

AN INVESTIGATION OF THE ELECTROWINNING OF COPPER WITH  
DIMENSIONALLY STABLE TITANIUM ANODES AND  
CONVENTIONAL LEAD ALLOY ANODES

**Zvanaka Senzeni Msindo**

A Dissertation submitted to the Faculty of Engineering and the Built Environment,  
University of the Witwatersrand, in fulfilment of the requirements of the degree of  
Master of Science in Engineering

February 2010

## **DECLARATION**

“I hereby declare that the thesis submitted for the degree MSc: Chemical Engineering, at the University of the Witwatersrand is my own work and has not previously been submitted to any other institution of higher education. I further declare that all sources cited are indicated and acknowledged by means of a comprehensive list of references”.

Z.S. Msindo

Copyright © University of the Witwatersrand 2009

*Dedicated to:*

*The Almighty: Thank you Lord for seeing me through. Without your help and guidance, I would not have made it this far.*

*My loving husband, Mordecai Mazhandu: Thank you for all the encouragement and support.*

*My daughter, Sasha: Thank you for being an inspiration.*

## **ACKNOWLEDGEMENTS**

I wish to express immeasurable gratitude to:

My supervisors: Prof. Potgieter and Dr Sibanda for their positive attitude and guidance. Your powerful contributions and constructive criticisms assisted me enormously in shaping this project. Without your persistent help this dissertation would not have been possible.

Anglo Platinum and the University of the Witwatersrand, for the financial assistance.

Bronwynne Ferreira, for availing her time and resources which assisted me in producing this piece of work.

Dr Marjanovic, for all the help she provided in ICP analysis of my samples.

Germaine Ntunka, for all the information he provided in the early stages of the project.

Evans Musapatika and Davison Nyabadza, for all the assistance offered on the use of AAS and XRD machines.

## ABSTRACT

The traditional anodes of choice in the electrowinning industry have been lead based anodes. However, these anodes display high energy consumption and low corrosion resistance during operation. These problems led to the investigation of other anode materials such as dimensionally stable anodes (DSAs), consisting of mixed metal oxide coatings on titanium or nickel substrates. In this study, electrochemical tests, physical characterisation techniques and electrowinning of copper from synthetic and industrial electrolytes were carried out on DSAs and lead anodes. These tests focused on stability, energy consumption and copper deposit quality. Potentiodynamic polarisation showed that the DSA plate anode exhibited the highest corrosion resistance while, lead and DSA mesh anodes showed spontaneous passivation in a synthetic solution. These anodes are therefore likely to succumb to failure earlier than the DSA plate anode. Lead anode dissolution was observed in galvanostatic chronopotentiometry tests. It was also observed that the failure mechanism of DSA anodes involves coating loss.

In electrowinning tests, copper deposits from the lead anode cell showed the presence of lead oxide. Furthermore, it was observed that, despite both mesh anodes (DSA 1 and DSA 2) exhibiting the lowest total energy consumption, they had the highest energy consumption per kilogramme of copper produced. The DSA 1 plate anode had the greatest current efficiency and therefore had the least energy consumption per kilogramme of copper. It was also noted that DSA anodes of the same composition may exhibit different behaviours as this depends on the method of preparation of the anode itself. The presence of iron or manganese in the electrolyte affected cathode quality, current efficiency, led to voltage fluctuations and an increase in anode potentials.

## GLOSSARY

Active - electrocatalytic

BMR solution – industrial electrolyte

Counter electrode - electrode in which an electrical current is expected to flow

Double layer capacitance - The measure of the ability of an electrical double layer to store electrical charge as a capacitor

Equivalents – electrons

Equivalent weight – weighted average for the major alloying elements in a specimen

Faradaic current – current due to a redox reaction

Galvanostatic – constant current

Limiting current density – maximum current density beyond which cell voltage must be significantly increased for a small increase in current density.

Metal values – valuable minerals in an ore

Open-circuit potential - potential of the working electrode relative to the reference electrode when no potential or current is being applied to the cell

Overpotential – extent of polarisation

Passivation - the spontaneous formation of a non-reactive surface film on a metal specimen

Polarisation - potential change from the equilibrium half-cell electrode potential caused by a net surface reaction rate for the half-cell reaction

Polarisation resistance – resistance of a specimen to corrode

Potentiodynamic – varying potential

Potentiostatic – constant potential

Reference electrode – electrode which establishes the electrical potential against which other potentials may be measured

Spalling – peeling off

Voltamperometric charges – Anodic charges

Working area – active surface area

Working electrode - electrode in an electrochemical system on which the reaction of interest is occurring

## LIST OF SYMBOLS

$A$  - Surface area in square metres.

$M$ - Molar mass or molecular mass of the substance in grams per mole.

$a$  - Atomic weight in grams per mole.

$a_i$  - Atomic weight of the *ith* alloying element in grams per mole.

$a$  and  $c$  - Anodic and cathodic coefficients.

$c$ - Specific heat capacity in kilocalories per kilogramme per degree Celsius.

$C$  - Constant.

$C_{dl}$  - Double layer capacitance in Farads per square centimetre.

CPE - Constant phase element in Farads.

$D$  – Constant.

$c_o$  - Concentration of the oxidised species in moles per unit volume or mass per unit volume.

$c_R$  - Concentration of the reduced species in moles per unit volume or mass per unit volume.

$\varepsilon_c$  - Cathode current efficiency (dimensionless).

$e_{H^+ / H_2}$  - Hydrogen half-cell reaction.

$E$  - Surface potential in volts.

$E_A^e$  - Equilibrium anode potentials in volts.

$E_C^e$  - Equilibrium cathode potentials in volts.

$E_{oc} / E_{corr}$  - Open circuit (corrosion) potential in volts.

$E_e$  - Equilibrium potential in volts.

$E_e^0$  - Standard potential in volts.

$E_0$  - Reversible potential in volts.

$E_{oc}$  - Open circuit potential in volts.

$E_p$  – Passivation potential in volts.

$\Delta E / \Delta V$  - Change in potential in volts.

$F$  - Faraday's constant (96 500 Coulombs per mole).  
 $f_i$  - Mass fraction of the  $i$ th alloying element (dimensionless).  
 $\Delta G$  - Standard Gibbs free energy change in Joules.  
 $i/I$  - Cell current in amperes.  
 $i_a$  - Anodic current in amperes  
 $i_c$  - Cathodic current in amperes.  
 $I_{corr}$  - Corrosion current in amperes.  
 $i_{pa}$  - Anodic peak current in amperes.  
 $i_{pc}$  - Cathodic peak current in amperes.  
 $\Delta i_{app}$  - Change in applied current in amperes.  
 $IR_{SOLN}$  - Voltage drop in solution in volts.  
 $j$  - Current density in amperes per square metre.  
 $j_o$  - Exchange current density in amperes per square metre.  
 $m$  - Mass in grams.  
 $N_{EQ}$  - Total number of equivalents.  
 $n$  - Number of electrons participating in the reaction.  
 $n$  - Surface roughness in electrochemical impedance spectroscopy data (dimensionless).  
 $P$  - Power in kilowatts.  
 $q^*$  - Voltammetric charge in coulombs per square centimetre.  
 $Q$  - Flow rate of the electrolyte per cell in millilitres per minute.  
 $r$  - Corrosion rate in grams per square metre per second, milli-inches per year, millimetres per year or micrometres per year.  
 $R$  - Gas constant in joules per Kelvin per mole.  
 $RF$  - Roughness factor (dimensionless).  
 $R_s$  - Solution resistance in ohms.  
 $R_{ct}$  - Charge transfer resistance in ohms.  
 $t$  - Time in seconds.  
 $T$  - Temperature in degrees Celsius or Kelvin.



$t_h$  - Heat-up time in hours.

$\Delta T$  - Temperature rise in degrees Celsius.

$V$  - Volume of solution per cell in litres.

$\Delta V_{\Omega}$  - Ohmic drop (IR) in the inter-electrode gap, in the electrodes and the connections in volts.

$\Delta V_t$  - Drift of  $\Delta V$  with time due to degradation of the electrode performance (stability) in volts.

$\Delta W$  - Weight gain in grams.

$\beta_a$  - Anodic Tafel constant in volts/decade.

$\beta_c$  - Cathodic Tafel constant in volts/decade.

$\alpha$  - Charge transfer coefficient (dimensionless)

$\eta$  - Overpotential in volts.

$\eta_a$  - Anodic polarisation in volts.

$\eta_c$  - Cathodic polarisation in volts.

$\Delta\eta$  - Sum of the anodic and cathodic overpotentials in volts.

$\rho$  - Density in grams per cubic centimetre.

## LIST OF ABBREVIATIONS

AAS - Atomic absorption spectrometer  
A.R. - Analytical reagent  
BMR - Base Metal Refinery  
CE - Counter electrode  
CV- Cyclic Voltammetry  
DC – Direct current  
DSAs - Dimensionally stable anodes  
e.m.f - electromotive force  
EASA - Electrochemically active surface area  
EDS - Energy dispersive spectroscopy  
EIS - Electrochemical Impedance Spectroscopy  
E.W. - Equivalent weight  
GPES - General Purpose Electrochemical System software  
IBCs - Intermediate Bulk Containers  
ICP - Inductively coupled plasma  
ICP-MS - Inductively coupled plasma-mass spectrometer  
Max. Maximum  
MoL - Mesh on Lead  
Min. - Minimum  
OCP - Open circuit potential  
OER - Oxygen evolution reaction  
OLP – Oxygen low potential  
PVC - Polyvinyl chloride  
RE - Reference electrode  
SEM - Scanning electron microscope  
SHE - Standard Hydrogen Electrode  
WE - Working electrode  
XRD – X-ray diffractometer  
XPS - X-ray photoelectron spectroscopy

## LIST OF FIGURES

|   |    |
|---|----|
| Figure 2.1: Potential-pH Diagram for the System Lead-Water, at 25 °C.....   | 12 |
| Figure 2.2: Potential-pH diagram for the System Lead-Sulphur-Water, at 25 °C. ....  | 13 |
| Figure 2.3: Potential-pH Equilibrium Diagram for the System Titanium-Water, at 25 °C. [Figure established by considering, as derivatives of tri- and tetravalent titanium, the anhydrous oxides Ti <sub>2</sub> O <sub>3</sub> and TiO <sub>2</sub> (rutile).]..... | 14 |
| Figure 2.4: Theoretical Domains of Corrosion, Immunity and Passivation of Titanium, at 25 °C. ....  | 15 |
| Figure 2.5: Potential-pH Equilibrium Diagram for the System Tantalum-Water, at 25 °C.....   | 16 |
| Figure 2.6: Potential-pH Diagrams for the Iridium-Water System at 25°C and Theoretical Conditions for the Corrosion, Immunity and Passivation of Iridium at 25°C Respectively.....  | 17 |
| Figure 2.7: Cathodic and Anodic Tafel Plot .....  | 22 |
| Figure 2.8: Cyclic Voltammogram.....  | 24 |
| Figure 2.9: Effect of Iron in the Electrolyte on Current Efficiency. ....   | 33 |
| Figure 3.1: log I-E Characteristic for a Metal which Shows Passivation .....  | 42 |
| Figure 3.2: Dependence of Service Life on Current Density, at Constant Electrolyte Concentration and Temperature. 150 g/l H <sub>2</sub> SO <sub>4</sub> – 60 °C.....   | 43 |
| Figure 3.3: Current Density-Voltage Curves for Copper Electrowinning Using Different Types of Anodes. Electrolyte: 50 g/l Cu, 50 g/l H <sub>2</sub> SO <sub>4</sub> , temperature: 40 °C; Cathode: copper clad graphite.....  | 48 |
| Figure 3.4: Cell Potential Difference (cell voltage) versus Current Density for De Nora Mercury Cells. (1) Graphite anodes; (2) activated Ti anodes (DSAs). NaCl concentration: 310 g/l. Temperature: 60 °C.....  | 49 |
| Figure 3.5: Polarisation measurements for the Oxygen Evolution Reaction on a TiO <sub>2</sub> /RuO <sub>2</sub> Dimensionally Stable Anode (DSA) and a Conventional Lead/Antimony anode. The electrolyte was 200 g/l sulphuric acid at 25 °C. ....                  | 50 |
| Figure 4.1: Potentiostat Equipped with a Personal Computer .....  | 55 |

|  |    |
|--|----|
| Figure 4.2: Electrowinning Cells .....   | 62 |
| Figure 4.3: Electrowinning Cells and Auxiliary Equipment.....  | 63 |
| Figure 4.4: Schematic Diagram of Experimental Setup.....   | 65 |
| Figure 4.5: Polystyrene Beads.....   | 65 |
| Figure 4.6: Sample anode with a copper hanger bar .....  | 67 |
| Figure 5.1: OCP Graphs for Ti-IrO <sub>2</sub> /Ta <sub>2</sub> O <sub>5</sub> Plate, Ti-IrO <sub>2</sub> /Ta <sub>2</sub> O <sub>5</sub> Mesh and Pb/Sb in 55 g/l Cu and 100 g/l H <sub>2</sub> SO <sub>4</sub> at Room Temperature (rt). ..... | 71 |
| Figure 5.2: Tafel Plots for DSA and Lead Alloy Anodes in Synthetic Electrolyte ....  | 73 |
| Figure 5.3: Tafel Plots for DSA Plate in the Potential range 0.4 V to 1.2 V and -0.4 V to 1.4 V in Synthetic Electrolyte. ....   | 74 |
| Figure 5.4: Anode potential-time curves for Pb-6% Sb and Ti-Ta <sub>2</sub> O <sub>5</sub> /IrO <sub>2</sub> (plate and mesh) in 55 g/l Cu and 100 g/l H <sub>2</sub> SO <sub>4</sub> at 190 A/m <sup>2</sup> .....                              | 76 |
| Figure 5.5: Cyclic Voltammograms for the Lead Alloy Anode in the Potential Range -0.5 to 2.2 V. ....   | 82 |
| Figure 5.6: Cyclic Voltammograms for the Lead Alloy Anode in the Potential Range 0 to 2.2 V.....   | 83 |
| Figure 5.7: Cyclic Voltammograms for Ti/IrO <sub>2</sub> -Ta <sub>2</sub> O <sub>5</sub> Electrodes in 0.5 M H <sub>2</sub> SO <sub>4</sub> at a Scan Rate of 100 mV/s.....  | 84 |
| Figure 5.8: Change of Voltammetric Charge of the DSA Mesh Specimen with Continuous Cycling.....  | 86 |
| Figure 5.9: Change of Voltammetric Charge of the DSA Plate Specimen with Continuous Cycling.....   | 86 |
| Figure 5.10: Change of Voltammetric Charge of the Lead Anode Specimen with Continuous Cycling.....   | 87 |
| Figure 5.11: Relationship between Current Density and Scan Rate at a Fixed Potential of 1.0 V for Ti/ IrO <sub>2</sub> -Ta <sub>2</sub> O <sub>5</sub> and Pb/Sb Anodes. ....  | 88 |
| Figure 5.12: Typical Graph of Anodic Charge, q* against Double Layer Capacitance, C <sub>dl</sub> for a DSA Anode. ....  | 89 |
| Figure 5.13: Nyquist Plots for the DSA Plate at Open Circuit Potential and Oxygen Evolution Potential.....   | 90 |

|   |     |
|---|-----|
| Figure 5.14: Nyquist Plots for the DSA Mesh Anode at Open Circuit Potential and Oxygen Evolution Potential. ....                | 91  |
| 5.15: Nyquist Plots for the Lead Anode at Open Circuit Potential and Oxygen Evolution Potential.....                            | 92  |
| Figure 5.16: Nyquist Plots for a Ti/IrO <sub>2</sub> -Ta <sub>2</sub> O <sub>5</sub> Plate Anode in Synthetic Electrolyte. .... | 94  |
| Figure 5.17: Nyquist Plots for a Ti/IrO <sub>2</sub> -Ta <sub>2</sub> O <sub>5</sub> Mesh Anode in Synthetic Electrolyte. ....  | 94  |
| Figure 5.18: Nyquist Plots for a Pb/Sb Anode in Synthetic Electrolyte .....   | 95  |
| Figure 5.19: Chronoamperometry Tests in Synthetic Electrolyte.....  | 96  |
| Figure 5.20: XRD Pattern for Unused DSA Anodes .....  | 97  |
| Figure 5.21: XRD Pattern for Used DSA Anodes .....  | 98  |
| Figure 5.22: XRD Pattern for an Unused Lead Alloy Anode .....   | 99  |
| Figure 5.23: XRD Pattern for a Used Lead Alloy Anode .....  | 99  |
| Figure 5.24: SEM Micrograph for an Unused Lead Alloy Anode.....   | 100 |
| Figure 5.25: SEM Micrograph for a Used Lead Alloy Anode.....  | 100 |
| Figure 5.26: SEM Micrograph for an unused DSA Anode.....  | 101 |
| Figure 5.27: SEM Micrograph for a used DSA Anode.....   | 101 |
| Figure 5.28: EDS Analysis for an Unused DSA Anode .....   | 102 |
| Figure 5.29: EDS Analysis for a Used DSA Anode .....  | 103 |
| Figure 5.30: Cell Voltage against Time in BMR Solution over a Period of 150 Hours. ....   | 106 |
| Figure 5.31: Cell Voltage against Time in BMR Solution over a Period of 150 Hours. ....   | 107 |
| Figure 5.32: Cell Voltage against Time in BMR Solution over a Period of 150 Hours. ....   | 108 |
| Figure 5.33: Cell Voltage against Time in BMR Solution over a Period of 150 Hours. ....   | 109 |
| Figure 5.34: Anode Potential against Time in BMR and Synthetic Solutions for a DSA Plate Specimen. ....                         | 111 |

|  |     |
|--|-----|
| Figure 5.35: Anode Potential against Time in BMR and Synthetic Solutions for a DSA Mesh Specimen. ....                 | 111 |
| Figure 5.36: Anode Potential against Time in BMR and Synthetic Solutions for a Lead Specimen. ....                     | 112 |
| Figure 5.37: Anode Potential against Time in Synthetic and Synthetic/Manganese Solution for a DSA Plate Specimen. .... | 114 |
| Figure 5.38: Anode Potential against Time in Synthetic and Synthetic/Manganese Solution for a DSA Mesh Specimen. ....  | 115 |
| Figure 5.39: Anode Potential against Time in Synthetic and Synthetic/Manganese Solution for a Lead Specimen. ....      | 116 |
| Figure 5.40: Heating Rod Showing Electrodeposited Copper in the Lead Anode Cell. ....                                  | 118 |
| Figure 5.41: Copper from DSA 1 Plate Anode .....   | 120 |
| Figure 5.42: Copper from DSA 2 Plate Anode .....   | 120 |
| Figure 5.43: Copper from DSA 1 Mesh Anode. ....  | 121 |
| Figure 5.44: Copper from DSA 2 Mesh Anode. ....  | 121 |
| Figure 5.45: Copper from Lead Anode Cell. ....   | 122 |
| Figure 5.46: Micrograph for Copper from DSA 1 Plate Anode Cell.....  | 122 |
| Figure 5.47: Micrograph for Copper from DSA 2 Plate Anode Cell.....  | 123 |
| Figure 5.48: Micrograph for Copper from DSA 1 Mesh Anode Cell.....   | 123 |
| Figure 5.49: Micrograph for Copper from DSA 2 Mesh Anode Cell.....   | 124 |
| Figure 5.50: Micrograph for Copper from Lead Anode Cell.....   | 124 |
| Figure 5.51: XRD Peak Height Intensity: DSA 1 Plate Anode Cell.....  | 125 |
| Figure 5.52: XRD Peak Height Intensity: DSA 1 Mesh Anode Cell.....   | 125 |
| Figure 5.53: XRD Peak Height Intensity: DSA 2 Plate Anode .....  | 126 |
| Figure 5.54: XRD Peak Height Intensity: DSA 2 Mesh Anode Cell.....   | 126 |
| Figure 5.55: XRD Peak Height Intensity: Lead Anode .....   | 127 |
| Figure 5.56: XRD Peak Height Intensity: Standard Copper Sample .....   | 127 |

## LIST OF TABLES

|   |     |
|---|-----|
| Table 2.1: Potential Values of Common Secondary Reference Electrodes. Standard Hydrogen Electrode Included for Reference..... | 8   |
| Table 2.2: Components of Cell Voltage in Copper Electrowinning .....  | 30  |
| Table 3.1: De Nora Mercury cells: Comparison of Performances with Graphite and DSA Anodes.....                                | 49  |
| Table 3.2: Conductivities of Some Conductive Polymers .....   | 52  |
| Table 4.1: Anode Type, Supplier and Composition.....  | 55  |
| Table 4.2: Reagents Used.....   | 56  |
| Table 4.3: Concentrations of Electrolytes Used.....   | 57  |
| Table 4.4: Equipment Used During Electrowinning Tests .....   | 61  |
| Table 4.5: Electrodes and Preparation.....  | 66  |
| Table 5.1: Linear Polarisation Parameters .....   | 75  |
| Table 5.2: Determination of Current Efficiency .....  | 78  |
| Table 5.3: Effect of anode substrates on anode potential and deposit morphology ....  | 79  |
| Table 5.4: Concentration of Lead in the Electrolyte and Standard Deviations.....  | 79  |
| Table 5.5: Concentrations of Titanium, Tantalum and Iridium in the Electrolyte.....   | 80  |
| Table 5.6: Voltammetric Charges for the Anode Specimens.....  | 85  |
| Table 5.7: Double Layer Capacitance and Roughness Factor for DSA Anodes.....  | 89  |
| Table 5.8: Equivalent Circuit Parameters for DSA Plate and Mesh Anodes and the Lead Anode at Open Circuit Potential .....     | 92  |
| Table 5.9: Equivalent Circuit Parameters for DSA Plate and Mesh Anodes and the Lead Anode at Oxygen Evolution Potential.....  | 92  |
| Table 5.10: Quantitative Analysis for Unused and Used DSA Anodes.....   | 104 |
| Table 5.11: Values of Minimum (Min.) and Maximum (Max.) Cell Voltages for DSA 1 and DSA 2 Plates. ....                        | 109 |
| Table 5.12: Values of Minimum and Maximum Cell Voltages for DSA 1 and DSA 2 Meshes.....                                       | 110 |

|  |     |
|--|-----|
| Table 5.13: Current Efficiencies Achieved Over a Period of 150 hrs Using DSA 1 Anodes and a Lead Anode ..... | 117 |
| Table 5.14: Current Efficiencies Achieved Over a Period of 150 hrs Using DSA 2 Anodes and a Lead Anode ..... | 117 |
| Table 5.15: Copper Diffraction Pattern (standard sample) .....   | 128 |
| Table 5.16: Simplified Economic Evaluation of Replacing Lead Anodes with a DSA Anode .....                   | 130 |
| Table 5.17: Other Fixed Costs in the Study .....   | 130 |



## TABLE OF CONTENTS

|  |          |
|--|----------|
| ACKNOWLEDGEMENTS.....  | iv       |
| ABSTRACT .....   | v        |
| GLOSSARY.....  | vi       |
| LIST OF SYMBOLS.....   | vii      |
| LIST OF ABBREVIATIONS.....   | x        |
| LIST OF FIGURES.....   | xi       |
| LIST OF TABLES .....   | xv       |
| <br>   |          |
| <b>1 INTRODUCTION.....</b>   | <b>1</b> |
| 1.1 Background and motivation .....                                | 1        |
| 1.2 Problem statement.....   | 2        |
| 1.3 Aim.....   | 3        |
| 1.4 Hypotheses .....   | 3        |
| 1.5 Research questions .....                                       | 4        |
| 1.6 Objectives.....  | 4        |
| 1.7 Research lay-out.....  | 5        |
| <b>2 THEORETICAL BACKGROUND.....</b>                               | <b>6</b> |
| 2.1 Electrochemical thermodynamics .....                           | 6        |
| 2.1.1 Electrode processes .....                                    | 6        |
| 2.1.2 Measurement of electrode potentials.....                     | 6        |
| 2.1.2.1 Nernst equation .....                                      | 7        |
| 2.1.2.2 Types of reference electrodes.....                         | 8        |
| 2.1.3 Electrochemical polarisation.....                            | 8        |
| 2.1.3.1 Butler-Volmer equation.....                                | 10       |
| 2.1.4 Measurement of cell voltages.....                            | 11       |
| 2.1.5 Pourbaix stability diagrams.....                             | 12       |
| 2.2 Electrochemical and physical characterisation techniques ..... | 18       |
| 2.2.1 Electrochemical characterisation.....                        | 18       |

|           |  |           |
|-----------|--|-----------|
| 2.2.1.1   | Corrosion rate measurements .....                            | 19        |
| 2.2.1.1.1 | Tafel extrapolation.....                                     | 22        |
| 2.2.1.1.2 | Polarisation resistance method .....                         | 23        |
| 2.2.1.2   | Cyclic voltammetry .....                                     | 23        |
| 2.2.1.2.1 | Qualitative analysis.....                                    | 24        |
| 2.2.1.2.2 | Quantitative analysis.....                                   | 25        |
| 2.2.1.3   | Chronoamperometry.....                                       | 25        |
| 2.2.1.4   | Galvanostatic chronopotentiometry .....                      | 26        |
| 2.2.1.5   | Electrochemical impedance spectroscopy.....                  | 26        |
| 2.2.2     | Physical characterisation techniques .....                   | 27        |
| 2.3       | Electrowinning of copper .....                               | 27        |
| 2.3.1     | Important parameters in electrowinning .....                 | 27        |
| 2.3.2     | Electrowinning reactions.....                                | 28        |
| 2.3.2.1   | Oxygen evolution .....                                       | 29        |
| 2.3.3     | Electrowinning products .....                                | 31        |
| 2.3.4     | Suppression of acid mist .....                               | 31        |
| 2.3.5     | Current density .....  | 31        |
| 2.3.6     | Electrolyte concentration.....                               | 32        |
| 2.3.7     | Additives .....  | 32        |
| 2.3.8     | Maximising copper purity .....                               | 32        |
| 2.3.9     | Maximising current efficiency .....                          | 33        |
| 2.3.10    | Amount of copper deposited .....                             | 34        |
| <b>3</b>  | <b>LITERATURE REVIEW.....</b>                                | <b>36</b> |
| 3.1       | Lead alloy anodes used in electrowinning .....               | 36        |
| 3.2       | DSA applications in electrochemistry.....                    | 36        |
| 3.2.1     | Manufacture of DSA anodes.....                               | 37        |
| 3.2.1.1   | Electrochemical oxidation on DSA-type oxide electrodes ..... | 38        |
| 3.2.1.2   | Electrocatalytic coatings for oxygen evolution.....          | 39        |
| 3.2.1.3   | Structure of oxide coating .....                             | 40        |
| 3.2.1.4   | Stability and success of DSA anodes .....                    | 40        |

|           |   |           |
|-----------|---|-----------|
| 3.2.1.5   | Deactivation mechanism of DSA anodes.....         | 40        |
| 3.2.1.5.1 | Passivation.....                                  | 40        |
| 3.2.1.5.2 | Coating consumption.....                          | 43        |
| 3.2.1.5.3 | Coating detachment.....                           | 44        |
| 3.2.1.5.4 | Mechanical damage.....                            | 44        |
| 3.2.1.5.5 | Mixed mechanism.....                              | 44        |
| 3.3       | Comparison of lead alloy and DSA anodes .....     | 45        |
| 3.4       | Alternative anode materials.....                  | 51        |
| <b>4</b>  | <b>EXPERIMENTAL PROCEDURES.....</b>               | <b>54</b> |
| 4.1       | Electrochemical tests.....                        | 54        |
| 4.1.1     | Electroanalytical equipment.....                  | 54        |
| 4.1.2     | Electrode preparation .....                       | 55        |
| 4.1.3     | Reagents .....                                    | 56        |
| 4.1.4     | Electrolyte solutions.....                        | 56        |
| 4.1.5     | Electrochemical measurements.....                 | 57        |
| 4.1.5.1   | Open circuit potential (OCP) measurements.....    | 58        |
| 4.1.5.2   | Potentiodynamic Polarisation.....                 | 58        |
| 4.1.5.3   | Chronopotentiometry (galvanostatic).....          | 58        |
| 4.1.5.4   | Cyclic Voltammetry (CV).....                      | 59        |
| 4.1.5.5   | Electrochemical Impedance Spectroscopy (EIS)..... | 60        |
| 4.1.5.6   | Chronoamperometry (< 1s).....                     | 60        |
| 4.1.6     | Reproducibility.....                              | 60        |
| 4.2       | Electrowinning tests .....                        | 61        |
| 4.2.1     | Equipment .....                                   | 61        |
| 4.2.2     | Electrowinning cell configuration and setup.....  | 61        |
| 4.2.2.1   | Control of pump flow rate.....                    | 63        |
| 4.2.3     | Suppression of acid mist .....                    | 64        |
| 4.2.4     | Electrodes .....                                  | 66        |
| 4.2.5     | Reagents .....                                    | 67        |
| 4.2.6     | Analytical equipment .....                        | 68        |

|          |  |           |
|----------|--|-----------|
| 4.2.7    | Equipment Design.....  | 68        |
| 4.2.7.1  | Pump sizing.....   | 68        |
| 4.2.7.2  | Heater sizing.....   | 69        |
| 4.3      | Physical characterisation.....   | 70        |
| 4.3.1    | Scanning electron microscope (SEM) and energy dispersive spectroscopy, EDS ..... | 70        |
| 4.3.2    | X-ray diffractometer.....  | 70        |
| 4.3.3    | Visual inspection.....   | 70        |
| <b>5</b> | <b>RESULTS AND DISCUSSIONS .....</b>   | <b>71</b> |
| 5.1      | Comparison of anode materials: Electrochemical Investigations .....              | 71        |
| 5.1.1    | Open circuit potential measurements .....  | 71        |
| 5.1.2    | Potentiodynamic polarisation.....  | 73        |
| 5.1.3    | Chronopotentiometry (galvanostatic).....   | 76        |
| 5.1.3.1  | Determination of current efficiency .....  | 77        |
| 5.1.3.2  | Electrolyte contamination .....  | 79        |
| 5.1.4    | Cyclic voltammetry.....  | 81        |
| 5.1.4.1  | Cyclic voltammograms for lead anodes.....  | 81        |
| 5.1.4.2  | Cyclic voltammograms for DSA anodes.....   | 83        |
| 5.1.4.3  | Electrochemically active surface area for the anode specimens .....              | 84        |
| 5.1.4.4  | Effect of continuous cycling on voltammetric charge .....                        | 85        |
| 5.1.4.5  | Determination of double layer capacitance.....                                   | 87        |
| 5.1.5    | Electrochemical impedance spectroscopy .....                                     | 90        |
| 5.1.6    | Chronoamperometry (<1s).....   | 96        |
| 5.1.7    | X-Ray Diffractometry (XRD) analysis .....  | 97        |
| 5.1.8    | Scanning Electron Microscopy (SEM) analysis.....                                 | 100       |
| 5.1.9    | Energy Dispersive Spectrometry (EDS) analysis.....                               | 102       |
| 5.2      | Comparison of anode materials: Electrowinning Experiments.....                   | 104       |
| 5.2.1    | Variation of Cell Voltage with Time.....   | 104       |
| 5.2.1.1  | Comparison of DSA 1 Plate and Mesh Anodes and the Lead Anode                     |           |

|           |   |            |
|-----------|---|------------|
| 5.2.1.2   | Comparison of DSA 2 Plate and Mesh Anodes and the Lead Anode                              | 107        |
| 5.2.1.3   | Comparison between the DSA 1 and DSA 2 plate and mesh anodes                              | 108        |
| 5.2.1.3.1 | Comparison between the DSA 1 and DSA 2 plate anodes.....                                  | 108        |
| 5.2.1.3.2 | Comparison between the DSA 1 and DSA 2 mesh anodes.....                                   | 109        |
| 5.2.1.4   | Comparison between BMR and Synthetic solutions.....                                       | 111        |
| 5.2.1.4.1 | Comparison between BMR and Synthetic solutions for a DSA plate                            | 111        |
| 5.2.1.4.2 | Comparison between BMR and Synthetic solutions for a DSA mesh anode.....                  | 111        |
| 5.2.1.4.3 | Comparison between BMR and Synthetic solutions for a lead anode                           | 112        |
| 5.3       | Impurities in BMR solution .....  | 113        |
| 5.3.1     | Effect of manganese on anode potential .....  | 113        |
| 5.3.1.1   | Comparison between synthetic and synthetic/manganese solutions                            | 114        |
| 5.3.1.1.1 | Comparison between synthetic and synthetic/manganese solutions for a DSA plate anode..... | 114        |
| 5.3.1.1.2 | Comparison between synthetic and synthetic/manganese solutions for a DSA mesh anode.....  | 115        |
| 5.3.1.1.3 | Comparison between synthetic and synthetic/manganese solutions for a lead anode.....      | 116        |
| 5.3.2     | Current efficiency.....   | 117        |
| 5.3.3     | Morphology of the copper produced.....  | 119        |
| 5.4       | XRD analysis for copper deposits.....   | 125        |
| 5.5       | Economic evaluation.....  | 130        |
| <b>6</b>  | <b>SUMMARY OF RESULTS.....</b>  | <b>132</b> |
| 6.1       | Comparison of anode materials.....  | 132        |
| 6.1.1     | Electrochemical Investigations .....  | 132        |

|           |  |            |
|-----------|--|------------|
| 6.1.1.1   | Open circuit potential measurements .....                            | 132        |
| 6.1.1.2   | Potentiodynamic polarisation .....                                   | 133        |
| 6.1.1.3   | Chronopotentiometry (galvanostatic) tests.....                       | 133        |
| 6.1.1.3.1 | Determination of current efficiency .....                            | 135        |
| 6.1.1.3.2 | Electrolyte contamination from anode deterioration .....             | 135        |
| 6.1.1.4   | Cyclic voltammetry .....   | 135        |
| 6.1.1.4.1 | Cyclic voltammograms for lead anodes .....                           | 136        |
| 6.1.1.4.2 | Cyclic voltammograms for DSA anodes .....                            | 136        |
| 6.1.1.4.3 | Electrochemically active surface area for the anode specimens<br>137 |            |
| 6.1.1.4.4 | Effect of continuous cycling on voltammetric charge.....             | 137        |
| 6.1.1.4.5 | Determination of double layer capacitance .....                      | 137        |
| 6.1.1.4.6 | Determination of Roughness Factor (RF) .....                         | 138        |
| 6.1.1.5   | Electrochemical impedance spectroscopy (EIS).....                    | 138        |
| 6.1.1.6   | Chronoamperometry (<1s) .....  | 139        |
| 6.1.2     | Physical Characterisation .....                                      | 139        |
| 6.1.2.1   | X-Ray Diffractometry (XRD) analysis of anode materials.....          | 139        |
| 6.1.2.2   | Scanning Electron Microscopy (SEM) analysis.....                     | 139        |
| 6.1.2.3   | Energy Dispersive Spectrometry (EDS) analysis.....                   | 140        |
| 6.1.3     | Electrowinning Experiments .....                                     | 140        |
| 6.1.3.1   | Variation of cell voltage with time.....                             | 140        |
| 6.1.3.2   | Current Efficiency .....   | 141        |
| 6.1.3.3   | XRD analysis and optical micrography of copper deposits .....        | 142        |
| 6.1.4     | Economic evaluation .....  | 143        |
| <b>7</b>  | <b>CONCLUSIONS AND RECOMMENDATIONS .....</b>                         | <b>144</b> |
| 7.1       | Conclusions .....  | 144        |
| 7.1.1     | Anode Stability.....   | 144        |
| 7.1.2     | Cell voltage .....   | 145        |
| 7.1.3     | Techno-economic evaluation .....                                     | 145        |
| 7.1.4     | Cathode contamination.....   | 146        |

|   |  |            |
|---|--|------------|
| 7.1.5   | Effect of impurities in the electrolyte..... | 146        |
| 7.2   | Recommendations for future research.....     | 146        |
| 7.3   | Expected contribution to knowledge.....      | 147        |
| <b>REFERENCES.....</b>                            |  | <b>149</b> |
| APPENDIX A: FLOW RATE CALCULATIONS.....           |  | 159        |
| APPENDIX B: OPERATING PARAMETERS.....             |  | 161        |
| APPENDIX C: HEATER SIZING.....                    |  | 162        |
| APPENDIX D: CURVES SHOWING REPRODUCIBILITY .....  |  | 164        |
| APPENDIX E: SIMILAR ANODE/CATHODE AREAS .....     |  | 174        |
| APPENDIX F: DATA FOR FIGURES .....                |  | 177        |
| APPENDIX G: COMPOSITION OF BMR ELECTROLYTE .....  |  | 203        |
| APPENDIX H: PHOTOGRAPH OF EXPERIMENTAL SETUP..... |  | 204        |
| <b>SUBMISSION OF RESEARCH PAPER.....</b>          |  | <b>205</b> |

# 1 INTRODUCTION

## 1.1 Background and motivation

Most of the world's copper produced is extracted using hydrometallurgical processes, with electrowinning being one of the most important final steps. The electrowinning process has been in existence since the 1800's and it has evolved ever since due to various researches undertaken. Electrowinning is an energy extensive process and as such it accounts for a significant part of the costs of copper production. In a conventional copper electrowinning cell, the cathodic reaction is the electrodeposition of copper from an aqueous solution of copper sulfate containing free sulphuric acid, and the anodic reaction is the dissociation of water into hydrogen ions and oxygen. The essential requirements for anodes in electrowinning are electrochemical stability in sulfate electrolytes, resistance to the chemical effects of oxygen liberated on the anode surface, low oxygen overvoltage, mechanical stability and structural integrity under operating conditions, product quality and environmental safety (Weems *et al.*, 2005, Gupta and Mukherjee, 1990).

The traditional anodes of choice in the electrowinning industry have been lead based anodes with typical compositions of lead-antimony (6%), lead-calcium (0.7%)-tin (1.3%) and lead-strontium (0.05%) tin (0.6%). The continued use of the lead based anodes in the electrowinning process has been mainly due to their relatively low cost compared to other materials. However, certain drawbacks in the use of these anodes have been documented, where the undesirable physical and chemical characteristics have prompted further research into alternative materials to replace them. The main disadvantages of lead based anodes are high energy consumption and low corrosion resistance. Corrosion results in shorter anode life spans and production of poor quality cathode deposits due to the incorporation of lead corrosion products (Moats *et al.*, 2003). Therefore, taking into consideration the low cost of lead based anodes, it is important that the replacement anodes offer high energy savings and low corrosion



rates. Various materials have been proposed by researchers as having the ability to replace the conventional lead anodes, such as dimensionally stable anodes (DSAs).

Dimensionally stable anodes consist of mixed metal oxide coatings, usually on titanium or nickel substrates. The oxides that can be used in the oxide coatings include tantalum oxide ( $\text{Ta}_2\text{O}_5$ ), iridium oxide ( $\text{IrO}_2$ ), ruthenium dioxide ( $\text{RuO}_2$ ) and tin oxide ( $\text{SnO}_2$ ). Since the discovery of DSAs by Henry Beer in 1957, much work has been done on these anodes. Initially, the use of the DSA mainly focussed on the  $\text{Ti/RuO}_2\text{-TiO}_2$  anodes, which are popular in the chlor-alkali industry. Although these anodes exhibited low energy consumption and low corrosion rates, they showed very poor performances when used as oxygen evolution anodes (Hine *et al.*, 1979). Nevertheless, the good performance of the  $\text{Ti/RuO}_2\text{-TiO}_2$  anode in chloride solutions suggested that, with an appropriate coating, a new DSA could be found for oxygen evolution. This motivated intensive research by many authors such as Rolewicz *et al.* (1988), which led to the  $\text{Ti/IrO}_2\text{-Ta}_2\text{O}_5$  electrode.

## 1.2 Problem statement

The electrowinning process is significantly affected by the electrode material. Conditions of high temperature ( $30\text{ }^{\circ}\text{C}$ - $60\text{ }^{\circ}\text{C}$ ), and a strongly acidic electrolyte, due to the decomposition of water into hydrogen ions and oxygen gas, create a corrosive environment in the cell. In spite of the low cost of lead anodes (about \$US 500/ $\text{m}^2$ ), high energy consumption and physical degradation associated with these anodes have been a major concern in the electrowinning of copper. During operation, a lead oxide layer forms on the anodes. Flakes of the lead oxide formed can attach to the growing copper deposit, leading to lead contamination in the final product. Physical degradation adversely affects anode life, cathode purity and the market grade of copper deposited (Weems *et al.*, 2005). Growths which occur on the cathode as a consequence of the oxide layer may also cause an electrical short circuit, thus decreasing the production of copper (Tyroler *et al.*, 1987). Cobalt sulphate is usually

added to the electrolyte circuit in order to stabilise the lead oxide layer and prevent spalling under controlled operating conditions. Levels of 120 ppm cobalt are considered to be sufficient (Weems *et al.*, 2005). However, since cobalt is expensive, this leads to an increase in operating costs. Other problems which result from the use of lead alloy anodes include disposal of the lead sludge produced, without violating environmental constraints and high maintenance costs incurred periodically to clean the anode surfaces and refurbish the anode area (Alfantazi and Moskalyk, 2003).

### **1.3 Aim**

This project will compare the performance of dimensionally stable anodes (Ti/ (70%) IrO<sub>2</sub>- (30%) Ta<sub>2</sub>O<sub>5</sub> against the conventional lead alloy anodes (lead- (6%) antimony) in synthetic and base metal refinery (BMR) solutions by investigating:

- (i) anode stability
- (ii) cell voltage
- (iii) cost of materials
- (iv) cathode contamination

An economic evaluation of the DSAs and lead alloy anodes will be provided.

### **1.4 Hypotheses**

In view of the reported problems of high energy consumption and corrosion associated with the conventional lead based anodes used in copper electrowinning, the dimensionally stable anodes (DSAs) may potentially be a good substitute. The research on DSAs, although still ongoing, suggests that there are advantages of using dimensionally stable anodes over lead based anodes. Based on the formulation of DSAs, these anodes are expected to have benefits such as low energy consumption and great stability. Therefore a number of indicators that include, corrosion resistance, anode potential, cell voltage and cathode purity will be investigated in this study in order to prove or disprove these hypotheses. Lead-antimony (6%) anodes and

dimensionally stable plate and mesh anodes will be tested in synthetic electrolyte and industrial electrolyte specific for the company concerned.

### **1.5 Research questions**

- ✓ What affects anode stability, cell voltage, life expectancy and cathode purity in electrowinning processes?
- ✓ What is the relationship between cell voltage and anode life?
- ✓ Is it technically and economically justifiable to replace conventional lead based anodes with dimensionally stable anodes in the copper electrowinning process?
- ✓ How does the behaviour of DSA anodes from different vendors compare during electrowinning?
- ✓ What are the harmful effects of impurities in the electrolyte on anode performance?

### **1.6 Objectives**

- ✓ To compare electrode stability and corrosion rates of DSA plate, DSA mesh and lead anodes.
- ✓ To assess the life expectancy of DSAs and lead anodes.
- ✓ To analyse the compositions and morphology of the copper deposits from electrowinning cells containing the DSA plate and mesh anodes and the lead anode.
- ✓ To compare energy consumption for the DSAs and lead anodes in the electrowinning of copper.
- ✓ To carry out a financial evaluation of the electrowinning process using the DSA anodes and lead anodes.
- ✓ To determine the effect of impurities in the electrolyte on the behaviour of the DSAs and lead anodes.

## **1.7 Research lay-out**

The rest of the project lay-out will be as follows:

- Chapter 2-Theoretical Background
- Chapter 3- Literature Review
- Chapter 4- Experimental Procedures
- Chapter 5- Results and Discussions
- Chapter 6- Summary of Results
- Chapter 7- Conclusions and Recommendations

## 2 THEORETICAL BACKGROUND

### 2.1 Electrochemical thermodynamics

#### 2.1.1 Electrode processes

Electrode processes are chemical reactions that involve the transfer of charge, usually electrons across the interface between an electrode and an electrolyte. For electrochemical reactions to occur, an anode, a cathode, ionic contact between the electrodes via an electrolyte and electronic contact are necessary. At the anode, oxidation of species occurs, which is a loss of electrons while at the cathode a simultaneous reduction process occurs. This reaction consumes those electrons provided by the oxidative process. Unless these electrons can be consumed, then the anodic reaction cannot occur (Scully, 1975).

#### 2.1.2 Measurement of electrode potentials

Electrochemical reactions that characterise a metal-solution interface occur at the surface of the metal, when a metal is immersed in a given solution. This leads to corrosion of the metal. The reactions create an electrochemical or equilibrium potential called electrode potential, or open circuit potential,  $E_{oc}$  (corrosion) potential. The potential of a metal is the means by which the anodic and cathodic reactions are kept in balance. Since the open circuit potential ends up at the potential where the cathodic and anodic currents are equal, it can also be referred to as a mixed potential.

The current from each half reaction depends on the electrochemical potential of the metal. If the anodic reaction releases too many electrons into the metal, the potential of the metal becomes more negative as a result of the excess electrons. This consequently slows the anodic reaction and speeds up the cathodic reaction thereby counteracting the initial perturbation of the system.

This follows Lechatelier’s principle which states that: “a system will always react to oppose a change imposed upon it” (Meyers, 2003). The value of either the anodic or cathodic current at  $E_{oc}$  is called the corrosion current,  $I_{corr}$ . The potential that exists between a metal and the solution in contact with it, is immeasurable in absolute terms and only the potential difference between the metal and another electrode can be measured. Furthermore, the changes in the potential difference can be related to the metal electrode under investigation, if the other electrode is a reference electrode. Such an electrode arrangement will enable direct measurement of electrode potential by using a potentiostat or a high impedance digital voltmeter (Scully, 1975). Experiments based on the measurement of the open circuit potential have important applications in corrosion measurements.

Corrosion current cannot be measured directly, but it can be estimated using electrochemical techniques. Corrosion current is an important parameter in the determination of the corrosion rate of a metal specimen in solution. In any real system,  $I_{corr}$  and corrosion rate are functions of many system variables such as type of metal, solution composition, temperature, solution movement and metal history (Jones, 1996).

*2.1.2.1 Nernst equation*

Electrode potentials can be calculated from the Nernst equation when the activity of metal cations is not at unit activity (non-standard conditions):

$$E_e = E_e^0 + \frac{2.3RT}{nF} \log \frac{c_o}{c_R} \dots\dots\dots 2.1$$

Where,  $E_e^0$  is the standard potential (the equilibrium potential when all reactants and products are at their standard states), n is the number of electrons participating in the reaction, R is the gas constant, T is temperature,  $c_o$  and  $c_R$  are the concentrations of the oxidised and reduced species respectively. The thermodynamic equation can also be written in terms of a ratio of activities.

### 2.1.2.2 Types of reference electrodes

There are several reference electrodes that are in common use in the field of electrochemistry. The Standard Hydrogen Electrode (SHE) is the primary reference electrode because it establishes the reference (zero) point on the electrochemical scale by definition. The hydrogen half-cell reaction has an electrode potential,  $e_{H^+/H_2} = 0$  for all reactants and products at standard state. This reference electrode is connected to another half-cell through a solution salt bridge which contains a porous glass barrier to permit charge transfer and potential measurement but not mass transfer of the acid solution in the electrode. Other reference electrodes are secondary reference electrodes and electrode potentials can also be reported with reference to these, as shown in table 2.1 (Jones, 1996).

**Table 2.1: Potential Values of Common Secondary Reference Electrodes. Standard Hydrogen Electrode Included for Reference**

| Name                       | Half-Cell Reaction               | Potential V vs. SHE | Area of Application   |
|----------------------------|----------------------------------|---------------------|---|
| Mercury-Mercurous Sulphate | $HgSO_4 + 2e^- = Hg + SO_4^{2-}$ | +0.615              | Possible contamination of cell by chloride is undesirable                     |
| Copper-Copper Sulphate     | $CuSO_4 + 2e^- = Cu + SO_4^{2-}$ | +0.318              | Buried metal structures   |
| Saturated Calomel          | $Hg_2Cl_2 + 2e^- = 2Hg + 2Cl^-$  | +0.241              | Laboratory use  |
| Silver-Silver Chloride     | $AgCl + e^- = Ag + Cl^-$         | +0.222              | Elevated temperatures (it has a smaller temperature coefficient of potential) |
| Standard Hydrogen          | $2H^+ + 2e^- = H_2$              | +0.000              |   |

### 2.1.3 Electrochemical polarisation

Polarisation is the potential change from the equilibrium half-cell electrode (open-circuit) potential caused by a net surface reaction rate for the half-cell reaction.

This causes current to flow via electrochemical reactions that occur at the electrode surface. The amount of current is controlled by the kinetics of the reactions and the diffusion of reactants both towards and away from the electrode.

The extent of polarisation is measured by the overpotential,  $\eta$ . For anodic polarisation, electrons are removed from the metal and a deficiency results in a positive potential change due to the slow liberation of electrons by the surface reaction, and  $\eta_a$  must be positive. For cathodic polarisation,  $\eta_c$ , electrons are supplied to the surface, and a build up in the metal due to the slow reaction rate causes the surface potential,  $E$ , to become negative compared to the equilibrium half-cell electrode potential,  $E_{eq}$ . Thus,  $\eta_c$  is negative by definition (Jones, 1996). Overpotential is determined from equations 2.2 and 2.3 given below:

$$\eta = E - E_{eq} \text{ (Bard and Faulkner, 1980) } \dots\dots\dots 2.2$$

$$\eta = C \log i + D \text{ (Jones, 1996) } \dots\dots\dots 2.3$$

Equation 2.3 is known as the Tafel equation, where C and D are constants and  $i$  is the cell current in amperes.

More specifically for the anode process the equation becomes:

$$\eta_a = \beta_a \log i_a - \beta_a \log j_o$$

For the cathode process:

$$\eta_c = \beta_c \log i_c - \beta_c \log j_o$$

Where,  $\beta_a = \frac{2.303RT}{\alpha nF}$  and  $\beta_c = \frac{2.303RT}{(1-\alpha)nF}$



The constants  $\beta_a$  and  $\beta_c$  are called the anodic and cathodic Tafel constants in volts/decade, R is the gas constant in joules per Kelvin per mole, T is the temperature in Kelvin, F is Faraday's constant in coulombs per mole,  $\alpha$  is the charge transfer coefficient, n is the number of electrons participating in the reaction,  $j_o$  is the exchange current density in amperes per square meter while  $i_a$  and  $i_c$  are the anodic and cathodic currents in amperes respectively .

2.1.3.1 Butler-Volmer equation

The potential of a cell in which two kinetically controlled reactions are occurring can be related to the current by the Butler-Volmer equation given as:

$$i = i_{corr} \left( 10^{\frac{(E-E_{OC})}{\beta_A}} - 10^{-\frac{(E-E_{OC})}{\beta_C}} \right) \dots\dots\dots 2.4$$

Where,

$i$  is the measured cell current in amperes,

$i_{corr}$  is the corrosion current in amperes,

$E_{oc}$  is the open circuit potential in volts,

$\beta_A$  is the anodic Tafel constant in volts/decade,

$\beta_C$  is the cathodic Tafel constant in volts/decade.

But *Overpotential* =  $E_{a/c} - E_{oc} = \eta_{a/c}$  where  $a$  and  $c$  are anodic and cathodic coefficients. Therefore, equation 2.4 becomes:

$$i = i_{corr} \left( 10^{\frac{(\eta_a)}{\beta_A}} - 10^{-\frac{(\eta_c)}{\beta_C}} \right) \dots\dots\dots 2.5$$

Rearranging equation 2.5 and differentiation gives an expression for the polarisation resistance,  $R_p$  (Stern and Geary, 1957):

$$R_p = \left[ \frac{\Delta E}{\Delta i_{app}} \right]_{\eta \rightarrow 0}$$

$$R_p = \frac{\beta_A \beta_C}{2.3(i_{corr})(\beta_A + \beta_C)} \dots\dots\dots 2.6$$

Where  $\beta_A$  and  $\beta_C$  are the Tafel constants of the anodic and cathodic reactions respectively.

The term  $\frac{\Delta E}{\Delta i_{app}}$  is given in ohms (volts/amperes or millivolts/milliamperes).

#### 2.1.4 Measurement of cell voltages

The magnitude of the equilibrium cell voltage is calculated from (Pletcher, 1991):

$$\Delta G = -nFE_{CELL}^e \dots\dots\dots 2.7$$

Where,

$E_{CELL}^e$  is equilibrium cell voltage.

$\Delta G$  is the standard Gibbs free energy change in Joules.

$F$  is Faraday's constant (96 500 Coulombs).

$n$  is number of electrons participating in the reaction.

For a reaction to proceed spontaneously;  $\Delta G$  is by convention negative and  $E_{CELL}^e$  positive (Scully, 1975). The equilibrium cell voltage can also be calculated from:

$$E_{CELL}^e = E_C^e - E_A^e \dots\dots\dots 2.8$$

Where  $E_C^e$  and  $E_A^e$  are the equilibrium cathode and anode potentials respectively.

### 2.1.5 Pourbaix stability diagrams

Pourbaix diagrams show the reactions and products that will be present when equilibrium is attained, assuming that all appropriate reactions have been included. More importantly, these diagrams show conditions in which corrosion is thermodynamically impossible (stability regions). Consequently, potential and/or pH can be adjusted in some cases to prevent corrosion (Jones, 1996). Figures 2.1-2.6 are Pourbaix diagrams for lead, titanium, tantalum and iridium which are the materials of concern in this study.

#### a. Stability of Lead

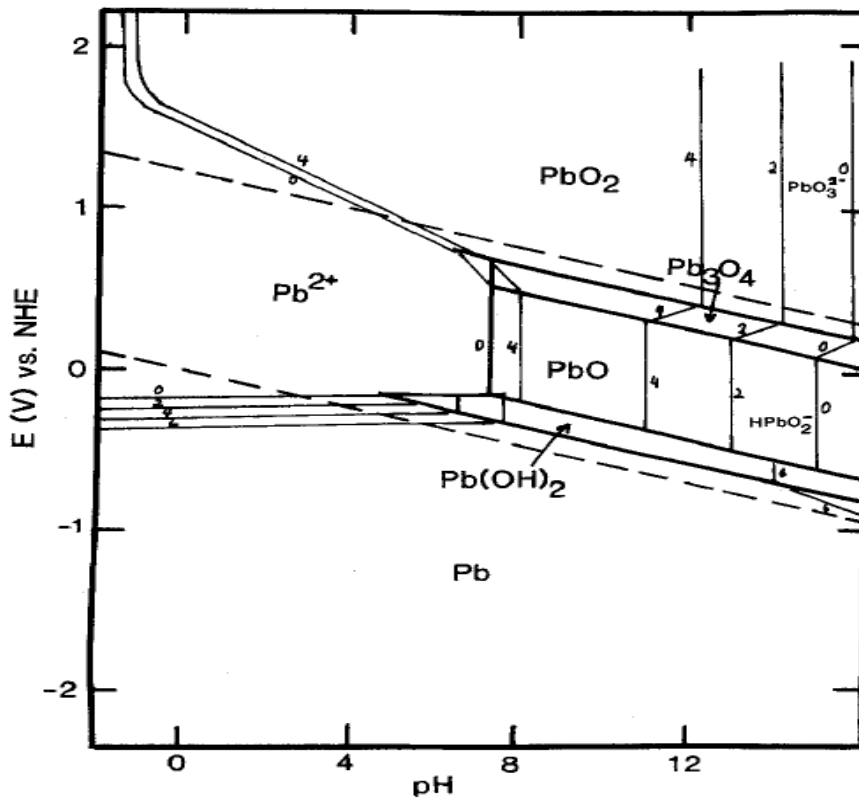


**Figure 2.1: Potential-pH Diagram for the System Lead-Water, at 25 °C.**

Adopted from Pourbaix, M. (1974) "Atlas of Electrochemical Equilibria in Aqueous Solutions" Pergamon Press, New York, USA.

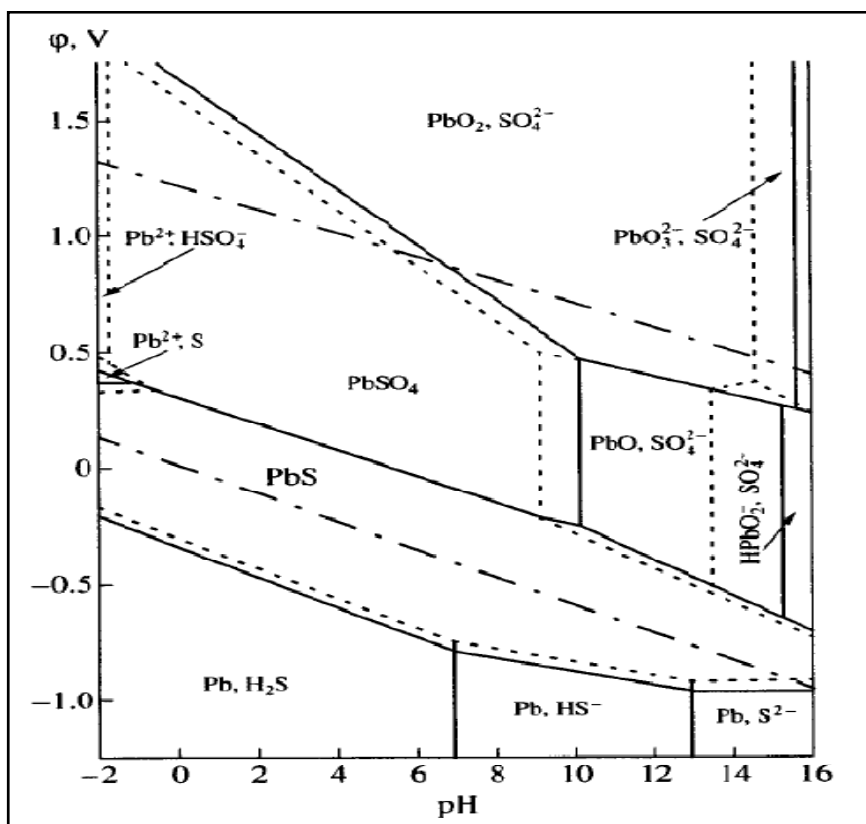


Figure 2.2: Potential-pH diagram for the System Lead-Sulphur-Water, at 25 °C.

In the presence of neutral and alkaline solutions free from oxidising agents, metallic lead is generally thermodynamically stable. However, under the influence of oxidising action, lead ions may be converted into brown quadrivalent lead peroxide (PbO<sub>2</sub>). Although lead peroxide is stable in alkaline solutions which are free from reducing agents, it is thermodynamically unstable at atmospheric pressure in acidic solutions, where it is reduced to plumbous ions (Pb<sup>++</sup>). Plumbous oxide (PbO) is amphoteric and as such, it dissolves in acid, neutral and alkaline solutions (Pourbaix, 1974). During electrowinning, the lead ions in solution react with sulphuric acid in the electrolyte to form lead sulphate which may migrate to the cathode and result in contamination of the copper deposit. Lead sulphate is stable in the presence of water and aqueous solutions of all pHs and both in the presence and in the absence of oxidising agents (Pourbaix, 1974).

## b. Stability of Titanium

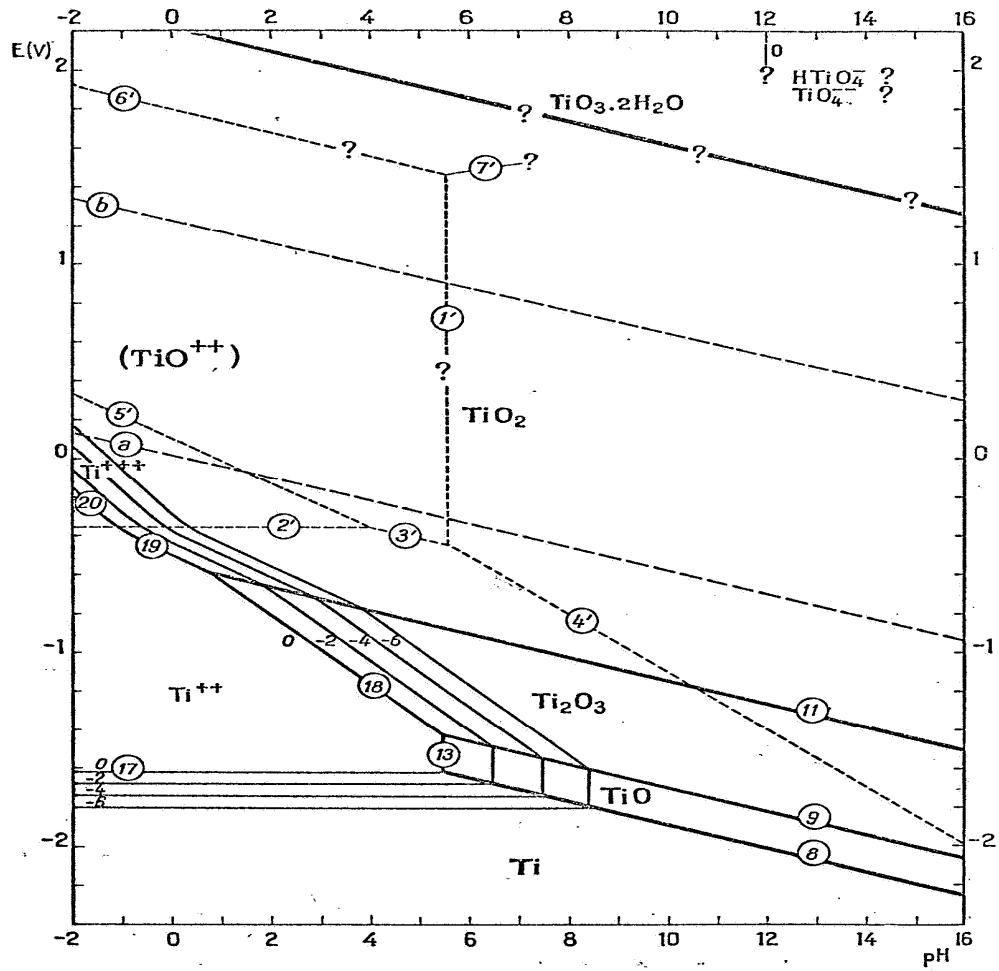
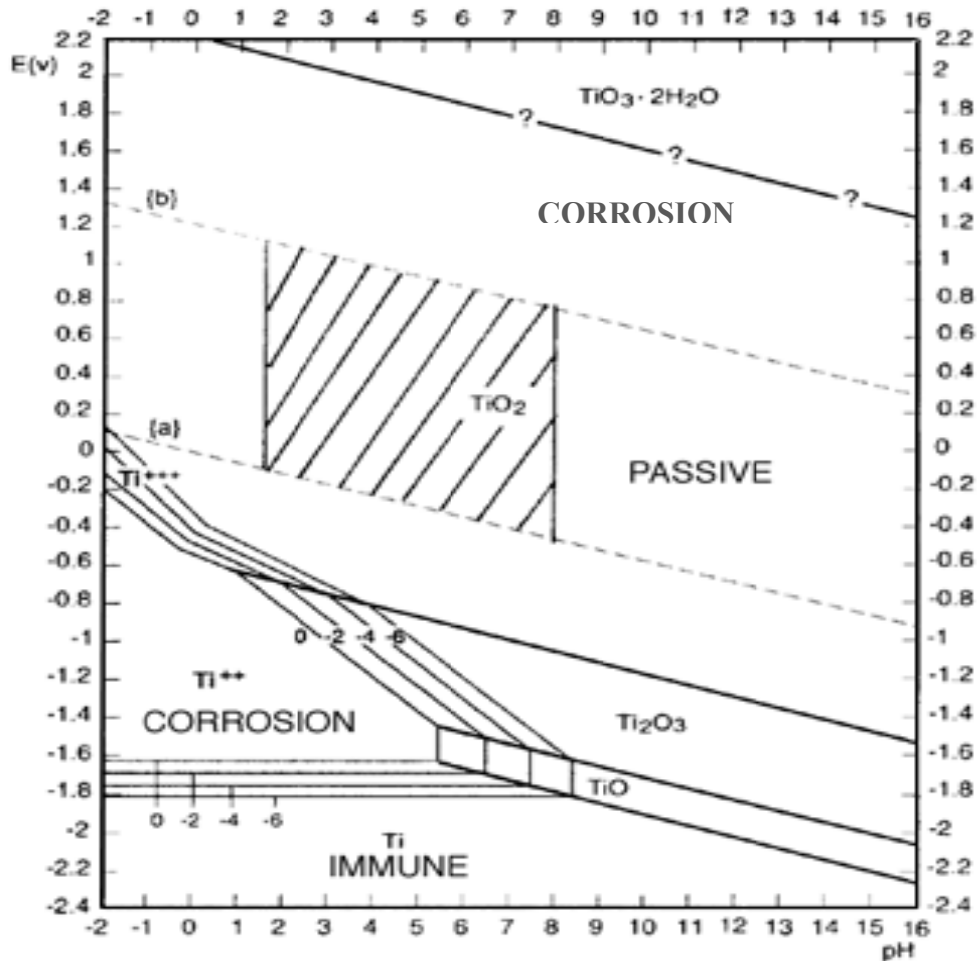


Figure 2.3: Potential-pH Equilibrium Diagram for the System Titanium-Water, at 25 °C. [Figure established by considering, as derivatives of tri- and tetravalent titanium, the anhydrous oxides  $\text{Ti}_2\text{O}_3$  and  $\text{TiO}_2$  (rutile).]

Adopted from Pourbaix, M. (1974) "Atlas of Electrochemical Equilibria in Aqueous Solutions" Pergamon Press, New York, USA.



**Figure 2.4: Theoretical Domains of Corrosion, Immunity and Passivation of Titanium, at 25 °C.**

[Deduced from figure 2.3, assuming passivation by the anhydrous oxide  $\text{TiO}_2$  (rutile).]

Adopted from Pourbaix, M. (1974) "Atlas of Electrochemical Equilibria," Pergamon Press, New York, USA.

Although titanium is not a noble metal, it is corrosion resistant because of a passivating film of rutile  $\text{TiO}_2$  that is formed on its surface. As cited by Pourbaix (1974), Gmelins stated that  $\text{TiO}_2$  is practically insoluble in acid. Titanium corrodes under reducing conditions and very powerful oxidising environments as these diminish the protective nature of the oxide film (Donachie, 2000). As indicated in the probable domain of corrosion in figure 2.4; titanium corrodes at high electrode potentials, if it is used as an electrolytic anode. However, Pourbaix (1974) reporting on the work of Preiser, stated that if titanium is partially coated with a noble metal

with low oxygen overpotential such as iridium, its electrode potential is lowered from the domain of corrosion situated on the upper part of figure 2.4 into the domain of passivation. This important feature enables titanium to be used in the manufacture of dimensionally stable anodes.

### c. Stability of Tantalum

The Pourbaix diagram for the tantalum-water system at 25 °C shows that the domain of immunity corresponds to the domain of stability of metallic tantalum (Ta) and the domain of passivation corresponds to the domain of stability of tantalum pentoxide (Ta<sub>2</sub>O<sub>5</sub>).

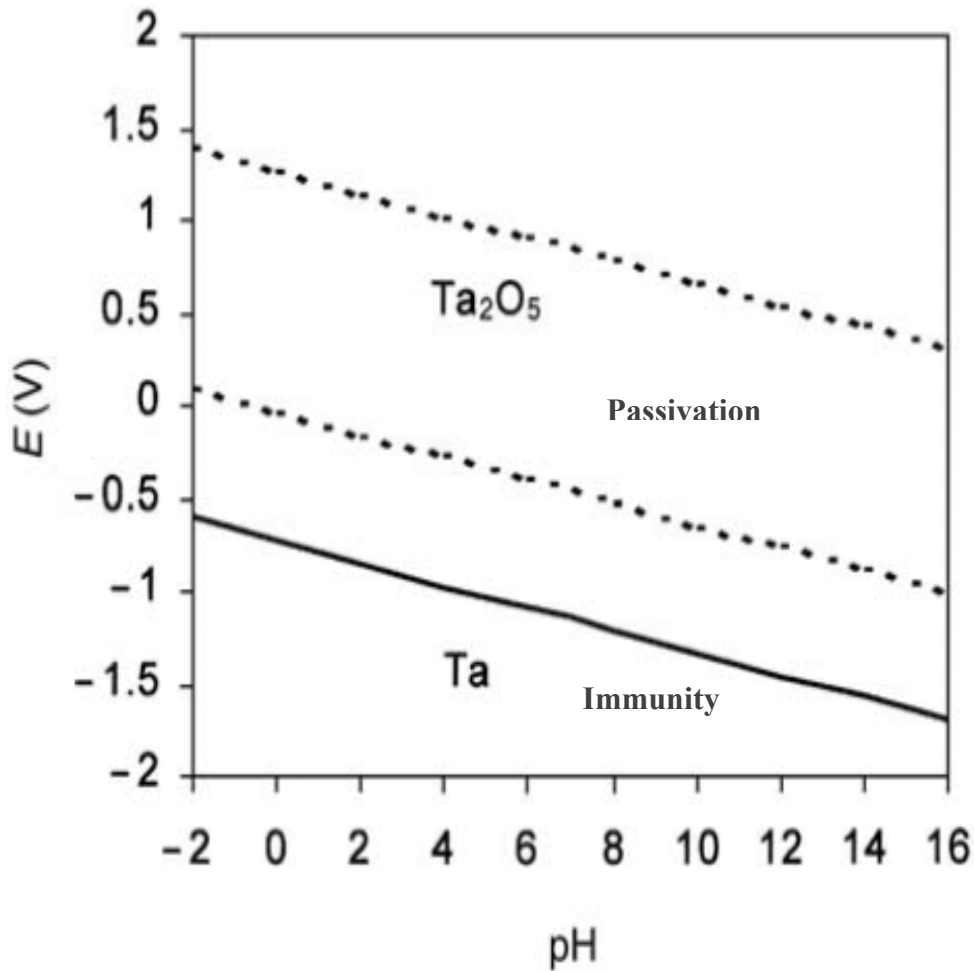


Figure 2.5: Potential-pH Equilibrium Diagram for the System Tantalum-Water, at 25 °C.

It is also unaffected by acids such as hydrochloric acid (HCl) and sulphuric acid (H<sub>2</sub>SO<sub>4</sub>) and their mixtures. This lead to the conclusion that tantalum pentoxide formed on the metal acts as a protective layer. The position of the domain of stability of tantalum pentoxide in figure 2.5 indicates that, Ta<sub>2</sub>O<sub>5</sub> is thermodynamically stable in the presence of water and acid. This is the reason why Ta<sub>2</sub>O<sub>5</sub> is used as a coating stabiliser in DSA anodes.

#### d. Stability of Iridium

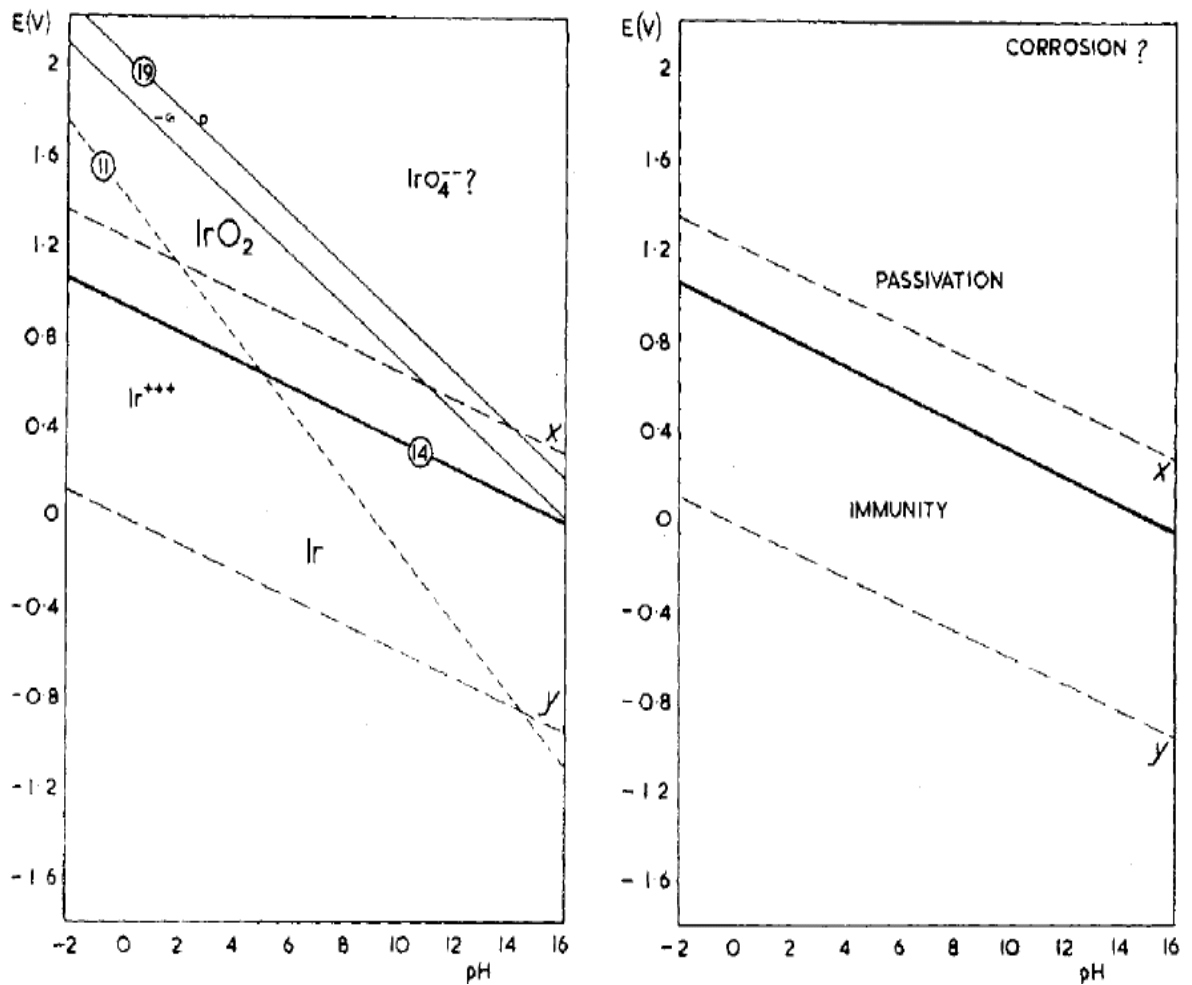
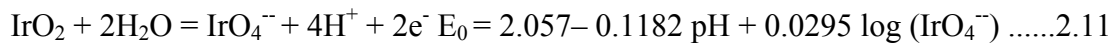
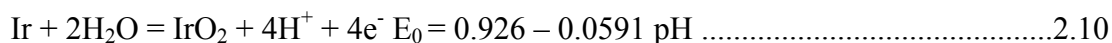


Figure 2.6: Potential-pH Diagrams for the Iridium-Water System at 25°C and Theoretical Conditions for the Corrosion, Immunity and Passivation of Iridium at 25°C Respectively.

(Pourbaix, 1974).



The numbers 11, 14 and 19 represent the following reactions respectively:



From figure 2.6, iridium appears to be noble since its domain of stability covers the majority of that of water. Iridium is stable in the presence of aqueous solutions of all pH's free from complexing substances. The oxide of tetravalent iridium, IrO<sub>2</sub>, is also insoluble in acid solutions. This is in line with practice. Furthermore, its position on the equilibrium diagram indicates that IrO<sub>2</sub> is the form of iridium which is stable in the presence of oxygen, hence its use as the active component in the coatings for DSAs.

## 2.2 Electrochemical and physical characterisation techniques

### 2.2.1 Electrochemical characterisation

Electrochemical characterisation techniques give information on processes occurring when an electric potential is applied to the system under study. Electrochemical methods such as open circuit potential tests, potentiodynamic polarisation, cyclic voltammetry and electrochemical impedance spectroscopy, can be applied in order to characterise different electrodes. All these techniques provide information on important parameters like corrosion rate, polarisation resistance, overvoltage and working area, thus making electrochemical methods versatile. Most electrochemical methods involve the use of three electrodes; namely the working electrode (WE), reference electrode (RE) and the counter electrode (CE) which is also called the secondary or auxiliary electrode. The three electrodes are connected to a

potentiostat /galvanostat, which is an instrument that can perform both controlled potential (potentiostatic) and controlled current (galvanostatic) experiments. The potential drop near the other current carrying electrode (the counter electrode) is not important when a three-electrode potentiostat is used.

### *2.2.1.1 Corrosion rate measurements*

Corrosion testing aims to achieve one or more of the following objectives (Sprowls, 1987):

- Screen available materials (alloys) to determine the best one for a specific application.
- Determine the probable service life of equipment or a product.
- Evaluate new commercial alloys.
- Study corrosion mechanisms.

Depending on the electrochemical system, the most suitable method may be applied with the aim of determining the corrosion behaviour of the material.

The reasons for the popularity of electrochemical techniques for corrosion measurement are:

#### **a) They are fast.**

While real-time weight loss measurements need days and sometimes weeks to make a reliable measurements of corrosion rate, electrochemical experiments will require at most several hours. The speed of electrochemical measurements is especially useful for those metals or alloys which are highly corrosion resistant.

#### **b) They are sensitive.**

Modern, electrochemical instrumentation can measure extremely low corrosion rates (less than 0.1 milli-inches per year) which are both tedious to perform with conventional weight-loss or chemical analytical techniques. Low current densities can also be precisely measured to values as low as  $10^{-9}$  A/cm<sup>2</sup>.

**c) They are accurate.**

Electrochemical techniques have been exhaustively tested before finding general acceptance.

In electrochemical reactions, electrons are either consumed or released. Thus, the rate of electron flow to or from a reacting interface is a measure of the reaction rate. The flow of electrons is measured as current,  $i$  in amperes where 1-ampere is equal to 1-coulomb of charge ( $6.2 \times 10^{18}$  electrons) per second. Faraday's law given below shows the proportionality between  $i$  and mass reacted in grams,  $m$ , in an electrochemical reaction (Jones, 1996):

$$m = \frac{Ita}{nF} \dots\dots\dots 2.12$$

Where  $F$  is the Faraday's constant (96 500 Coulombs/mole),  $n$  is the number of equivalent (electrons transferred) exchanged,  $a$  is the atomic weight in grams per mole, and  $t$  is the time in seconds.

Dividing equation (2.12) by  $t$  and the surface area in square metres,  $A$  yields the corrosion rate in grams per square metre per second,  $r$ :

$$r = \frac{m}{tA} = \frac{ja}{nF} \dots\dots\dots 2.13$$

Where  $j$  is the current density  $\left(\frac{i}{A}\right)$ .

Equation 2.13 shows the proportionality between mass loss per unit area per unit time and current density in which case the proportionality constant includes  $\frac{a}{nF}$  and any conversion factors for units. Since the same current concentrated into a smaller

surface area results in a larger corrosion rate, current density rather than current is proportional to corrosion rate whilst corrosion rate is inversely proportional to area for the same dissolving current. Dividing equation 2.13 by the density,  $\rho$ , of the alloy gives the units of penetration per unit time. For corrosion rate in milli-inches per year (mpy), equation 2.13 becomes:

$$r = 0.129 \frac{aj}{n\rho} \text{ (in mpy)} \dots\dots\dots 2.14$$

For units of  $j$ ,  $\mu A/cm^2$  and  $\rho$ ,  $g/cm^3$ . The proportionality constant, 0.129 changes to 0.00327 and 3.27 for mm/yr and  $\mu M/yr$ .

Calculation of the corrosion rate requires the determination of the equivalent weight (E.W.),  $a/n$  for the alloy. The alloy equivalent weight is a weighted average of  $a/n$  for the major alloying elements in the alloy (Jones, 1996).

Dean (1987) proposed a procedure for calculating the equivalent weight of an alloy. He recommended that the fractional number of equivalents of all alloying elements should be summed up in order to determine the total number of equivalents,  $N_{EQ}$ , which result from dissolving unit mass of the alloy. This is given below as:

$$N_{EQ} = \sum \left( \frac{f_i}{a_i/n} \right) = \sum \left( \frac{f_i n_i}{a_i} \right) \dots\dots\dots 2.15$$

Where  $f_i$ ,  $n_i$  and  $a_i$  are mass fraction, electrons exchanged, and atomic weight, respectively, of the  $i$ th alloying element. Equivalent weight is then the reciprocal of  $N_{EQ}$ :

$$E.W. = N_{EQ}^{-1} \dots\dots\dots 2.16$$

Although, the measurement of open circuit potential ( $E_{oc}$ ) is the first step in most electrochemical corrosion experiments, the two main electrochemical polarisation techniques available for the measurement of corrosion rate are Tafel extrapolation and polarisation resistance.

2.2.1.1.1 Tafel extrapolation

Tafel plots are used to measure corrosion rates of metal specimens in solution by polarising the specimen about 300mV anodically (positive-going potential) and cathodically (negative-going potential) from the corrosion potential,  $E_{corr}$ . The resulting current is plotted on the logarithmic scale as shown in 2.7.

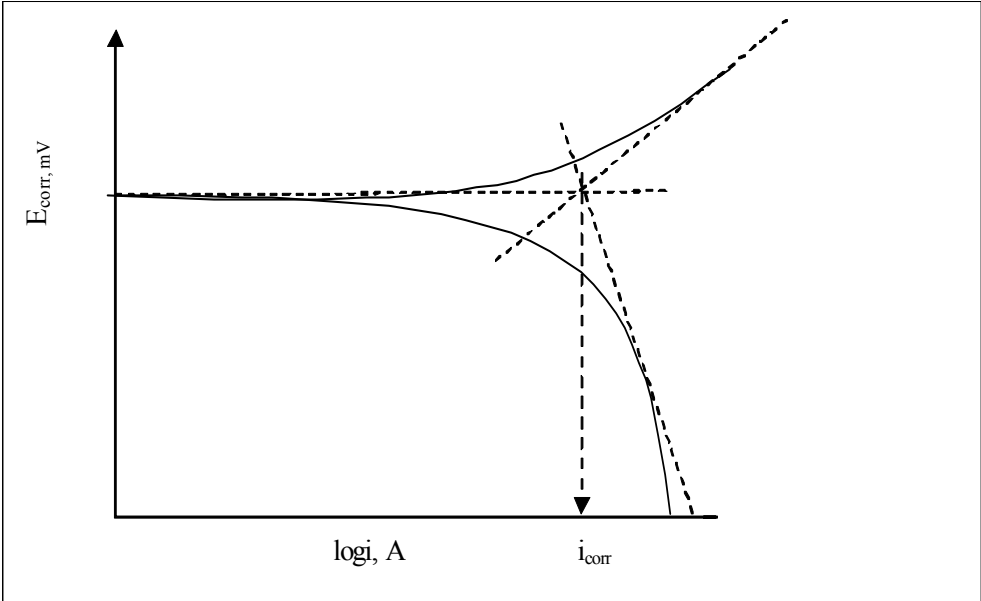


Figure 2.7: Cathodic and Anodic Tafel Plot

Tafel plots yield values of the corrosion current,  $i_{corr}$  by extrapolating the linear portion of the curve to  $E_{corr}$ . The corrosion rate can then be calculated from  $i_{corr}$  by using equation 2.17:

$$Corrosion\ Rate = \frac{0.129i_{corr}(E.W.)}{A.\rho} \dots\dots\dots 2.17$$

where A, is the surface area of specimen.

#### 2.2.1.1.2 Polarisation resistance method

A potential is applied to the specimen, +/-20 mV about  $E_{corr}$  (open circuit potential) and plots of applied potential versus measured current are made at a typical scan rate of 0.1 mV/sec. An apparent linearity is observed at the origin of the polarisation curve for overvoltages up to a few millivolts. The slope of the curve gives the polarisation resistance,  $R_p$  (equation 2.6). Not only does the value of  $R_p$  measure the corrodibility of a specimen after a potential has been applied, it is also used in the determination of the corrosion current,  $I_{corr}$  for use in the determination of corrosion rate (equation 2.17) if the Tafel constants are known. However, if  $\beta_A$  and  $\beta_C$  are unknown, the corrosion rate can still be estimated within a factor of 2 since  $\beta_A\beta_C/\beta_A + \beta_C$  varies little in magnitude. From equation 2.6, it is evident that the degree of polarisation of a specimen at a given applied current is greater for a lower corrosion rate. Overall, the slope of this linear curve is inversely proportional to the corrosion rate (Scully, 1975).

#### 2.2.1.2 Cyclic voltammetry

In a cyclic voltammetry experiment, as in other controlled potential experiments, a potential is applied to the system, and the faradaic current (current due to a redox reaction) is measured over a range of potentials often referred to as a potential window. The potential is varied in a linear manner starting at an initial value up to a pre-defined limiting value. At this potential, (switching potential) the direction of the potential scan is reversed, and the same potential window is scanned in the opposite direction, hence the term cyclic. This means that, for example, species formed by oxidation on the first (forward) scan can be reduced on the second (reverse) scan (Bard and Faulkner, 2001). Figure 2.8 below shows a typical cyclic voltammogram.

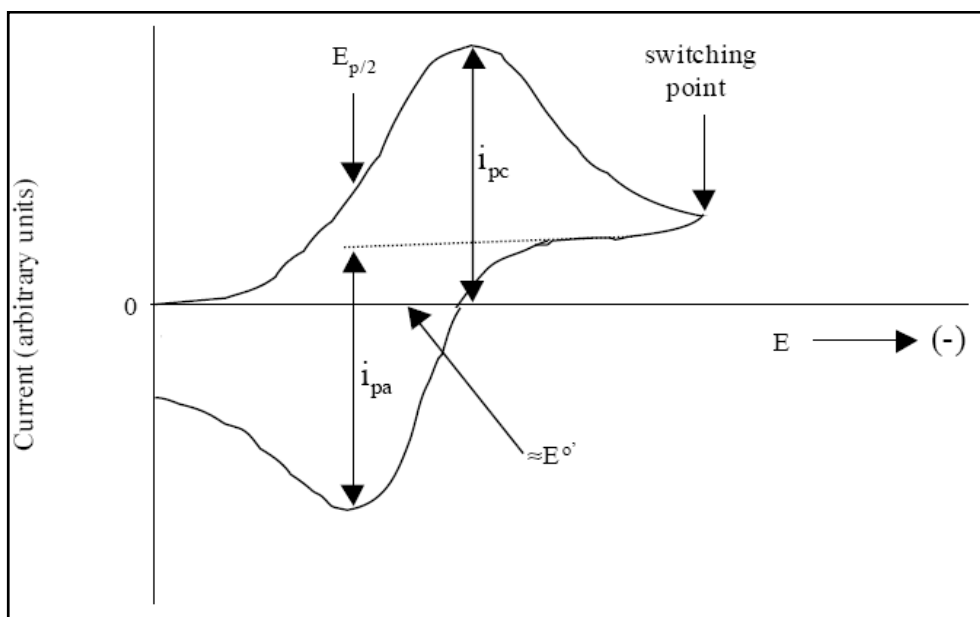


**Figure 2.8: Cyclic Voltammogram**

The anodic peak current,  $i_{pa}$ , and cathodic peak current,  $i_{pc}$ , are equal in magnitude when the transport of the reduced and oxidised species in the solution is controlled only by diffusion to a planar electrode surface immersed in an unstirred solution. Furthermore, the electrode potential  $E_{0.85}$  found at 85% up the CV wave to  $i_{pa}$  (or  $E_{pa}$ ), is equal to the reversible potential,  $E_0$  (Gosser, 1993).

Cyclic voltammetry (CV) is thus a potentiodynamic electrochemical measurement which is used to monitor the surface properties of metal specimens. Not only is it a fast and reliable characterisation tool, it also provides both qualitative and quantitative information. The method uses a reference electrode, working electrode, and counter electrode. The range of potential is determined by a combination of the solvent, electrolyte and specific working electrode material.

#### 2.2.1.2.1 Qualitative analysis

a) Passivation tendencies of electrode materials can be detected from cyclic voltammograms on performing repetitive scans (Cheng and Hiskey, 1996).

b) Since the area under a voltammogram represents electrical charge on a metal specimen and electrical charge is proportional to the electrode area, the working area (active surface area) of different materials can be compared (Ortiz *et al.*, 2004). In electrode processes, a larger working area results in an increase in the number of active sites which in turn leads to an increase in reaction rate or rate of electron transfer (Pletcher, 1991).

#### 2.2.1.2.2 Quantitative analysis

a) Voltamperometric (anodic) charges can also be used to determine the anode with the largest electrochemically active surface area (Hu *et al.*, 1996).

b) The potential for oxygen evolution can be determined from a voltammogram in electrode processes involving the oxygen evolution reaction (OER) thus enabling conclusions on the most energy efficient working electrode (anode) to be drawn.

c) Evaluation of remaining activity can be carried out by calculating the anodic (voltamperometric) charges before and after chronopotentiometry tests (Ortiz *et al.*, 2004).

#### 2.2.1.3 Chronoamperometry

Chronoamperometry is an electrochemical technique in which the potential of the working electrode is stepped, and the resulting current from faradic processes occurring at the electrode (caused by the potential step) is monitored as a function of time. Chronoamperometry techniques are used to assess the activity of anode materials since the potential is changed instantaneously. As with all pulsed techniques, chronoamperometry generates high charging currents, which in this case, decay exponentially with time. A three electrode system is commonly used. The potential steps used in chronoamperometry are selected from Tafel plots in the passivation region.



#### 2.2.1.4 Galvanostatic chronopotentiometry

In galvanostatic chronopotentiometry, a constant current is applied between the auxiliary and working electrodes and the working electrode potential is recorded with time with respect to the reference electrode. Galvanostatic chronopotentiometry can also be referred to as constant current electrolysis. A three electrode arrangement is used. From this test, the anode potential that characterises a specific anode material can be deduced.

#### 2.2.1.5 Electrochemical impedance spectroscopy

Electrochemical Impedance Spectroscopy (EIS) is a powerful technique for the characterisation of electrochemical systems. It has found widespread applications in the characterisation of coatings and corrosion phenomena. EIS has also been used extensively as a tool for investigating mechanisms in electrodeposition, electrodisolution and passivity. An important advantage of EIS over other laboratory techniques is the possibility of using very small amplitude signals without significantly disturbing the properties being measured. To make an EIS measurement, a small amplitude signal, usually a voltage between 5 to 50 mV is applied to a specimen over a range of frequencies of 0.001 Hz to 100,000 Hz. The resistance and capacitance of the impedance response of the system are recorded by the EIS instrument (potentiostat). In the characterisation of coatings, when the EIS data has been fit into a frequency response, a set of parameters which can be correlated with the coating condition can be obtained. High impedance values obtained from medium to low frequencies suggest high corrosion resistance of specimen in a given electrolyte.

EIS retains all the advantages of direct-current methods because it is sensitive, can be conducted in situ, and often does not require artificial accelerating factors such as temperature and concentration for testing (de Assisa *et al.*, 2006).

### 2.2.2 Physical characterisation techniques

Physical characterisation techniques are divided on the basis of the interrogating radiation. Some techniques utilise X-ray techniques, optical or electron microscopy. These techniques enable composition and surface morphology of specimens to be studied (Flewitt and Wild, 2003).

## 2.3 **Electrowinning of copper**

Electrowinning involves:

- (a) immersing metal cathodes and inert, conductive anodes in an aqueous solution of copper sulphate containing free sulphuric acid ( $\text{CuSO}_4\text{-H}_2\text{SO}_4\text{-H}_2\text{O}$  electrolyte),
- (b) applying an electrical potential between the anodes and cathodes,
- (c) plating pure metallic copper from the electrolyte onto the cathodes.

Cathodes may be stainless steel blanks or copper 'starter sheets'. Copper is electrodeposited on the cathodes for about one week, after which harvesting is done while water dissociates into hydrogen ions and oxygen at the anode (Biswas *et al.*, 2002).

### 2.3.1 Important parameters in electrowinning

In electrowinning processes, efficient operation can be achieved by manipulating temperature and current density. Temperatures of between 30 °C and 60 °C are considered suitable for the electrowinning of copper. Electrolysis can also be carried out at low or high current densities. When operating at low current densities (up to 430 A/m<sup>2</sup>), a cooling coil made of lead or aluminium can be placed in the cell in order to control the temperature. Higher current densities (861 to 1076 A/m<sup>2</sup>), are only used if the copper concentration, acid concentration, purity of the electrolyte and circulation rate are high.

In such a case, Gupta and Mukherjee (1990) stated that the value of copper concentration should be greater than 170 g/l copper while the acid concentration is around 200 g/l H<sub>2</sub>SO<sub>4</sub> and external cooling is also employed. They also mentioned that for each current density applied; a narrow range of acidity exists at which copper deposition is efficient. Although most plants operate at low current densities and low acidities, operating at high current density improves throughput and energy efficiency for the copper cells. Limiting current density is also taken into consideration during electrowinning. This is defined as the maximum current density beyond which cell voltage must be increased significantly for a small increase in current density and is a function of the mass transfer coefficient of the electrode and the concentration of copper ions in solution. The metal deposited at or above the limiting current density is rough, less dense, and less pure and consequently has a low market grade. According to Gupta and Mukherjee (1990), in a conventional electrowinning cell, high quality metal is produced at a current density of about 200 A/m<sup>2</sup> which may be an indication that it is slightly below the limiting current density.

### 2.3.2 Electrowinning reactions

During copper electrowinning, the following reactions occur at the electrodes:

**Cathode:**



---


$$\Delta G_{298}^0 = -64,410 \text{ J} ; E_e^0 = +0.334 \text{ V}$$

Copper ions (Cu<sup>2+</sup>) are preferentially discharged because the hydrogen cations also present in the solution are more electropositive than the Cu<sup>2+</sup> ions.

**Anode:**



---

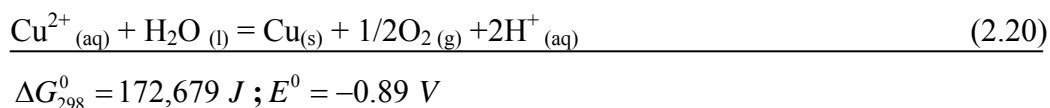

$$\Delta G_{298}^0 = 237,089 \text{ J} ; E_e^0 = -1.229 \text{ V}$$

Although hydroxyl ions are also oxidised at the anode, they produce negligible anodic current since their concentration in the acidic solution is low. Preferential decomposition of water also occurs at the anode, over the oxidation of sulphate anions because the electrode potential for their oxidation is much greater than that for decomposition of water (-1.229 V). Equation 2.19 above is known as the oxygen evolution reaction (OER). Thus, an oxygen evolution reaction is an electrode reaction in which oxygen gas is produced at the anode of an electrolytic cell by the oxidation of hydroxyl (OH-) ions or the oxidation of the water molecules of an aqueous solution.

### 2.3.2.1 Oxygen evolution

Oxygen evolution is one of the most important technological reactions in electrochemistry taking place in many industrial processes namely water electrolysis, metal electrowinning, cathodic protection and electro-organic synthesis (Fierro *et al.*, 2007). This reaction has a large bearing on the economics of the process as it operates at a high overpotential. Furthermore, this reaction enhances the harsh corrosive environment for the electrode material in acidic media.

Thus the overall cell reaction in copper electrowinning involves the reduction of copper ions to copper and the oxidation of water to oxygen and hydrogen ions as indicated by the reaction below:



The value -0.89 V is a measure of the electromotive force (e.m.f) which would have to be opposed to prevent the reverse reaction from taking place. Therefore, from the overall reaction above, if a potential of 0.89 V is applied across the electrodes, there is no net reaction since the cell will be in equilibrium (Gilchrist, 1989). However, for copper deposition to occur from the solution to the cathode a larger potential is

necessary since the potential difference applied to the cell consists of several components as shown below (Trasatti, 2000):

$$\Delta V = \Delta E + \Delta \eta + \Delta V_{\Omega} + \Delta V_t \dots\dots\dots 2.21$$

Where,

$\Delta V$  is potential difference in volts.

$\Delta E$  is the thermodynamic (equilibrium) potential difference for the given electrode reactions in volts.

$\Delta \eta$  is the sum of the anodic and cathodic overpotentials in volts.

$\Delta V_{\Omega}$  is ohmic drop (IR) in the inter-electrode gap, in the electrodes and the connections in volts.

$\Delta V_t$  = Drift of  $\Delta V$  with time due to degradation of the electrode performance (stability) in volts.

The overpotential,  $\eta$  is applied to each electrode in order to enhance the rate of electron transfer processes and also to supply a potential while  $IR_{SOLN}$  (voltage drop in the solution) is used to drive the current through the electrolyte. Therefore, the energy requirement is approximately 2 000 kWh/tonne of copper produced while the electrical potential needed for electrowinning is about 2 V. It is made up of:

**Table 2.2: Components of Cell Voltage in Copper Electrowinning**

|   |                  |
|---|------------------|
| Theoretical voltage for reaction 2.11                                       | $\approx 0.9 V$  |
| Oxygen deposition overvoltage   | $\approx 0.5 V$  |
| Copper deposition overvoltage   | $\approx 0.05 V$ |
| Electrical resistance at cathode current density<br>(300 A/m <sup>2</sup> ) | $\approx 0.5 V$  |

Adopted from Biswas *et al.*, (2002) "Extractive Metallurgy of Copper", 4<sup>th</sup> edition, Pergamon.

Gupta and Mukherjee (1990) gave the power requirement in conventional electrowinning cells as 0.16 to 2.5 kWh/kg copper.

### 2.3.3 Electrowinning products

The electrowinning products are:

- (a) copper metal at the cathode (less than 20 ppm undesirable impurities) (Biswas *et al.*, 2002)
- (b) oxygen gas at the anode
- (c) regenerated sulphuric acid in the solution

The copper is manually or machine-stripped from the stainless steel cathode blanks, washed and sent to the market or the entire copper 'starter sheet' is washed and sent to the market. The oxygen enters the atmosphere while the acid is recirculated to the leaching circuit.

### 2.3.4 Suppression of acid mist

"Acid mist" is used to describe the oxygen bubbles that form on the anode and burst at the electrolyte interface, giving rise to sulphuric acid mist. In electrowinning plants, hollow polyethylene balls (approximately 2 cm in diameter) are usually floated, 5 to 10 cm deep, on the electrolyte together with fluorocarbon surfactant. Polypropylene BB's, usually 0.3 cm in diameter and 0.15 cm long are also commonly used. Mechanical mist suppressant systems that include polymer brushes around the anode tops, are also used while in some plants large blowers are used in order to minimise generation of acid mist (Pfalzgraff, 1999).

### 2.3.5 Current density

Copper plating rate increases with increasing current density. However, excessive current density gives rough, nodular cathode deposits and decreased copper purity. Therefore, each plant chooses its current density as a balance between these opposing factors.

### 2.3.6 Electrolyte concentration

Electrowinning electrolyte typically contains 44 kg  $\text{Cu}^{2+}$  and 170 kg  $\text{H}_2\text{SO}_4$  per  $\text{m}^3$  as it enters an electrowinning cell. It contains about 5 kg  $\text{Cu}^{2+}$  less per  $\text{m}^3$  as it leaves the cell.

### 2.3.7 Additives

All electrowinning plants dissolve guar gum in their electrolytes (about 250 g/t of cathode copper) or glue. As cited by Biswas *et al.* (2002), Stanke reported that these additives promote dense, level copper deposits with minimum impurity entrainment. Cobalt sulphate ( $\text{CoSO}_4$ ) solution is also added to provide about 150 ppm cobalt ions ( $\text{Co}^{2+}$ ) in the electrowinning electrolyte. Biswas *et al.* (2002) reporting the work of Prengaman and Siegmund mentioned that  $\text{Co}^{2+}$  promotes oxygen ( $\text{O}_2$ ) evolution at the anode rather than lead (Pb) oxidation.

### 2.3.8 Maximising copper purity

The three main impurities in electrowon copper are:

- (a) Lead (1 or 2 ppm) from anode corrosion product entrapment
- (b) Sulphur (4 or 5 ppm) from lead sulphate anode corrosion product and electrolyte entrapment and
- (c) Iron (1 or 2 ppm) from electrolyte entrapment.

According to Maki (1999), cathode purity may be maximised by:

- (a) straight vertical equispaced cathodes and anodes with no anode-cathode contact
- (b) immediate thorough washing of the deposited copper
- (c) frequent removal of anode corrosion products from the bottom of the electrowinning cells
- (d) Iron in electrolyte below  $2 \text{ kg/m}^3$  to minimise iron in cathode copper.

### 2.3.9 Maximising current efficiency

Current efficiencies in modern electrowinning plants may be around 90 %. The unused current is wasted by:

- (a) anode/cathode short circuits
- (b) stray current to the ground
- (c) reduction of  $\text{Fe}^{3+}$  to  $\text{Fe}^{2+}$  at the cathode and re-oxidation of  $\text{Fe}^{2+}$  to  $\text{Fe}^{3+}$  at the anode (Das and Gopala, 1996; Biswas *et al.*, 2002).

High current efficiency is important because it maximises copper plating rate and minimises electrical energy consumption (Biswas *et al.*, 2002).

Some results of the effect of iron on the current efficiency at a total current density of  $280 \text{ A/m}^2$  are shown below.

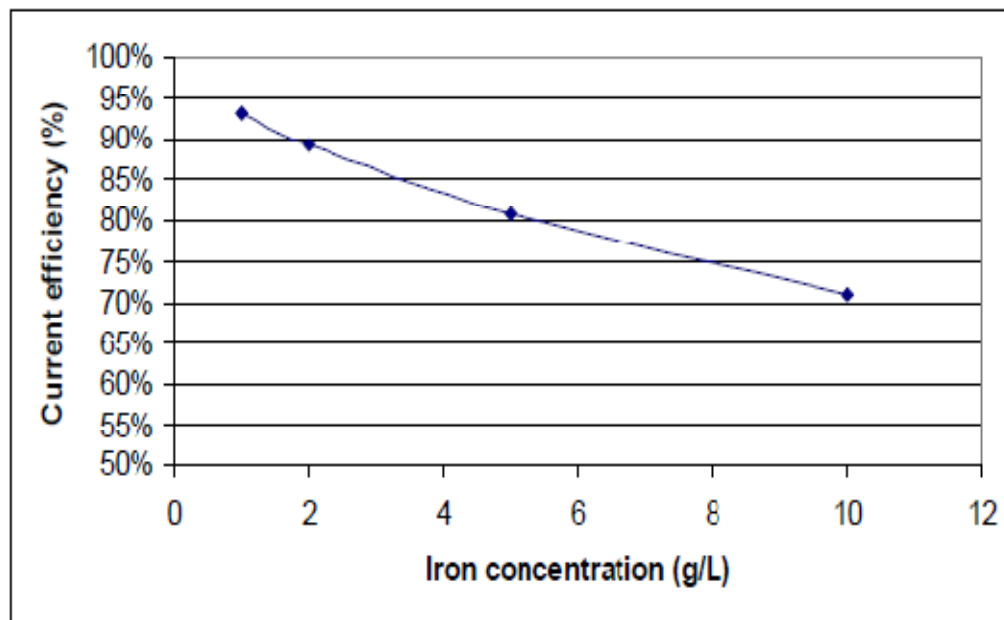


**Figure 2.9: Effect of Iron in the Electrolyte on Current Efficiency.**

Adapted from “Electrowinning and Electrorefining of Metals: A Course Presented to Anglo Research by Nicol, M.J. (2006).



2.3.10 Amount of copper deposited

According to Faraday's law (equation 2.12), which gives the theoretical amount of metal deposited, a gram equivalent of copper is deposited if 96 500 Coulombs (26.8 Ah) of electricity is passed.

However, in practice, the actual amount of electricity required is greater than the theoretical amount due to current loss which results from (Gupta and Mukherjee, 1990):

- ✓ Inadequate circulation of the electrolyte
- ✓ Poor connections
- ✓ Circuit leakages
- ✓ Short circuitry of the electrode caused by the dendritic growth of the copper during deposition.

The ratio between the theoretical and actual amount of electricity used is known as the current efficiency. Current efficiency can be calculated from the weight gained by the cathode as shown below:

$$\varepsilon_c(I) = \frac{nF\Delta W}{ItM} \dots\dots\dots 2.22$$

Where,

$\varepsilon_c$  is Cathode current efficiency.

$\Delta W$  is weight gain.

$F$  is Faraday's constant.

$I$  is applied current.

$M$  is atomic weight of copper.

$t$  is time taken for the copper to be deposited.

$n$  is the number of electrons participating in the reaction (2 electrons).

Another important parameter, which describes the performance of a cell, is the energy consumption which was given by Pletcher (1991) as:

$$\text{Energy Consumption} = \frac{-nFE_{cell}10^{-3}}{3.6\varepsilon_c M} \dots\dots\dots 2.23 (a)$$

Where, n – number of electrons, M – molecular weight,  $E_{cell}$  – cell voltage,  $\varepsilon_c$  - current efficiency and F- Faraday’s constant.

The energy efficiency of a cell can then be calculated from equation 2.23 (b) below:

$$\text{Energy efficiency (\%)} = \frac{\text{reversible decomposition voltage}}{\text{applied voltage}} * \text{current efficiency (\%)} \quad 2.23 (b)$$

### **3 LITERATURE REVIEW**

#### **3.1 Lead alloy anodes used in electrowinning**

Biswas *et al.* (2002) citing the work of Prengaman and Siegmund mentioned that electrowinning anodes are almost always cold rolled lead-tin-calcium (Pb-Sn-Ca) alloys containing about 98.4% lead (oxygen scavenged prior to alloying), 1.5% tin and 0.1% calcium. Tin provides corrosion resistance and corrosion layer conductivity while calcium and cold rolling add strength. These authors also stated that, the Pb-Sn-Ca blades are soldered onto slotted copper hanger bars for support in the electrolytic cells. Lead is then electrodeposited around the joints to protect them from corrosion. The Pb-Sn-Ca alloy forms an adherent corrosion layer which minimises lead contamination of the cathode copper and extends anode life. Other lead alloy anodes also used in electrowinning contain silver or antimony additions (Yu and O'Keefe, 2002).

#### **3.2 DSA applications in electrochemistry**

Dimensionally stable anodes (DSAs) are used in a number of important industrial applications (Martelli *et al.*, 1994) and have found a wide application in chlorine gas production for example, chlor-alkali and sodium chlorate production, since their introduction in the late 1960s. These anodes proved to override the shortcomings of the previously used magnetite and graphite electrodes which had high overvoltage and had a tendency to degrade during the process. The life of DSA electrodes in chlorine evolution is claimed to be up to 10 years (Herlitz, 2004). Recently, there has been a marked increase in the use of DSA anodes in the field of oxygen evolution processes (Martelli *et al.*, 1994). DSA electrodes have also found application in oxygen reduction (Yoshio *et al.*, 2008), organic oxidation (fuel cells and air batteries) and molten salt electrolysis (Uchida *et al.*, 1981).

### 3.2.1 Manufacture of DSA anodes

Different methods can be used to manufacture DSA anodes. However, the performance of these anodes is critically dependent on their composition and the procedure of preparation (solvent of the painting solution, firing temperature). The morphology and structure of the coating were found to be essential factors influencing the properties and performances of the Ti/IrO<sub>2</sub>-Ta<sub>2</sub>O<sub>5</sub> electrode (Vercesi *et al.*, 1991). Kulandaisamy *et al.* (1997) also mentioned that an increase in resistivity of the surface coating for DSA anodes increased the anode potential; the resistivity being a function of the method of preparation of the oxide coating on the anode. Martelli *et al.* (1994) reported that even DSA anodes with the same chemical composition would show different electrocatalytic activities when their microstructures are different.

The first operation for the preparation of dimensionally stable electrodes based on titanium sheets is the pretreatment of titanium (Krysa *et al.*, 1996). The valve metal substrate (titanium) is degreased in acetone and then etched in boiling oxalic acid solution or hydrochloric acid. To achieve good adhesion of the coating, the surface of the base metal must be pretreated to an appropriate degree of roughness. The active oxides are subsequently applied as a solution of precursor salts using a roller or brush until the required coating loading has been reached (Martelli *et al.*, 1994). Coating loading depends on the conditions and type of solution in which the anodes will be used. As thermal decomposition of precursor salts occurs during the drying stage, the metallic oxides are produced. One of the oxides will be the catalyst and conducting component while the other oxide is the stabiliser and dispersant of the catalyst.

The conventional thermal deposition method of film preparation involves the use of H<sub>2</sub>IrCl<sub>6</sub>·6H<sub>2</sub>O and TaCl<sub>5</sub> precursors dissolved in hydrochloric acid and alcohol, respectively. However, Angelinetta *et al.* (1989) and Spinolo *et al.* (1997) reported that oxide anodes prepared from organic solvent systems display better performance.

It was also shown that IrO<sub>2</sub>-Ta<sub>2</sub>O<sub>5</sub> coatings prepared at low temperature display a low stability due to incomplete thermal decomposition resulting in the dissolution of the coating during electrolysis (Hu *et al.*, 2002). However, at higher temperatures (>500 °C), partial oxidation of the base metal leads to low adhesion of the film to the support. Therefore, an in situ study of the thermolysis processes is indispensable in order to improve the design of thermally prepared electrode coatings.

Morimitsu *et al.* as cited by Moats (2008) stated that decreasing the curing temperature used in the thermal decomposition process during coating preparation lowers the anode overpotential although this may be at the expense of anode life.

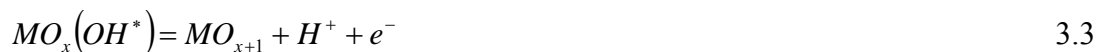
### 3.2.1.1 Electrochemical oxidation on DSA-type oxide electrodes

The electrochemical oxidation processes on DSA-type oxide electrodes occur via oxygen-atom transfer from water in the solvent phase to the oxidation product. The overall processes of anodic oxygen transfer can be represented by the generic equation (Savall, 1995).

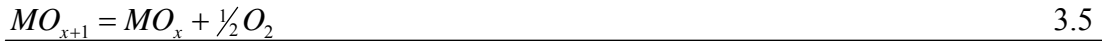


Where R is the reactant and the RO<sub>x</sub> is the oxidation product.

In the mechanism proposed for oxidative degradation in aqueous solutions, the first step is the discharge of water or OH<sup>-</sup> ions, which leads to the production of hydroxyl radical (OH\*) adsorbed on the electrode surface. The coating of MO<sub>x</sub> forms an active species (MO<sub>x+1</sub>) on DSA-type oxide electrodes by the discharge of H<sub>2</sub>O according to the reactions (Comninellis, 1994):



The  $MO_{x+1}$  species are responsible for both reactant oxidation and oxygen evolution in a competitive process as shown below:



### 3.2.1.2 *Electrocatalytic coatings for oxygen evolution*

Although the service life of DSA anodes is strictly dependent on the operating conditions, the long and stable operation of these anodes has been attributed to the mixed metal oxide coatings deposited on the valve metal substrate (Martelli *et al.*, 1994). The oxides that have been commonly used in the oxide coatings are tantalum oxide ( $Ta_2O_5$ ), iridium oxide ( $IrO_2$ ), ruthenium dioxide ( $RuO_2$ ) and tin oxide ( $SnO_2$ ). Although the material that is available commercially is Ti/ $Ta_2O_5$ - $IrO_2$  (Rolewicz *et al.*, 1988), mixtures of tin oxide and iridium oxide ( $SnO_2 + IrO_2$ ) have also gained popularity in acidic environments due to the impressive surface segregation of  $IrO_2$ , which increases electroactivity, while at the same time reducing power consumption. Ruthenium is also considered as an active oxide for the oxygen evolution reaction (OER). A number of other electrode coatings on titanium or nickel substrates are also available for oxygen and hydrogen evolution in other common electrochemical processes (Cardarelli *et al.*, 1998).

In view of the number of metallic oxides available as catalysts for the oxygen evolution reaction (OER), various couplings between noble metal oxides such as  $RuO_2$ ,  $IrO_2$ ,  $PtO_x$  and valve metal oxides, for example  $TiO_2$ ,  $ZrO_2$ ,  $Ta_2O_5$  can be applied as a paint on the substrates of different valve metals, such as Ti, Zr, Ta and Nb.

### 3.2.1.3 Structure of oxide coating

Martelli *et al.*, (1994) using an X-ray diffractometer (XRD), noticed that IrO<sub>2</sub>-Ta<sub>2</sub>O<sub>5</sub> coating contained pure crystalline IrO<sub>2</sub> and Ta<sub>2</sub>O<sub>5</sub> amorphous phase. They attributed this to the temperatures used during the drying stage of the precursor salts. Surface morphology as analysed by a scanning electron microscope (SEM) showed a mud-cracked structure of the oxide coating and some crystalline agglomerates at the surface. The electrical and electrochemical properties of DSA anodes are found to depend strongly on the characteristics of the morphology and structure of Ti substrate/noble metal interface.

### 3.2.1.4 Stability and success of DSA anodes

Not only does chemical composition of DSA anodes have great effect on the chemical stability but also on the electrocatalytic properties of these anodes. Different types of noble metals will result from quite different properties, and even the anodes with the same chemical composition would show the different electrocatalytic activities when their microstructures are different (Martelli *et al.*, 1994).

### 3.2.1.5 Deactivation mechanism of DSA anodes

Martelli *et al.* (1994) classified the deactivation mechanism of Ti/IrO<sub>2</sub>-Ta<sub>2</sub>O<sub>5</sub> anodes into five classes, namely: metal base passivation, coating consumption, coating detachment, mechanical damages and mixed mechanism. However, they also mentioned that these classes were not independent of each other since deactivation may occur by more than one mechanism. Process related conditions (temperature, current density and concentration) or internal factors (related to the coating) have an influence on the deactivation mechanism that occurs. Factors related to the coating can be reduced by proper fabrication of the coating.

#### 3.2.1.5.1 Passivation

Passivation influences the kinetics of metal dissolution. Passivation is the formation of a thin, non-porous layer usually 1-15 nm thick, of a corrosion product on the

surface which is able to act as a barrier to further oxidation of the metal. A passive surface is formed over some metals or alloys when exposed to oxygen or other chemical reactions which can lead to the formation of non-reactive and low solubility films on metal surfaces. The surface is also electron conducting although it is not able to transport ions and thus there is no mechanism for the thickening of the film.

The formation of passivating films can be irreversible and their removal may require quite harsh conditions. Figure 3.1 shows a characteristic curve for a metal undergoing passivation over a wide range of potential (E). The curve is obtained by scanning the potential from the potential where there is no corrosion and as the potential becomes more positive, the metal is oxidised and contains three regions namely (Pletcher, 1991):

a. Active Corrosion Region

The exponential increase in current in the active corrosion region is attributed to the dissolution of metal into ions. At more positive potentials, there is a sharp drop in current.

b. Passive Region

In the passive region, the current remains at a low value over a wide potential range and the corrosion rate is low.

c. Oxide Conversion ( $\text{H}_2\text{O}$  to  $\text{O}_2$ )

Due to oxygen evolution and further oxidation of the metal ions in the oxide layer, the current rises again as depicted in figure 3.1.



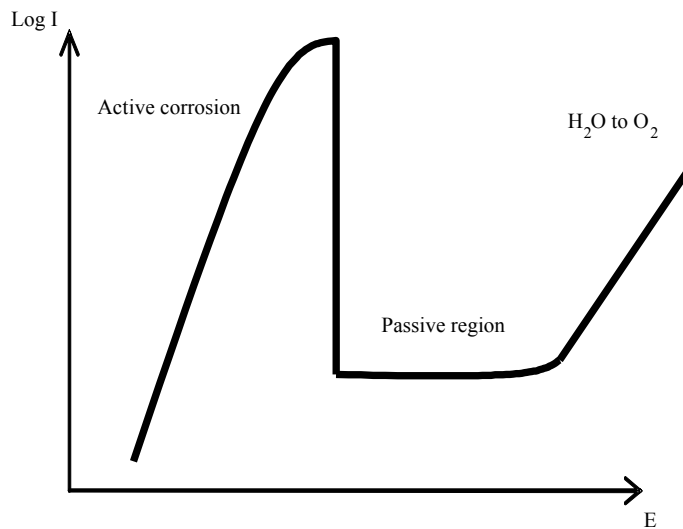


**Figure 3.1: log I-E Characteristic for a Metal which Shows Passivation**

Adapted from "A first course in Electrode Processes", (Derek Pletcher, 1991).

In operations involving DSA anodes containing titanium as a substrate, passivation is attributed to the formation of a thin, insulating layer of TiO<sub>2</sub> at the interface between the metallic base and the active coating. Operations at high current densities are characterised by passivation as the most frequent deactivation mechanism. From studies by Martelli *et al.* (1994), it was discovered that rate of anode passivation is related to current density, as shown in figure 3.2 below, and at the moment of deactivation a certain amount of catalyst remains non-utilised on the electrode surface.

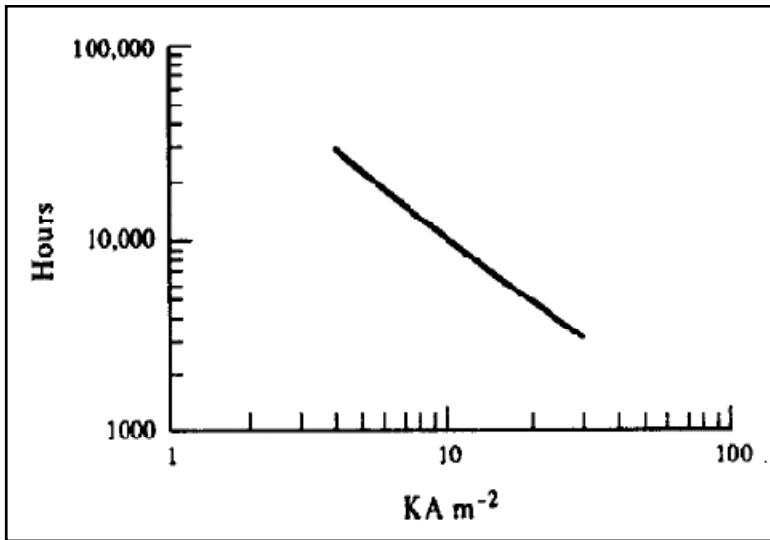


**Figure 3.2: Dependence of Service Life on Current Density, at Constant Electrolyte Concentration and Temperature. 150 g/l H<sub>2</sub>SO<sub>4</sub> – 60 °C**

Adapted from “Deactivation Mechanisms Of Oxygen Evolving Anodes at High Current Densities”, (Martelli *et al.*, 1994).

As cited by Martelli *et al.* (1994), Denora *et al.* defined the wear rate as being equal to:

$$r = \frac{\text{initial loading (gNm}^{-2}\text{)}}{j(\text{kAm}^{-2})x(\text{hours})} \dots\dots\dots 3.6$$

Ling *et al.* (1994) also concluded that electrolyte circulation, direction of electrolyte circulation and high current densities between 0.23 to 1.50 kA m<sup>-2</sup> accelerated anode passivation. Ling *et al.* (1994) also cited Sedzimir and Gumowska as having found similar results pertaining to the effect of current density on the onset of passivation. Higher temperatures were observed to delay the onset of anode passivation.

### 3.2.1.5.2 Coating consumption

Coating consumption occurs as a result of electrochemical corrosion and /or chemical consumption. Electrochemical corrosion is the oxidation and dissolution of a noble oxide at high potentials. For a coating containing IrO<sub>2</sub>, dissolution is possible. For

example, at potentials greater than 2.0 V vs. SHE,  $\text{IrO}_4^{2-}$  is formed. However, research has shown that iridium rarely reaches such high potentials in oxygen evolution reactions. Chemical consumption is a consequence of the interactions which occur between the electrode, electrolyte and/or the impurities in solution. Martelli *et al.* (1994) reporting the work of Hardee, mentioned that phosphates and chromates preferentially react with tantalum in a coating containing  $\text{Ta}_2\text{O}_5$ , while organic impurities may also react with the precious metal oxides leading to a mixed deactivation mechanism.

#### 3.2.1.5.3 Coating detachment

Chemical attack of the valve metal substrate by an acidic electrolyte, may lead to the weakening of the bond between the substrate and the coating, thus promoting detachment. Furthermore, since the coating is porous, it provides a large surface area for gas evolution, which can erode loosely bonded particles.

#### 3.2.1.5.4 Mechanical damage

Mechanical damage is known as the trivial cause of deactivation, which usually destroys a good coating within a few seconds.

#### 3.2.1.5.5 Mixed mechanism

In practice, at least two of the afore-mentioned mechanisms result in anode deactivation.

Hu *et al.* (2002) also carried out a standard accelerated electrolysis test in 0.5 M  $\text{H}_2\text{SO}_4$  solution, at a current density of  $2 \text{ A cm}^{-2}$  and a temperature of  $50 \pm 1 \text{ }^\circ\text{C}$ . These authors reported that over the whole electrolysis time in  $\text{H}_2\text{SO}_4$  solution, performance of the long service life Ti/70%  $\text{IrO}_2$ -30%  $\text{Ta}_2\text{O}_5$  anodes prepared at  $450 \text{ }^\circ\text{C}$  can be divided into three stages, namely 'active', 'stable' and 'de-active' regions.

They found that the following three types of destruction were occurring during the electrolysis:

- (i) dissolution of the active component,
- (ii) penetration of electrolyte through the porous structure of the thermally prepared oxide layer, and
- (iii) dissolution and anodic oxidation of the titanium base.

In the active and stable regions, loss of oxide coatings was dominated by dissolution of the active component, while in the 'de-active' region, oxide coatings were lost mainly by the peeling-off taking place in the Ti/oxide layer interface region. Furthermore electrocatalytic activity of the oxide catalyst decreased slowly with electrolysis time. Hu *et al.* (2002) noticed a sudden increase in electrode potential in the de-active region which was caused by the degradation in Ti/oxide layer interface. They concluded that dissolution and anodic oxidation of Ti base, ultimately leads to deactivation of DSA anodes.

### **3.3 Comparison of lead alloy and DSA anodes**

According to Alfantazi and Moskalyk (2003) and Weems *et al.* (2005), lead alloys are not dimensionally stable, since they slowly dissolve in electrolytes, leading to problems such as changes in the gap between the anode and cathode and product contamination by lead. Beer (1980) mentioned that dimensionally stable anodes have brought considerable improvements to the field of electrowinning which include:

- (i) lower half-cell potential,
- (ii) use of higher current densities,
- (iii) lower gas bubble effect through special anode designs,
- (iv) no loss of anode material, thus keeping the electrolyte pure,
- (v) no contamination of cathode deposits
- (vi) high current efficiency, and simple cell constructions.

Trasatti (2000) also agrees that the success of DSA anodes has been attributed to their chemical stability that allows them to maintain nearly constant dimensions during the life of the anode even when operating in environments with very low pH values. DSA anodes have been reported to have consumption rates as low as 1 mg/amp.yr due to their stability, and thus can be operated at high current densities (greater than 200 A/m<sup>2</sup>) (Alfantazi and Moskalyk, 2003). High current densities result in high yields of metal deposits. Gupta and Mukherjee (1990) reported that DSA technology can result in up to 20-25% power savings compared to the lead counterparts.

As cited by Kristóf *et al.* (2004), Alves *et al.* reported that IrO<sub>x</sub> is the most widely investigated electrocatalyst for O<sub>2</sub> evolution. It presents a service life almost 20 times longer than that of the equivalent RuO<sub>2</sub>. However, since IrO<sub>x</sub> is much more expensive than RuO<sub>2</sub> and its activity is slightly lower, in order to save cost and/or to improve the coating property; other components such as Ta<sub>2</sub>O<sub>5</sub> are usually added.

Balko and Nguyen (1991) also reported that the major technological advantage of titanium metal anodes activated with iridium oxide based coatings, is their ability to evolve oxygen in strongly acidic environments while maintaining good catalytic activity and dimensional stability. According to Trasatti (2000), thermally prepared IrO<sub>2</sub>-based coatings deposited on titanium metal supports are the most promising anodes in electrometallurgy where cheaper, but environmentally undesired materials like lead alloys, have to be dismissed. Kristóf *et al.* (2004) also mentioned that in industrial processes where oxygen evolution is one of the electrochemical reactions occurring at the anode, IrO<sub>2</sub>-based coatings may be a success. The authors also mentioned that tantalum pentoxide would be the optimal stabilising component of IrO<sub>2</sub>-based film anodes.

In the search for the most suitable DSA-type electrode for oxygen evolution in acidic solutions, Comninellis and Vercesi (1991) analysed nine binary coatings with IrO<sub>2</sub>, RuO<sub>2</sub> and Pt as the conducting component, and TiO<sub>2</sub>, ZrO<sub>2</sub>, Ta<sub>2</sub>O<sub>5</sub> as inert oxides,

deposited on titanium in  $\text{H}_2\text{SO}_4$ . These authors examined the microstructural properties, electrocatalytic activity and anodic stability. In agreement with Rolewicz *et al.*'s findings, Comminellis and Vercesi found that  $\text{Ti}/\text{IrO}_2$  (70 mol %)- $\text{Ta}_2\text{O}_5$  (30 mol %) was the best electrode for oxygen evolution in acidic media. The anode was associated with high catalytic activity and service life. The service life of  $\text{Ti}/\text{IrO}_2$ - $\text{Ta}_2\text{O}_5$  with 70 mol %  $\text{IrO}_2$  was estimated to be 5–10 years in electroflotation applications (Mraz and Krysa, 1994).

After analysing the behaviours of various coatings on a titanium substrate, Kotz *et al.* (1983) reported that the best coating for oxygen evolution in acidic solutions is  $\text{Ti}/\text{IrO}_2$  (70% mol)- $\text{Ta}_2\text{O}_5$  (30% mol). Their conclusion was based on the concept of anodic efficiency ( $\text{Ah mol}^{-1}$  of active component that can be supplied) and stability. Mraz and Krysa (1994) and Krysa *et al.* (1996) also agree that among the many  $\text{IrO}_2$ -based film electrodes, an important advantage offered by mixed oxide coatings consisting of  $\text{IrO}_2$  and  $\text{Ta}_2\text{O}_5$  is the remarkable catalytic activity for the oxygen evolution reaction, which allows lower energy consumption in the process of interest.

The decisive feature is, however, the service life of these electrodes, which are so far satisfactory for many practical applications, in spite of the fact that the performance can be still improved by proper optimisation of the electrode film preparation (Kristóf *et al.*, 2004). Cooper (1985) carried out experiments in an electrolyte containing 50 g/l Cu and 50 g/l  $\text{H}_2\text{SO}_4$ . The author reported that, although the addition of cobalt (II) to the copper electrowinning electrolyte can lower the oxygen overvoltage on the Pb-Sb anodes, an even greater reduction of 500-600 mV in the overvoltage can be realised by the replacement of lead alloy anodes with dimensionally stable anodes (DSA) as shown in figure 3.3. The particular anodes referred to in figure 3.3 are titanium anodes with an oxygen low potential (OLP) coating of iridium and platinum.

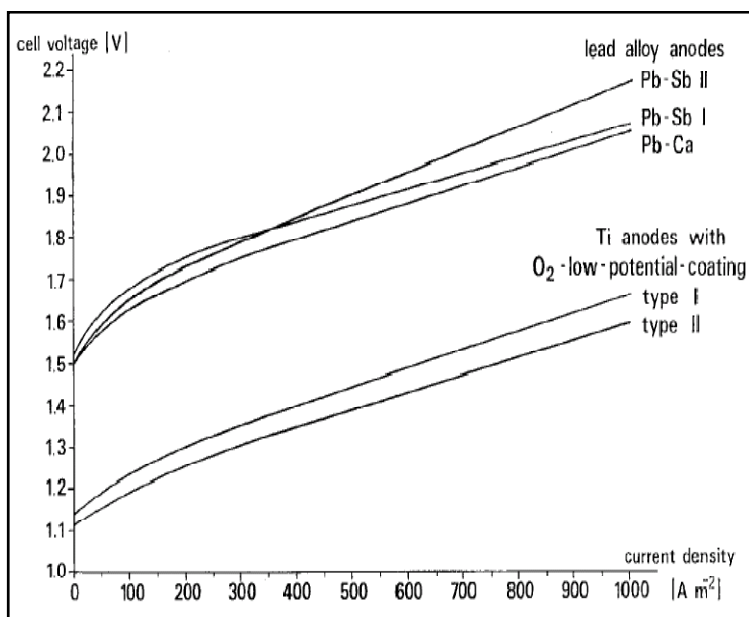


**Figure 3.3: Current Density-Voltage Curves for Copper Electrowinning Using Different Types of Anodes. Electrolyte: 50 g/l Cu, 50 g/l H<sub>2</sub>SO<sub>4</sub>, temperature: 40 °C; Cathode: copper clad graphite.**

Adapted from “Advances and Future Prospects in Copper Electrowinning”, *Journal of Applied Electrochemistry*, 15 (6), (Cooper, 1985)

The author also mentioned that, although the reduction of the oxygen overvoltage via the use of DSA anodes may be expensive, continuing advances in anode materials and further increases in energy costs will undoubtedly lead to the wider acceptance of anodes having low oxygen overpotential such as DSA anodes in copper electrowinning. Forti *et al.* (2001), in agreement with other authors, mentioned that DSA-type electrodes show good technological performance and their success is due to desirable features such as high stability of the active coating, good overall performance under mild conditions, high conductivity and commercial availability. However, these authors (Forti *et al.*, 2001) seem to contradict other authors such as Loufty and Leroy (1978), Alfantazi and Moskalyk (2003) and Moats *et al.* (2003) by mentioning that DSA electrodes are inexpensive.

Trasatti (2000) reported that Vittorio and Oronzio carried out experiments using mercury cells with graphite and DSA electrodes. After plotting graphs of cell voltage versus current, these authors noted that the slope of the graph was higher for graphite

electrodes. Furthermore, values of cell voltage at constant current were also higher (4.97 V) than those with the DSA electrode (3.90 V). In this case, although the composition of the DSA anodes used in the experiments was not revealed, the conclusion drawn was that DSA anodes were more suitable for the process. Table 3.1 and its corresponding graph show the results of the comparison.

**Table 3.1: De Nora Mercury cells: Comparison of Performances with Graphite and DSA Anodes.**

|  | <b>Graphite</b> | <b>DSA</b> |
|--|-----------------|------------|
| Anode potential (V)                                  | 1.47            | 1.37       |
| Cathode potential (V)                                | -1.85           | -1.85      |
| Anode ohmic drop (V)                                 | 0.15            | 0.15       |
| Electrolyte ohmic drop (V)                           | 0.60            | 0.40       |
| Gas bubble effect (V)                                | 0.90            | 0.13       |
| Current efficiency (%)                               | 96              | 97         |
| Energy consumption (kWh <sup>t</sup> <sup>-1</sup> ) | 3910            | 3040       |

Adapted from "Electrocatalysis: understanding the success of DSA<sup>®</sup>", *Electrochimica Acta*, 45 (15-16), (Trasatti, 2000)

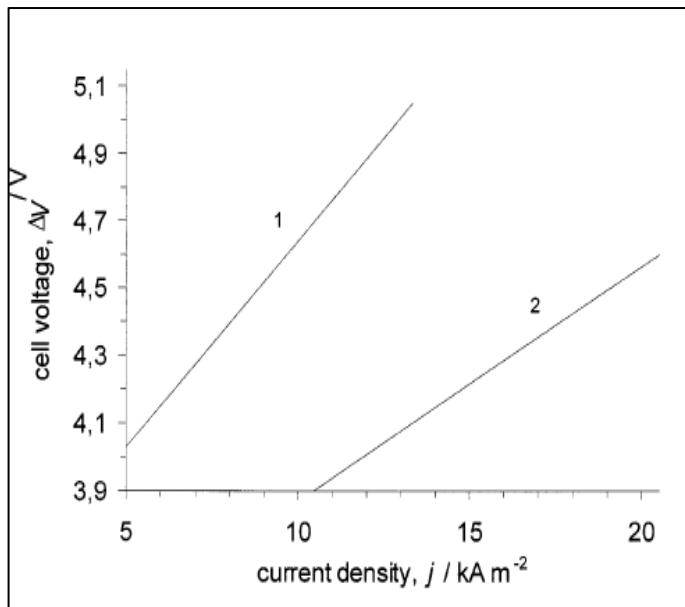


**Figure 3.4: Cell Potential Difference (cell voltage) versus Current Density for De Nora Mercury Cells. (1) Graphite anodes; (2) activated Ti anodes (DSAs). NaCl concentration: 310 g/l. Temperature: 60 °C.**



Kulandaisamy *et al.* (1997) reported that the energy consumed in the electrowinning of metals accounted for a substantial portion of the overall cost of the metal production. According to these authors, since 50-60% of the energy is consumed in the anode reaction alone, the appropriate selection of the anode is crucial. They carried out potentiodynamic studies in 2 M sulphuric acid and achieved about 450 mV reduction in anode potential compared to the lead anode. Although their study focused on the Ti/Ir-Co anode, these authors also agreed that catalytically activated anodes reduced anode potential significantly. Loufty and Leroy (1978) carried out an experiment comparing a dimensionally stable anode and an antimonial lead anode in 200 g/l sulphuric acid and found that the anode potential for the lead alloy anode was 500 mV higher than that of the DSA anode as shown in figure 3.5.

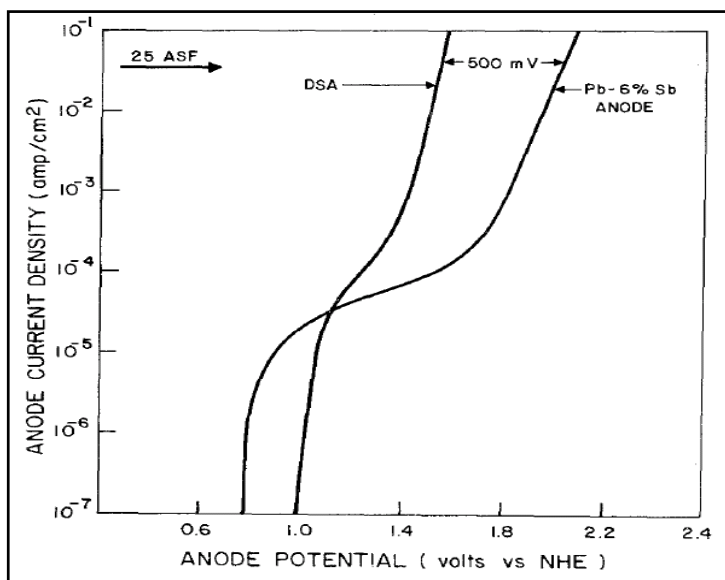


**Figure 3.5: Polarisation measurements for the Oxygen Evolution Reaction on a  $\text{TiO}_2/\text{RuO}_2$  Dimensionally Stable Anode (DSA) and a Conventional Lead/Antimony anode. The electrolyte was 200 g/l sulphuric acid at 25 °C.**

Adapted from “Energy Efficiency in Metal Electrowinning”, *Journal of Applied Electrochemistry*, 8 (6), (Loufty and Leroy, 1978)

They attributed the high anode potential of the lead alloy anode to the  $\text{PbO}_2$  surface formed on the anode, which exhibits one of the largest oxygen overpotentials known.

However, Loufty and Leroy (1978) also reported that although the use of dimensionally stable anodes seems attractive in this case, the energy saving benefit may not be as great as that which would be expected from considerations of the electrode overvoltages alone. The limited electronic resistivity of the valve metals (titanium), and their relatively high cost, may result in a limitation on the cell-voltage reduction which is economically achievable.

### **3.4 Alternative anode materials**

Some researchers have proposed that the cell voltage in electrowinning may also be reduced by utilising other anode materials that have been developed. Rubel *et al.* (1994) and De Pauli and Trasatti (1995) reported on the surface properties of Ti/(SnO<sub>2</sub> + IrO<sub>2</sub>), a dimensionally stable anode by using Scanning Electron Microscopy (SEM), X-ray photoelectron spectroscopy (XPS) and cyclic voltammetry. They claimed that these anodes showed stability under excessive oxygen production, thus making them suitable for practical applications. Ortiz *et al.* (2004) carried out research on the properties of this anode Ti/(SnO<sub>2</sub> + IrO<sub>2</sub>) by analysing the surface response using cyclic voltammetry and impedance measurements in the potential range where no reactions occurred. The electrode samples were prepared at 10 mol % intervals of composition from pure SnO<sub>2</sub> to pure IrO<sub>2</sub>, with a few more concentrations between 0 and 10 mol % IrO<sub>2</sub>. Electrocatalytic properties were studied using the chlorine evolution reaction while the reaction mechanism was analysed using Tafel slopes and reaction orders with respect to hydrogen and chloride ions. After comparing the voltammetric charges for fresh electrodes and those that had been used in the study, it was concluded that the oxide electrodes showed stability.

Although Alfantazi and Moskalyk (2003) mentioned that DSA anodes are chemically stable and they reduce anode potential, they suggested that DSA anodes are not the ideal replacements for lead alloy anodes due to their prohibitive capital cost and the requirement of periodic recoating with precious metals.

In the same year, Alfantazi and Moskalyk carried out a preliminary study on the use of conductive polymers, namely polyaniline and poly 3, 4, 5-trifluoro phenylthiophene (TFPT) as protective coatings on lead alloy anodes. The coatings successfully reduced physical degradation and overpotential of the anodes without hindering the flow of current. Table 3.2 below shows the conductivities of some conductive polymers.

**Table 3.2: Conductivities of Some Conductive Polymers**

| POLYMER                        | CONDUCTIVITY (S/cm)                      |
|--------------------------------|--|
| Polyacetylene                  | $10^2$ - $10^5$ (stretched)              |
| Polythiophene                  | $10^2$ - $10^4$                          |
| Polypyrrole                    | $10$ - $10^3$ (stretched)                |
| Poly-phenylenevinylene         | $10^3$                                   |
| Polyaniline                    | $10$ - $150$ (heated)<br>$10^2$ - $10^3$ |
| Poly 1,2,3-ethyldioxythiophene | $10$ - $780$ (in nanopores)              |

Adopted from "Conductive Polymer Coatings for Anodes in Aqueous Electrowinning" (Alfantazi and Moskalyk, 2003)

Thus as an alternative to DSA anodes, they proposed the application of conductive polymer coatings on lead alloy anodes. They reported that this would be a cheaper means of addressing the shortcomings of traditional lead alloy anodes. Hrussanova *et al.* (2001) carried out a comprehensive study on the behaviour of the Pb–Co<sub>3</sub>O<sub>4</sub> composite anode in copper electrowinning using synthetic electrolyte (30 g/l Cu in 85 g/l H<sub>2</sub>SO<sub>4</sub>). They reported that the Pb–Co<sub>3</sub>O<sub>4</sub> anode had a considerable depolarising effect on the oxygen evolution reaction compared to commonly used metallurgical Pb–Sb 5.85% and Pb–Ca 0.08%–Sn 0.74% anodes. As a result, the anode potential was 40 mV lower than Pb–Sb and about 70 mV lower than the Pb–Ca–Sn anode. The corrosion rate of the anode during prolonged polarization (96 h) under galvanostatic conditions was approximately 6.7 times lower than that of Pb–Sb anode. These authors concluded that the use of a Pb–Co<sub>3</sub>O<sub>4</sub> anode under conditions similar to those used industrially should cause a decrease in energy consumption.

Lead based metal oxide anodes such as the Mesh on Lead (MoL) anodes developed by Eltech Systems Corporation have also been studied by many researchers. These anodes utilise conventional lead alloy anodes as the anode substrate, while their electrocatalytic activity is increased by the addition of electrocatalytic metal oxides to the lead anode surface. Moats *et al.* (2003) reported that MoL anodes are very promising and have lifetimes of 12–16 months in commercial copper electrowinning tank houses.

After this time the electrocatalytic activity of the anode is lost and oxygen evolution begins to occur predominantly at the lead anode surface. The reported advantages of MoL anodes include energy savings of 12-17%, enhanced current efficiency (up to 5%), lower cost compared to dimensionally stable anodes, ease of preparation and as such they can be prepared on site, reduction in sludge generation and improved cathode quality (< 1 ppm Pb).

Another anode of interest is the titanium-lead anode (Ti-Pb), which is reported to have life times of 10 to 12 years. Ferdman (2000) claims that when using this anode, spalling does not occur and as such lead content in copper cathodes is ten times lower than that obtained with conventional lead alloy anodes.

It has also been mentioned that anodes with oxide coatings such as IrO<sub>2</sub>-Bi<sub>2</sub>O<sub>3</sub> are likely to inhibit MnO<sub>2</sub> deposition even with high concentrations of Mn (5 g/l) and are therefore less susceptible to passivation. Manganese has been reported to form either soluble species or insoluble manganese dioxide that may passivate the anode surface and hinder the OER reaction (Kao and Weibel, 1992). Passivation of the anode surface results in an increase in anode potential. Thus, IrO<sub>2</sub>-Bi<sub>2</sub>O<sub>3</sub> oxide coatings are claimed to have high overpotential for the deposition of MnO<sub>2</sub> such that this reaction is practically inhibited at temperatures up to 60 °C (Tuffrey *et al.*, 2006).

## 4 EXPERIMENTAL PROCEDURES

In these investigations, three main tests were performed in order to analyse and characterise the anode materials being compared. These methods were:

- i. Electrochemical tests
- ii. Electrowinning tests
- iii. Morphological tests

Electrochemical tests were carried out in order to compare stability, corrosion resistance, and electrocatalytic activities of the lead alloy and dimensionally stable anodes. Electrowinning tests were done in order to assess cell voltages with the aim of determining energy consumption, cathode contamination and stability of the same anode materials. Morphological studies and determination of composition of the anodes were carried out using a scanning electron microscope and x-ray diffractometer respectively. All tests were conducted at room temperature unless stated otherwise.

### 4.1 Electrochemical tests

#### 4.1.1 Electroanalytical equipment

An Autolab, potentiostat/galvanostat/ (Eco Chemie)/PGSTAT302 was used to obtain a three-electrode cell configuration for all the electrochemical tests. The control of the equipment, real time monitoring of experiments and data acquisition were accomplished by use of General Purpose Electrochemical System 4.9 (GPES) software, installed on a personal computer as shown in figure 4.1. The electrochemical cell used in the study was a 500 ml pyrex beaker, covered with a perspex lid with three guidance holes through which the working electrode (WE), counter electrode (CE) and reference electrode (RE) could be inserted.

A graphite rod and a silver/silver chloride electrode (0.222 V vs Standard Hydrogen Electrode) were used as the counter and reference electrodes respectively. The Ag/AgCl reference electrode was positioned as close as possible to the working electrode in order to minimise ohmic drop due to uncompensated resistance. The base electrolyte in the RE was a 3 M solution of potassium chloride (3 M KCl).



Figure 4.1: Potentiostat Equipped with a Personal Computer

#### 4.1.2 Electrode preparation

Table 4.1: Anode Type, Supplier and Composition

| Anode Type                         | Supplier                    | Composition   |
|------------------------------------|-----------------------------|---|
| Antimonial lead (Pb/Sb)            | Anglo Platinum              | 94% lead and 6% antimony                            |
| Dimensionally stable anodes (DSAs) | DISA Anodes, NMT Electrodes | Ti-IrO <sub>2</sub> /Ta <sub>2</sub> O <sub>5</sub> |

The titanium substrate used in the DSAs was ASTM grade 1. The composition of the coating was:

- Inner layer: 30/70% IrO<sub>2</sub>-Ta<sub>2</sub>O<sub>5</sub>; 10 g/m<sup>2</sup>, followed by
- Outer layer: 70/30% IrO<sub>2</sub>- Ta<sub>2</sub>O<sub>5</sub>; 10 g/m<sup>2</sup>

The anode pieces were cut to provide a 1 cm<sup>2</sup> surface area unless where stated otherwise. For all DSA mesh anode samples, the true area was taken into consideration after consultation with other experts in the field.

Conductive wire was taped on the back of each specimen using electrically conductive tape, before mounting it in epoxy resin. The sample surfaces for lead alloy anodes to be analysed were ground and polished with silicon carbide paper successively from 240-grit to 1 000 grit, to ensure complete removal of pits. However, for the DSA plate anode specimens, only 1 000 grit paper was used to clean the surface in order to prevent removal of the coating. Microscopic investigations were done to ensure that the coating was still intact. After grinding and polishing, the samples were cleaned with deionised water.

#### 4.1.3 Reagents

**Table 4.2: Reagents Used**

| Reagent  | Supplier | Grade             | Molecular Mass (g/mol) |
|--|----------|-------------------|------------------------|
| Concentrated sulphuric acid (H <sub>2</sub> SO <sub>4</sub> )    | Merck    | <sup>a</sup> (AR) | 98.01                  |
| Hydrated copper sulphate (CuSO <sub>4</sub> .5 H <sub>2</sub> O) | Merck    | <sup>a</sup> (AR) | 249.69                 |

<sup>a</sup> AR – Analytical Reagent

#### 4.1.4 Electrolyte solutions

The test electrolytes used in this study were 0.5 M sulphuric acid, synthetic solution and base metal refinery electrolyte. The 0.5 M H<sub>2</sub>SO<sub>4</sub> was prepared by diluting 28 ml of concentrated H<sub>2</sub>SO<sub>4</sub> with 1 litre of distilled water. The synthetic solution was prepared from 216.23 g reagent grade copper sulphate (CuSO<sub>4</sub>. 5H<sub>2</sub>O), 100 g sulphuric acid and 1 litre of distilled water in order to simulate the primary constituents for industrial operating conditions. Table 4.3 summarises the concentrations of the two electrolytes used in the electrochemical tests.

**Table 4.3: Concentrations of Electrolytes Used**

| Electrolyte Solution           | Concentration (M)              |     |
|--------------------------------|--------------------------------|-----|
|                                | H <sub>2</sub> SO <sub>4</sub> | Cu  |
| H <sub>2</sub> SO <sub>4</sub> | 0.5                            | -   |
| Synthetic                      | 1                              | 0.9 |
| Base Metal Refinery            | 1                              | 0.9 |

#### 4.1.5 Electrochemical measurements

In this work, the following electrochemical methods were used to monitor the properties of the anode materials:

- (i) open circuit potential
- (ii) potentiodynamic polarisation
- (iii) cyclic voltammetry
- (iv) chronoamperometry
- (v) chronopotentiometry (galvanostatic)
- (vi) electrochemical impedance spectroscopy.

Prior to carrying out open circuit potential tests, potentiodynamic polarisation, and galvanostatic chronopotentiometry tests, the lead anode samples were conditioned in order to replicate a commercial surface by forming a stable lead (IV) dioxide layer on the oxide. This was done by following a procedure outlined by Cifuentes *et al.* (1998). A constant anodic current density of 200 A/m<sup>2</sup> was applied over a period of two and half hours in a solution of 55 g/l Cu, 100 g/l H<sub>2</sub>SO<sub>4</sub> and 120 ppm cobalt (Co). The cobalt was used to stabilise the oxide layer (Weems *et al.*, 2005).

In the electrochemical impedance spectroscopy tests, initially, 50 consecutive cyclic voltammetry scans were performed on the lead anode followed by 20 minutes of conditioning prior to the experiments, in order to produce a more stable and reproducible surface layer (Yu and O'Keefe, 2002).



#### *4.1.5.1 Open circuit potential (OCP) measurements*

Open circuit potential (OCP) measurements were carried out for a period of two hours using synthetic solution in order to assess the stability of the anodes under investigation. The tests also furnished information on the anode material with the highest corrosion resistance and the redox transitions controlling the surface electrochemistry of the anodes. The measurements were carried out in synthetic solution.

#### *4.1.5.2 Potentiodynamic Polarisation*

In potentiodynamic polarisation the specimens were polarised in synthetic solution from 250 mV below the corrosion potential ( $E_{\text{corr}}$ ) to a final potential of approximately 1-1.2 V above  $E_{\text{corr}}$ . A scan rate of 20 mV/s was used. Plots of potential (volts) against log. current density ( $\text{A}/\text{cm}^2$ ) were constructed. These potentiodynamic plots were used to assess:

- corrosion rate of the metal specimens in synthetic solution
- the ability of materials to passivate spontaneously in the synthetic solution and
- the potential region over which the specimen remains passive.

#### *4.1.5.3 Chronopotentiometry (galvanostatic)*

Chronopotentiometry tests were carried out in order to evaluate electrode potentials and chemical stability under galvanostatic conditions in synthetic electrolyte. A current density of  $190 \text{ A}/\text{m}^2$  (similar to plant conditions) was applied to the electrochemical cell and the anode potential was recorded with time. The three electrode arrangement was used, although the graphite rod was replaced with a 316 stainless steel cathode plate of dimensions 12 cm x 2 cm x 1 mm. The cell used was a 500 ml pyrex beaker covered with a perspex lid with three guidance holes through which the anode, cathode and reference electrode could be inserted. The anode sizes for this experiment are indicated in table 5.2 as  $1 \text{ cm}^2$ ,  $1.36 \text{ cm}^2$  and  $1.90 \text{ cm}^2$  for the lead anode, DSA plate anode and the DSA mesh anode respectively. The active cathode area used in all these tests was constant. Therefore the cathodic current

density was the same for all the experiments. Visual inspection of the copper deposits was also done while current efficiencies for all the anodes were determined from the weight gained by the cathodes.

Galvanostatic chronopotentiometry tests were also carried out in base metal refinery electrolyte and manganese containing synthetic electrolyte in order to assess the extent to which contaminants in the electrolyte can affect the anode potential or cell voltage during electrowinning operations.

#### *4.1.5.4 Cyclic Voltammetry (CV)*

Cyclic voltammetry tests were performed in order to monitor the surface properties of metal specimens. The CV tests were also used to determine the potential for oxygen evolution and assess working area of the electrode materials. The experiments were performed in 0.5 M sulphuric acid in order to avoid masking of the anode surface by copper cations.

In each CV experiment, a potential was applied to the system, and the faradaic current measured over a range of potentials referred to as a potential window. The potential was varied in a linear manner starting at an initial value up to a pre-defined limiting value. At this potential, (switching potential) the direction of the potential scan was reversed, and the same potential window scanned in the opposite direction. Therefore any species formed on the anode material by oxidation on the first (forward) scan would probably be reduced on the second (reverse) scan.

Multiple, consecutive scans for the lead alloy specimens were performed at a low scan rate (2 mV/s). According to Yu and O'Keefe (1999), consecutive CV tests on the lead anodes at a lower scan rate of 2 mV/s provide more stable, consistent, and comparable trends. The lead anode curves were generated over potential ranges of 0 to 2 V and -0.5 to 2.2 V; which covered the reactions from metallic lead,  $Pb^0$  to  $Pb$  (IV) and oxygen evolution.

Voltammetric curves for the DSA anodes (plate and mesh) were recorded between -0.6 to 1.5 V (the oxygen evolution potential) and measured at a scan rate of 100 mV/s. Nijjer *et al.* (2001) reported that the anodic peaks for DSA anodes, resulting from the Ir(III)/Ir(IV) redox transition are clearly visible at scan rates higher than 20 mV/s. Hence beyond 20 mV/s, as scan rate increases much broader peaks are exhibited.

#### 4.1.5.5 *Electrochemical Impedance Spectroscopy (EIS)*

EIS was used as a tool for investigating the corrosion phenomena of DSA anode specimens (plate and mesh) and the lead anode in synthetic electrolyte. The impedance spectra were initially obtained at open circuit and oxygen evolution potentials. A single sine wave was used with a perturbation amplitude of 5 mV for the rest potential measurements. The frequency was swept from 100 mHz to 1 kHz. Impedance tests were also carried out at different potentials in the region of the oxygen evolution reaction (OER). Frequency response analyser software (FRA) was used to analyse the EIS data.

#### 4.1.5.6 *Chronoamperometry (< 1s)*

Chronoamperometry (< 1s) was carried out in synthetic solution in order to rapidly characterise the anode materials by reducing the sampling time. This aided in the assessment of anode activity. A potential step of 1.5 V was used for all the anode specimens.

#### 4.1.6 Reproducibility

To assess reproducibility of results, a number of experiments were performed for each test. Some of the raw data and corresponding graphs have been included in the appendices section.

## 4.2 Electrowinning tests

### 4.2.1 Equipment

The major equipment used in this work is indicated in table 4.4 below:

**Table 4.4: Equipment Used During Electrowinning Tests**

| Equipment  | Purpose  | Technical Data         |
|--|--|------------------------|
| DC power supply and 3 data loggers   | To supply current to the electrowinning cell and record cell voltage with time | 100 A power supply     |
| 3 electrowinning cells   | Electrowinning   | 16 litres/cell         |
| 3 intermediate bulk containers (IBCs)                                      | Bulk storage of electrolyte  | 1 000 litres/container |
| 1 industrial peristaltic pumps   | For draining the IBCs  | 165 rpm maximum        |
| 1 laboratory scale peristaltic pump  | For electrolyte feed   | 110 ml/minute          |
| 2 electrolyte tanks  | Storage of fresh and spent electrolyte   | 200 litres/tank        |
| Titanium mini hot rod, with temperature control box and PT100 sensor HALAR | To heat the solution from room temperature to 55 °C                            | 600 W, 230 V           |
| Thermometer  | To measure electrolyte temperature   | -                      |

### 4.2.2 Electrowinning cell configuration and setup

The electrowinning cells rig shown in figure 4.2 was constructed of polyvinyl chloride (PVC) material. Each cell measured 0.375 m x 0.12 m x 0.365 m and contained two cathodes and one anode spaced 2 cm apart. The cells had electrolyte overflow chambers. Overflow would drain through the outlet ports (figure 4.3) at one end of the cell into the spent solution tank (Appendix H). Electrolyte was pumped by a peristaltic pump from the fresh electrolyte tank at a constant flow rate of 110 ml/minute. A four-way valve was then used to divide the flow into three equal

streams of flow rate 36.7 ml/minute for the three cells. The total plating cycle was 150 hours which required 330 litres of electrolyte per cell. Thus a total of 990 litres of solution per plating cycle was used for the experiments. Three Intermediate Bulk Containers (IBCs) containing the electrolyte were supplied from the Base Metal Refinery in Rustenburg. Heating rods were used for maintaining the desired electrolyte temperature (50-55 °C).



**Figure 4.2: Electrowinning Cells**

The electrodes were connected externally to an electrical circuit (figure 4.3) while the current was supplied by a DC power supply unit (0-10 V; 0-100 A) to give a constant current density of  $190 \text{ A/m}^2$  as shown in figure 4.4. Since the project focused on the anode, the anode was put into the centre of each cell and the two cathodes on the outside.

Necessary safety measures which included the use of an emergency switch on the power supply unit were also put in place in order to ensure safe operation. Real-time measurements of cell voltage with time were recorded by data loggers for all the three cells.

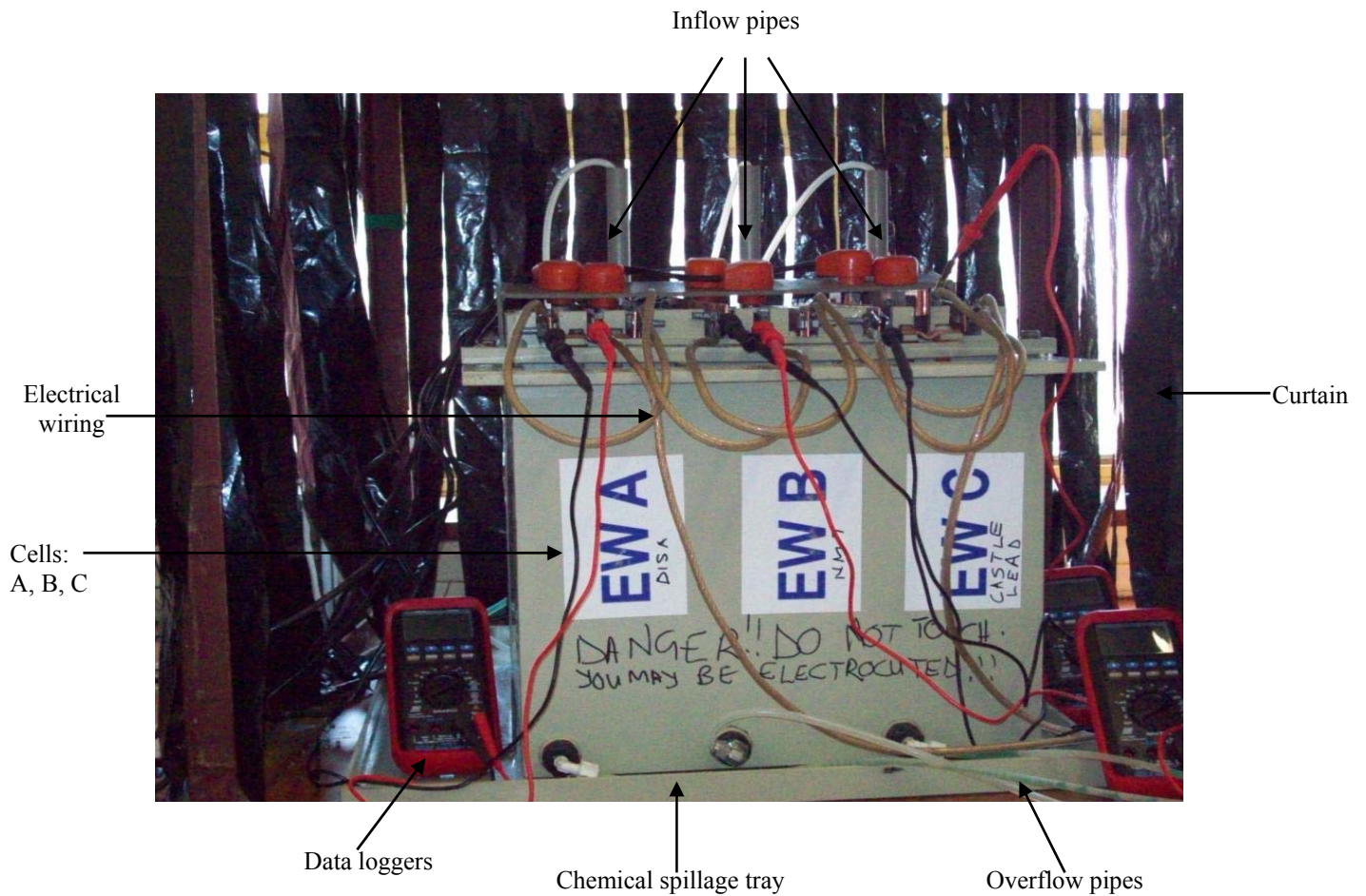


**Figure 4.3: Electrowinning Cells and Auxiliary Equipment**

#### 4.2.2.1 Control of pump flow rate

Peristaltic pumps are characterised by unstable pumping rates. However, to ensure accuracy the following procedures were carried out:

- a) The peristaltic pump fitted with its new tubing was operated for half an hour before calibration. Most tubing materials have a break-in period, during which the shape memory of the tubing and the fluid flow rate adjust and stabilise. The length of this break-in period is dependent on the size of tubing and material (<http://www.coleparmer.com>).

b) The pump was periodically calibrated by first adjusting the variable speed on the analog control knob and then using a stopwatch. A 2-litre measuring cylinder was filled with BMR solution using the peristaltic pump and when the BMR level reached a predetermined volume (2 litres, 1 litre, 0.5 litres and 0.25 litres), the timer was stopped and the time recorded was rounded to the nearest second.

Once the electrowinning process had begun, the pump, pumped out BMR solution from a 200-litre tank. At a flow rate of 110 ml/min and within 24 hours, 158.4 litres of fluid was depleted from the 200-litre tank which needed to be replaced. Throughout the experiments, 158.4 litres +/- 500 ml per day were used to fill the tank to capacity; an indication that the pump was consistently pumping out solution at a flow rate acceptably close or equal to 110 ml/min.

#### 4.2.3 Suppression of acid mist

Three measures were put in place to ensure the suppression of acid mist.

These are:

- Addition of an aluminium foil pipe to the cell fume hood and directing it to the fume extractor fan as shown in Appendix H.
- Making use of curtains as highlighted in Appendix H.
- The use of polystyrene beads of diameter approximately 0.3 cm as indicated in figure 4.5.

Figure 4.4 shows a schematic diagram of the experimental setup.

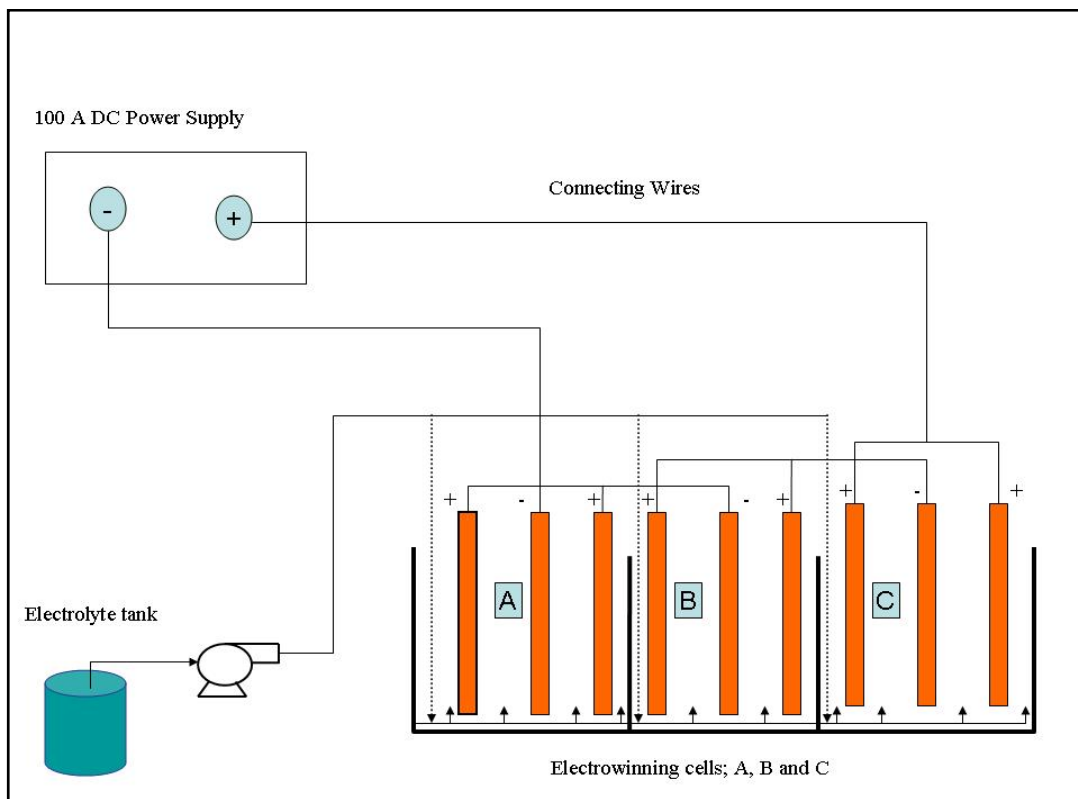


Figure 4.4: Schematic Diagram of Experimental Setup



Figure 4.5: Polystyrene Beads



#### 4.2.4 Electrodes

**Table 4.5: Electrodes and Preparation**

| <b>Electrodes</b>     | <b>Material</b>  | <b>Dimensions<br/>(mm)</b> | <b>Hanger bar<br/>material</b> | <b>Supplier</b>      |
|-----------------------|--|----------------------------|--------------------------------|----------------------|
| <b>Cathodes</b>       | Copper   | 405 *330                   | Copper                         | Anglo<br>Platinum    |
| <b>Anodes</b>         |  |                            |                                |                      |
| <b>Lead<br/>Alloy</b> | Pb (6% Sb)   | 405 *330                   | Copper                         | Castle Lead<br>Works |
| <b>DSA 1</b>          | Ti- (70%)IrO <sub>2</sub> /(30%)Ta <sub>2</sub> O <sub>5</sub> plate<br>and mesh | 405 *330                   | Titanium                       | DISA Anodes          |
| <b>DSA 2</b>          | Ti- (70%)IrO <sub>2</sub> /(30%)Ta <sub>2</sub> O <sub>5</sub> plate<br>and mesh | 405 *330                   | Titanium                       | NMT<br>Electrodes    |

The dimensionally stable anodes from DISA Anodes and NMT electrodes were denoted as DSA 1 and DSA 2 anodes respectively and their performance was assessed in order to determine the best anode to use in the electrowinning of copper at Anglo Platinum in comparison to the antimonial lead anode which is currently being used.

The hanger bars were screwed to the top edge of each electrode in order to establish electrical connection as shown in figure 4.6. During operation the electrolyte level was kept constant at 360 mm above the lower edge of the anode.

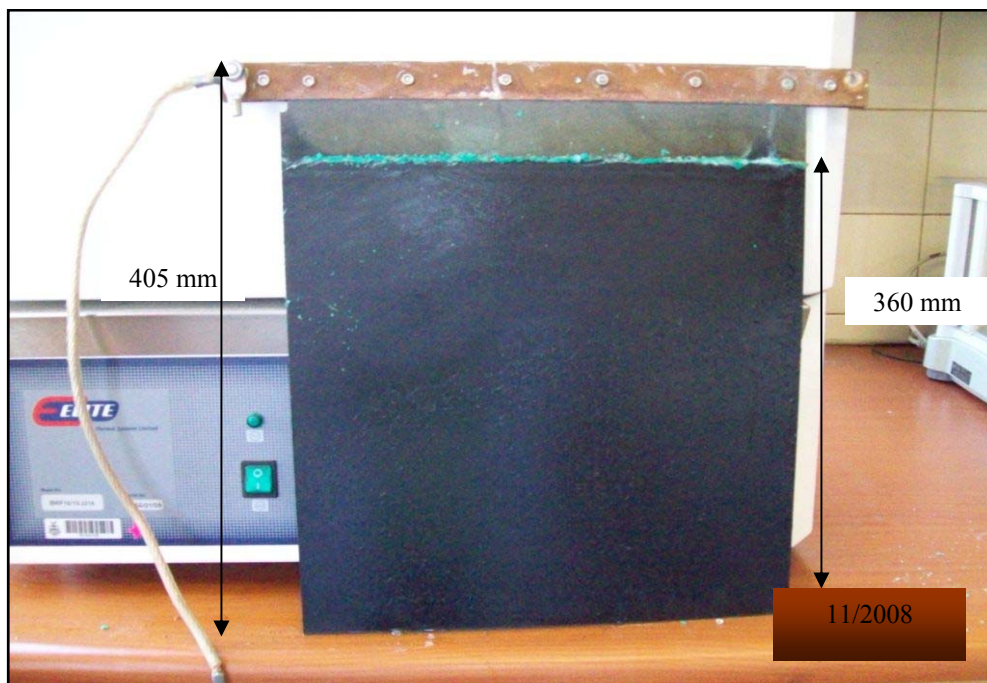


**Figure 4.6: Sample anode with a copper hanger bar**

#### 4.2.5 Reagents

- Copper feed to the electrowinning cells at base metal refinery (BMR) was used as the main solution. The solution contained 55 g/l Cu and 100 g/l H<sub>2</sub>SO<sub>4</sub>.
- Hydrated copper sulphate solution was used to prepare standards to calibrate the Atomic absorption spectrometer.

After electrolysis, the cathodes were removed and thoroughly washed with tap water followed by distilled water and air dried after washing it in acetone. The current efficiency was calculated from the weight gained by the cathodes using equation 2.22:

$$\varepsilon_c(I) = \frac{nF\Delta W}{ItM} \dots\dots\dots 2.22$$

Where,

$\Delta W$  - Weight gained by the cathode.

F - Faraday's constant.

I - Applied current

M - Atomic weight of copper

t - Time taken for the copper to be deposited

n – Number of electrons participating in the reaction (2 electrons)

#### 4.2.6 Analytical equipment

In the study an atomic absorption spectrometer (AAS) was used to periodically analyse the copper concentration in the overflow solution. An inductively coupled plasma (ICP) and inductively coupled plasma-mass spectrometer (ICP-MS) were also used to provide a compositional analysis of the base metal refinery electrolyte.

#### 4.2.7 Equipment Design

##### 4.2.7.1 *Pump sizing*

Calculations for pump sizing were carried out initially by assuming, 90% current efficiency and using equations 2.22 and 4.1 as shown in Appendix A.

$$t = \frac{nF\Delta W}{\varepsilon IM} \dots\dots\dots 2.22$$

$$Q = \frac{V}{t} \dots\dots\dots 4.1$$

Where, V - volume of solution per cell

t - time taken for the copper to be deposited (from equation 2.22)

Q- flowrate of the electrolyte per cell

The spreadsheet supplied by Anglo Platinum (Appendix B) was then used to validate the result.

#### 4.2.7.2 Heater sizing

The following equations supplied by Hi-tech Elements were used in the sizing of the heating rods. Calculations on the sizing of the heating rods are shown in Appendix C.

a) Calculation of the power required to heat the solution and container:

$$P = \frac{mc\Delta T}{860 * t_h} \dots\dots\dots 4.2$$

Where,

P- power (kW)

m- mass (kg)

c- specific heat capacity (kcalories/kg<sup>0</sup>C)

$\Delta T$  - temperature rise (<sup>0</sup>C)

$t_h$  - heat-up time (hours)

b) Calculation of the power required to heat the container:

- Same as equation 4.2.

c) Calculation of the power required to overcome heat losses:

Heat losses are governed by the installation; that is, indoors, outdoors, thermal insulation and in most cases between 10-20% of the sum of steps (a) and (b) above is sufficient. In the study, heat losses were assumed to be 20%, which gives a good overdesign factor.

Therefore the total power rating of the heater is given by the sum of steps (a), (b) and (c).

### **4.3 Physical characterisation**

#### 4.3.1 Scanning electron microscope (SEM) and energy dispersive spectroscopy, EDS

Surface morphology and elemental composition of the DSAs and antimonial lead were analysed using a JSM-840 (JEOL) scanning electron microscope, with energy dispersive spectroscopy (EDS). Morphological studies were carried out in order to establish the relationship between surface morphology and anode behaviour. EDS analysis was performed in order to determine the elemental compositions of the anode materials. The operating voltage of the electronic beam was 20 keV for both morphological studies and EDS analysis.

#### 4.3.2 X-ray diffractometer

Compositional analysis of the anode materials and crystallographic orientation of the copper deposits from electrowinning were done using a Philips-PW1710, X-ray diffractometer with a copper K-alpha as anode. The generator settings were set at 40 kV and 50 mA. The start and end angles were  $20^{\circ}$  and  $80^{\circ}$  respectively for the continuous scan while the scan step time was 1 second. Xpert Highscore Software was then used to match the resulting peaks.

#### 4.3.3 Visual inspection

Visual inspection of cathodes was carried out after the experiments. This assisted in assessing the physical appearance of the copper deposits.

## 5 RESULTS AND DISCUSSIONS

### 5.1 Comparison of anode materials: Electrochemical Investigations

#### 5.1.1 Open circuit potential measurements

Open circuit potential (OCP) measurements were carried out in order to assess the stability of the anodes under investigation. The tests also furnished information on the anode material with the highest corrosion resistance and the redox transitions controlling the surface electrochemistry of the anodes. Figure 5.1 shows the graphs for open circuit potential measurements for the DSA anodes and lead anode. The experiments were conducted within a period of two hours each.

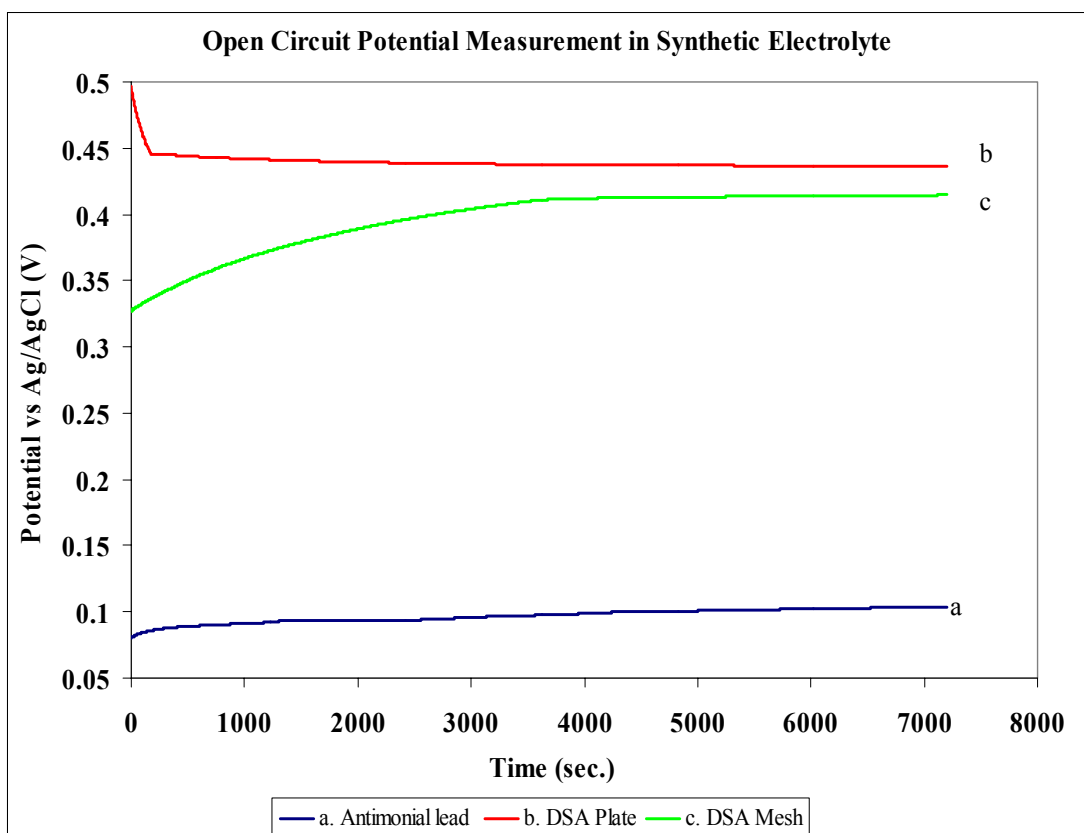


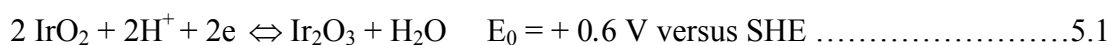
Figure 5.1: OCP Graphs for  $\text{Ti-IrO}_2/\text{Ta}_2\text{O}_5$  Plate,  $\text{Ti-IrO}_2/\text{Ta}_2\text{O}_5$  Mesh and Pb/Sb in 55 g/l Cu and 100 g/l  $\text{H}_2\text{SO}_4$  at Room Temperature (rt).

The results indicate that for the DSA plate, there is initially a sharp decrease in potential from 0.49 V to 0.45 V, within the first 200 s, after which the potential stabilizes for the remaining duration of the measurement. The initial decrease in OCP can be attributed to the erosion of coating particles that are weakly bonded to the substrate once there is interaction between the electrolyte and the anode (Martelli *et al.*, 1994). For the DSA mesh anode, the potential is shifted more rapidly towards the nobler potentials from 0.33 V to 0.41 V within the first 3750 seconds and then tends to stabilise. For the antimonial lead specimen, there is a small increase of the potential from 0.08 V to 0.10 V for the whole duration of the experiment.

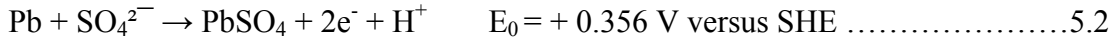
It can be observed that the DSAs showed differences in behaviour despite being of similar composition. However, it would not be possible to relate the differences in behaviours to the mechanisms of these anodes since there was not enough information about their manufacture. The manufacturers were not at liberty to disclose this information. Despite this, the purpose of the investigation, which was to establish if these DSA anodes (plate and mesh) had different behaviours and if so, to what extent, was achieved.

Figure 5.1 also shows that the DSA anodes have nobler potentials compared to the lead alloy anode with the DSA plate having the largest average  $E_{oc}$  value of 0.44 V. These results suggest that the DSA plate has the highest corrosion resistance followed by the DSA mesh and lastly the lead alloy anode.

$E_{oc}$  measurements also provide information about the electrodes surface active sites. Comparison of the  $E_{oc}$ -data with the theoretical value of the standard potential of the solid-state transitions present in the coating suggests that the surface electrochemistry for the DSA anodes could be controlled by hydrated Ir(III)/Ir(IV) redox transition (Alves *et al.*, 1998).



The surface electrochemistry for the lead anodes can be said to be controlled by the Pb/Pb(II) redox transition.



### 5.1.2 Potentiodynamic polarisation

Potentiodynamic polarisation was used to determine the corrosion rate of the anodes in synthetic electrolyte. Figure 5.2 shows the potential against log. current graphs used in the evaluation of cathodic and anodic Tafel constants and corrosion rate.

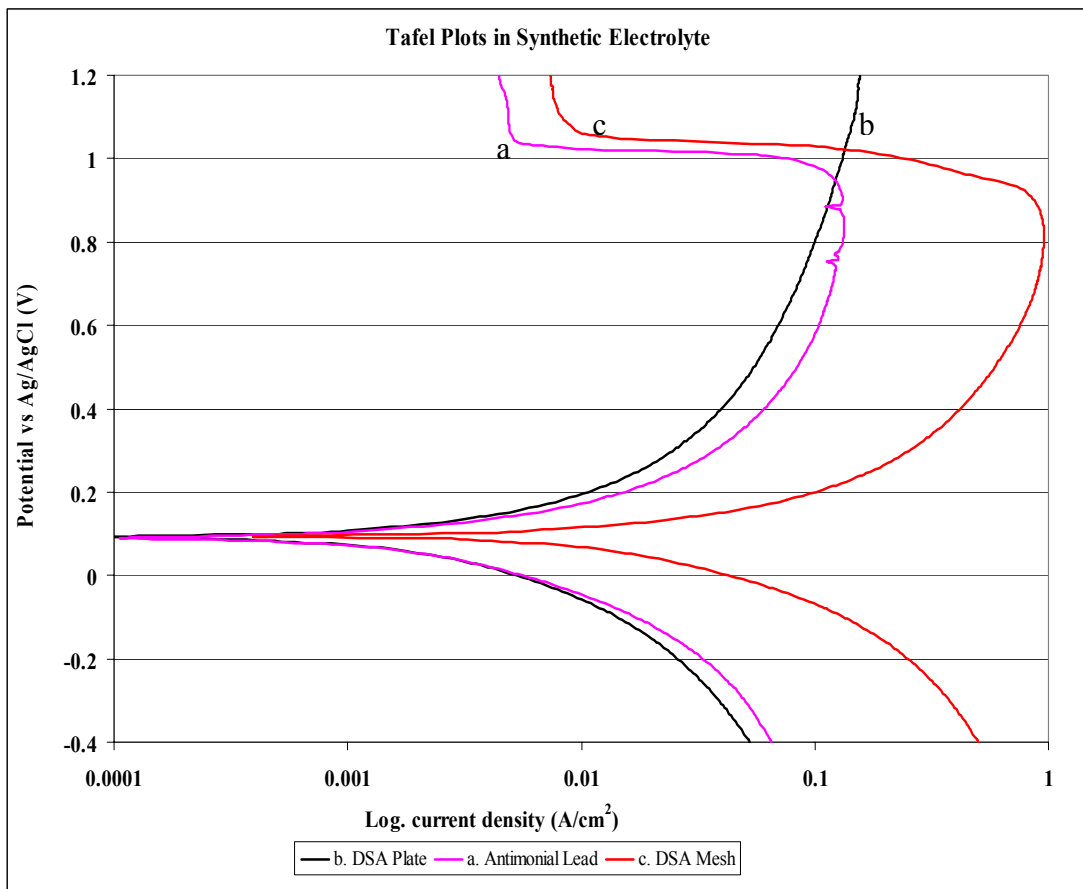


**Figure 5.2: Tafel Plots for DSA and Lead Alloy Anodes in Synthetic Electrolyte**



Unlike the lead alloy and DSA mesh anodes, the DSA plate does not show passivation tendencies, in the potential range of -0.4 V to 1.2 V despite it having the same composition as the mesh anode. Only the active and pseudo-passive behaviour is evident. However, in the potential range of -0.4 V to 1.4 V the DSA plate anode also shows active-passive behaviour as shown in figure 5.3 below.

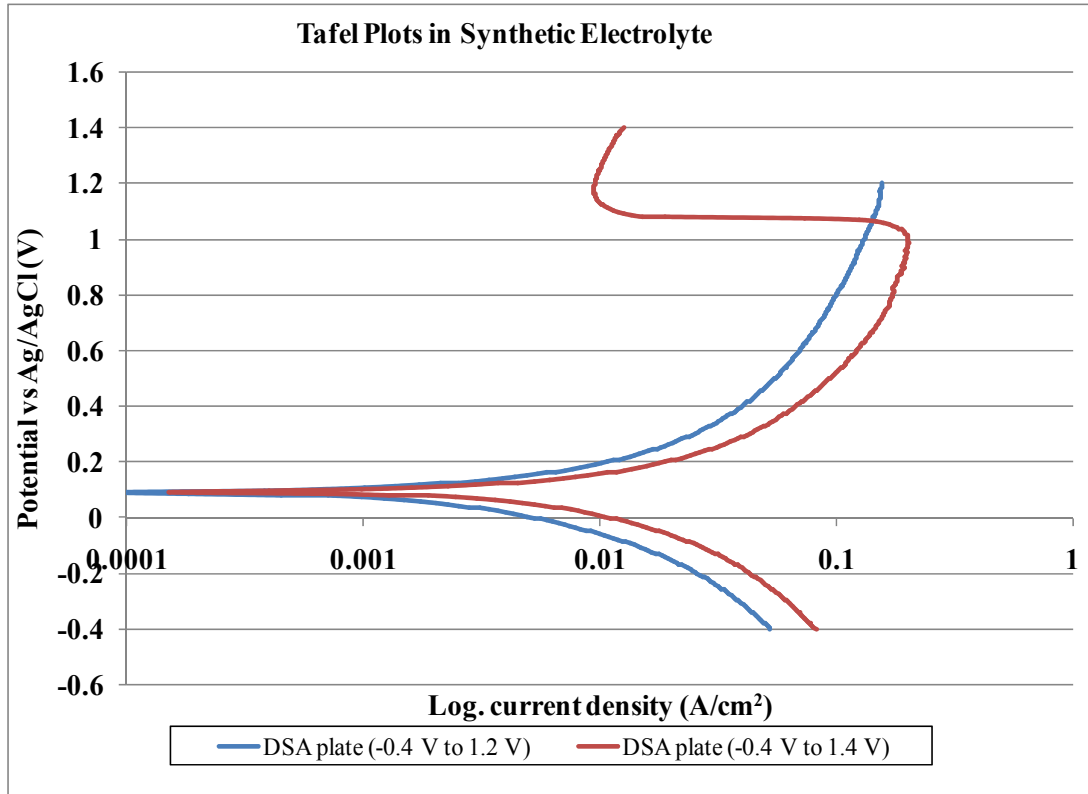


Figure 5.3: Tafel Plots for DSA Plate in the Potential range 0.4 V to 1.2 V and -0.4 V to 1.4 V in Synthetic Electrolyte.

There has been no documented data on the behaviours of dimensionally stable mesh and plate anodes. However, despite the two anodes having similar chemical composition, the differences in behaviour may be attributed to the adhesion of the coating, which in plate anodes could probably be higher than in mesh anodes. As a result mesh anodes are likely to passivate earlier than plate anodes under the same operating conditions.

The passivation of the DSA anodes is attributed to the formation of a thin, insulating layer of TiO<sub>2</sub> at the interface between the metallic base and the active coating. The passivation is also indicative of coating consumption which exposes the titanium substrate to the electrolyte.

Table 5.1 shows that the lowest corrosion rate (maximum polarisation resistance) was observed for the DSA plate anode followed by the DSA mesh anode and lastly the lead anode, which is in agreement with open circuit potential measurements. The corrosion rates for the lead and DSA mesh anodes were 210% and 197% greater than the corrosion rate for the DSA plate anode.

The high corrosion rate of the lead anode shows that the anode is associated with the problem of physical degradation which has an adverse effect on anode life and cathode purity (Weems *et al.*, 2005). For the DSA mesh anode, more area is available for corrosion to occur due to the anode's large working area, hence the high corrosion rate.

**Table 5.1: Linear Polarisation Parameters**

| Anode Material               | DSA Plate | DSA Mesh | Lead Alloy (Pb/Sb) |
|------------------------------|-----------|----------|--------------------|
| $i_{corr}$ (A)               | 7.434E-5  | 1.031E-3 | 1.13E-4            |
| $E_{corr, obs}$ (V)          | 0.088     | 0.082    | 0.090              |
| $I$ (A/cm <sup>2</sup> )     | 9.29E-5   | 2.75E-4  | 1.13E-4            |
| $\beta_c$ (V/dec)            | 0.0034    | 0.0220   | 0.0031             |
| $\beta_a$ (V/dec)            | 0.0081    | 0.0800   | 0.0076             |
| $R_p$ (ohm)                  | 13.89     | 3.61     | 8.46               |
| Begin potential              | 0.088     | 0.079    | 0.091              |
| End potential (V)            | 0.093     | 0.089    | 0.096              |
| Equivalent weight (g)        | 11.97     | 11.97    | 99.41              |
| Density (g/cm <sup>3</sup> ) | 4.54      | 4.54     | 14.82              |
| Corrosion rate (mm/year)     | 0.80      | 2.37     | 2.48               |

Table 5.1 also shows that the anodic ( $\beta_a$ ) and cathodic ( $\beta_c$ ) Tafel constants for the DSA mesh anode were an order of magnitude greater than those for the DSA plate and lead anodes. These higher Tafel constant values may have been due to surface film formation on the DSA mesh anode as a result of passivation. This resulted in high film resistances being encountered at the electrolyte/electrode interface (Kear and Walsh, 2005). The lead anode was associated with low Tafel constants while for the DSA plate anode, no passivation layer was detected as indicated in figure 5.2.

### 5.1.3 Chronopotentiometry (galvanostatic)

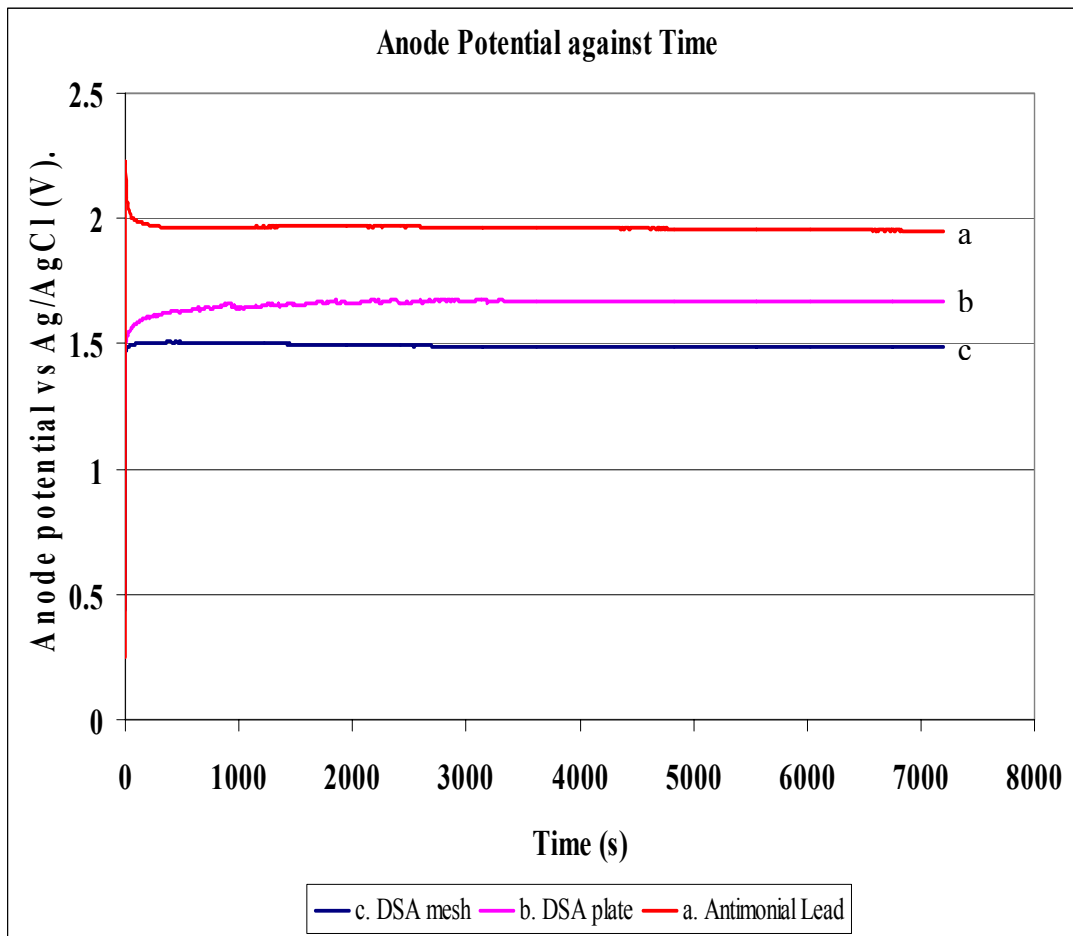


Figure 5.4: Anode potential-time curves for Pb-6% Sb and Ti-Ta<sub>2</sub>O<sub>5</sub>/IrO<sub>2</sub> (plate and mesh) in 55 g/l Cu and 100 g/l H<sub>2</sub>SO<sub>4</sub> at 190 A/m<sup>2</sup>

Figure 5.4 compares the performance of the DSA anodes (Ti-Ta<sub>2</sub>O<sub>5</sub>/IrO<sub>2</sub>) and the traditional Pb-6%Sb under oxygen evolution conditions. Since in the entire investigation the bath composition, temperature, electrode distance, current density and cathode material were kept constant, the differences observed in the anode potentials may be attributed to the nature of these anode materials.

In this study, the lead anode is found to be associated with the highest anode potential of 1.97 V. This may be due to higher oxygen over-potential with this anode material. When the anode potentials for the DSA plate and mesh anodes were compared with that of the lead anode they were found to be 19% and 24% lower, respectively. Anode potential is a major component of the cell voltage, also making it a significant cost issue in the electrowinning process. Thus, if lead anodes are replaced by DSA anodes which have low anode potentials, energy savings around 19% to 24% could be realised. The anode potentials for the DSA anodes were observed to increase with time until they reached constant values while that for the lead anode decreased until it also attained a constant potential. For both DSA anodes, this can be a result of some erosion of the porous outer layer of the active coating due to intense oxygen evolution (Mraz and Krysa, 1994) while for the lead anode this could be attributed to the passive film of PbO<sub>2</sub>.

*5.1.3.1 Determination of current efficiency*

Current efficiency was also determined in each of the three cells from the weight gained by the cathode as indicated by equation 2.22 below:

$$\epsilon_c(I) = \frac{nF\Delta W}{ItM} \dots\dots\dots 2.22$$

Where,

$\epsilon_c$  - Cathode current efficiency.

$\Delta W$  - Weight gained by cathode.

F - Faraday's constant.

I - Applied current

M - Atomic weight of copper

t - Time taken for the copper to be deposited

n – Number of electrons participating in the reaction (2 electrons)

In this study, fresh anodes were used.

**Table 5.2: Determination of Current Efficiency**

| <b>Pb/Sb</b>  | <b>Value</b> |
|---|--------------|
| Initial weight of cathode (g)                                 | 18.885       |
| Final weight of cathode (g)                                   | 18.929       |
| Weight gained by the cathode (g)                              | 0.044        |
| Area of specimen (cm <sup>2</sup> )                           | 1.00         |
| Current density (A/cm <sup>2</sup> )                          | 0.019        |
| Current (A)   | 0.019        |
| <b>Current efficiency (%)</b>                                 | <b>97.6</b>  |
| <b>Ti-Ta<sub>2</sub>O<sub>5</sub>/IrO<sub>2</sub> (plate)</b> |              |
| Initial weight of cathode (g)                                 | 19.653       |
| Final weight of cathode (g)                                   | 19.713       |
| Weight gained by the cathode (g)                              | 0.060        |
| Area of specimen (cm <sup>2</sup> )                           | 1.36         |
| Current density (A/cm <sup>2</sup> )                          | 0.019        |
| Current (A)   | 0.026        |
| <b>Current efficiency (%)</b>                                 | <b>97.9</b>  |
| <b>Ti-Ta<sub>2</sub>O<sub>5</sub>/IrO<sub>2</sub> (mesh)</b>  |              |
| Initial weight of cathode (g)                                 | 19.653       |
| Final weight of cathode (g)                                   | 19.714       |
| Weight gained by the cathode (g)                              | 0.061        |
| True area of specimen (cm <sup>2</sup> )                      | 1.90         |
| Current density (A/cm <sup>2</sup> )                          | 0.019        |
| Current (A)   | 0.036        |
| <b>Current efficiency (%)</b>                                 | <b>97.9</b>  |

**Table 5.3: Effect of anode substrates on anode potential and deposit morphology**

| Electrode material | Anode potential (V)     | Cathode Current Efficiency (%) | Deposit morphology           |
|--------------------|-------------------------|--------------------------------|------------------------------|
| DSA plate          | 1.67, 1.67 <sup>a</sup> | 97.9                           | Bright, smooth, compact      |
| DSA mesh           | 1.50, 1.51 <sup>a</sup> | 97.9                           | Bright, smooth, compact      |
| Antimonial Lead    | 1.96, 1.95 <sup>a</sup> | 97.6                           | Dull, adheres to the surface |

Cu concentration, 55 g/L; H<sub>2</sub>SO<sub>4</sub> concentration, 100 g/L; current density, 190 A/m<sup>2</sup>; bath temperature, 55 °C; duration of electrolysis, 2 h.

<sup>a</sup> Data obtained in 1 h of electrolysis.

The results from tables 5.2 and 5.3 indicate that there is an insignificant difference between all the anodes in terms of initial current efficiency in synthetic electrolyte. These results are substantiated by the work reported by Panda and Das (2001).

#### 5.1.3.2 Electrolyte contamination

The electrode stability was also evaluated under galvanostatic conditions in 55 g/l Cu and 100 g/l H<sub>2</sub>SO<sub>4</sub>. The electrolytes were analysed for lead, titanium, iridium and tantalum contamination after two hours of galvanostatic chronopotentiometry using the Atomic Absorption Spectrometer. The results are shown in tables 5.4 and 5.5 below for the three runs carried out.

**Table 5.4: Concentration of Lead in the Electrolyte and Standard Deviations**

| SAMPLE No.                | Run 1               | Run 2 | Run 3 |
|---------------------------|---------------------|-------|-------|
|                           | CONCENTRATION (ppm) |       |       |
| 1                         | 8.8                 | 8.5   | 8.5   |
| 2                         | 6.8                 | 7.0   | 6.8   |
| 3                         | 7.1                 | 6.9   | 7.3   |
| <b>AVERAGE</b>            | 7.6                 | 7.5   | 7.5   |
| <b>STANDARD DEVIATION</b> | 0.9                 | 0.7   | 0.7   |

**Table 5.5: Concentrations of Titanium, Tantalum and Iridium in the Electrolyte**

| <b>SAMPLE</b>  | <b>1 (containing DSA plate anode)</b> |           |           | <b>2 (containing DSA mesh anode)</b> |           |           |
|----------------|---------------------------------------|-----------|-----------|--------------------------------------|-----------|-----------|
|                | <b>CONCENTRATION (ppm)</b>            |           |           |                                      |           |           |
| <b>ELEMENT</b> | <b>Ti</b>                             | <b>Ta</b> | <b>Ir</b> | <b>Ti</b>                            | <b>Ta</b> | <b>Ir</b> |
| Run 1          | 0.017                                 | 0.001     | 0.003     | 0.015                                | 0.000     | 0.004     |
| Run 2          | 0.017                                 | 0.001     | 0.003     | 0.015                                | 0.000     | 0.004     |
| Run 3          | 0.017                                 | 0.001     | 0.003     | 0.016                                | 0.000     | 0.004     |
| <b>AVERAGE</b> | 0.017                                 | 0.001     | 0.003     | 0.015                                | 0.000     | 0.004     |

The results in table 5.4 indicate that during electrowinning of copper using lead alloy anodes, anodic dissolution of lead occurs. The lead ions in solution are most likely to result in cathode contamination when they form lead sulphate which in turn attaches to the growing copper deposit. Dissolution of the lead alloy anodes may also contribute to a reduced life span for the anodes and varying current distribution due to changing electrode thickness and flatness. The resultant lead sludge that must be removed from the cells and handled with environmental constraints is also a major environmental problem.

From table 5.5 the presence of traces of tantalum (coating stabiliser) and iridium (active component) shows that during electrowinning operations using DSA anodes, some loss of coating occurs. The amount of iridium loss is 3 times greater than the tantalum loss. This is attributed to the high stability of tantalum in the coating. Traces of the titanium substrate were also detected in the samples analysed. The amount of iridium loss in the electrochemical cell containing the DSA mesh anode was 33% greater than the iridium loss in the cell containing the DSA plate specimen. This can be attributed to the large electrochemically active surface area (EASA) characteristic of mesh anodes. A greater EASA, results in more area being available for corrosion. Hu and co-workers (1996) investigated the degradation mechanism of the Ti - (70%) IrO<sub>2</sub>/ (30%) Ta<sub>2</sub>O<sub>5</sub> anodes in H<sub>2</sub>SO<sub>4</sub> and found out that the deactivation mechanism of

these anodes during electrolysis was in three stages, namely; active, stable and de-active. In the first two stages, the dissolution of the coating dominated (with IrO<sub>2</sub> component preferential loss over Ta<sub>2</sub>O<sub>5</sub>).

#### 5.1.4 Cyclic voltammetry

Cyclic voltammetry was carried out in order to assess the surface characteristics and determine the electrochemically active surface area (EASA) for the anodes. The voltammetric charge, obtained usually by integration between hydrogen and oxygen gas evolution region of a cyclic voltammetric curve, has been proven to be proportional to the EASA of metal oxide electrode, and thought to be able to represent the number of electrochemically active sites (Hu *et al.*, 1996).

##### 5.1.4.1 *Cyclic voltammograms for lead anodes*

For the lead anode, curves were generated over a potential range of 0 to 2 V and -0.5 to 2.2 V; ranges that cover the reactions from metallic lead, Pb<sup>0</sup> to Pb (IV) and oxygen evolution in 0.5 M sulphuric acid. Figure 5.5 and 5.6 characterise the electrochemical behaviour of Pb–Sb anodes in synthetic electrolyte at a scan rate of 2 mV/s.

All curves show two anodic peaks at scanning in a positive direction while only figure 5.5 shows two cathodic peaks at scanning in the negative direction. The first process which takes place is the anodic dissolution of lead and formation of a PbSO<sub>4</sub> layer, which has passivating properties, followed by a wide passive region. As the anodic potential increases to about 1.75 V, lead (IV) oxide forms at the surface of the electrode, and with a further increase in the potential, O<sub>2</sub> evolution commences around 1.9 V. Oxygen evolution intensifies with the increase in cycle number. The cathodic peak which appeared at 1.4 V in the reverse scan could be attributed to the reduction of PbO<sub>2</sub> formed on the surface, back into PbSO<sub>4</sub>. For figure 5.5, another



small cathodic peak is evident at -0.5 V. This is attributed to the reduction of  $\text{PbSO}_4$  to Pb.

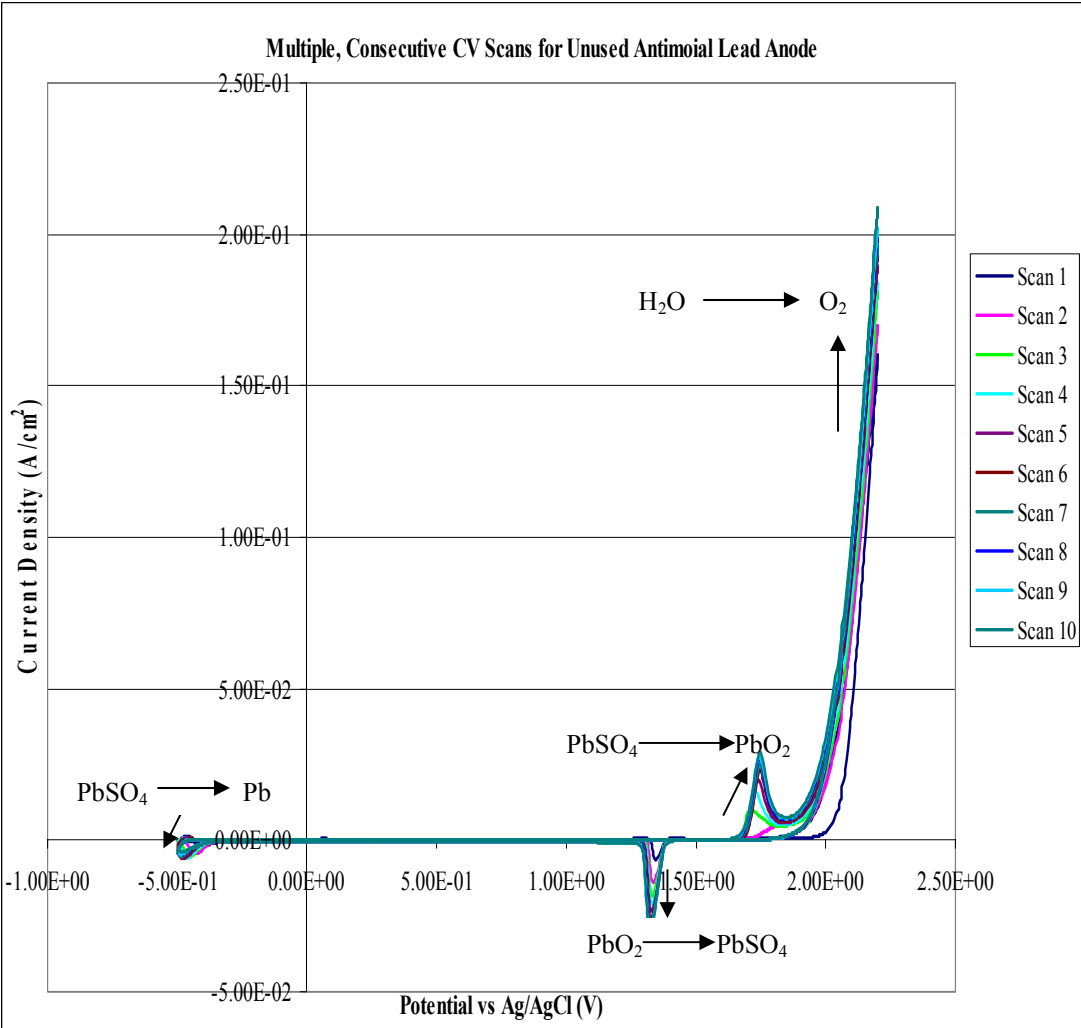


**Figure 5.5: Cyclic Voltammograms for the Lead Alloy Anode in the Potential Range -0.5 to 2.2 V.**

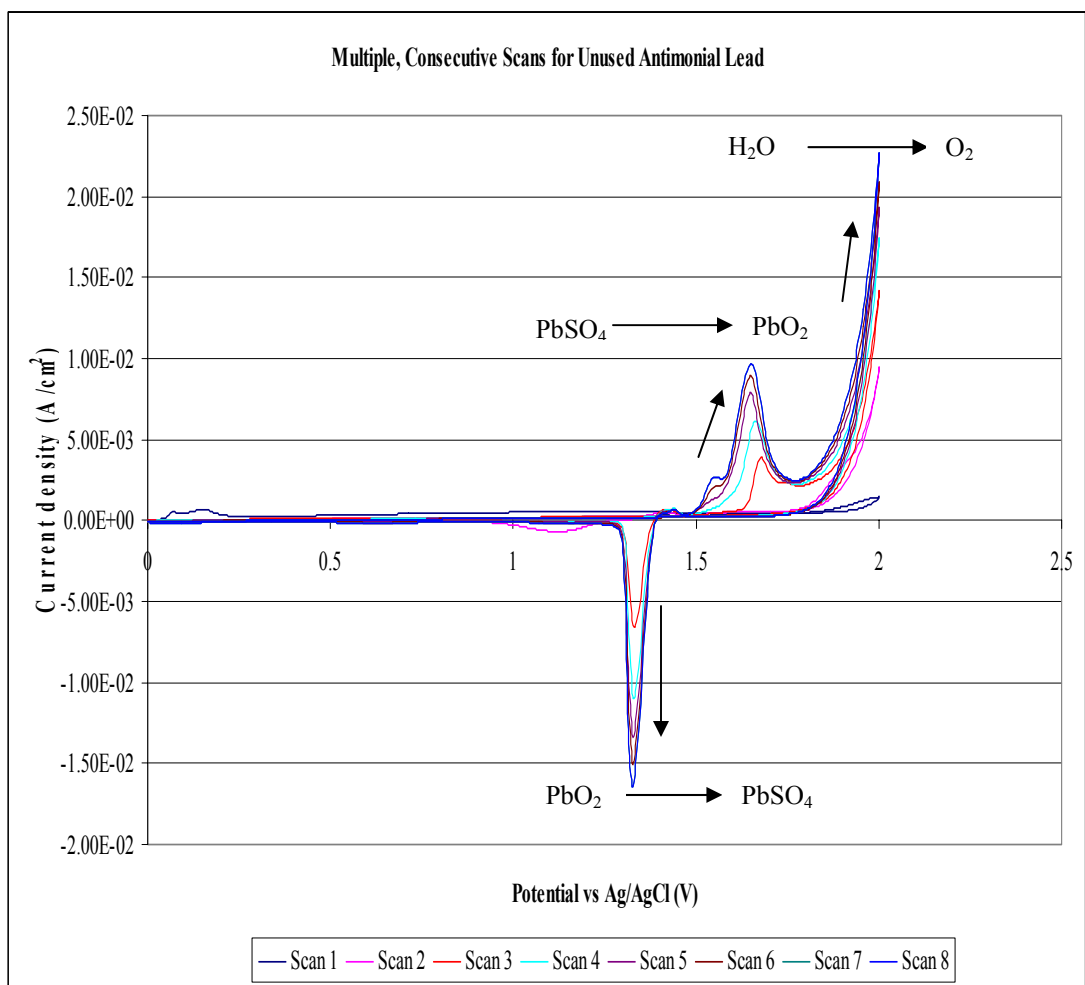


**Figure 5.6: Cyclic Voltammograms for the Lead Alloy Anode in the Potential Range 0 to 2.2 V.**

#### 5.1.4.2 Cyclic voltammograms for DSA anodes

Voltammetric curves for these anodes were recorded between -0.6 to 1.5 V in 0.5 M sulphuric acid at a scan rate of 100 mV/s.

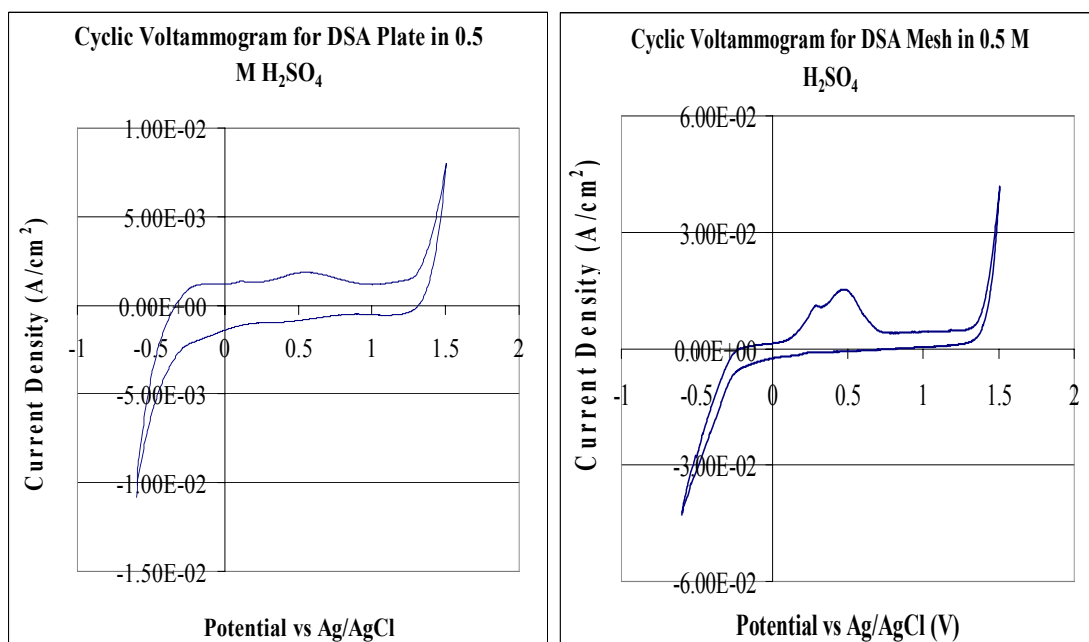


**Figure 5.7: Cyclic Voltammograms for Ti/IrO<sub>2</sub>-Ta<sub>2</sub>O<sub>5</sub> Electrodes in 0.5 M H<sub>2</sub>SO<sub>4</sub> at a Scan Rate of 100 mV/s.**

Figure 5.7 shows the CV curves for DSA mesh and plate anodes in 0.5 M H<sub>2</sub>SO<sub>4</sub> solution. These curves were recorded in the potential range -0.6 to 1.5 V (the oxygen evolution potential). It can be seen that the CV curves have a similar shape. Several current peaks are present in both voltammograms. The anodic peak at a potential of  $\approx$  1.5 V is due to the oxygen evolution reaction, while the cathodic peak at a potential of about -0.6 V is indicative of intensive hydrogen evolution. A pair of peaks observed at potentials between 0.3 and 0.5 V for the DSA mesh is likely to be a result of the redox transition, Ir(III)/Ir(IV) while for the DSA plate a smaller current peak appearing around 0.5 V is also attributed to the same redox transition as that of the mesh. The broad nature of these peaks is attributed to the heterogeneity of the surface active sites on the electrodes.

#### 5.1.4.3 Electrochemically active surface area for the anode specimens

Table 5.5 below shows the voltammetric charges  $q^*$  measured at a scan rate of 20 mV/s for the three anode specimens; in the potential range 0 to 1.5 V.

The mesh has the greatest value of  $q^*$ . Since the voltammetric charge has been proven to be proportional to the EASA of metal oxide electrode, and thought to be able to represent the number of electrochemically active sites, the results in table 5.6 indicate that the mesh has the largest working area for oxygen evolution. This may be attributed to its structure. In electrode processes, a larger working area results in increased catalytic activity. The high activity facilitates lowering of the effective current density, resulting in reduced anode potential (Kulandaisamy *et al.*, 1997).

**Table 5.6: Voltammetric Charges for the Anode Specimens**

| Anode Specimen  | $q^*$ (mC/cm <sup>2</sup> ) |
|---|-----------------------------|
| Ti/IrO <sub>2</sub> -Ta <sub>2</sub> O <sub>5</sub> Plate | 51                          |
| Ti/IrO <sub>2</sub> -Ta <sub>2</sub> O <sub>5</sub> Mesh  | 226                         |
| Pb/ 6 % Sb  | 26                          |

#### 5.1.4.4 Effect of continuous cycling on voltammetric charge

Figures 5.8, 5.9 and 5.10 show the variation of voltammetric charge with continuous cycling for the DSA mesh and plate and the lead anode specimens respectively.

The voltammetric charge  $q^*$ , calculated by graphical integration of the CV curves in figure 5.7 in the range between 0 and 1.5 V, increases with cycling time. In the first 40 cycles for the plate and 20 cycles for the mesh,  $q^*$  increases, after which there is little change in the voltammetric charge. This suggests that after these cycles, the DSA anode specimens attain a stable condition.

Xu and Scantlebury (2003) reported that such behaviour is typical of stable oxide electrodes. The increase in  $q^*$  is attributed to the further hydration and activation of the inside pores or microcracks which are not activated in the first few cycles. The cracked, porous structure of the oxide coating is shown on the SEM micrograph in figure 5.23. Of the two DSA anodes, figure 5.8 indicates that the mesh stabilises faster (after 20 cycles) since it has a greater EASA which consequently results in shorter hydration time of the inner layer.

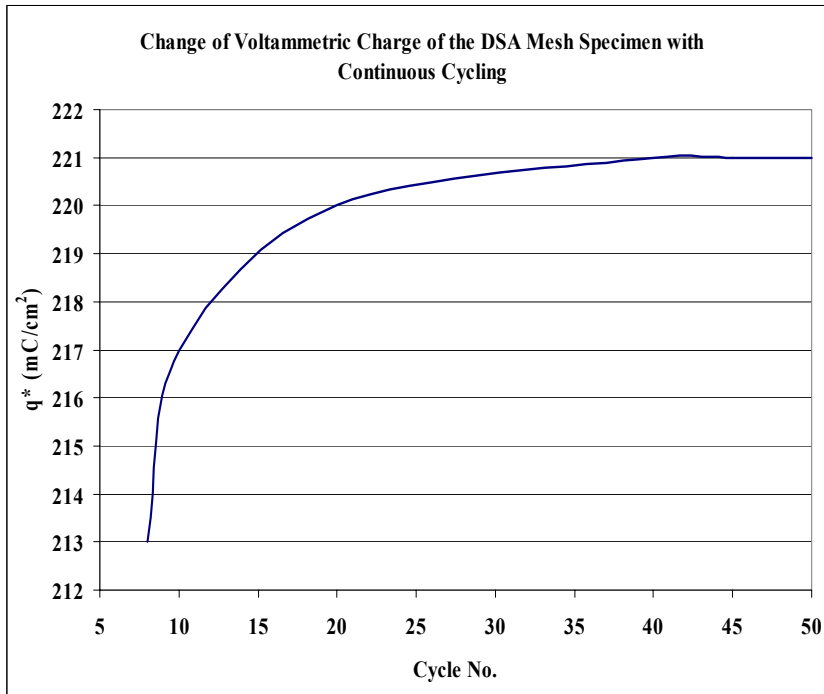


**Figure 5.8: Change of Voltammetric Charge of the DSA Mesh Specimen with Continuous Cycling.**

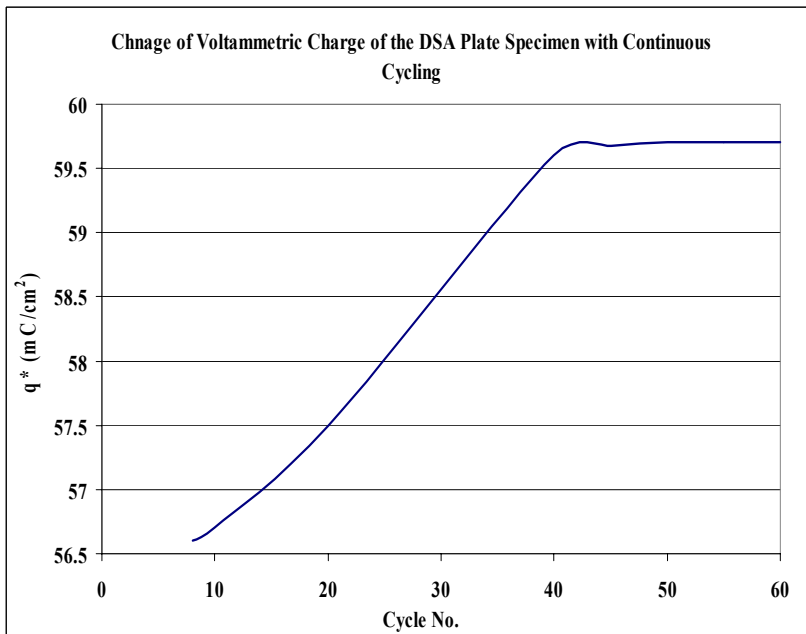


**Figure 5.9: Change of Voltammetric Charge of the DSA Plate Specimen with Continuous Cycling.**

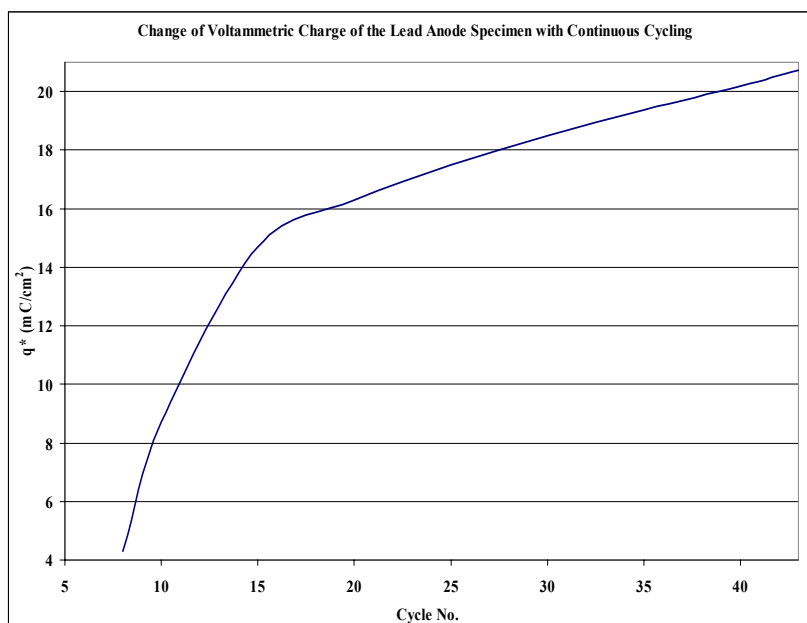


**Figure 5.10: Change of Voltammetric Charge of the Lead Anode Specimen with Continuous Cycling.**

The voltammetric charge  $q^*$ , calculated by graphical integration of the CV curve in figure 5.6 in the range between 0 and 2.0 V, also increases with cycling times for the lead anode specimen. In the first 15 cycles there is a rapid increase in  $q^*$ , after which there is a steady continuous increase in voltammetric charge which can be attributed to the formation of a passive film of porous lead (IV) oxide as cycling progresses.

#### 5.1.4.5 Determination of double layer capacitance

The value of the double layer capacitance ( $C_{dl}$ ) depends on many variables including electrode potential, temperature, ionic concentrations and types of ions, oxide layers and electrode roughness. For the DSA anode materials the double layer capacitance was determined by evaluating the slopes of the graphs of current density against scan rate at a fixed potential at which no main redox transitions occurred on the surface, according to the method proposed by Xu and Scantlebury (2003). In this study a potential of 1.0 V vs Ag/AgCl was selected to give the graphs below.

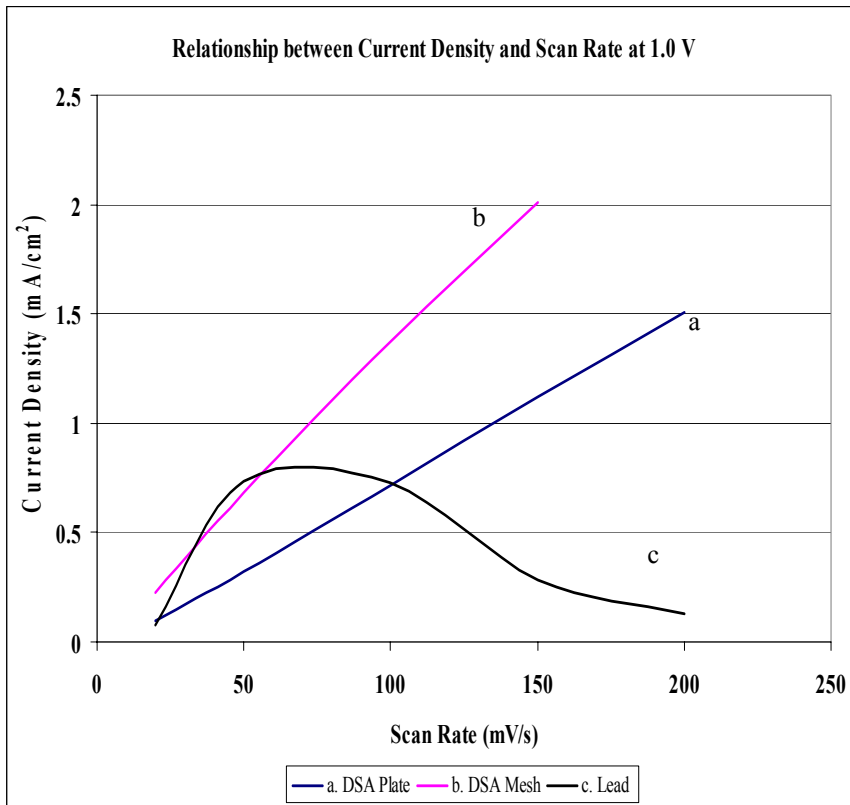


**Figure 5.11: Relationship between Current Density and Scan Rate at a Fixed Potential of 1.0 V for Ti/ IrO<sub>2</sub>-Ta<sub>2</sub>O<sub>5</sub> and Pb/Sb Anodes.**

Figure 5.11 above indicates that a linear relationship exists between current density and scan rate for the DSA anodes. For the lead anode specimen, the relationship between current density and scan rate showed a large deviation from linearity and for this reason, the double layer capacitance,  $C_{dl}$  was replaced by the constant phase element (CPE). Similarly to the anodic charge,  $q^*$ , the DSA mesh has a higher double layer capacitance and as such  $C_{dl}$  can be used to describe the EASA of each anode. A linear relationship has been found to exist between the anodic charge  $q$ , and the double layer capacitance,  $C_{dl}$  as indicated in figure 5.12 (Xu and Scantlebury, 2003).

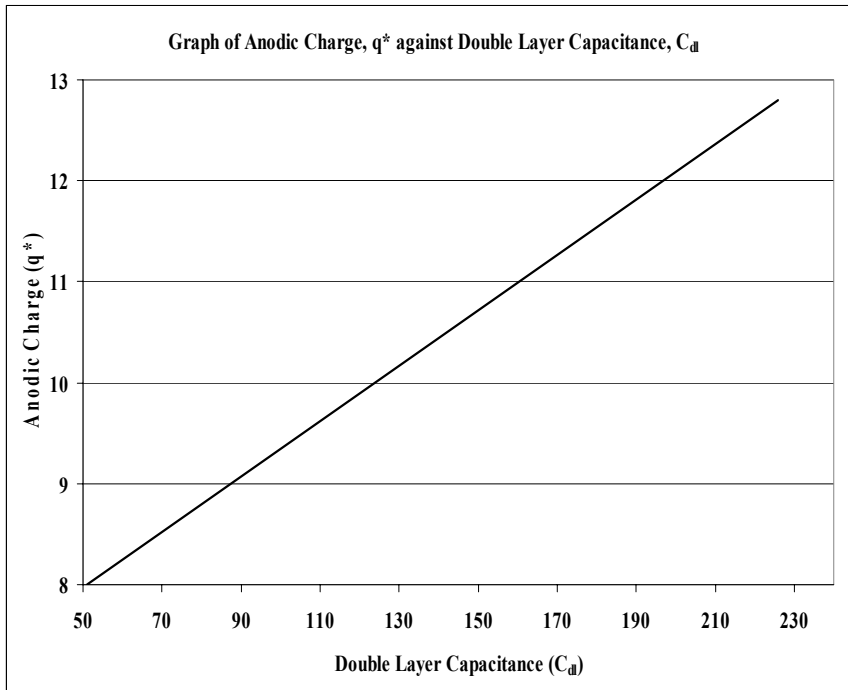


**Figure 5.12: Typical Graph of Anodic Charge,  $q^*$  against Double Layer Capacitance,  $C_{dl}$  for a DSA Anode.**

The roughness factor was also evaluated for the DSA anode specimens by dividing the values of the double layer capacitance with  $60 \mu\text{Fcm}^{-2}$ . This is the value for a smooth and compact  $\text{TiO}_2$  film with a rutile structure (Lassali *et al.*, 1997). Table 5.7 shows the capacitances and roughness factors for the DSA anodes. The RF value for the  $\text{Ti}/\text{IrO}_2\text{-Ta}_2\text{O}_5$  mesh is 60% greater than that of the  $\text{Ti}/\text{IrO}_2\text{-Ta}_2\text{O}_5$  plate. This suggests that both porous morphology and the structure of oxide anodes have an influence on the surface roughness and consequently the electrochemically active surface area. RF values in the range 83-395 for the oxide electrodes have been reported by Xu and Scantlebury (2003).

**Table 5.7: Double Layer Capacitance and Roughness Factor for DSA Anodes**

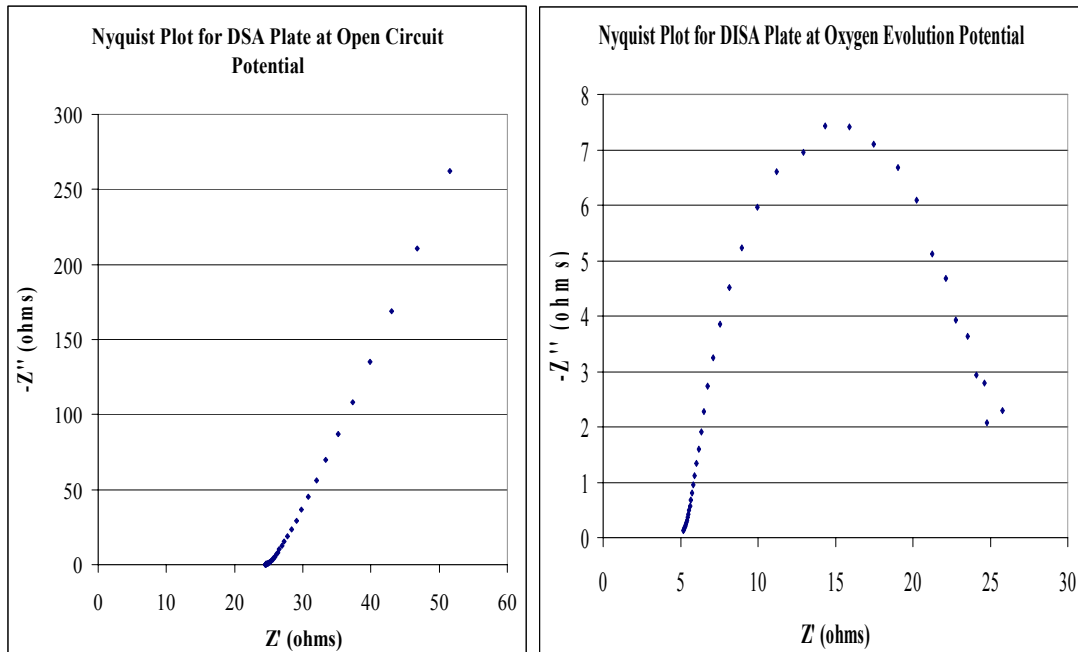
| Electrode  | $C_{dl}$ ( $\text{mFcm}^{-2}$ ) | Roughness factor (RF) |
|--|---------------------------------|-----------------------|
| $\text{Ti}/\text{IrO}_2\text{-Ta}_2\text{O}_5$ plate | 8.0                             | 133                   |
| $\text{Ti}/\text{IrO}_2\text{-Ta}_2\text{O}_5$ mesh  | 12.8                            | 213                   |



### 5.1.5 Electrochemical impedance spectroscopy

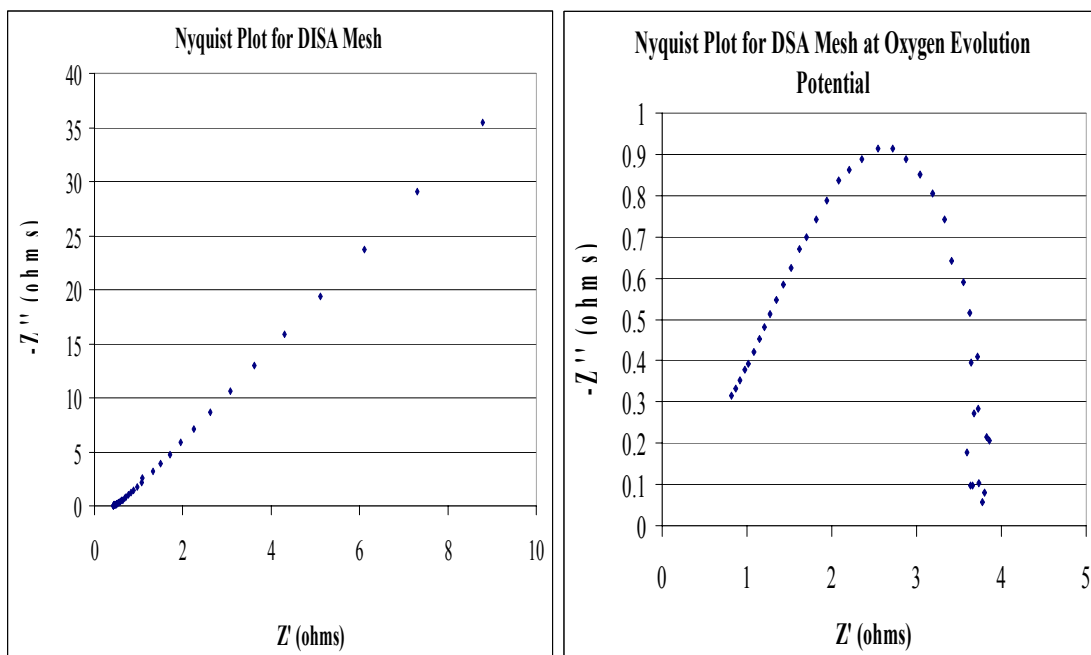
Impedance measurements were carried out in order to provide supportive evidence for the above results. The tests were carried out at the open circuit potential for each material and the potential for oxygen evolution as determined from cyclic polarisation and galvanostatic chronopotentiometry measurements. The impedance behaviour of the metal specimens was expressed in Nyquist plots of  $Z''$  ( $\omega$ ) as a function of  $Z'$  ( $\omega$ ).

Figure 5.13 shows the Nyquist plots for the DSA plate anode at open circuit potential and oxygen evolution potential.



**Figure 5.13: Nyquist Plots for the DSA Plate at Open Circuit Potential and Oxygen Evolution Potential.**

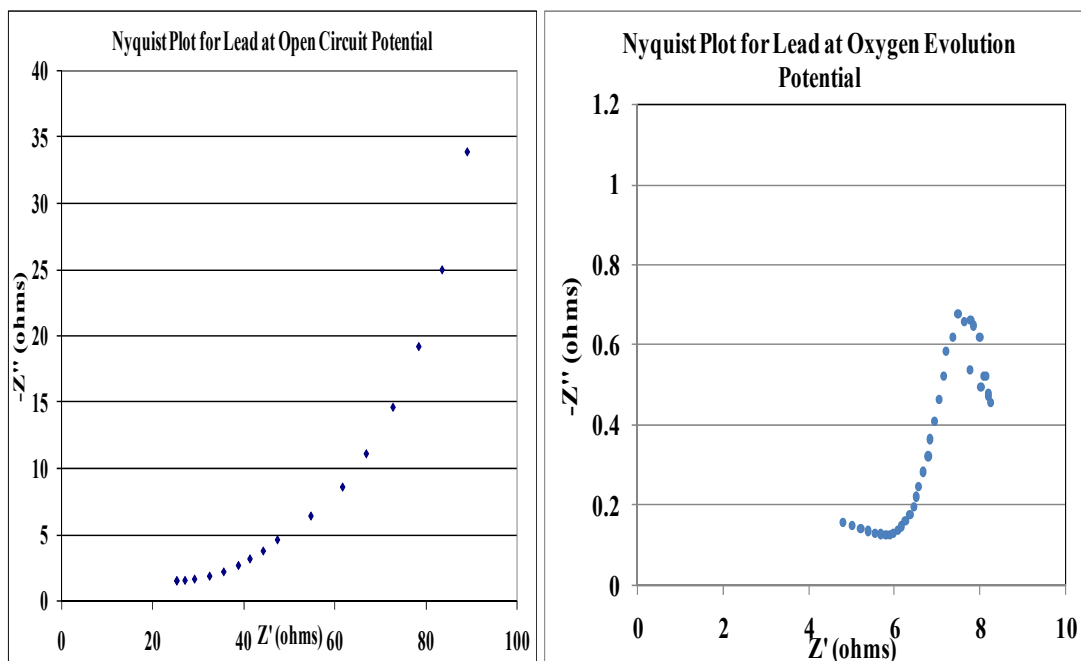
Figure 5.14 shows the Nyquist plots for the DSA mesh anode at open circuit potential and oxygen evolution potential.



**Figure 5.14: Nyquist Plots for the DSA Mesh Anode at Open Circuit Potential and Oxygen Evolution Potential.**

It can be noted that the Nyquist plots for the DSAs are similar in shape.

Figure 5.15 shows the Nyquist plots for the lead anode at open circuit potential and oxygen evolution potential.



**5.15: Nyquist Plots for the Lead Anode at Open Circuit Potential and Oxygen Evolution Potential**

Tables 5.8 and 5.9 give the equivalent circuit parameters evaluated from the Nyquist plots for all the anodes.

**Table 5.8: Equivalent Circuit Parameters for DSA Plate and Mesh Anodes and the Lead Anode at Open Circuit Potential**

| Anode     | Potential (V) | $R_p$ (ohm)        | CPE (F)               | n    |
|-----------|---------------|--------------------|-----------------------|------|
| DSA plate | 0.72          | $1.33 \times 10^4$ | $5.90 \times 10^{-7}$ | 1.08 |
| DSA mesh  | 0.36          | $2.76 \times 10^3$ | $1.98 \times 10^{-6}$ | 1.56 |
| lead      | 0.08          | $5.24 \times 10^2$ | $1.67 \times 10^{-7}$ | 0.23 |

**Table 5.9: Equivalent Circuit Parameters for DSA Plate and Mesh Anodes and the Lead Anode at Oxygen Evolution Potential**

| Anode     | $E_p$ (V) | $R_s$ (ohm)           | $R_p$ (ohm)        | CPE (F)               | n    |
|-----------|-----------|-----------------------|--------------------|-----------------------|------|
| DSA plate | 1.50      | $0.51 \times 10^1$    | $2.19 \times 10^1$ | $9.26 \times 10^{-3}$ | 0.60 |
| DSA mesh  | 1.50      | $5.90 \times 10^{-1}$ | $0.33 \times 10^1$ | $1.32 \times 10^{-2}$ | 0.67 |
| lead      | 1.96      | $0.48 \times 10^1$    | $0.87 \times 10^1$ | $7.76 \times 10^{-4}$ | 0.15 |

$E_{oc}$  – open circuit potential in volts.

$E_p$  – passivation potential in volts.

$R_s$  – solution resistance in ohms.

$R_p$  – polarisation resistance in ohms.

CPE (in Farads) is the constant phase element that depicts the double layer capacitance including surface roughness ( $Q_{dl,n}$ ).

$n$  – surface roughness

It can be seen from the tables that the polarisation resistance for all the anodes are higher at the open circuit potential compared to the oxygen evolution potential. This indicates that an unused anode in the case of lead anodes or an anode covered with an undamaged or fresh coating in the case of DSAs generally has very high corrosion resistance. At both potentials at which EIS studies were carried out, the polarisation resistance measured with the help of Nyquist plots clearly confirms the superior performance of the DSA plate anode with respect to its corrosion resistance over the DSA mesh and lead anodes.

Comparing the polarisation resistances in tables 5.1, 5.8 and 5.9, it can be observed that the resistances from linear polarisation tests in table 5.1, differ by orders of magnitude with those evaluated at open circuit potential (table 5.8) while they are of the same order with the resistances evaluated at the oxygen evolution potential (table 5.9). This is an indication that when investigating the polarisation resistance of an anode at the oxygen evolution potential, linear polarisation can also be used.

The variation of the constant phase element, CPE and surface roughness,  $n$  in tables 5.8 and 5.9 determined from impedance plots shows that the DSA mesh has the greatest working area among the three anode materials tested. These results are also in agreement with the values of double layer capacitance,  $C_{dl}$  and roughness factor shown in table 5.7.

Impedance tests were also carried out at different potentials in the region of the oxygen evolution reaction. The influence of the potentials on the complex plane plots is shown in figures 5.16, 5.17 and 5.18.

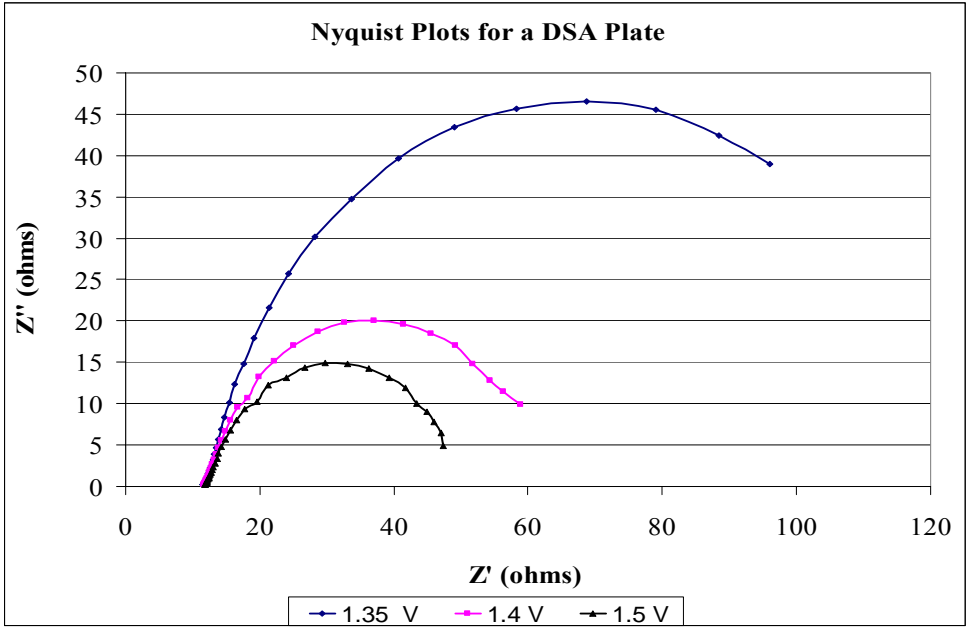


Figure 5.16: Nyquist Plots for a Ti/IrO<sub>2</sub>-Ta<sub>2</sub>O<sub>5</sub> Plate Anode in Synthetic Electrolyte.

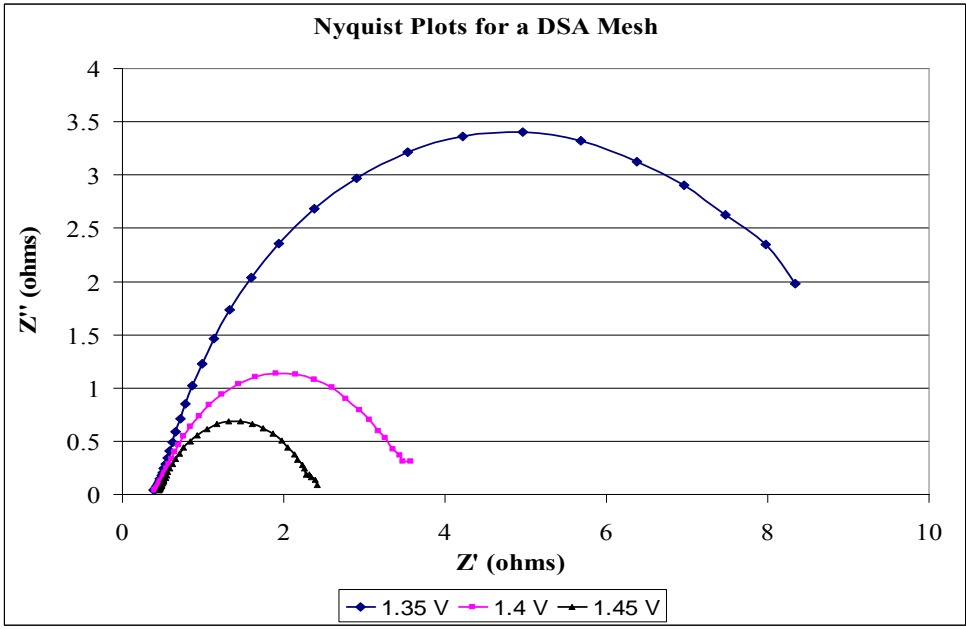


Figure 5.17: Nyquist Plots for a Ti/IrO<sub>2</sub>-Ta<sub>2</sub>O<sub>5</sub> Mesh Anode in Synthetic Electrolyte.

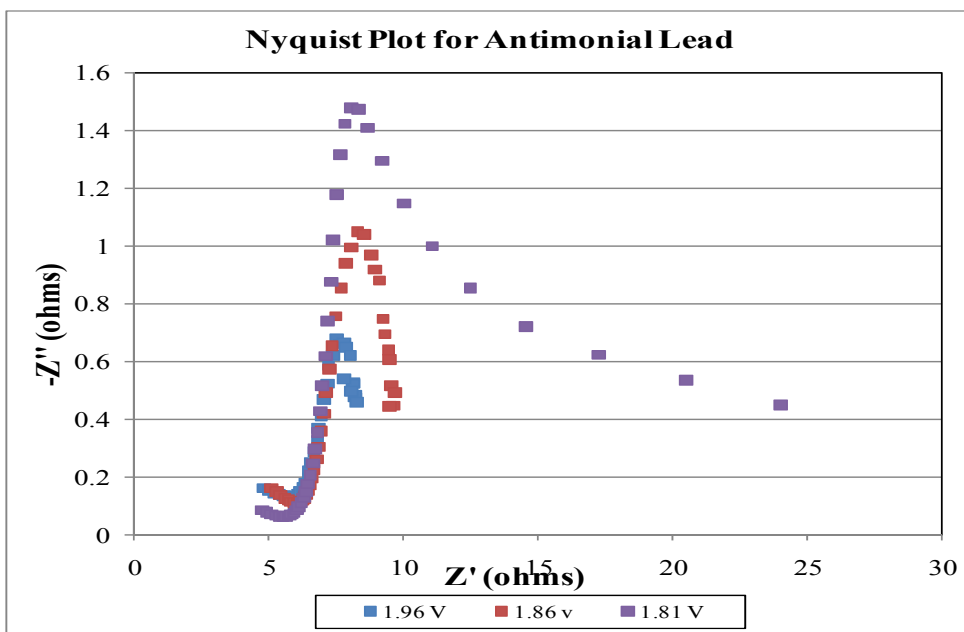


Figure 5.18: Nyquist Plots for a Pb/Sb Anode in Synthetic Electrolyte

The analysis of the low frequency domain of the impedance spectra for all the anodes shows a marked decrease in charge transfer,  $R_{ct}$  for oxygen evolution as the potential increases. The resistances are in the region of 120  $\Omega$ , 60  $\Omega$  and 40  $\Omega$  at potentials of 1.35 V, 1.40 V and 1.45 V respectively, for the plate. For the mesh, the resistances decrease in the order 10  $\Omega$ , 4  $\Omega$  and 2  $\Omega$  as potential increases while for the lead anode the resistances are in the region of 25  $\Omega$ , 10  $\Omega$  and 8  $\Omega$ . Comparing the values of  $R_{ct}$  for these anodes, the mesh has the lowest  $R_{ct}$  values. This may be attributed to better catalytic performance of the mesh as a result of its greater EASA.

### 5.1.6 Chronoamperometry (<1s)

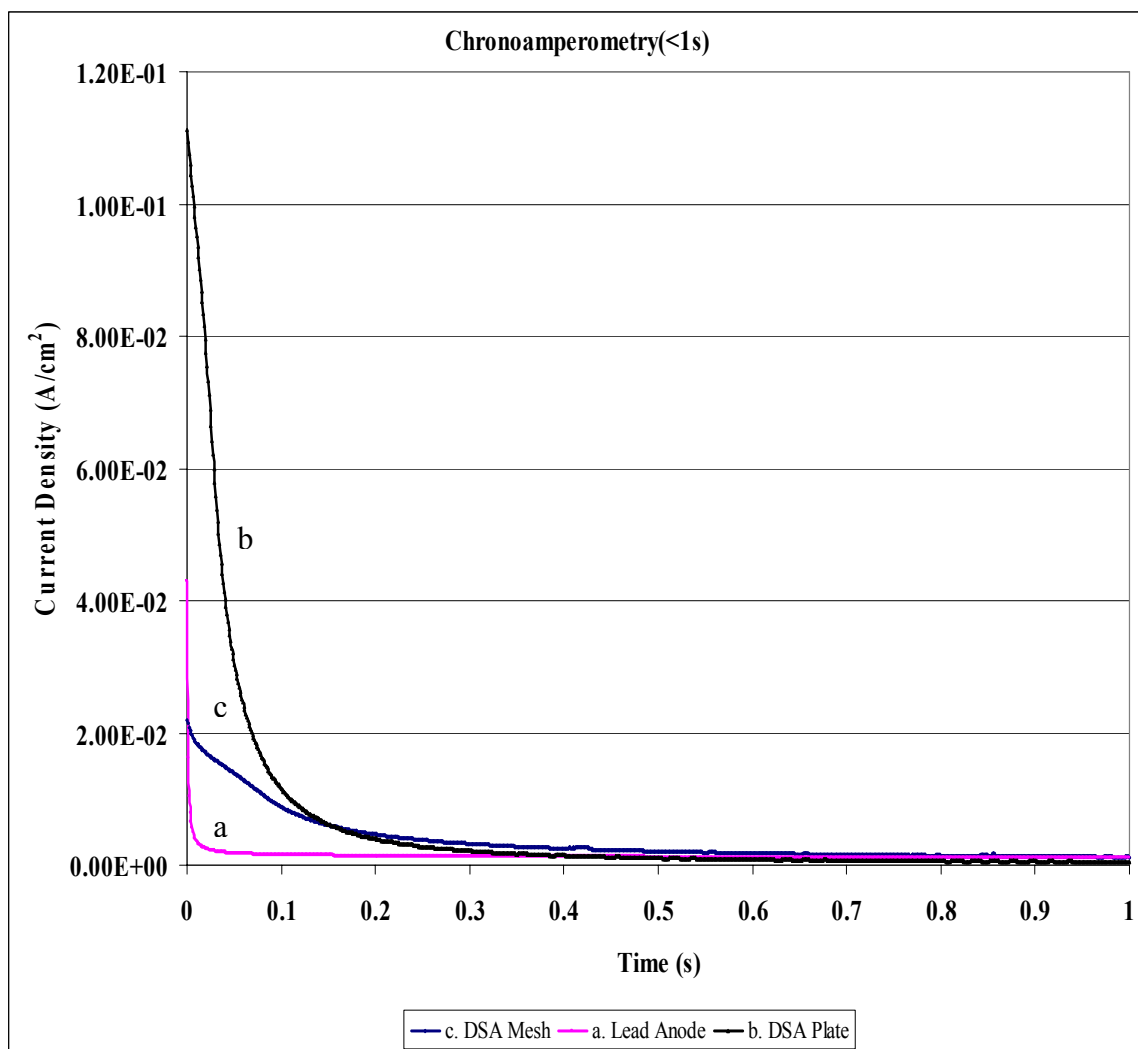


Figure 5.19: Chronoamperometry Tests in Synthetic Electrolyte

Chronoamperometry (1s) was used for the rapid characterisation of the three anodes. The results in synthetic electrolyte show that upon applying a potential step of 1.5 V, the resulting OER current initially decreases and quickly reaches a quasi steady-state value. However, in this case the corresponding steady-state oxidation currents were slightly lower than each other. Figure 5.19 indicates that, for the DSA anodes, the decrease in current density represents the dissolution of the active component occurring during electrolysis. As penetration of the electrolyte occurs through the

mud cracked, porous structure of the thermally prepared oxide layer, the DSA anodes becomes stable around 0.3 seconds. As a consequence of dissolution of the active component, electrocatalytic activity of oxide catalyst decreases slowly with time until deactivation is reached by base metal passivation. For the lead alloy anode, the initial decrease in current density may be attributed to the partial blockage of the electrode surface due to the formation of a passivating layer. As the layer grows in thickness, the anode tends to stabilise as evidenced by the constant current density at 0.05 seconds.

5.1.7 X-Ray Diffractometry (XRD) analysis

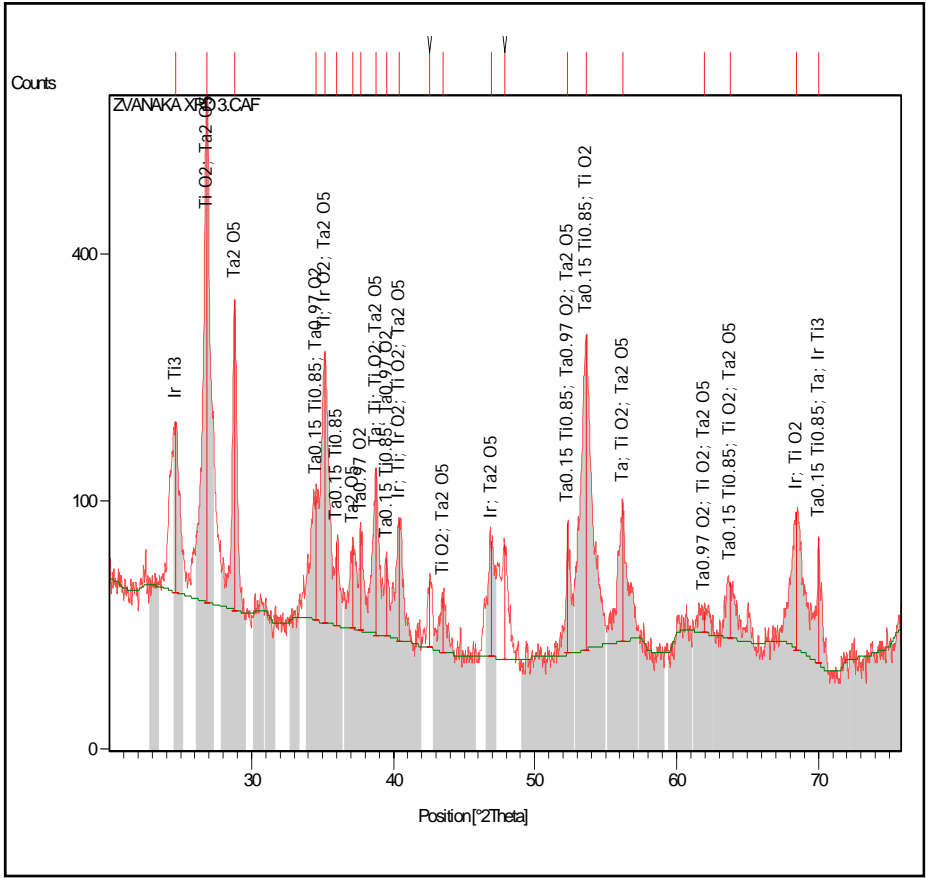


Figure 5.20: XRD Pattern for Unused DSA Anodes





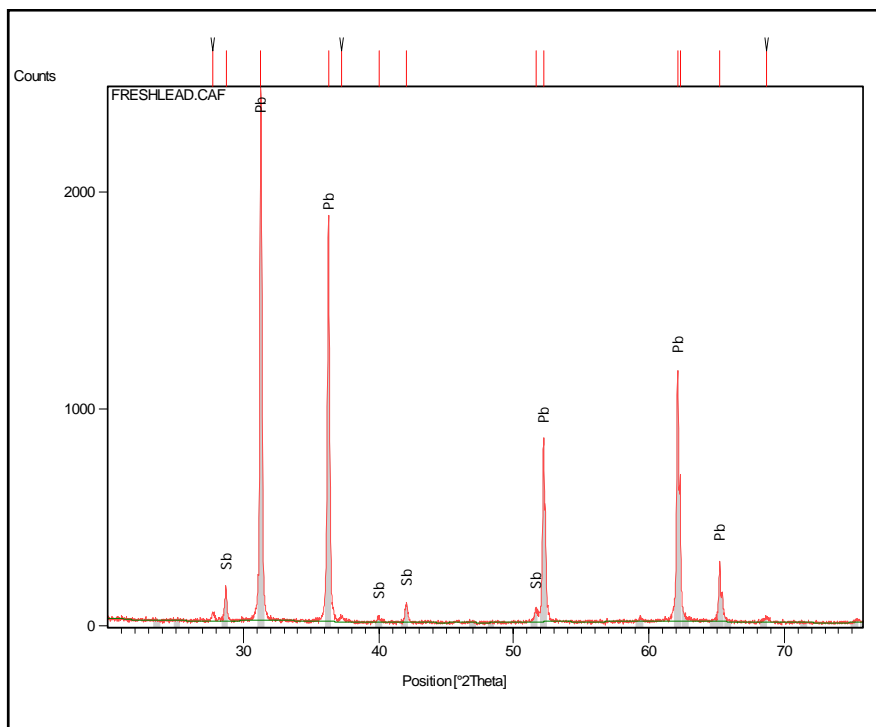


Figure 5.22: XRD Pattern for an Unused Lead Alloy Anode

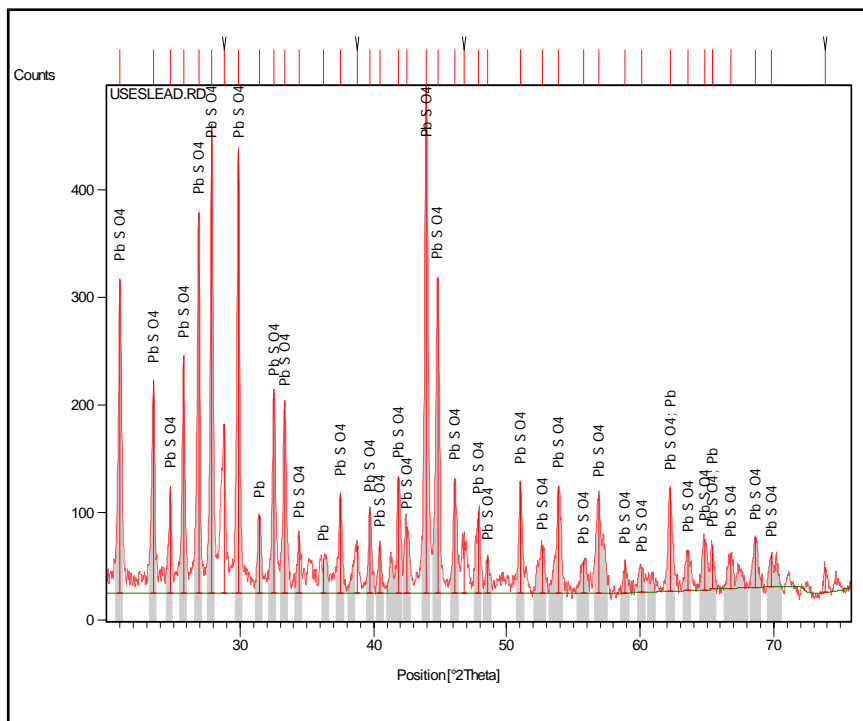
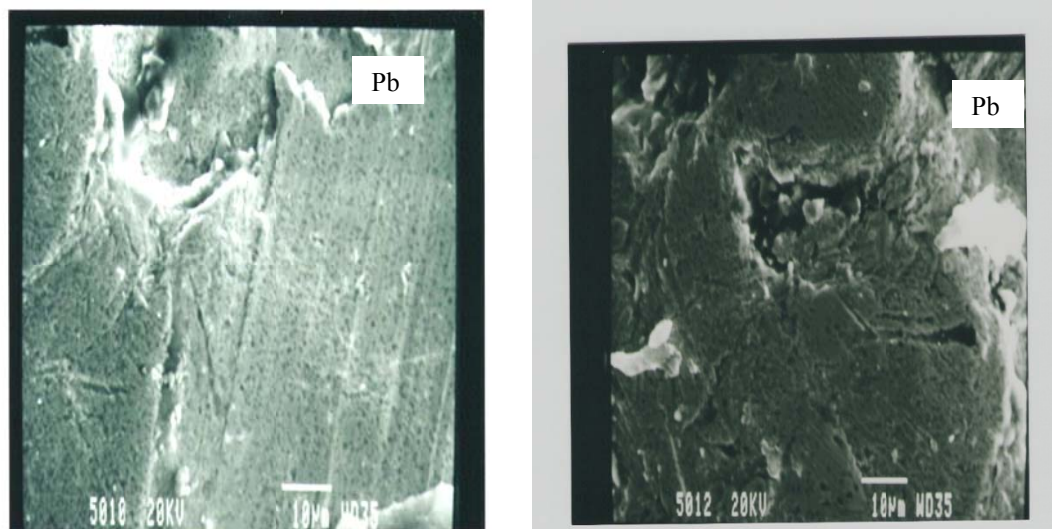


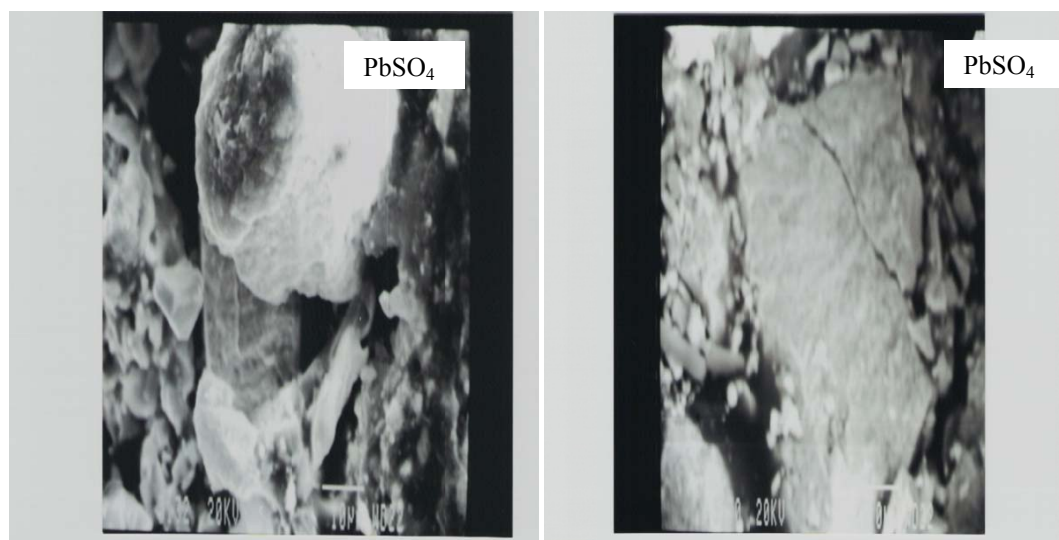
Figure 5.23: XRD Pattern for a Used Lead Alloy Anode

The unused lead alloy anode spectrum showed only lead and traces of antimony as indicated in figure 5.22 while the XRD spectrum for a used lead alloy anode revealed the presence of lead sulphate ( $\text{PbSO}_4$ ) on the anode surface as shown in figure 5.23.

#### 5.1.8 Scanning Electron Microscopy (SEM) analysis

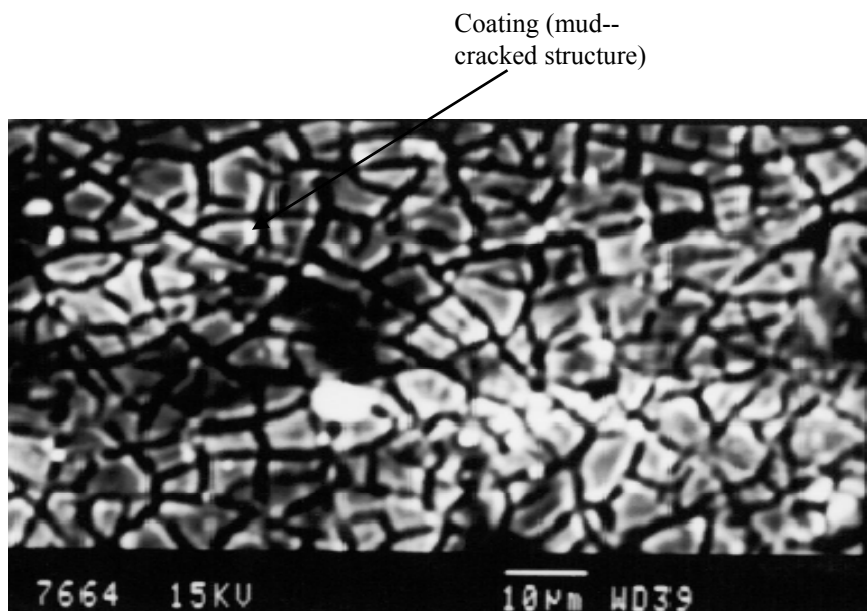


**Figure 5.24: SEM Micrograph for an Unused Lead Alloy Anode**



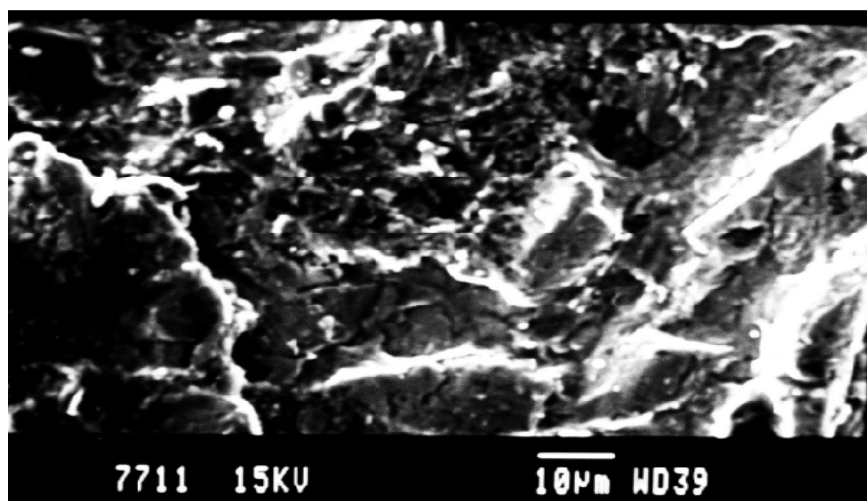
**Figure 5.25: SEM Micrograph for a Used Lead Alloy Anode**

Figure 5.25 indicates that the Pb/Pb(II) redox transition controls the surface of the lead alloy anode as previously suggested from the open circuit potential measurements and XRD analysis.



**Figure 5.26: SEM Micrograph for an unused DSA Anode**

Surface morphology of unused DSA anodes as analysed by a scanning electron microscope (SEM) showed a mud-cracked structure of the oxide coating as shown in figure 5.26 above.



**Figure 5.27: SEM Micrograph for a used DSA Anode**

Figure 5.27 shows the morphology of a used DSA anode. The absence of the mud-cracked structure is further proof that, during electrowinning operations using dimensionally stable anodes, coating loss occurs (Martelli *et al.*, 1994, Hu *et al.*, 2002).

### 5.1.9 Energy Dispersive Spectrometry (EDS) analysis

Figures 5.28 and 5.29 are the EDS patterns of the Ti/ IrO<sub>2</sub>-Ta<sub>2</sub>O<sub>5</sub> anodes before and after long term use. No EDS analysis was performed on the lead alloy anodes since the results from XRD analysis were conclusive.

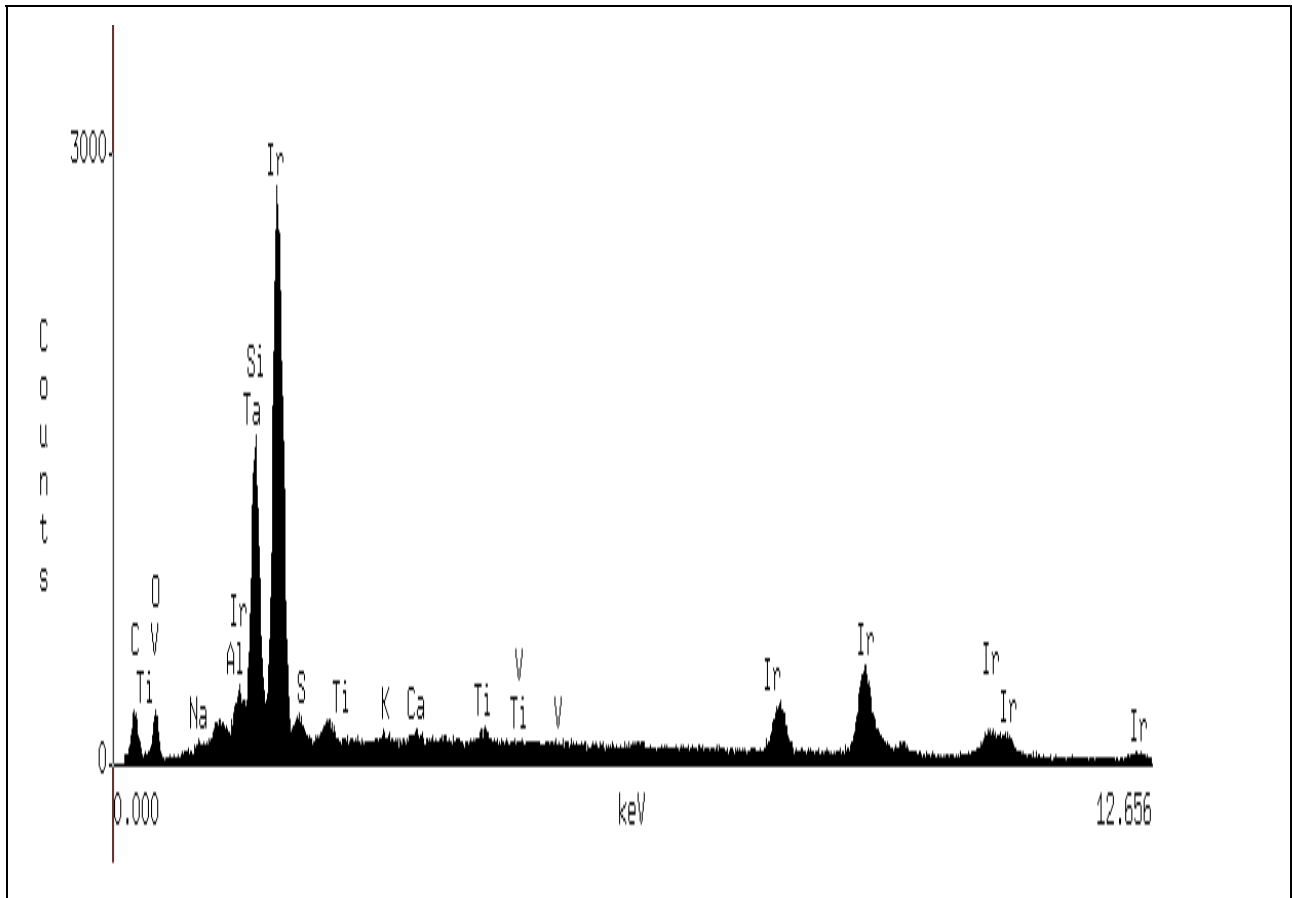


**Figure 5.28: EDS Analysis for an Unused DSA Anode**

Figure 5.28 indicates that iridium and tantalum are the major elements on the surface of the titanium substrate for an unused DSA anode. Other trace elements such as carbon, silicon and aluminium may be attributed to impurities coming from the preparation method of the anode.

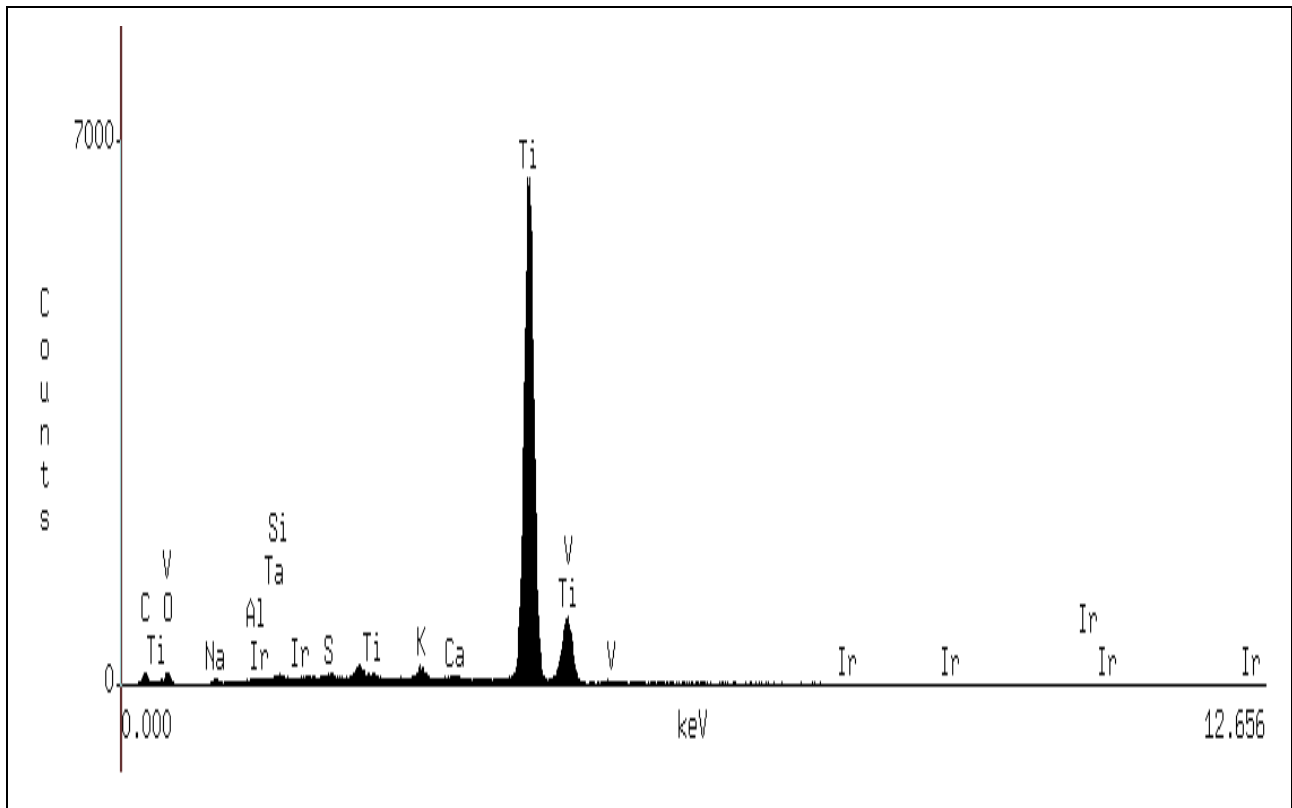


**Figure 5.29: EDS Analysis for a Used DSA Anode**

Figure 5.29 shows the heavy presence of the titanium substrate and traces of iridium and tantalum which are the active and inert components respectively. This EDS result suggests that the failure mechanism of the DSA anodes is due to coating consumption (reduction in coating thickness) which results in a stronger titanium signal. The results also indicate that some residual coating remains on the DSA anodes, after deactivation. The results from figure 5.28 and 5.29 are further substantiated by the quantitative analysis for unused and used DSA anodes in Table 5.10. The percentage compositions of iridium and tantalum were much higher in a fresh (unused) anode

than in a used anode while for titanium, the composition was greater in a used anode than in a fresh anode.

**Table 5.10: Quantitative Analysis for Unused and Used DSA Anodes.**

| Element Wt %       | Ti    |       | Ir    |      | Ta    |      |
|--------------------|-------|-------|-------|------|-------|------|
|                    | Fresh | Used  | Fresh | Used | Fresh | Used |
| <b>Composition</b> | 1.47  | 96.77 | 64.33 | 0.00 | 28.16 | 0.47 |

## 5.2 Comparison of anode materials: Electrowinning Experiments

### 5.2.1 Variation of Cell Voltage with Time

Cell voltage is a function of a number of variables, which may be varied to enhance the overall efficiency; the major contributor being the decomposition potential (section 2.3.2.1). Anode overpotential and resistance according to Ohm's law also significantly affect the cell voltage. The different cell voltage values recorded for the three electrowinning cells can thus be attributed to the difference in the anode materials since all the other conditions (temperature, electrode distance, concentration, electrode connections, and cathode material) were kept constant.

Figures 5.30 and 5.31 show the graphs of cell voltage with time for the anode materials considered under the study in BMR solution of concentration 55 g/l Cu and 100 g/l sulphuric acid, at a current density of 190 A/m<sup>2</sup> and a temperature of 55 °C. Despite the voltage fluctuations which characterised the electrowinning operation, mean cell voltages and the corresponding energy consumption were calculated in order to give some form of basis for comparison of these anodes. The voltage fluctuations could have been due to a number of factors such as electrode stability, differences in cell hydrodynamics and impurities in the electrolyte.

### 5.2.1.1 Comparison of DSA 1 Plate and Mesh Anodes and the Lead Anode

Generally the DSA 1 mesh anode cell had the lowest mean cell voltage of the three anode materials used, followed by the DSA 1 plate anode cell and the lead anode cell. However despite this trend, the cell voltage values in the DSA 1 plate containing cell were higher than the cell voltage values in the cell containing the lead anode in the first 95 hours of operation. These high voltage values may be attributed to erosion of the porous outer layer of the active coating due to intense oxygen evolution. Mraz and Krýsa (1994) reported that the initial dissolution rate for the IrO<sub>2</sub> based coating is reported to be several orders higher than the steady state dissolution rate. Beyond that the cell voltage values decreased to around 1.57 V as shown in figure 5.30. This voltage was lower than that of the lead anode during the same period by a magnitude of 15%. Thus the decrease in cell voltage for the DSA 1 plate around 95 hours as seen in figure 5.30 may indicate that a stable voltage of 1.57 V has been attained for the anode (Cardarelli *et al.*, 1998).

Any increase in the cell voltage from 1.57 V after continuous operation will therefore be a result of anode deactivation (Cardarelli *et al.*, 1998). The cell voltage values in the cell containing the DSA 1 mesh anode were also initially higher than the cell voltage values in the cells containing the DSA 1 plate and lead anodes. The values were in the range 1.98 V to 2.2 V but dropped after about 15 hours. This can also be attributed to erosion of the porous outer layer of the coating.



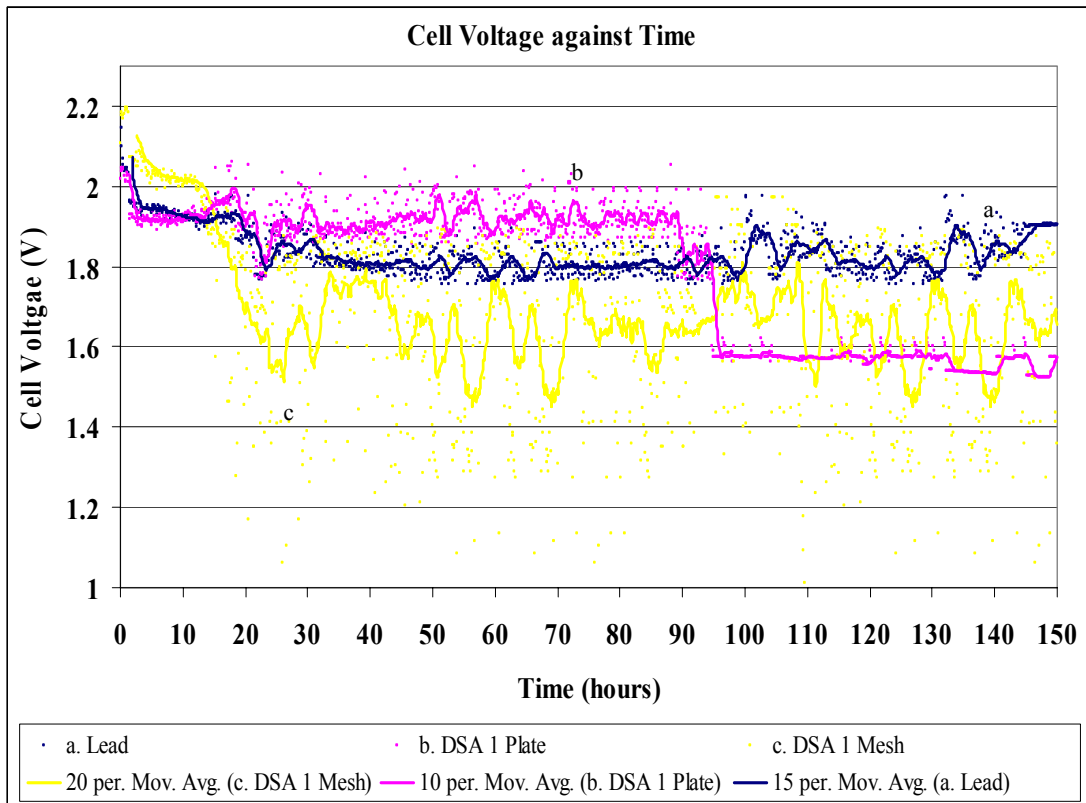


**Figure 5.30: Cell Voltage against Time in BMR Solution over a Period of 150 Hours.**

**a) Mean Voltages for DSA 1 Anodes and the Lead Anode**

The mean voltages for the DSA 1 plate, DSA 1 mesh and lead anodes were 1.787 V, 1.688 V and 1.838 V respectively over a period of 150 hours of electrowinning. This shows that the lead anode had the highest average energy consumption which was calculated to be 45 656 kJ. The DSA 1 plate and mesh anodes’ average energy consumption was 3% and 8% lower than that of the lead anode respectively.

After performing electrowinning tests in synthetic electrolyte, Hu *et al.* (1996) and other authors have also reported that the DSA anodes should have the least energy consumption when compared to the lead anode. Furthermore, this trend is in agreement with the results from chronopotentiometry tests carried out in synthetic solution earlier in the study.

### 5.2.1.2 Comparison of DSA 2 Plate and Mesh Anodes and the Lead Anode

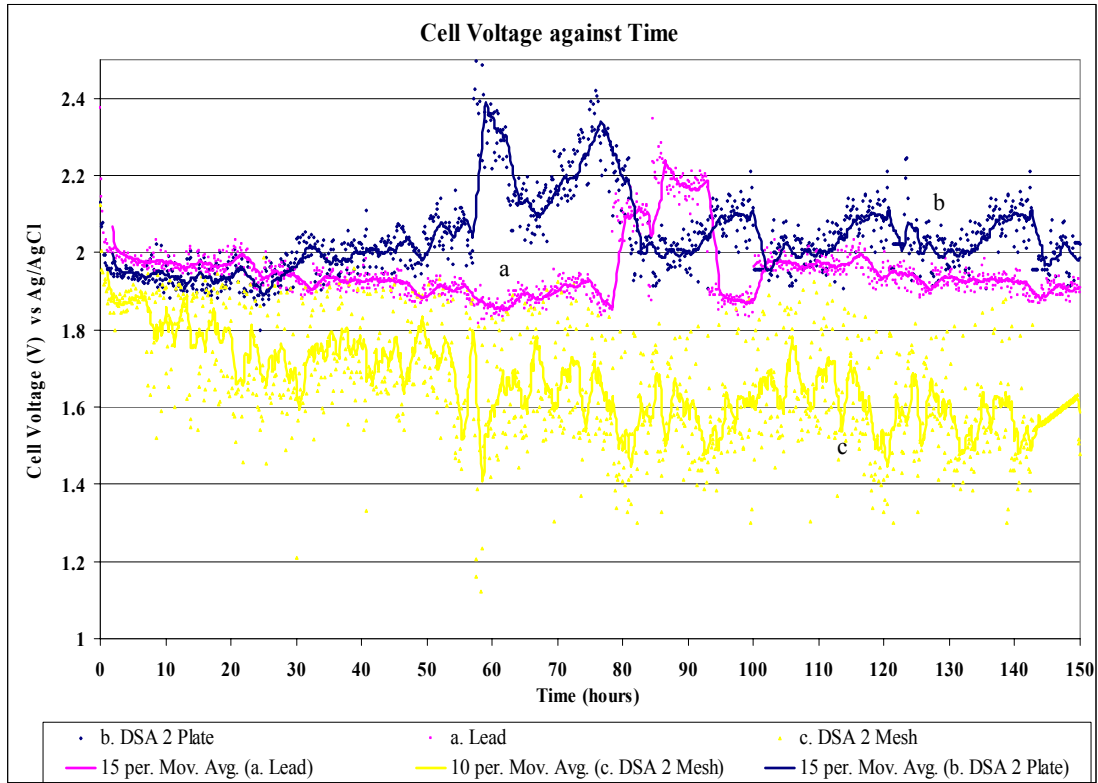


Figure 5.31: Cell Voltage against Time in BMR Solution over a Period of 150 Hours.

#### b) Mean Voltages for DSA 2 Anodes and the Lead Anode

The mean voltages for the DSA 2 plate, DSA 2 mesh and lead anode cells were 2.042 V, 1.661 V and 1.952 V respectively over a period of 150 hours of electrowinning. This shows that the lead anode cell had an average energy consumption of 48 488 kJ. The average energy consumption for the DSA 2 plate anode cell was found to be 5% higher than that of the lead anode cell while the average energy consumption for the DSA 2 mesh anode cell was 15% lower than that of the lead anode cell. However, as was seen for the DSA 1 plate anode cell, the cell voltage values for the DSA 2 plate anode cell might decrease to values below the lead anode cell and stabilise with continued operation if steady state dissolution is reached. This will however, depend on the method of preparation (solvent of the painting solution, firing temperature) of this anode. The morphology and structure of the coating were found to be essential factors influencing the properties and performances of the Ti/IrO<sub>2</sub>-Ta<sub>2</sub>O<sub>5</sub> electrode

(Vercesi *et al.*, 1991). Kulandaisamy *et al.* (1997) also mentioned that an increase in resistivity of the surface coating for DSA anodes increased the anode potential. The resistivity is a function of the method of preparation of the oxide coating on the anode. Martelli *et al.* (1994) also reported that even DSA anodes with the same chemical composition would show different electrocatalytic activities when their microstructures are different. Morimitsu *et al.*, as cited by Moats (2008), stated that decreasing the curing temperature used in the thermal decomposition process during coating preparation lowers the anode overpotential and in turn the cell voltage.

5.2.1.3 Comparison between the DSA 1 and DSA 2 plate and mesh anodes

DSA 1 and DSA 2 anodes (both plate and mesh) were also compared over a period of 150 hours in order to determine the best DSA anode. Figures 5.32 and 5.33 show the comparison between these plates and mesh anodes.

5.2.1.3.1 Comparison between the DSA 1 and DSA 2 plate anodes

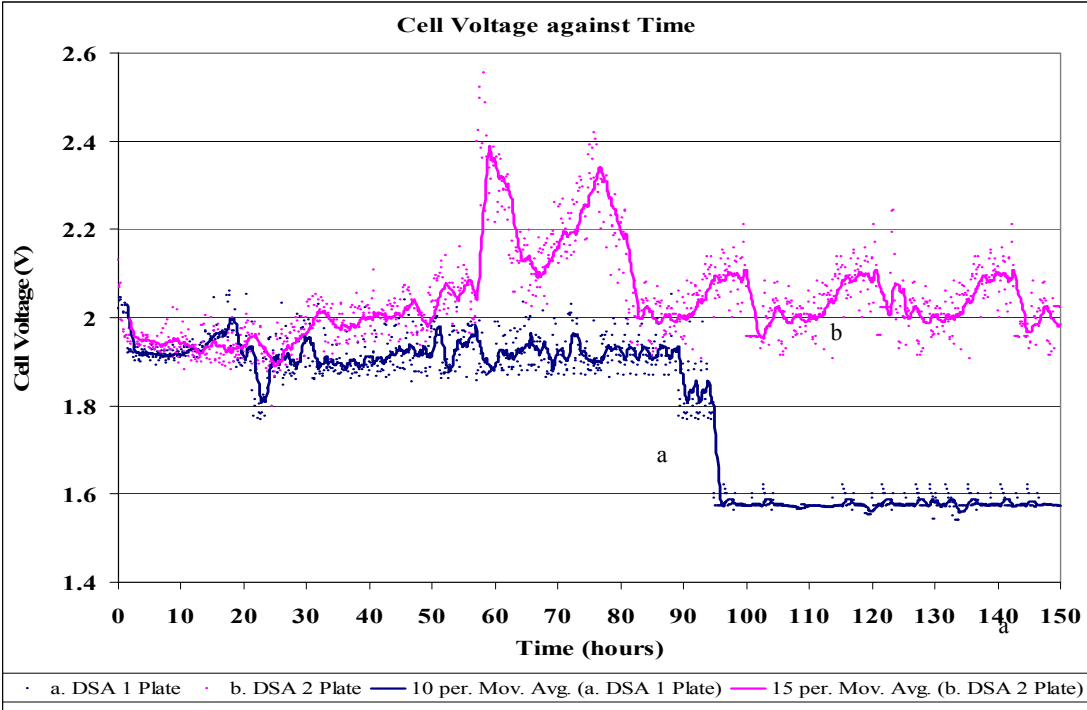


Figure 5.32: Cell Voltage against Time in BMR Solution over a Period of 150 Hours.

The initial cell voltages in the DSA 1 plate and DSA 2 plate cells were 2.019 V and 2.131 V. Overall, the DSA 1 plate cell had lower cell voltage values than its DSA 2 plate counterpart. The mean cell voltage for the DSA 1 plate cell over a period of 150 hours was 1.787 V; 12% lower than the DSA 2 plate cell which had a mean voltage of 2.042 V. This can be attributed to the high resistivity of the mixed metal oxide coating on the DSA 2 plate anode. Since current and duration of the study were constant, the energy saving also translates to 12% when using the DSA 1 plate anode instead of the DSA 2 plate anode. Table 5.11 below shows other parameters evaluated for the two plate anodes.

**Table 5.11: Values of Minimum (Min.) and Maximum (Max.) Cell Voltages for DSA 1 and DSA 2 Plates.**

| Anode | Min. Cell Voltage | Max. Cell Voltage |
|-------|-------------------|-------------------|
| DSA 1 | 1.539             | 2.061             |
| DSA 2 | 1.799             | 2.555             |

5.2.1.3.2 Comparison between the DSA 1 and DSA 2 mesh anodes

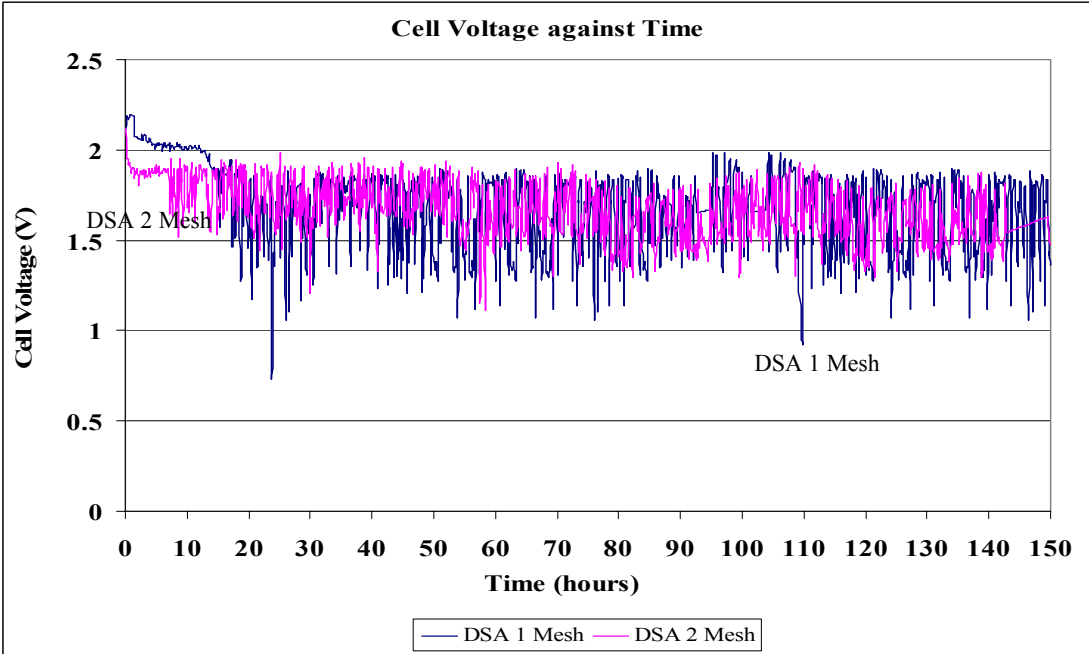


**Figure 5.33: Cell Voltage against Time in BMR Solution over a Period of 150 Hours.**

The initial cell voltages in the DSA 1 mesh and DSA 2 mesh cells were 2.108 V and 2.123 V. Figure 5.33 shows that the cell voltage values in the cell containing the DSA 1 mesh anode were higher than the values from the DSA 2 mesh cell in the first 15 hours of electrowinning. Beyond that, the cell voltage values are almost equal. The mean cell voltage for the DSA 1 mesh cell was 1.688 V; 1.6% higher than the DSA 2 mesh cell which had a mean voltage of 1.661 V. Thus in terms of operation, the DSA 2 mesh anode will result in energy consumption, 1.6% lower than that of the DSA 1 mesh anode.

**Table 5.12: Values of Minimum and Maximum Cell Voltages for DSA 1 and DSA 2 Meshes.**

| Anode | Min. Cell Voltage | Max. Cell Voltage |
|-------|-------------------|-------------------|
| DSA 1 | 0.736             | 2.196             |
| DSA 2 | 1.121             | 2.122             |

Figures 5.34, 5.35 and 5.36 below show the graphs of galvanostatic tests carried out in BMR and synthetic solutions using a potentiostat/galvanostat over eight hours and a current density of 190 A/m<sup>2</sup> at room temperature.

5.2.1.4 Comparison between BMR and Synthetic solutions

5.2.1.4.1 Comparison between BMR and Synthetic solutions for a DSA plate

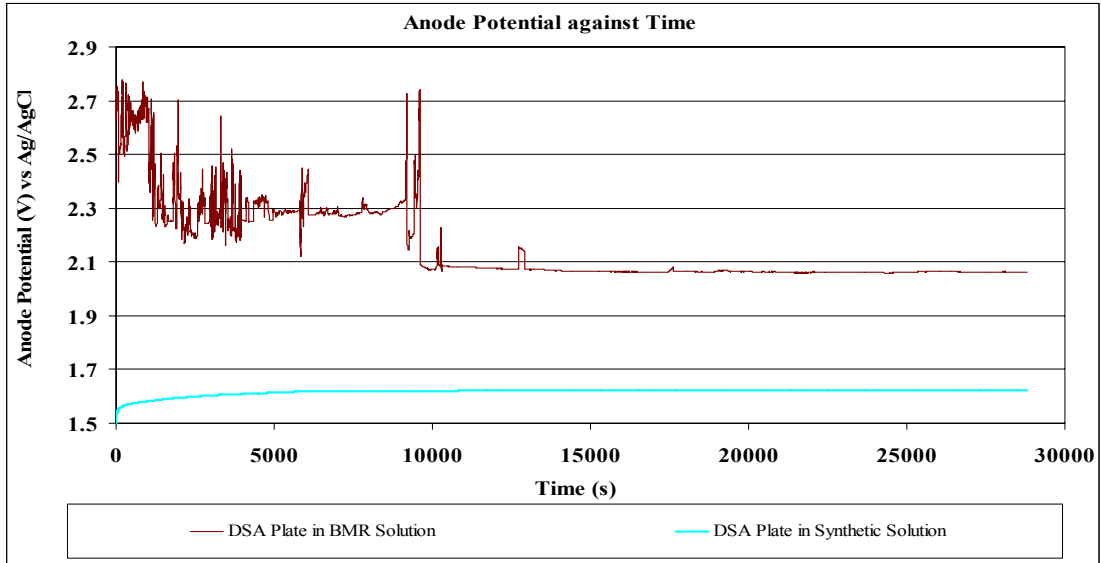


Figure 5.34: Anode Potential against Time in BMR and Synthetic Solutions for a DSA Plate Specimen.

5.2.1.4.2 Comparison between BMR and Synthetic solutions for a DSA mesh anode

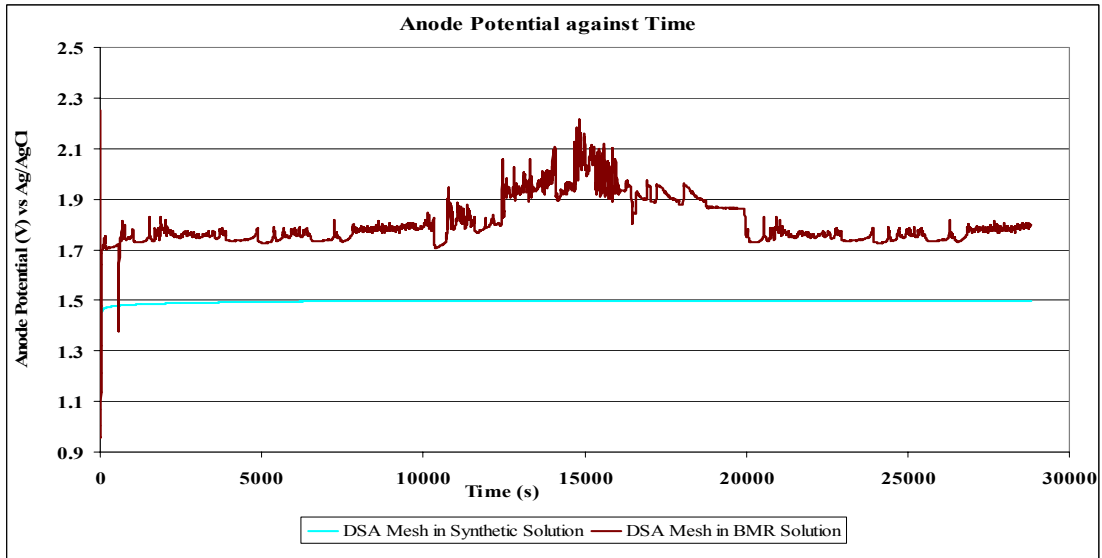
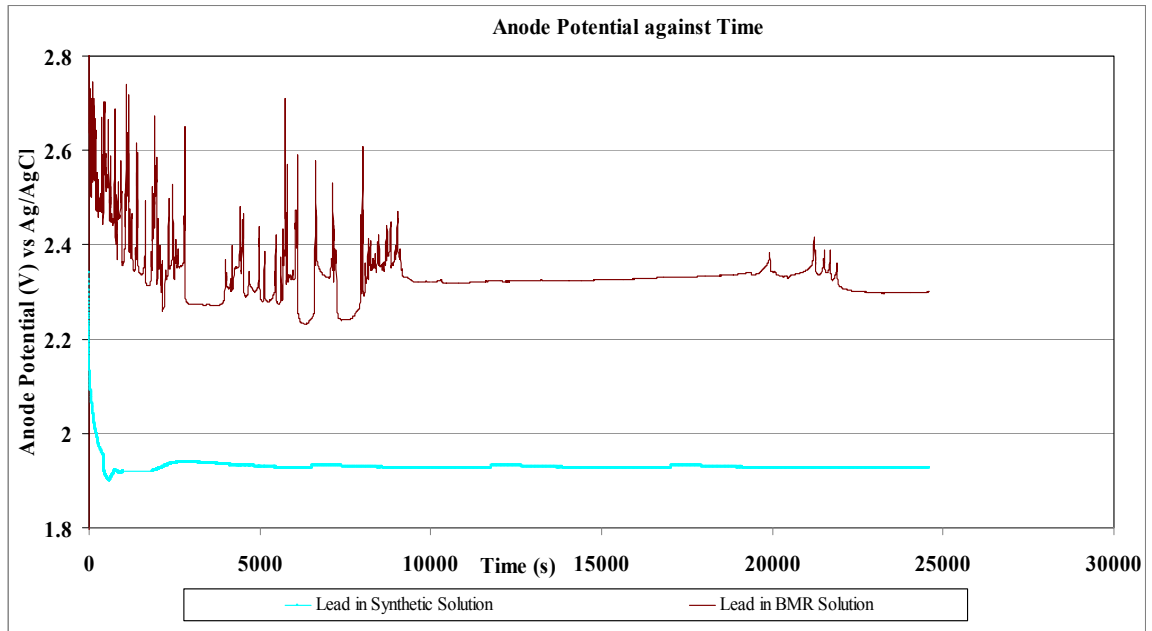


Figure 5.35: Anode Potential against Time in BMR and Synthetic Solutions for a DSA Mesh Specimen.

#### 5.2.1.4.3 Comparison between BMR and Synthetic solutions for a lead anode



**Figure 5.36: Anode Potential against Time in BMR and Synthetic Solutions for a Lead Specimen.**

An analysis of figures 5.34, 5.35 and 5.36 for the different anode materials indicates that the anode potentials for the DSA plate, DSA mesh and lead anodes are higher in BMR solution than in synthetic solution. The average values of anode potential in BMR solution were 1.91 V, 2.16 V and 2.33 V for the DSA mesh, DSA plate and lead anodes respectively. This would result in energy savings of 7% for the DSA plate anode and 18% for the DSA mesh anode if the lead anode were to be replaced. These energy savings differ from the range of 19-24% given in earlier tests carried out using synthetic electrolyte. Furthermore, in the BMR solution voltage fluctuations were also common, while in synthetic solution the anode potentials stabilised within the first hour. This can be attributed to the difference in composition of the two solutions used.

### **5.3 Impurities in BMR solution**

#### **5.3.1 Effect of manganese on anode potential**

From the various impurities in industrial electrolytes, manganese ions were added to synthetic electrolyte in order to assess their effect on the magnitude of the anode potential for the different anodes. Manganese has been reported to cause an increase of 10–15% in energy consumption in zinc electrowinning electrolytes (Zhang and Cheng, 2007). The manganese was added as aliquots from stock solutions prepared from its sulphate salt. Yu and O’Keefe (2002) reported that, despite oxygen evolution being the main reaction, in copper electrowinning, secondary reactions may occur in the presence of manganese impurities. Manganese may react at the anode surface during oxidation to form either soluble species or insoluble manganese dioxide that may passivate the anode surface and hinder the OER reaction (Kao and Weibel, 1992). Passivation of the anode surface results in an increase in anode potential.

Figures 5.37, 5.38 and 5.39 show the variation of anode potential with time in the presence and absence of manganese ions for the DSA plate and mesh anodes and the lead anode. The manganese concentration was 8 mg Mn/l; similar to the BMR solution used in the study.



5.3.1.1 Comparison between synthetic and synthetic/manganese solutions

5.3.1.1.1 Comparison between synthetic and synthetic/manganese solutions for a DSA plate anode

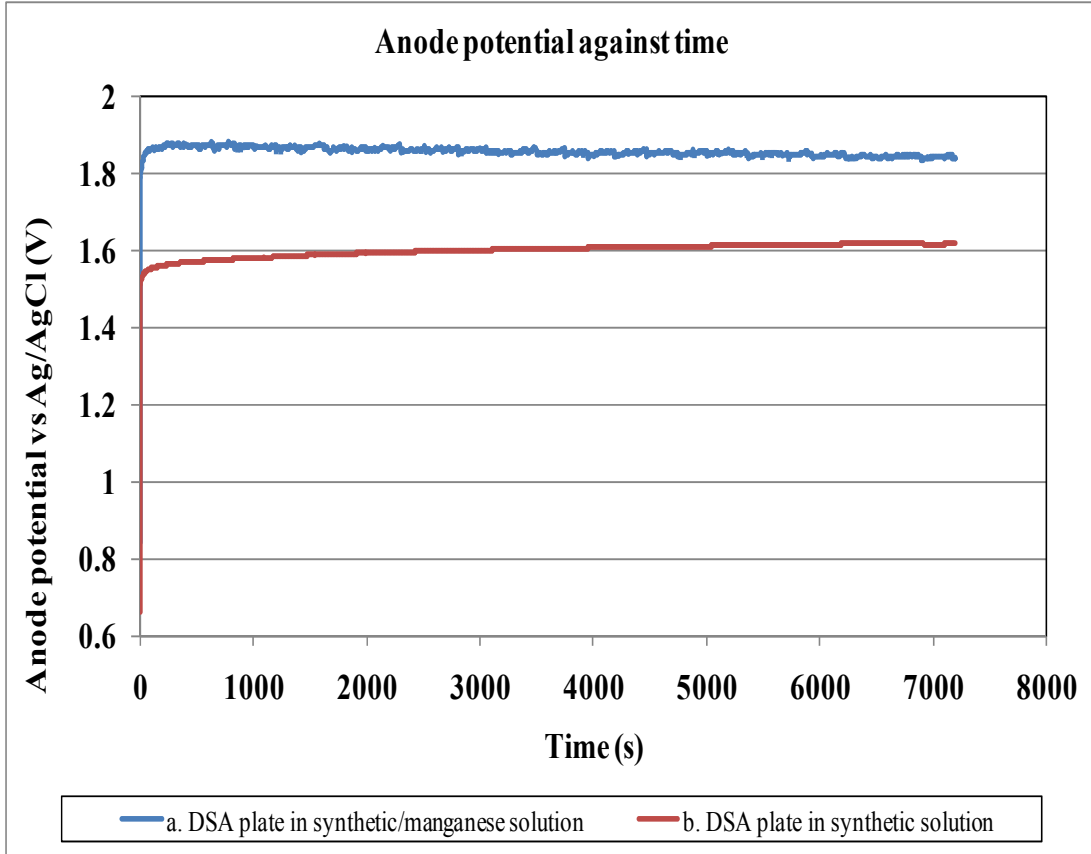


Figure 5.37: Anode Potential against Time in Synthetic and Synthetic/Manganese Solution for a DSA Plate Specimen.

5.3.1.1.2 Comparison between synthetic and synthetic/manganese solutions for a DSA mesh anode

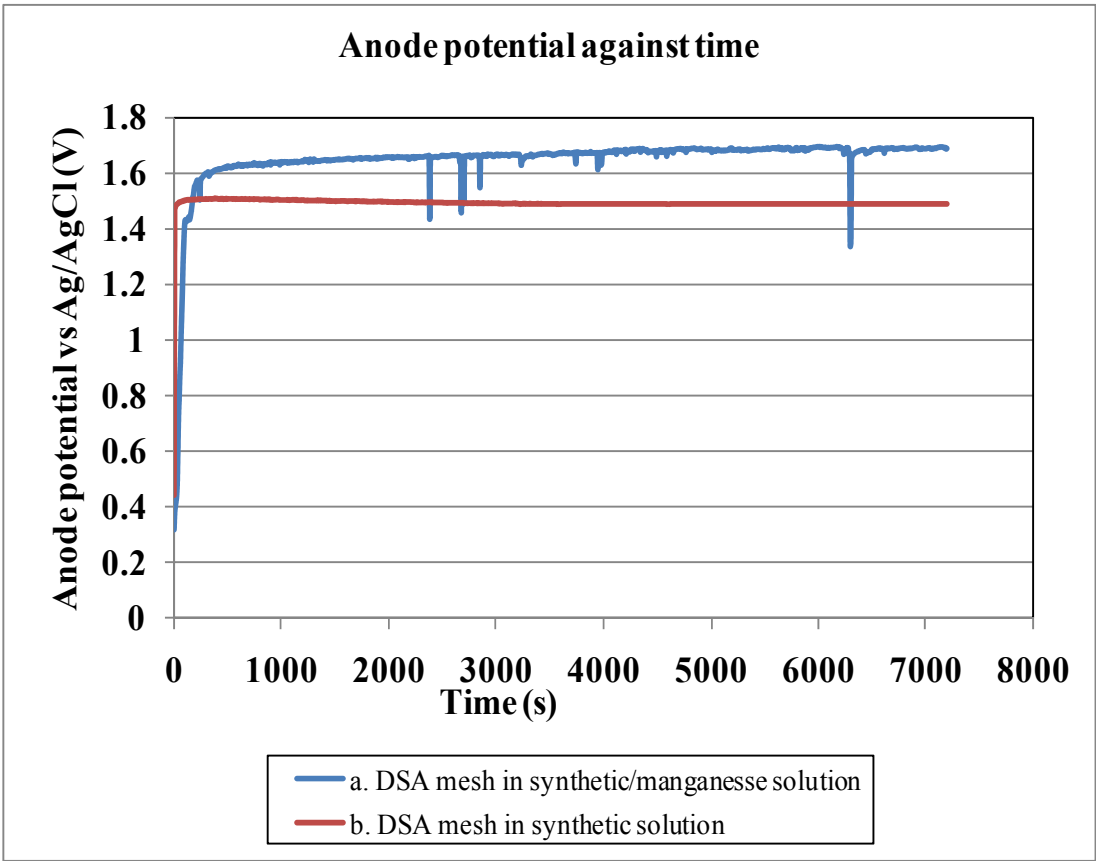


Figure 5.38: Anode Potential against Time in Synthetic and Synthetic/Manganese Solution for a DSA Mesh Specimen.

5.3.1.1.3 Comparison between synthetic and synthetic/manganese solutions for a lead anode

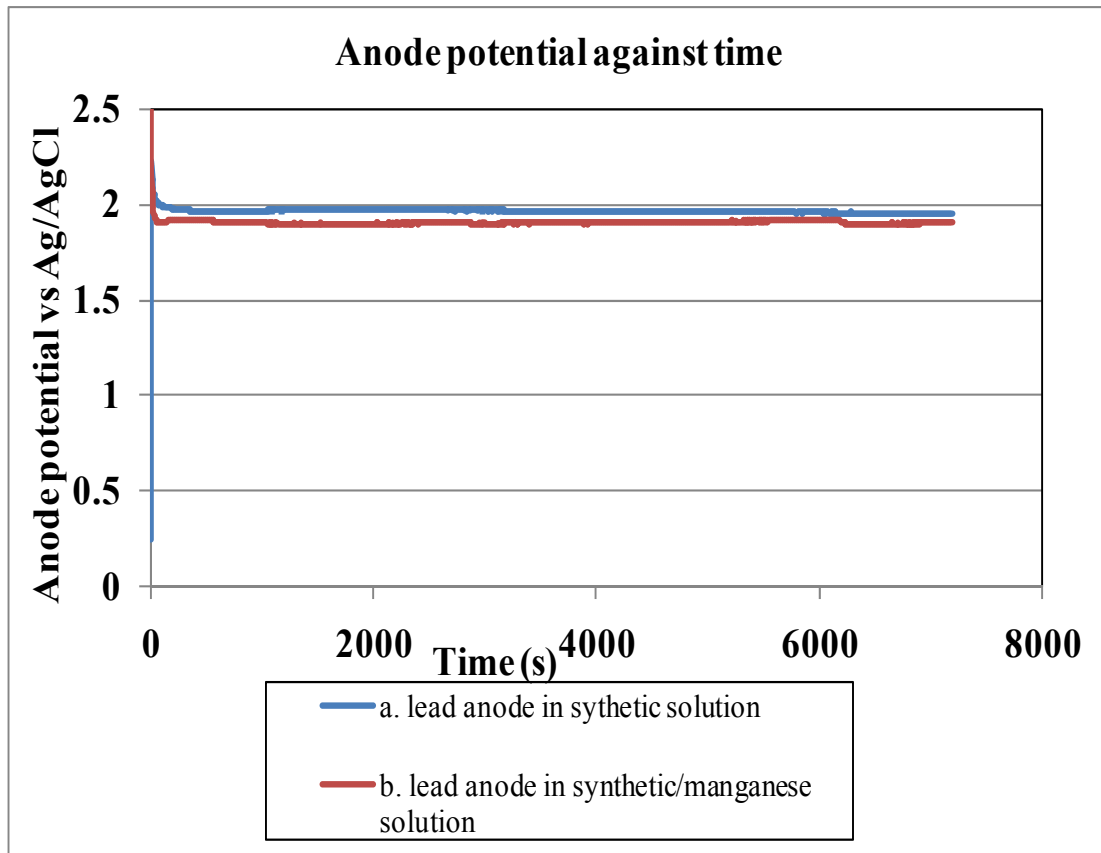


Figure 5.39: Anode Potential against Time in Synthetic and Synthetic/Manganese Solution for a Lead Specimen.

It can be observed that addition of manganese into the synthetic solution increased anode potential for both DSA anodes while for the lead anode; manganese had a slight depolarising effect. Yu and O'Keefe (2002) found out that when oxygen evolution became more significant, manganese depolarised the Pb-Ca-Sn anode. Anode potential is a major component of cell voltage; therefore, the cell voltage for the DSA anodes is also expected to increase. This in turn, decreases the energy saving benefit that otherwise could have been realised. The average energy saving in synthetic/manganese solution was 6% for the DSA plate and 14% for the DSA mesh as compared to 19% and 24% previously reported for the synthetic solution. The graphs also show that addition of manganese into synthetic solution resulted in some

voltage fluctuations, for the DSA anodes. Manganese, in electrowinning processes utilising lead anodes, has also been reported to decrease lead anode corrosion by forming a film of manganese dioxide (MnO<sub>2</sub>).

### 5.3.2 Current efficiency

The tables below show the current efficiencies achieved for the duration of the study using five anodes (lead anodes and DSA anodes). The current efficiency was determined using the equation 2.22 given below:

$$\varepsilon_c(I) = \frac{nF\Delta W}{ItM} \dots\dots\dots 2.22$$

**Table 5.13: Current Efficiencies Achieved Over a Period of 150 hrs Using DSA 1 Anodes and a Lead Anode**

| CELL | ANODE TYPE         | TOTAL MASS OF COPPER DEPOSITED (kg) | PLATING RATE (kg/hr) | CURRENT EFFICIENCY (%) |
|------|--------------------|-------------------------------------|----------------------|------------------------|
| A    | DSA 1 Plate        | 7.3                                 | 0.05                 | 89.3                   |
| B    | DSA 1 Mesh         | 4.4                                 | 0.03                 | 53.5                   |
| C    | Lead alloy (6% Sb) | 6.1                                 | 0.04                 | 74.1                   |

**Table 5.14: Current Efficiencies Achieved Over a Period of 150 hrs Using DSA 2 Anodes and a Lead Anode**

| CELL | ANODE TYPE         | TOTAL MASS OF COPPER DEPOSITED (kg) | PLATING RATE (kg/hr) | CURRENT EFFICIENCY (%) |
|------|--------------------|-------------------------------------|----------------------|------------------------|
| A    | DSA 2 Plate        | 6.7                                 | 0.05                 | 82.5                   |
| B    | DSA 2 Mesh         | 4.2                                 | 0.03                 | 51.0                   |
| C    | Lead alloy (6% Sb) | 7.0                                 | 0.05                 | 86.2                   |

Overall, in the electrowinning studies conducted using DSA and lead anodes in BMR solution, the current efficiencies for all the anodes in BMR solution were markedly lower than the current efficiencies in synthetic electrolyte (table 5.3). Das and Gopala (1996) mentioned that during hydrometallurgical extraction of copper from its ores, the leach liquors often contain a substantial amount of iron. The presence of Fe (III) in the electrolyte not only leads to production of poor quality cathode copper but also causes a loss in current efficiency due to the reduction of  $\text{Fe}^{3+}$  to  $\text{Fe}^{2+}$  at the cathode and re-oxidation of  $\text{Fe}^{2+}$  to  $\text{Fe}^{3+}$ .

The differences observed in the current efficiencies for the lead alloy anode (74% and 86%) were not due to the failure of the experiment itself, but rather copper deposition which occurred on the heating rod inside the lead anode cell as shown in figure 5.40. So theoretically, the results were the same within acceptable experimental error.



**Figure 5.40: Heating Rod Showing Electrodeposited Copper in the Lead Anode Cell.**

DSA 1 and 2 mesh anodes had the lowest current efficiencies as indicated in tables 5.13 and 5.14. A number of factors could have contributed to this problem. Firstly, since coated titanium electrode have been reported to oxidise ferrous ions to ferric

ions, which has a bearing on current efficiency; the oxidation with mesh anodes may have been more profound than that resulting from DSA plate anodes. Therefore, this may have inadvertently led to reduced cathode current efficiency in the cells containing these anodes.

Furthermore, other factors such as; precise material composition, impurities, cross-sectional areas of the cathodes or anode current density, could have played a role too in affecting the cathode current efficiency. Ettel *et al.* (1974) suggested that there could be a relationship between anode current density and cathode current efficiency since gas evolution at the anode results in electrolyte movement and in turn affects mass transfer coefficients at the cathode.

### 5.3.3 Morphology of the copper produced

Some nodules were observed on the copper produced in the cells containing the lead anode and both DSA plate anodes. This could be attributed to the likelihood of varying current distributions in these cells since some areas on the copper deposits were uniform. Varying current distributions are mainly caused by imperfections on the surface of the electrode (Nicol, 2006). The copper deposited in the cells containing both mesh anodes was uniform. Figures 5.41 to 5.45 show these copper deposits.



**Figure 5.41: Copper from DSA 1 Plate Anode**



**Figure 5.42: Copper from DSA 2 Plate Anode**

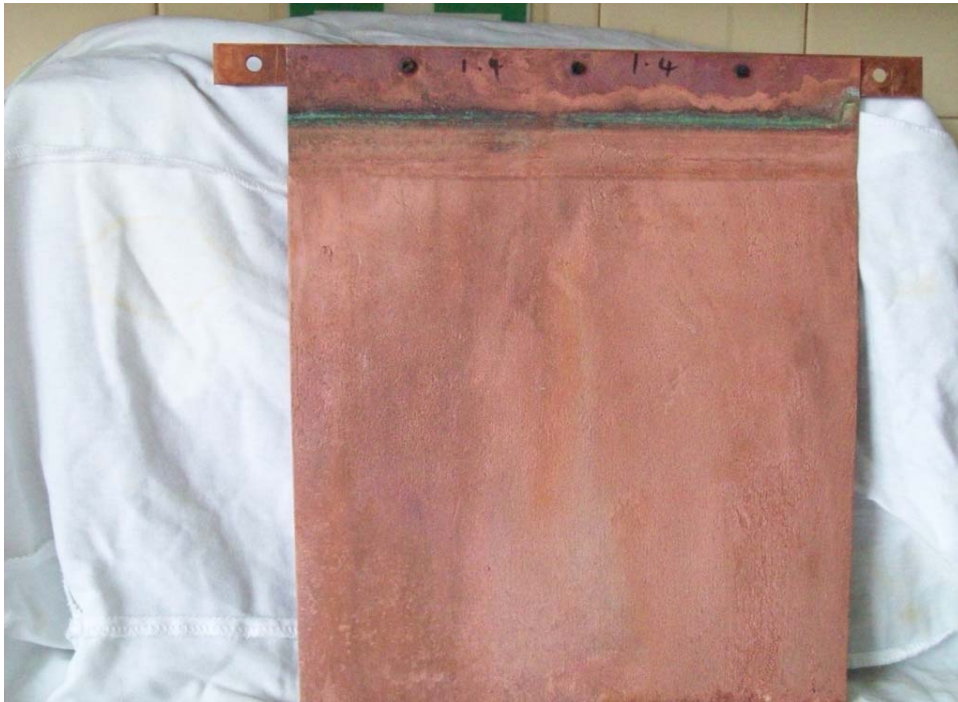


**Figure 5.43: Copper from DSA 1 Mesh Anode.**



**Figure 5.44: Copper from DSA 2 Mesh Anode.**





**Figure 5.45: Copper from Lead Anode Cell.**

The optical micrographs below also show the deposit morphology for copper deposited in cells containing the DSA 1 and DSA 2 plate anodes, DSA 1 and DSA 2 mesh anodes and the lead anode.

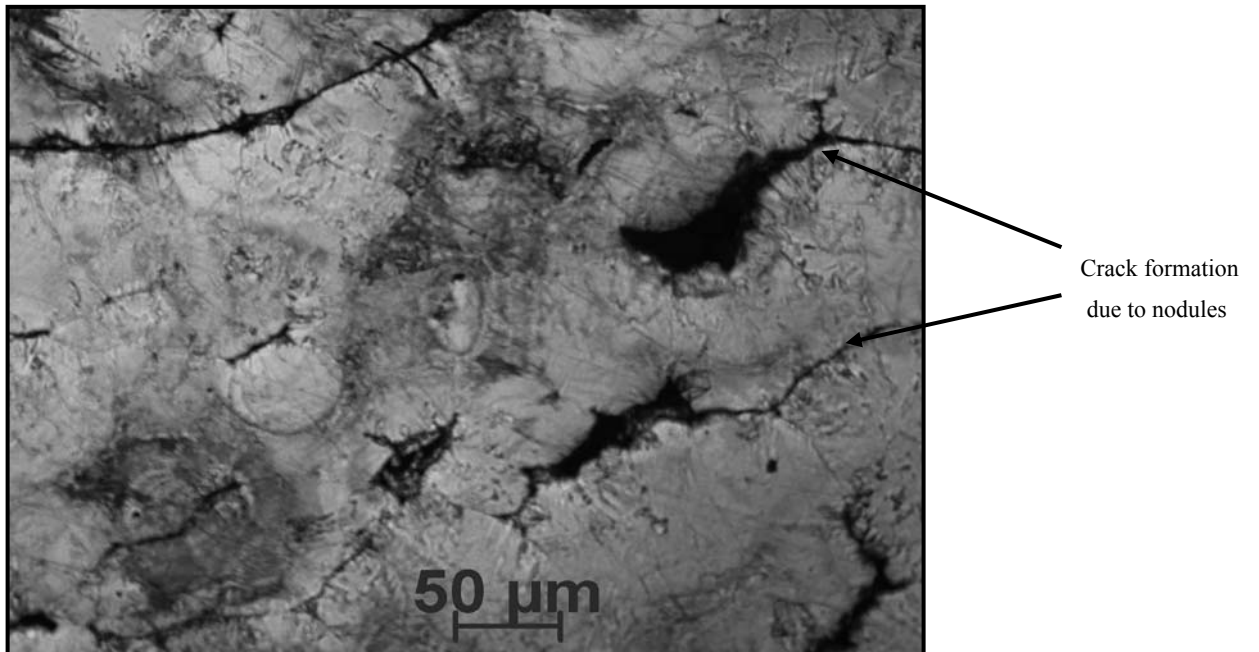


**Figure 5.46: Micrograph for Copper from DSA 1 Plate Anode Cell**

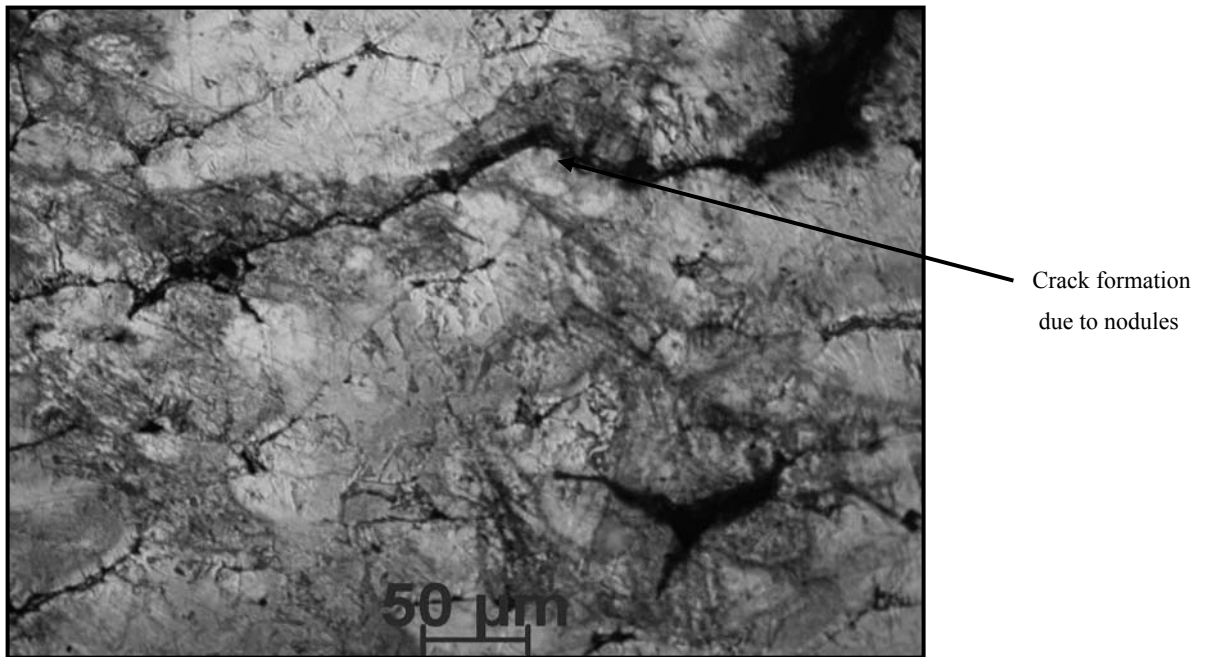


**Figure 5.47: Micrograph for Copper from DSA 2 Plate Anode Cell**

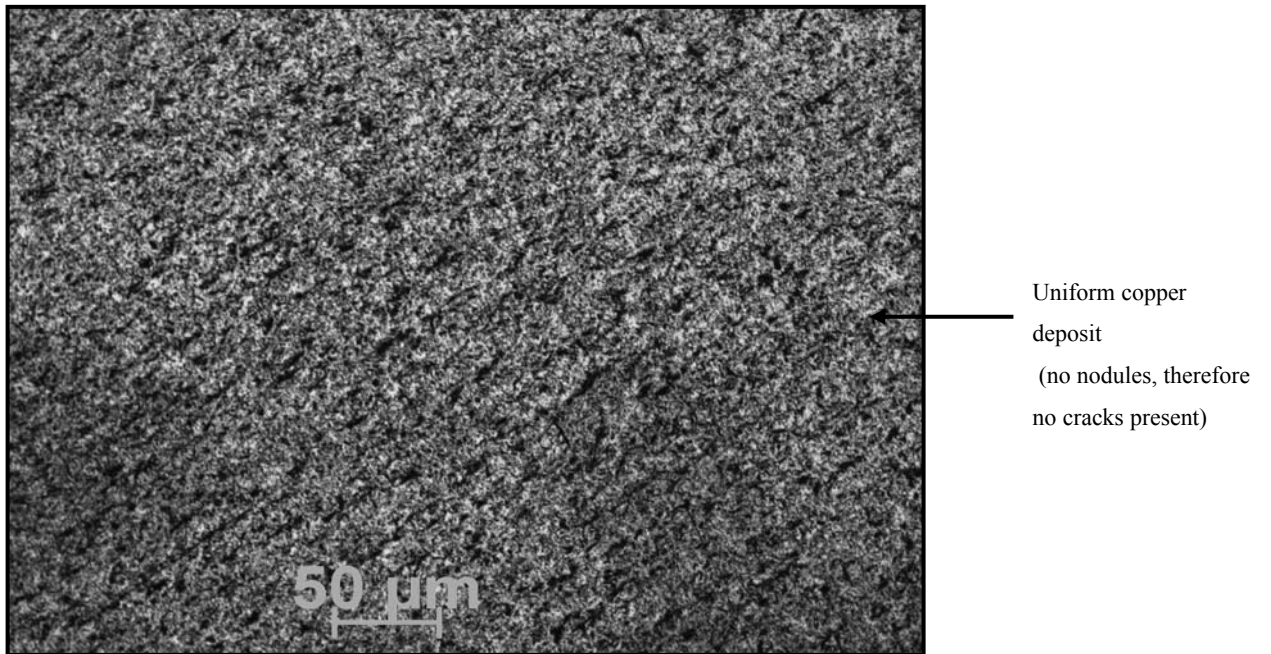
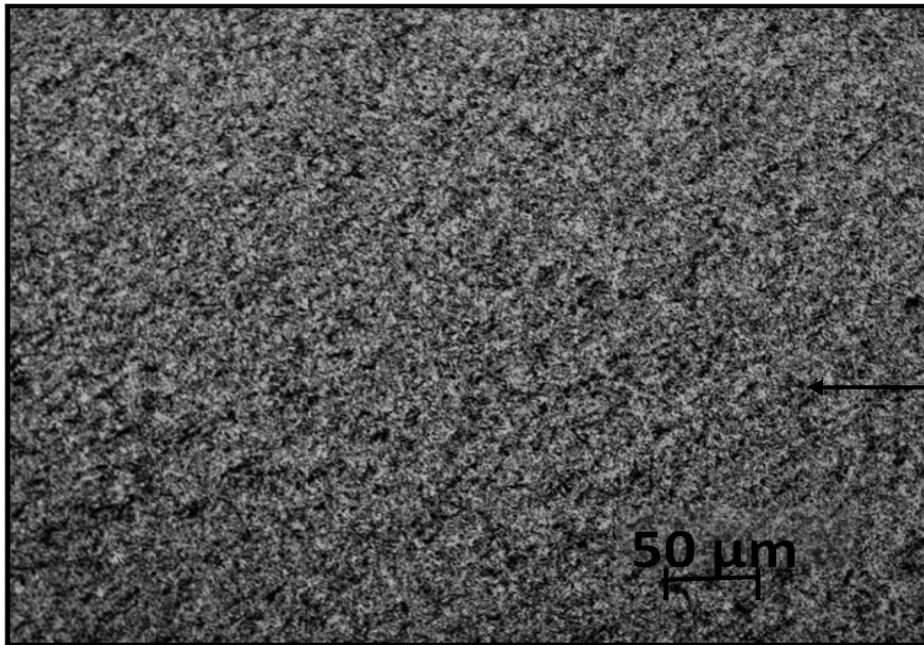
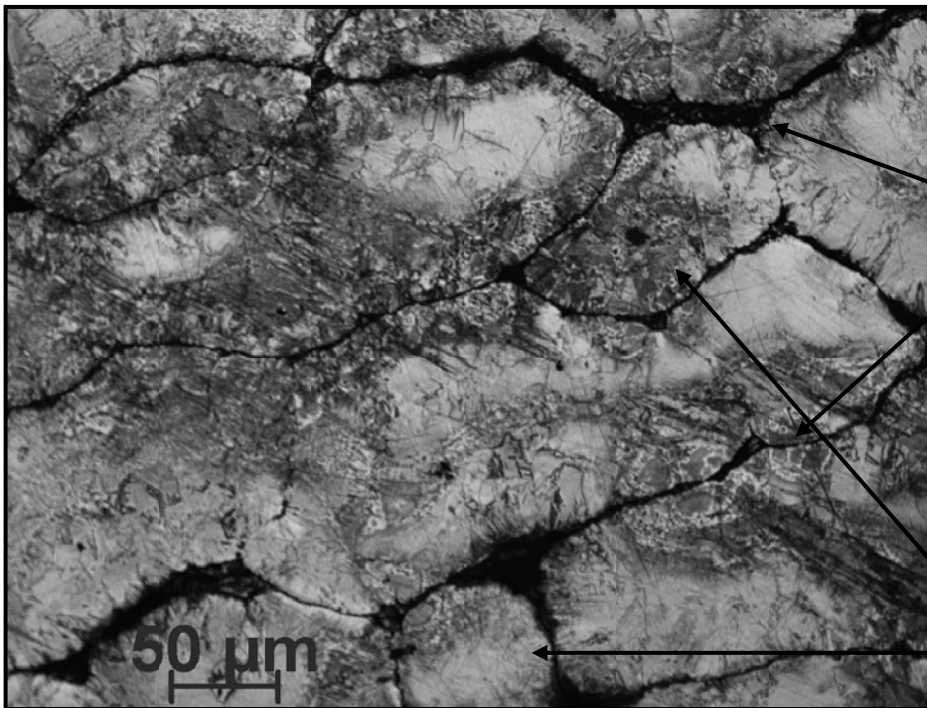


**Figure 5.48: Micrograph for Copper from DSA 1 Mesh Anode Cell.**



Uniform copper deposit  
(no nodules, therefore no cracks present)

Figure 5.49: Micrograph for Copper from DSA 2 Mesh Anode Cell.



Heavy presence of cracks on copper deposit as a result of nodule formation

Nodules

Figure 5.50: Micrograph for Copper from Lead Anode Cell

#### 5.4 XRD analysis for copper deposits

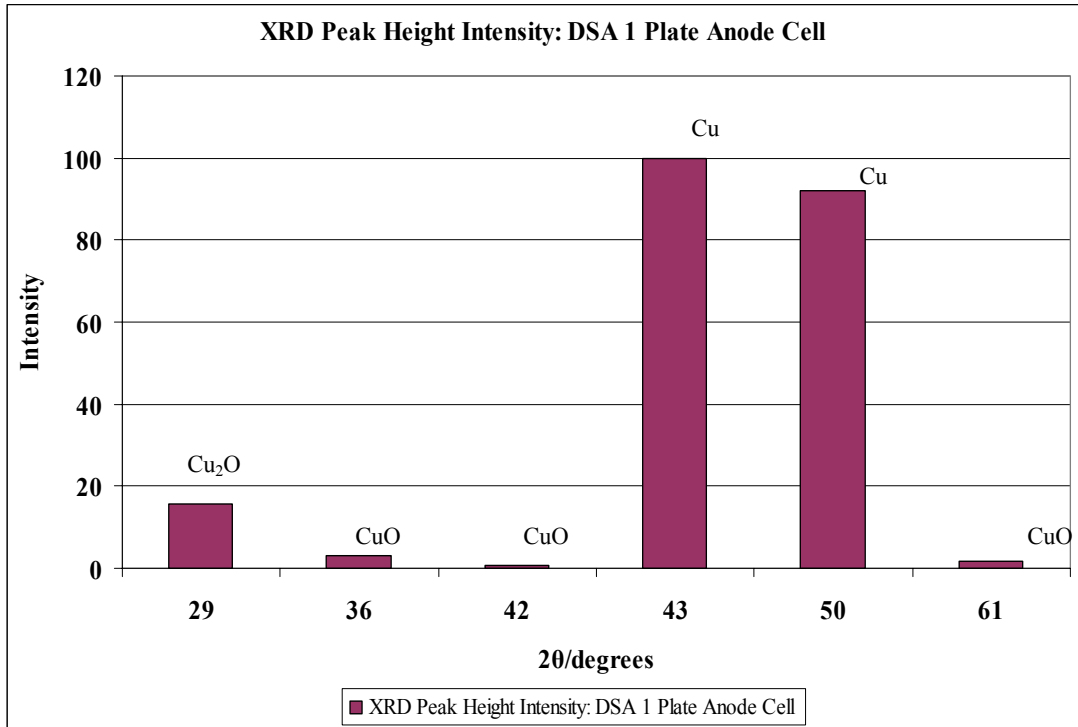


Figure 5.51: XRD Peak Height Intensity: DSA 1 Plate Anode Cell

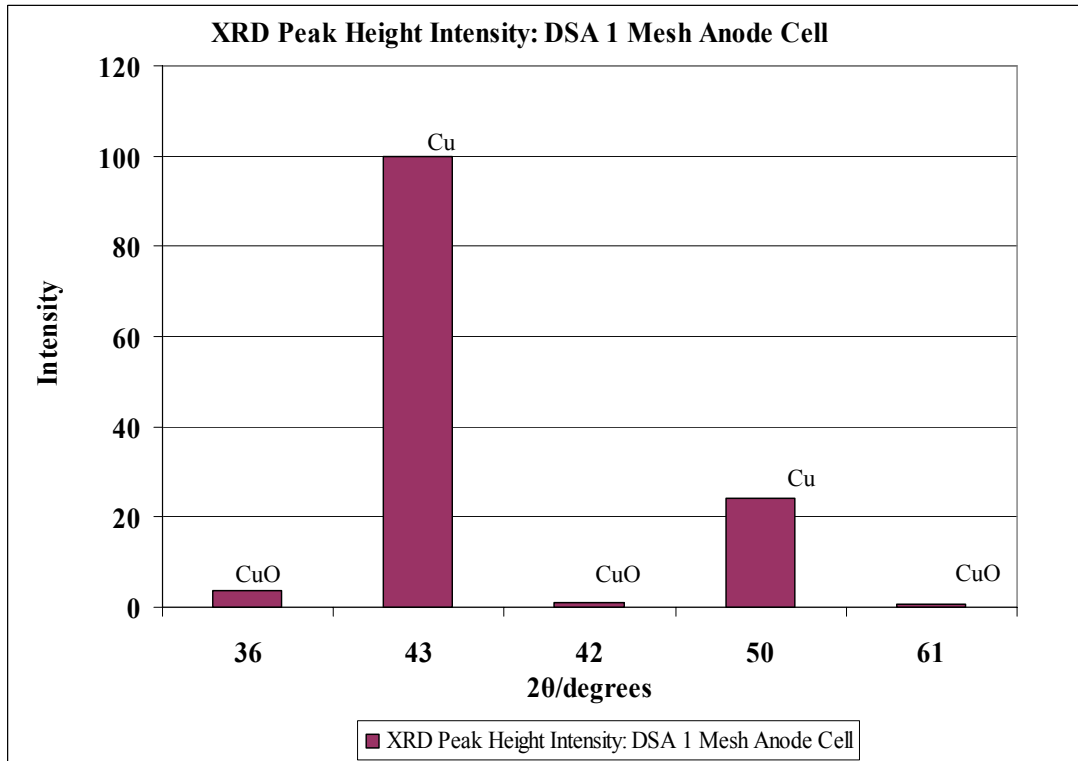


Figure 5.52: XRD Peak Height Intensity: DSA 1 Mesh Anode Cell

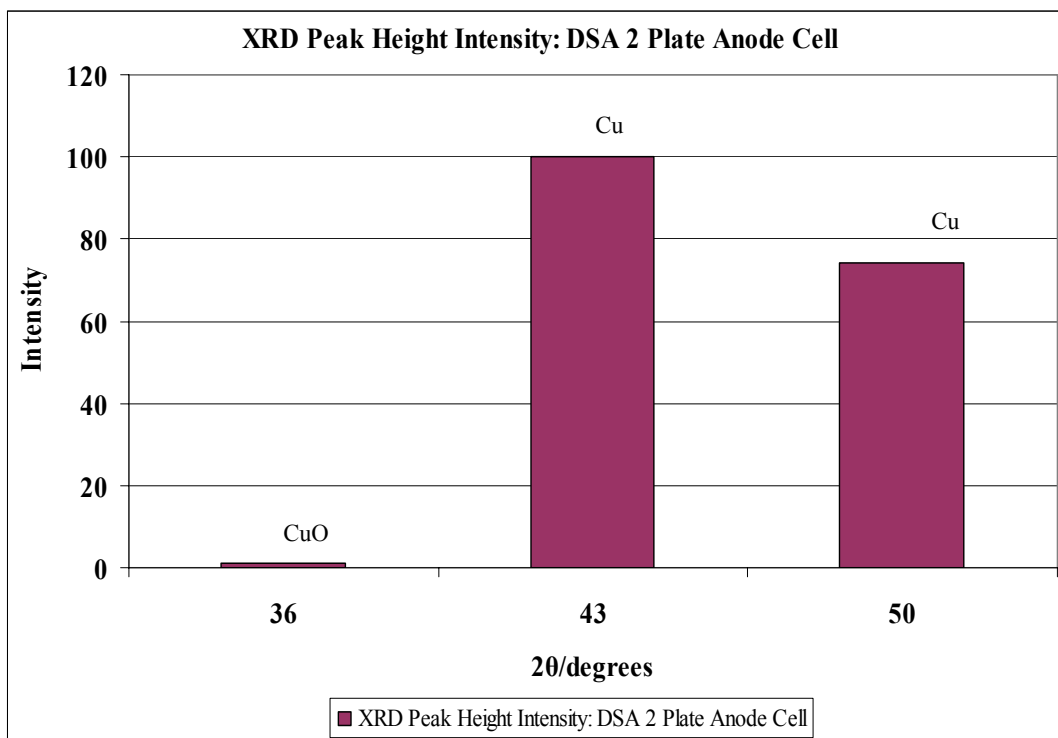


Figure 5.53: XRD Peak Height Intensity: DSA 2 Plate Anode

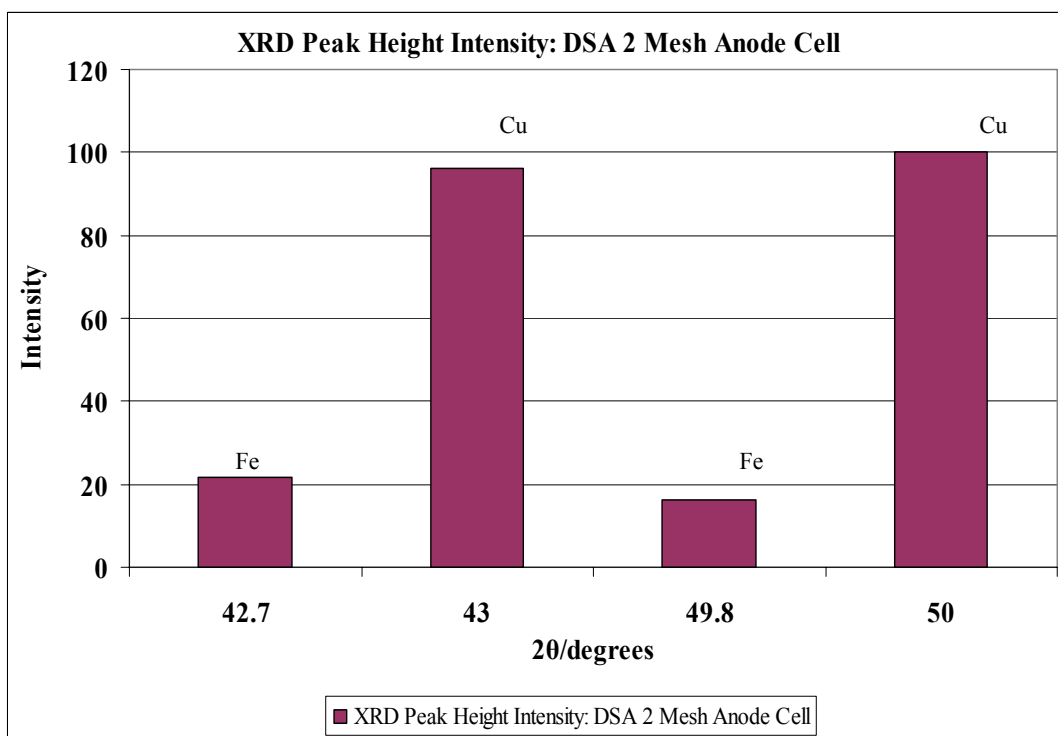


Figure 5.54: XRD Peak Height Intensity: DSA 2 Mesh Anode Cell

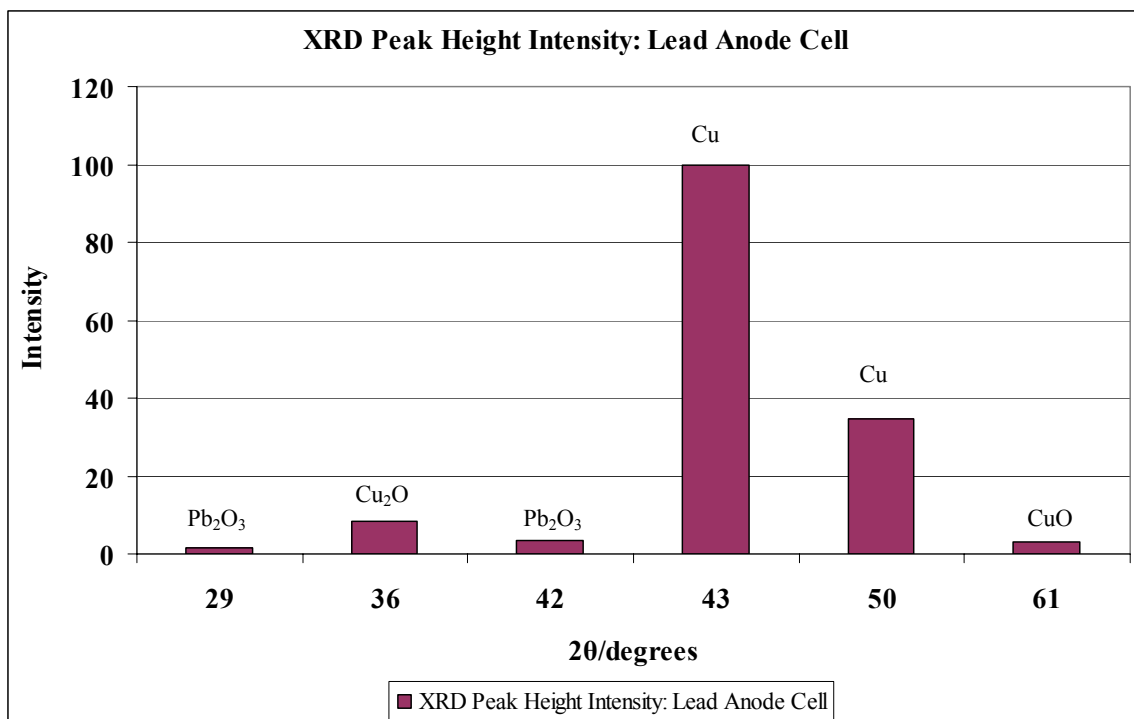


Figure 5.55: XRD Peak Height Intensity: Lead Anode

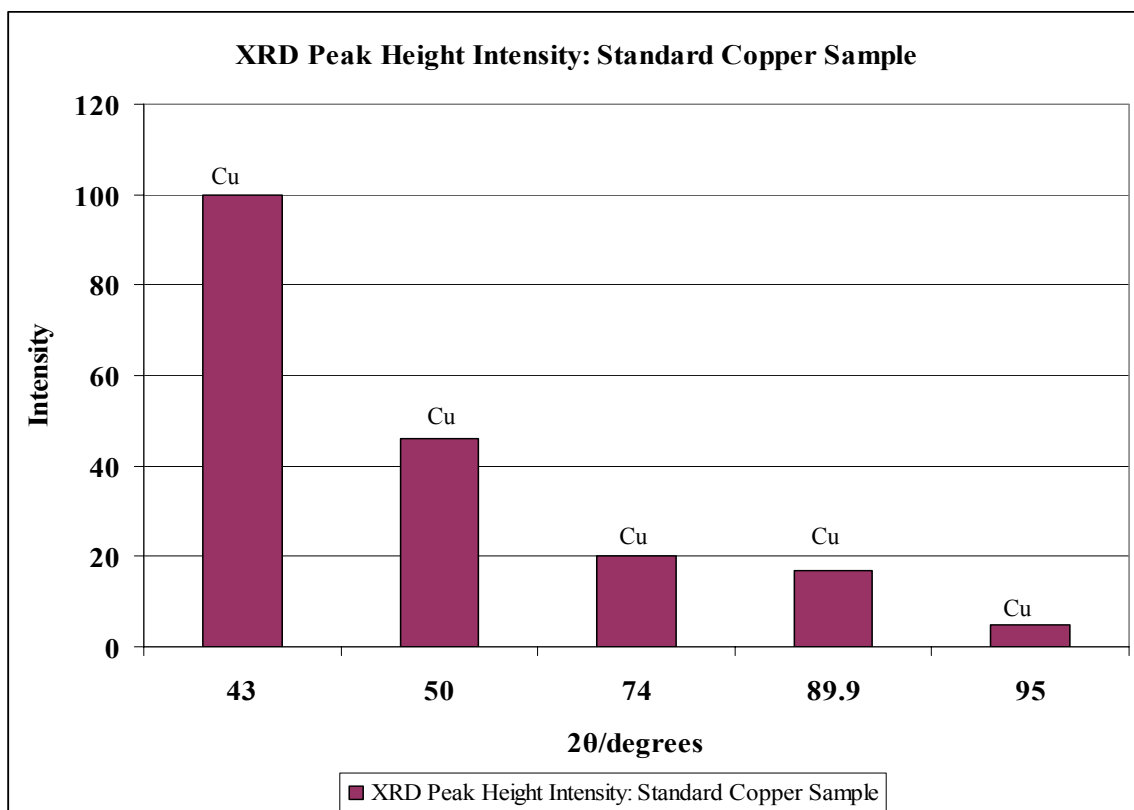


Figure 5.56: XRD Peak Height Intensity: Standard Copper Sample

Figures 5.51 to 5.55 show the peak height intensities measured from the XRD spectra while table 5.17 below lists the preferential planes along with their relative intensities for a standard copper sample (International Center for Diffraction Data, 1980).

**Table 5.15: Copper Diffraction Pattern (standard sample)**

| <b>Bragg angle (<math>2\theta</math>)</b> | <b>Plane (h k l)</b> | <b>Intensities (<math>I/I_1</math>)</b> |
|---|----------------------|---|
| 43.30                                     | (111)                | 100                                     |
| 50.44                                     | (200)                | 46                                      |
| 74.12                                     | (220)                | 20                                      |
| 89.91                                     | (311)                | 17                                      |
| 95.14                                     | (222)                | 5                                       |

In four of the copper deposit samples, the (111) plane was preferred as shown in figures 5.51, 5.52, 5.53 and 5.55. These were deposits from the DSA 1 plate and mesh anode cells, DSA 2 plate anode cell and the lead anode cell. This is similar to a standard copper sample as shown in figure 5.56.

However, for the DSA 2 mesh anode cell, the dominant crystal orientation was in the (200) crystal plane as shown in figure 5.54. This is a deviation from the standard crystal orientation, which can be attributed to the iron contaminant from electrolyte entrapment (Biswas *et al.* 2002), found in the deposit. Iron has been reported to adversely affect the morphology of copper deposits by hindering the formation of copper seeds in such a way that it cannot undergo any mechanical working (De Filippo *et al.*, 1989).

The BMR solution used in the study contained  $12.4 \text{ kg/m}^3$  Fe in comparison to  $2 \text{ kg/m}^3$ , stated by Maki (1999) as the concentration necessary to minimise iron in cathode copper. Therefore, in this study, the high level of iron in the BMR solution significantly increased the chances of iron contamination through electrolyte entrapment, despite washing the cathodes thoroughly.

According to Alfantazi and Valic (2003), good quality copper deposits are produced when a single crystal growth plane is dominant. In this study, copper deposits from the cells containing the DSA 1 mesh and lead anodes had one dominant plane (111). However a good quality deposit was only produced in the cell containing the DSA 1 mesh anode. As previously mentioned the deposit was also uniform (figures 5.43 and 5.48) and had no traces of harmful cations like iron or lead which exert a detrimental effect on the deposit quality thereby reducing its grade. The copper from the lead cell was contaminated with lead. Lead which accumulates on the edges of the copper grains inhibits growth of the seeds, thus reducing the final dimensions of the microcrystals. This leads to a reduction in copper conductivity and consequently reduces not only its grade but also its competitiveness in the market.

Copper deposits from the DSA 1 plate, DSA 2 plate and DSA 2 mesh cells had more than one dominant crystal plane ((111) and (200) planes); the (200) plane being the second preferred plane for the DSA 1 plate and DSA 2 plate cells. These copper deposits both exhibited nodular growth as shown in pictures 1 and 2 and micrographs 1 and 2. In the DSA 2 mesh cell, the (111) crystal plane was the second preferred plane and although the deposit was uniform it was impure as shown in figure 5.54.

All copper deposits also contained traces of copper oxide either as CuO or Cu<sub>2</sub>O. This may have been the reason why other crystal planes were not evident in the copper deposits as is the case with a standard copper sample. In consultation with other experts in the field, it was noted that there is always some oxygen present in a cathode. Furthermore, occlusion of electrolyte could have been another main source of oxygen in the copper deposit (Nicol, 2006). It is therefore possible that these oxides may or may not have been formed after removal from the cell.



## 5.5 Economic evaluation

A simplified economic evaluation was carried out as shown in table 5.18. The energy consumption per kg copper for the five anodes was in the range 1.7 to 2.7 kWh/kg copper; close to the range reported by Gupta and Mukherjee (1990) of 0.16 to 2.5 kWh/kg copper.

**Table 5.16: Simplified Economic Evaluation of Replacing Lead Anodes with a DSA Anode**

| Anode Material (405 mm*330 mm) | Materials Costs <sup>a</sup> (\$) | Energy Consumption (kWh) | Copper Deposited in 150 hrs (kg) | Current Efficiency (%) | Energy Consumption (kWh/kg Cu) | Energy Consumption (kWh/t Cu) | Energy Cost/kg Cu (\$/kg) <sup>b</sup> |
|--------------------------------|-----------------------------------|--------------------------|----------------------------------|------------------------|--------------------------------|-------------------------------|--|
| Pb-6%Sb                        | 124                               | 13.1                     | 6.6                              | 86.2                   | 2.0                            | 2 000                         | 0.300                                  |
| DSA 1 Plate                    | 410                               | 12.3                     | 7.3                              | 89.3                   | 1.7                            | 1 700                         | 0.255                                  |
| DSA 2 Plate                    | 755                               | 14.1                     | 6.7                              | 82.5                   | 2.1                            | 2 100                         | 0.315                                  |
| DSA 1 Mesh                     | 434                               | 11.6                     | 4.4                              | 53.5                   | 2.6                            | 2 600                         | 0.390                                  |
| DSA 2 Mesh                     | 578                               | 11.5                     | 4.2                              | 51.0                   | 2.7                            | 2 700                         | 0.405                                  |

<sup>a</sup> Material costs were calculated in U.S. dollars and they include prices of hanger bars.

<sup>b</sup> Energy costs were calculated at US\$0.15/kWh.

**Table 5.17: Other Fixed Costs in the Study**

| Equipment                        | Fixed Capital Costs (US\$) |
|----------------------------------|----------------------------|
| Power Supply Unit                | 3300                       |
| Pump                             | 1840                       |
| Cathodes                         | 600                        |
| Heating Elements & Control boxes | 965                        |
| Piping                           | 245                        |
| <b>Total</b>                     | <b>6950</b>                |

The economic evaluation shows that the DSA 1 plate anode had the least energy consumption per kilogramme of copper produced among all the five materials considered under the investigation. As a result its energy cost was 15% lower than that of the conventional lead anode. Moats and Free (2007) reported that DSA anodes coated with a precious metal oxide coating based on IrO<sub>2</sub> resulted in power consumption 10-17% lower than that of the conventional lead anodes.

Although both DSA 1 and 2 mesh anodes exhibited the lowest total energy consumption, they had the highest energy consumption per kilogramme of copper produced. As a result, their energy costs per kg copper were significantly high (30%-35% greater than the lead anode respectively). This can be attributed to the low current efficiencies of 53.5% and 51% respectively in the cells containing these anodes. Biswas *et al.* (2002) reported that high current efficiency is important because it maximises copper plating rate and minimises electrical energy consumption. Energy cost per kg of copper produced for the DSA 2 plate anode was also 5% higher than that of the lead anode due to the high cell voltage values in its cell.

## 6 SUMMARY OF RESULTS

### 6.1 Comparison of anode materials

#### 6.1.1 Electrochemical Investigations

Several tests were conducted in order to determine the best anode under conditions of constant current, temperature and concentration. All electrochemical tests were performed in a single compartment, 500 ml Pyrex beaker at room temperature and in synthetic solution of concentration 55 g/l Cu and 100 g/l H<sub>2</sub>SO<sub>4</sub>.

##### *6.1.1.1 Open circuit potential measurements*

Open circuit potential (OCP) measurements were carried out in order to assess the stability of the anodes under investigation. The tests also furnished information on the anode material with the highest corrosion resistance and the redox transitions controlling the surface electrochemistry of the anodes.

The results indicated that the initial sharp decrease in potential from 0.49 V to 0.45 V, within the first 200 s for the DSA plate, could have been caused by the erosion of coating particles that are weakly bonded to the substrate once there is interaction between the electrolyte and the anode (Martelli *et al.*, 1994). For the DSA mesh, the potential shifted more rapidly towards the nobler potentials from 0.33 V to 0.41 V within the first 3750 seconds and then stabilised while for the antimonial lead specimen, a small increase in potential from 0.08 V to 0.10 V was observed for the whole duration of the experiment.

The OCP measurements showed that the DSA anodes had nobler potentials compared to the lead alloy anode with the DSA plate having the largest average open circuit potential ( $E_{oc}$ ) value of 0.44 V vs Ag/AgCl. These results suggest that the DSA plate had the highest corrosion resistance.

The OCP measurements also indicated that the DSA anodes could be controlled by hydrated Ir(III)/Ir(IV) redox transition (Alves *et al.*, 1998) while the lead anode surface is controlled by the Pb/Pb(II) redox transition.

#### 6.1.1.2 Potentiodynamic polarisation

Potentiodynamic polarisation was used to assess:

- the ability of materials to passivate spontaneously in the synthetic solution and
- the potential region over which the specimen remained passive
- corrosion rate of the metal specimens in the synthetic solution.

Unlike the lead alloy and DSA mesh anodes, the DSA plate anode did not show early passivation tendencies in the potential range of -0.4 V to 1.2 V. Only active and pseudo-passive behaviour were evident. However, in the potential range of -0.4 V to 1.4 V the DSA plate anode also showed active-passive behaviour. Since passivation is the most frequent deactivation mechanism for DSA anodes (Martelli *et al.*, 1994), it can be concluded that the DSA mesh anode is likely to succumb to failure earlier than the DSA plate anode after continuous operation.

The potentiodynamic polarisation tests also showed that the DSA plate anode exhibited the highest corrosion resistance of 0.8 mm/year against 2.37 mm/year for the DSA mesh anode and 2.48 mm/year for the lead anode. These results reveal the corrodible nature of lead alloy anodes over DSA plate anodes (Alfantazi and Moskalyk, 2003). Despite the mesh anode being a dimensionally stable anode, its high corrosion (3 times greater than the DSA plate anode) can be attributed to the large electrochemically active surface area (EASA) available for corrosion.

#### 6.1.1.3 Chronopotentiometry (galvanostatic) tests

Chronopotentiometry tests were carried out in order to evaluate anode potentials and electrode stability under galvanostatic conditions at a current density of 190 A/cm<sup>2</sup>. The results showed that the lead anode has the highest anode potential of 1.97 V vs

Ag/AgCl, followed by the DSA plate anode (1.6 V vs Ag/AgCl) and lastly, the DSA mesh anode (1.5 V vs Ag/AgCl). Since anode potential is a major component of the cell voltage, and is directly related to energy consumption, the use of dimensionally stable anodes in the place of the lead anodes can considerably lower the energy demand of electrowinning. An energy reduction of 19% and 24% can be achieved with the DSA plate anode and the DSA mesh anode, respectively.

The extent to which contaminants in the electrolyte can affect the cell voltage during electrowinning was also investigated using galvanostatic chronopotentiometry tests. The tests showed that addition of manganese to the synthetic electrolyte increased the anode potential values for the DSAs from averages of: 1.6 V to 1.8 V for the DSA plate anode and 1.5 V to 1.65 V for the DSA mesh anode. However, for the lead anode, a slight depolarising effect to the magnitude of 3% was observed. The results indicate that, if lead anodes were to be replaced, the average energy savings in synthetic/manganese solution would be 6% for the DSA plate anode and 14% for the DSA mesh anode as compared to 19% and 24% previously reported for the synthetic solution.

Manganese oxide deposition blocks the catalytic sites on the DSA anodes, leading to an increase in anode potential and inevitably the cell voltage. This reduces the energy saving benefit that would have otherwise been achieved. On the lead anode the presence of a manganese oxide layer has been reported to result in the reduction of the anode's corrosion rate.

Chronopotentiometry tests were also carried out for base metal refinery (BMR) electrolyte and higher average anode potential values than those in the synthetic solution were recorded. These mean values were 2.33 V, 2.16 V and 1.91 V for the lead anode, DSA plate and mesh anodes respectively.

#### 6.1.1.3.1 Determination of current efficiency

The current efficiencies as determined for the three anodes from the weight gained by the cathode were 97.9% for both DSA anodes (plate and mesh) and 97.6% for the lead anode. This shows an insignificant difference between all the anodes in terms of initial current efficiency for fresh anodes in synthetic electrolyte. These results are substantiated by the work reported by Panda and Das (2001).

#### 6.1.1.3.2 Electrolyte contamination from anode deterioration

The electrolytes were analysed for lead, titanium, iridium and tantalum contamination after two hours of galvanostatic chronopotentiometry using the Atomic Absorption Spectrometer. The results revealed that during electrowinning of copper using lead alloy anodes, anodic dissolution of lead occurs. This is likely to result in cathode contamination and reduced life span for the anodes.

The presence of traces of tantalum (coating stabiliser) and iridium (active component) in electrolytes containing both DSA anodes was also confirmed in the AAS analysis. This indicates that during electrowinning operations using DSA anodes, some loss of coating occurs. The amount of iridium loss was 0.003 ppm; three times greater than the tantalum loss. This is attributed to the high stability of tantalum in the coating. Traces of the titanium substrate were also detected in the samples analysed.

The amount of iridium loss in the electrochemical cell containing the DSA mesh anode was 33% greater than the iridium loss in the cell containing the DSA plate specimen (0.004 ppm against 0.003 ppm) as a result of the large electrochemically active surface area (EASA) characteristic of the mesh anodes.

#### 6.1.1.4 Cyclic voltammetry

Cyclic voltammetry was carried out in order to assess the surface characteristics and determine the anode with the greatest electrochemically active surface area (EASA). All experiments were carried out in 0.5 M sulphuric acid solution.

#### 6.1.1.4.1 Cyclic voltammograms for lead anodes

For the lead anode, curves generated over the potential ranges of 0 to 2 V and -0.5 to 2.2 V, covered the reactions from metallic lead,  $\text{Pb}^0$ , to Pb (IV) and oxygen evolution. All the curves showed two anodic peaks at scanning in the positive direction, the first peak being attributed to the anodic dissolution of lead and formation of a  $\text{PbSO}_4$  layer, which has passivating properties. This was followed by a wide passive region. As the anodic potential increased to about 1.75 V, lead (IV) oxide formed at the surface of the electrode. A further increase in the potential resulted in  $\text{O}_2$  evolution around 1.9 V. The results also showed that oxygen evolution intensified with the increase in cycle number. The cathodic peak which appeared at 1.4 V in the reverse scan could be attributed to the reduction of  $\text{PbO}_2$  formed on the surface, back into  $\text{PbSO}_4$ , while a small cathodic peak at -0.5 V was attributed to the reduction of  $\text{PbSO}_4$  to Pb.

#### 6.1.1.4.2 Cyclic voltammograms for DSA anodes

Voltammetric curves for the DSA anodes were recorded between -0.6 to 1.5 V (up to the oxygen evolution potential). Several current peaks were observed in both voltammograms. The anodic peak at a potential of approximately 1.5 V was due to the oxygen evolution reaction, while the cathodic peak at a potential of about -0.6 V indicated intensive hydrogen evolution. A pair of peaks observed at potentials between 0.3 and 0.5 V for the DSA mesh was likely to be a result of the redox transition, Ir (III)/Ir (IV) while for the DSA plate a smaller current peak appearing around 0.5 V was also attributed to the same redox transition as that of the mesh. The broad nature of these peaks showed the heterogeneity of the surface active sites on these electrodes.

#### 6.1.1.4.3 Electrochemically active surface area for the anode specimens

Voltammetric charges ( $q^*$ ) were measured at a scan rate of 20 mV/s for the three anode specimens in the potential range 0 to 1.5 V. The results showed that the mesh had the greatest value of  $q^*$  and as such it has the largest working area for oxygen evolution. This may be attributed to its structure. The larger working area results in increased catalytic activity, thereby facilitating the lowering of the effective current density and resulting in reduced anode potential (Kulandaisamy *et al.*, 1997).

#### 6.1.1.4.4 Effect of continuous cycling on voltammetric charge

The variation of voltammetric charge with continuous cycling for the DSA mesh and plate anodes and the lead anode specimens was also investigated. It was observed that the voltammetric charge  $q^*$ , calculated by graphical integration of the cyclic voltammetry (CV) curves in the range between 0 and 1.5 V, increased with cycling time in the first 40 cycles for the plate and 20 cycles for the mesh,  $q^*$ , after which there was little change in the voltammetric charge. These results suggested that the DSA anode specimens had attained a stable condition (Xu and Scantlebury, 2003). Of the two DSA anodes, the mesh stabilised faster (after 20 cycles) due to its large EASA which consequently results in shorter hydration time of the inner layer.

The voltammetric charge  $q^*$  calculated in the range between 0 and 2.0 V for the lead anode also increased with cycling time. There was a rapid increase in the first 15 cycles, which was followed by a steady continuous increase in voltammetric charge. This may have been due to the formation of a passive film of porous lead (IV) oxide as cycling progressed.

#### 6.1.1.4.5 Determination of double layer capacitance

Determination of the double layer capacitance for both DSA mesh and plate anodes indicated that a linear relationship exists between current density and scan rate. For the lead anode specimen, the relationship between current density and scan rate showed a large deviation from linearity and for this reason, the double layer



capacitance,  $C_{dl}$ , was replaced by the constant phase element (CPE). Similarly to the anodic charge,  $q^*$ , the DSA mesh had a higher double layer capacitance than the DSA plate anode and as such it can be concluded that  $C_{dl}$  can be used to describe the EASA of each anode (Xu and Scantlebury, 2003). A linear relationship was also found to exist between the anodic charge  $q$ , and the double layer capacitance,  $C_{dl}$ .

#### 6.1.1.4.6 Determination of Roughness Factor (RF)

The RF value for the Ti/IrO<sub>2</sub>-Ta<sub>2</sub>O<sub>5</sub> mesh anode was 60% greater than that for Ti/IrO<sub>2</sub>-Ta<sub>2</sub>O<sub>5</sub> plate anode, suggesting that both porous morphology and the structure of oxide anodes have an influence on the surface roughness and consequently the electrochemically active surface area.

#### 6.1.1.5 *Electrochemical impedance spectroscopy (EIS)*

Impedance measurements were carried out in order to provide supportive evidence for the above results. The tests were carried out at the open circuit potential and the oxygen evolution potential as determined from cyclic polarisation and galvanostatic chronopotentiometry measurements. The results showed that polarisation resistances for all the anode materials were higher at the open circuit potential compared to the oxygen evolution potential.

This is an indication that an unused metal in the case of lead anodes or a metal covered with an undamaged or fresh coating in the case of DSAs generally has very high impedance. At both potentials at which EIS studies were carried out, the polarisation resistances measured confirmed the superior performance of the DSA plate anode with respect to its corrosion resistance over the DSA mesh and lead anodes. The variation of the constant phase element, CPE and  $n$ , from impedance plots was also in agreement with the calculated values of double layer capacitance,  $C_{dl}$ , and roughness factor previously mentioned for the DSAs.

Impedance tests were also carried out at different potentials in the region of the OER reaction. The DSA mesh anode had the lowest  $R_{ct}$  values among the three anode materials probably due to its greater EASA which results in better catalytic performance.

#### *6.1.1.6 Chronoamperometry (<1s)*

Chronoamperometry (<1s) was used for the rapid characterisation of the three anodes. The results in synthetic electrolyte showed that upon applying a potential step of 1.5 V, the resulting OER current initially decreases and quickly reaches a quasi steady-state value. For the DSA anodes, the initial decrease in current density represented the dissolution of the active component occurring during electrolysis. As penetration of the electrolyte occurred through the mud cracked, porous structure of the thermally prepared oxide layer, the DSA anodes stabilised at 0.3 seconds. For the lead alloy anode, the initial decrease in current density may be attributed to the partial blockage of the electrode surface due to the formation of a passivating layer. However, as the thickness of the layer increased, the anode stabilised at 0.05 seconds.

### 6.1.2 Physical Characterisation

#### *6.1.2.1 X-Ray Diffractometry (XRD) analysis of anode materials*

The XRD analysis for unused DSAs showed  $\text{IrO}_2$  and  $\text{Ta}_2\text{O}_5$  phases while for used DSAs the XRD spectrum only showed the presence  $\text{Ta}_2\text{O}_5$  and titanium phases. This is an indication of  $\text{IrO}_2$  loss from the coating during anode use (Hu *et al.*, 2002). The unused lead alloy anode spectrum showed only lead and traces of antimony while the XRD spectrum for a used lead alloy anode revealed the presence of lead sulphate ( $\text{PbSO}_4$ ) on the anode surface.

#### *6.1.2.2 Scanning Electron Microscopy (SEM) analysis*

Results from the SEM analysis showed that the Pb/Pb(II) redox transition controls the surface of the lead alloy anode as previously suggested from the open circuit potential

measurements and XRD analysis. Surface morphology of the unused DSAs showed a mud-cracked structure of the oxide coating while for the used DSAs, the absence of the mud-cracked structure indicated that coating loss had occurred during operation.

#### *6.1.2.3 Energy Dispersive Spectrometry (EDS) analysis*

EDS analysis revealed that iridium and tantalum are the major elements on the surface of the titanium substrate for an unused DSA anode. However, an analysis of a used DSA anode showed a heavy presence of the titanium substrate and traces of iridium and tantalum which are the active and inert components respectively. This EDS result suggests that the failure mechanism of the DSA anodes is due to coating consumption (reduction in coating thickness) which results in a stronger titanium signal. The results also indicate that some residual coating remains on the DSA anodes, after deactivation.

### 6.1.3 Electrowinning Experiments

Electrowinning tests were carried out in a PVC cell having three separated compartments, using base metal refinery (BMR) solution of concentration 55 g/l Cu and 100 g/l H<sub>2</sub>SO<sub>4</sub> at 55 °C and a current density of 190 A/m<sup>2</sup>. Anodes tested were two types of DSA plate anodes, two types of DSA mesh anodes and one type of lead anode.

#### *6.1.3.1 Variation of cell voltage with time*

The results show that both DSA 1 and 2 mesh anodes had the lowest average energy consumption of 41 760 kJ and 41 400 kJ respectively. The cell voltage values in the cells containing the DSA 1 plate and lead anodes were almost similar in the first 95 hours of operation with mean cell voltages of 1.92 V and 1.84 V respectively. However, the significant drop in cell voltage for the DSA 1 plate anode to approximately 1.57 V may indicate that the anode had reached a stable condition at which any increase in cell voltage after continuous operation would indicate failure or

anode deactivation. The cell voltage values for the lead anode remained in the region of 1.80 V.

For the DSA 2 plate and lead anodes the cell voltage values remained quite high for the whole duration of the experiment (150 hours), with mean voltages of 2.05 V and 1.96 V respectively. From these results it can be seen that the traditional lead anodes result in high energy consumption during electrowinning. The DSA 2 plate anode showed a deviation from DSA 1 anode behaviour since the cell voltage values remained high during the investigation. This may be attributed to the methods used during the preparation of this anode, causing the anode to take a longer time than its DSA 1 plate counterpart to attain its stable condition.

#### *6.1.3.2 Current Efficiency*

Overall, the current efficiencies in the electrowinning tests were lower than those from electrochemical tests which were  $\gg 90\%$  for all the anodes. This may be attributed to the presence of iron in the BMR solution which is not contained in synthetic solution.

The DSA 1 plate anode had the greatest current efficiency of 89.3%, while DSA 1 and DSA 2 mesh anodes had the lowest current efficiencies of 53.5% and 51.0%, respectively.

A number of factors could have contributed towards the low current efficiencies which characterised both DSA mesh anodes. Firstly, since coated titanium electrode have been reported to oxidise ferrous ions to ferric ions, which has a bearing on current efficiency; the oxidation with mesh anodes may have been more profound than that resulting from DSA plate anodes. This may have led to reduced cathode current efficiency in the cells containing these anodes. Other factors such as; precise material composition, impurities, cross-sectional areas of the cathodes and anode

current density could have played a role too in affecting the cathode current efficiency.

#### *6.1.3.3 XRD analysis and optical micrography of copper deposits*

XRD analysis and optical micrography were carried out in order to characterise the crystallographic orientation and morphology of the copper deposits produced. In four of the copper deposit samples, the (111) plane was preferred; similar to a standard copper sample. These were deposits from the DSA 1 plate and mesh anode cells, DSA 2 plate anode cell and the lead anode cell. However, for the DSA 2 mesh anode cell, the dominant crystal orientation was in the (200) crystal plane. This is a deviation from the standard crystal orientation, which can be attributed to the iron contaminant found in the deposit, which affected the morphology of the copper deposit (De Filippo *et al.*, 1989).

Copper deposits from the DSA 1 plate, DSA 2 plate and DSA 2 mesh cells had more than one dominant crystal plane ((111) and (200) planes); the (200) plane being the second preferred plane for the DSA 1 plate and DSA 2 plate cells. These copper deposits both exhibited nodular growth. In the DSA 2 mesh cell, the (111) crystal plane was the second preferred plane and, although the deposit was uniform, it was impure.

Copper deposits from the cells containing the DSA 1 mesh and lead anodes had one dominant plane (111). However, a good quality deposit was only produced in the cell containing the DSA 1 mesh anode. The deposit was uniform and had no traces of harmful cations like iron or lead which exert a detrimental effect on the deposit quality thereby reducing its grade.

The copper from the lead cell was contaminated with lead; an indication that the anode degrades during electrowinning. Lead which accumulates on the edges of the copper grains inhibits growth of the seeds, thus reducing the final dimensions of the

microcrystals. This leads to a reduction in copper conductivity and consequently reduces not only its grade but also its competitiveness in the market.

All copper deposits also contained traces of copper oxide either as CuO or Cu<sub>2</sub>O. This may have been the reason why crystal planes 220, 311 and 222 were not evident in the copper deposits as is the case with a standard copper sample. In consultation with other experts in the field, it was noted that there is always some oxygen present in a cathode. Furthermore, occlusion of electrolyte could have been another main source of oxygen in the copper deposit. It is therefore possible that these oxides may or may not have been formed after removal from the cell.

#### 6.1.4 Economic evaluation

The economic evaluation showed that the DSA 1 plate anode had the least energy consumption per kilogramme of copper produced among all the five anode materials considered under the investigation. As a result its energy cost was 15% lower than that of the conventional lead anode. Although both DSA 1 and 2 mesh anodes exhibited the lowest total energy consumption, they had the highest energy consumption per kilogramme of copper produced. As a result, their energy costs per kg copper were 30%-35% greater than the lead anode respectively. This can be attributed to the low current efficiencies of 53.5% and 51% respectively in the cells containing these anodes. Energy cost per kg of copper produced for the DSA 2 plate anode was also 5% higher than that of the lead anode due to the high cell voltage values in its cell.

## 7 CONCLUSIONS AND RECOMMENDATIONS

### 7.1 Conclusions

A good anode material should remain inert and enable oxygen to be evolved at the lowest possible overpotential during the electrowinning process. Electrochemical tests, physical characterisation techniques and electrowinning of copper from acidic sulphate media were carried out on DSA and lead anodes in order to determine the most suitable anode based on stability, energy consumption and copper deposit quality. The following key findings were made:

#### 7.1.1 Anode Stability

Potentiodynamic polarisation tests showed that the DSA plate anode exhibited the highest corrosion resistance followed by the DSA mesh anode and lead anode respectively. The DSA mesh anode's corrosion rate was three times greater than the DSA plate anode and almost equivalent to that of the lead anode. This could be a result of the large electrochemically active surface area (EASA) associated with mesh anodes as determined from cyclic voltammetry tests. Open circuit potential measurements performed were also in agreement with these results.

Galvanostatic chronopotentiometry tests showed that lead anode dissolution occurs during electrowinning of copper, since lead ions were detected in the electrolyte containing the lead anode. Furthermore, there were traces of iridium, and tantalum in the electrolyte from both DSA plate and mesh anodes; an indication that the failure mechanism of DSA anodes not only involves passivation but also coating consumption due to the interaction between the anodes and the electrolyte (Martelli *et al.*, 1994, Hu *et al.* 2002).

Life expectancies of the DSA plate, DSA mesh and lead anodes were also assessed using potentiodynamic polarisation. The lead and DSA mesh anodes showed spontaneous passivation in synthetic solution, an indication that these anodes are likely to succumb to failure by passivation earlier than the DSA plate anode.

### 7.1.2 Cell voltage

Generally, DSA mesh anodes had the lowest mean cell voltages compared to the DSA plates and lead anodes. Furthermore, it was also noted that DSA anodes of the same composition may exhibit different behaviours as this depends on the method of preparation of the anode itself. This was seen for the DSA 2 plate anode cell, whose mean cell voltage was higher than that of the lead anode cell while the DSA 1 plate anode had a lower mean cell voltage. Therefore, oxygen overpotential and conditioning times in DSA anodes depend critically on the method of preparation of the anode itself.

### 7.1.3 Techno-economic evaluation

The results from the economic evaluation indicated that although both DSA 1 and 2 mesh anodes exhibited the lowest total energy consumption as a result of the low mean cell voltages in their cells, these anodes were associated with the highest energy consumption per kilogramme of copper produced among the five anodes considered under the electrowinning investigation. This was due to the low current efficiencies of these mesh anodes. Energy cost per kg of copper produced for the DSA 2 plate anode was comparable to that of the lead anode due to the high cell voltage values in its cell. In this investigation, the DSA 1 plate anode had the greatest current efficiency and as such was associated with the least energy consumption per kilogramme of copper produced. Therefore, energy saving is not entirely dependent on cell voltage but also on current efficiency.



#### 7.1.4 Cathode contamination

Copper deposits harvested from the lead anode cell, during the electrowinning process, showed the presence of lead oxide on analysis with an X-ray diffractometer.

#### 7.1.5 Effect of impurities in the electrolyte

Electrowinning tests and galvanostatic chronopotentiometry tests conducted in BMR solution and synthetic solution containing manganese, revealed that the presence of contaminants such as iron or manganese in the electrolyte is not only detrimental to cathode quality and current efficiency, but may also lead to voltage fluctuations and an increase in anode potential or cell voltage for dimensionally stable anodes.

Therefore, an overall analysis taking all the electrode materials studied under this investigation into account, indicates that the best electrode option for the electrowinning of copper in industrial electrolytes is the DSA 1 plate anode.

### **7.2 Recommendations for future research**

- There is a need for further classification of dimensionally stable anodes in terms of the preparation method (solvent of the painting solution, firing temperature) and composition since it was shown that DSA anodes with the same material compositions may have different behaviours (anode potentials, conditioning times). Therefore, the conventional lead anodes used in the electrowinning of copper may be replaced once a proper classification of the DSA anodes has been established.
- BMR solution contains other impurities such as arsenic, selenium and chromium, all of which may have an adverse effect on the anode potential and stability of the anode itself. Thus more research should be done in this area in

order to determine how much impurities can override the said benefits of DSA anodes and to what extent the structure of the titanium substrate and coating can be modified in order to make it less susceptible to attack by impurities. Chromates in BMR solution have also been mentioned to react with  $Ta_2O_5$  in DSA anode coatings resulting in early deactivation of the anode.

- Further investigations can be carried out on other anode materials such as the Mesh on Lead (MoL), the Pb-Co (0.5-6% Co) and  $Pb-Co_3O_4$ , the titanium-lead anode (Ti-Pb) and the  $IrO_2-Bi_2O_3$  based anodes, which have been documented to have advantages over the conventional lead based anodes.
- In order to improve the economics of the DSA anodes, the power savings can be improved further by lowering the oxygen overpotential. The use of stabilised ruthenium oxide ( $RuO_2$ ) has been reported to be economically attractive because not only do ruthenium based coatings have a lower oxygen overpotential than their iridium based counterparts, the cost of ruthenium is half that of iridium.
- More investigation into the effects of anode current density on cathode current efficiency is required especially on the DSA mesh anodes.

### **7.3 Expected contribution to knowledge**

- Most researchers have focused on the behaviour of anode materials in synthetic solution (copper in sulphuric acid) but this project has shown that results obtained in synthetic solution are only ideal conditions and do not exactly satisfy plant conditions, due to the impurities in industrial (BMR) electrolytes. Therefore, in order to carry out laboratory scale experiments to simulate electrowinning processes, additional elements found in BMR electrolytes need to be added in synthetic solutions in order to determine the

extent to which each contaminant has a bearing on anode potentials, cell voltages and deposit morphology.

- The research also showed that DSA anodes of the same composition may exhibit different behaviours as this depends on the method of preparation of the anode itself.
- In this investigation, tests were carried out on DSA mesh anodes which most researchers have not focused on. The results from this study suggested that, anode current density may play a role in the determination of cathode current efficiency. Therefore, further investigations should be done by varying anode current density in order to determine the extent to which anode current density may affect cathode current efficiency.
- The study also showed that the presence of manganese in copper electrowinning electrolytes increases anode potentials for the DSAs while it has a slight depolarising effect on the antimonial lead anode.

## REFERENCES

- Alfantazi, A.M. and Valic, D. (2003) “A Study of Copper Electrowinning Parameters Using a Statistically Designed Methodology”, *Journal of Applied Electrochemistry*, 33 (2), 217-225.
- Alfantazi, A.M. and Moskalyk, R.R. (2003) “Conductive Polymer Coatings for Anodes in Aqueous Electrowinning”, *Journal of the Minerals, Metals and Materials Society* 55 (7), 49-55, 57.
- Alves, V. A. L., da Silva, A. and Boodts, J. F. C. (1998) “Surface Characterisation of IrO<sub>2</sub>/TiO<sub>2</sub>/CeO<sub>2</sub> Oxide Electrodes and Faradaic Impedance Investigation of the Oxygen Evolution Reaction from Alkaline Solution”, *Electrochimica Acta.*, 44 (8-9), 1525-1534.
- Angelinetta, C., Trasatti, S., Atanasoska, Lj.D., Minevski, Z.S. and Atanasoski, R.T. (1989) “Effect of Preparation on the Surface and Electrocatalytic Properties of RuO<sub>2</sub> + IrO<sub>2</sub> Mixed Oxide Electrodes”, *Journal of Materials, Chemistry and Physics*, 22 (1-2), 535-546.
- Balko, E.N. and Nguyen, P.H. (1991): “Iridium-Tin Mixed Oxide Anode Coatings”, *Journal of Applied Electrochemistry*, 21 (8), 678-682.
- Bard, A.J., and Faulkner, L.R. “Electrochemical Methods-Fundamentals and Applications”, John Wiley & Sons, Inc., New York, USA, 1980.
- Bard, A. J.; Faulkner, L. R. “Electrochemical Methods. Fundamentals and Applications” 2nd Ed., John Wiley& Sons, New York, USA, 2001.
- Beer, H.B. (1980) “The Invention and Industrial Development of Metal Anodes”, *Journal of the Electrochemical Society*, 127 (8) 303C-307C.
- Biswas, A.K., Davenport, W.G., King, M., and Schlesinger, M. “Extractive Metallurgy of Copper”, 4<sup>th</sup> edition, Pergamon, New York, USA, 2002.
- Cardarelli, F., Taxil, P., Savall, A., Comninellis, C., Manoli, G. & Leclerc, O. (1998) “Preparation of Oxygen Evolving Electrodes With Long Service Life Under Extreme Conditions” *Journal of Applied Electrochemistry*, 28 (3), 245-250.

- Cheng, X. and Hiskey, J.B. (1996) “Fundamental Studies of Copper Anode Passivation During Electrorefining: Part I. Development of Techniques”, *Metallurgical and Materials Transactions B*, 27 (3), 393-398.
- Cifuentes, G., Cifuentes, L. and Crisostomo, G. (1998) “A Lead-Acid Battery Analogue to In Situ Anode Degradation in Copper Electrometallurgy”, *Corrosion Science*, 40 (2-3), 225-234.
- Comninellis, Ch. and Vercesi, G. P. (1991) “Characterisation of DSA-Type Oxygen Evolving Electrodes: Choice of a Coating”, *Journal of Applied Electrochemistry*, 21 (4), 335-345.
- Comninellis, C. (1994) “Electrochemical oxidation of organic pollutants for wastewater treatment”, In *Environmental Oriented Electrochemistry*; Sequeira, C. A. C., Ed.; Elsevier: Amsterdam, Netherlands, 77-102.
- Cooper, W.C. (1985) “Advances and Future Prospects in Copper Electrowinning”, *Journal of Applied Electrochemistry*, 15 (6), 789-805.
- Das, S.C. and Gopala K.P. (1996) “Effect of Fe (III) During Copper Electrowinning at Higher Current Density”, *International Journal of Mineral Processing*, 46 (1-2), 91-105.
- Da Silva, L.M., Boodts, J. F. C. and De Faria, L.A. (2001) “Oxygen Evolution at  $\text{RuO}_2(x) + \text{Co}_3\text{O}_4 (1-x)$  Electrodes from Acid Solution”, *Electrochimica Acta*, 46 (9), 1369-1375.
- Dean, S.W. (1987) “Technical Note: Calculation of Alloy Equivalent Weight”, *Materials Performance*, 25 (12), 51-52.
- De Assisa, S.L., Wolyneec, S. and Costa, I. (2006) “Corrosion characterization of titanium alloys by electrochemical techniques”, *Electrochimica Acta*, 51 (8-9), 1815-1819.
- De Filippo, D., Dessi', L. and Rossi, A. (1989) “Effect of Iron (III) and Lead (II) on the Quality of Copper Electrodeposited from a Pyrophosphate Bath”, *Journal of Applied Electrochemistry*, 19 (1), 37-42.

- De Pauli, C.P. and Trasatti, S. (1995) “Electrochemical Surface Characterization of IrO<sub>2</sub> + SnO<sub>2</sub> Mixed Oxide Electrocatalysts”, *Journal of Electroanalytical Chemistry*, 396 (1-2), 161-168.
- Donachie, M.J. “Titanium: A Technical Guide”, 2nd Ed., ASM International, Ohio, USA, 2000.
- Ferdman, A., (2000) “Insoluble Titanium-Lead Anode for Sulphate Electrolytes”, *US Patent 6129822*.
- Fierro, S., Nagel, T., Baltruschat, H. and Comminellis, C. (2007) “Investigation of the Oxygen Evolution Reaction On Ti/IrO<sub>2</sub> Electrodes Using Isotope Labelling and On-Line Mass Spectrometry” *Electrochemistry Communications*, 9(8), 1969-1974.
- Flewitt, P.E.J. and Wild, R.K. “Physical Methods for Materials Characterisation”, 2nd Edition, Institute of Physics Publishing, Philadelphia, USA, 2003.
- Forti, J.C., Olivi, P. and De Andrade, A.R. (2001) “Characterisation of DSA®-Type Coatings with Nominal Composition Ti/Ru<sub>0.3</sub>Ti<sub>(0.7-x)</sub> Sn<sub>x</sub>O<sub>2</sub> Prepared via a Polymeric Precursor”, *Electrochimica Acta*, 47 (6), 913-920.
- Gilchrist, J.D. “*Extraction Metallurgy*”, 3<sup>rd</sup> Edition, Pergamon Press, Oxford, UK, 1989.
- Gosser, D.K. (Jr). “Cyclic Voltammetry: Simulation and Analysis of Reaction Mechanisms”, VCH Publishers, New York, USA, 1993.
- Gupta, C.K. and Mukherjee, T.K. “*Hydrometallurgy in Extraction Processes*”, Volume 2, CRC Press, Florida, USA, 1990.
- Herlitz, F. (2004) “Titanium in the Electrochemical Industry-Use and Protection”, Permascand AB, Sweden, [WWW].
- Hine, F., Yasuda, M., Noda, T., Yoshida, T. and Okuda, J. (1979) “Electrochemical Behavior of the Oxide-Coated Metal Anodes”, *Journal of Electrochemical Society*, 126 (9), 1439-1445.
- Hine, F. “Electrode Processes and Electrochemical Engineering”, Plenum Press, New York and London, USA&UK, 1985.

- Hrussanova, A., Mirkova, L. and Dobrev, Ts. (2001) “Anodic Behaviour of the Pb–Co<sub>3</sub>O<sub>4</sub> Composite Coating in Copper Electrowinning”, *Hydrometallurgy*, 60 (3), 199-213.
- Hu, C. C., Lee, C. H. and Wen, T. C. (1996) “Oxygen Evolution and Hypochlorite Production on Ru-Pt Binary Oxides” *Journal of Applied Electrochemistry*, 26(1), 72-82.
- Hu, J.M., Meng, H.M., Zhang, J.Q. and Cao, C.N. (2002) “Degradation Mechanism of Long Service Life Ti/IrO<sub>2</sub>–Ta<sub>2</sub>O<sub>5</sub> Oxide Anodes in Sulphuric Acid”, *Corrosion Science*, 44 (8), 1665-1668.
- Hu, J., Zhang, J. and Cao, C. (2004) “Oxygen evolution reaction on IrO<sub>2</sub>-based DSA<sup>®</sup> type electrodes: kinetics analysis of Tafel lines and EIS”, *International Journal of Hydrogen Energy*, 29 (8), 791-797.
- International Center for Diffraction Data (1980), “Mineral Powder Diffraction File”, JCPDS, Pennsylvania, USA.
- Jones, D.A. “Principles and prevention of corrosion, 2nd edition, Prentice Hall, Upper Saddle River, New Jersey, USA, 1996.
- Kao, W.H. and Weibel, V. J. (1992) “Electrochemical Oxidation of Manganese (II) at a Platinum Electrode” *Journal of Applied Electrochemistry*, 22 (1), 21-27.
- Kear, G. and Walsh, C. (2005) “The Characteristics of a True Tafel Slope”, *Journal of Corrosion and Materials*, 30 (6), 51-55.
- Kotz, R., Lewerenz, H.J. and Stucki, S. (1983) “XPS Studies of Oxygen Evolution on Ru and RuO<sub>2</sub> Anodes”, *Journal of Electrochemical Society*, 130 (4), 825-829.
- Kristóf, J., Szilágyi, T., Horváth, E., De Battisti, A., Frost, R.L. and Rédey, Á. (2004) “Investigation of IrO<sub>2</sub>/Ta<sub>2</sub>O<sub>5</sub> Thin Film Evolution”, *Thermochimica Acta*, 413 (1-2), 93-99.
- Krysa, J., Kule, L., Mraz, R. and Rousar, I. (1996) “Effect of Coating Thickness and Surface Treatment of Titanium on the Properties of IrO<sub>2</sub>-Ta<sub>2</sub>O<sub>5</sub> Anodes”, *Journal of Applied Electrochemistry*, 26 (10), 999-1005.

- Kulandaisamy, S., Prabhakar, R.S., Chockalingam, S.C., Visvanathan, S., Venkateswaran, K.V., Ramachandran, P. and Nandakumar, V. (1997) “Performance of Catalytically Activated Anodes in the Electrowinning of Metals”, *Journal of Applied Electrochemistry*, 27 (5), 579-583.
- Lassali, T.A., Bulhoses, L.O., Abeid, L.M. and Boodts, J.F. (1997) “Surface Characterisation of Thermally Prepared, Ti-Supported, Ir-Based Electrocatalysts Containing Ti and Sn”, *Journal of the Electrochemical Society*, 144(10), 3348-3354.
- Ling, X., Gu, Z.H. and Fahidy, T.Z. (1994) “Effect of Operating Conditions on Anode Passivation in the Electrorefining of Copper “, *Journal of Applied Electrochemistry*, 24 (11), 1109-1115.
- Loufty, R.O. and Leroy, R.L. (1978) “Energy Efficiency in Metal Electrowinning”, *Journal of Applied Electrochemistry*, 8 (6), 549-555.
- Maki, T. (1999) “Evolution of Cathode Quality at Phelps Dodge Mining Company” In *Copper Leaching, Solvent Extraction, and Electrowinning Technology*, ed. Jergensen II, G.V., SME, Littelton, CO., USA, 223-225.
- Martelli, G.N., Ornelas, R. and Faita, G. (1994) “Deactivation Mechanisms Of Oxygen Evolving Anodes at High Current Densities”, *Electrochimica Acta*, 39 (11-12), 1551-1558.
- Meyers, R. “The Basics of Chemistry (Basics of the Hard Sciences)”, Greenwood Press, Westport, USA, 2003.
- Moats, M., Hardee, K., and Brown, C., (2003) “Mesh-on-Lead Anodes for Copper Electrowinning”, *Journal of Metals*, 55(7), 46-48.
- Moats, M. and Free, M. (2007) “A Bright Future for Electrowinning”, *Journal of the Minerals, Metals and Materials Society*, 59 (10), 34-36.
- Moats, M.S. (2008) “Will Lead-based Anodes Ever be Replaced in Aqueous Electrowinning?”, *Journal of Minerals, Metals and Materials Society*, 60 (10), 46-49.
- Mráz, R. and Krýsa, J. (1994) “Long Service Life IrO<sub>2</sub>/Ta<sub>2</sub>O<sub>5</sub> Electrodes for Electroflotation”, *Journal of Applied Electrochemistry*, 24 (12), 1262-1266.



- Nicol, M.J. (2006) “Electrowinning and Electrorefining of Metals”, A Course Presented To Anglo Research.
- Nijjer, S., Thonstad, J., and Haarberg, G.M. (2001) “Cyclic and Linear Voltammetry on Ti/IrO<sub>2</sub>-Ta<sub>2</sub>O<sub>5</sub>-MnO<sub>x</sub> Electrodes in Sulphuric Acid Containing Mn<sup>2+</sup> Ions”, *Electrochimica Acta*, 46(23), 3503-3508.
- Ortiz, P.I., De Pauli, C.P. and Trasatti, S. (2004) “Composite Materials for Electrocatalysis: Ti/(SnO<sub>2</sub>+IrO<sub>2</sub>) Surface and Electrocatalytic Properties Studied by Impedance and Chlorine Evolution”, *Journal of New Materials for Electrochemical Systems*, 7 (2), 153-159.
- Panda B. and Das S. C. (2001) “Electrowinning of Copper from Sulphate Electrolyte in the Presence of Sulfurous Acid”, *Hydrometallurgy*, 59 (1), 55-67.
- Pfalzgraff, C.L. (1999) “Do’s and Don’t’s of Tankhouse Design and Operation” In *Copper Leaching, Solvent Extraction, and Electrowinning Technology*, ed. Jergensen II, G.V., SME, Littelton, CO., USA, 217-221.
- Pletcher, D. “Industrial Electrochemistry”, Chapman and Hall, UK, 1982.
- Pletcher, D. “A first course in Electrode Processes”, Alresford Press Ltd., Alresford, Hants, UK, 1991.
- Pourbaix, M. “Atlas of Electrochemical Equilibria, in Aqueous Solutions” Pergamon Press, New York, USA, 1974.
- Rolewicz, J., Comninellis, C., Plattner, E. and Hinden, J. (1988) “Characterisation of DSA-type electrodes for Oxygen Evolution- 1. Titanium/Iridium Dioxide-Tantalum Pentoxide Electrode”, *Journal of Electrochimica Acta*, 33 (4), 573-580.
- Rubel, M., Haasch, R., Mrozek, P., Wieckowski, A., De Pauli, C. and Trasatti, S. (1994) “Characterization of IrO<sub>2</sub>-SnO<sub>2</sub> Thin Layers by Electron and Ion Spectroscopies”, *Vacuum*, 45 (4), 423-427.
- Savall, A. (1995) “Electrochemical treatment of industrial organic effluents”, *Chimia International Journal for Chemistry*, 49 (1-2), 23-27.

- Scully, J. C. “The Fundamentals of Corrosion”, 2nd edition, Pergamon Press Ltd, Headington Hill Hall, Oxford, UK, 1975.
- Spinolo, G., Ardizzone, S. and Trasatti, S. (1997) “Surface Characterisation of  $\text{Co}_3\text{O}_4$  Electrodes Prepared by the Sol-Gel Method” *Journal of Electroanalytical Chemistry*, 423 (1-2), 49-57.
- Sprowls, D.O. “Metals Handbook”, Volume 13, 9th edition, *Corrosion*, ASM International, Metals Park, OH., USA, 1987.
- Stern, M. and Geary, A.L. (1957) “Electrochemical Polarization: A Theoretical Analysis of the Shape of Polarization Curves”, *Journal of Electrochemical Society*, 104 (1), 56-63.
- Trasatti, S. (2000) “Electrocatalysis: understanding the success of DSA<sup>®</sup>”, *Electrochimica Acta*, 45 (15-16), 2377-2385.
- Tuffrey, N. Fletcher, H., Marinovich, Y. and McGinnity, J. (2006) “Improved Anode and Cathode Processes in Base Metal Electrowinning”, AMIRA Project.
- Tyroler, P.M., Sanmiya, T.S., Krueger, D.W. and Stupavsky, S. (1987) “Copper Electrowinning at Inco's Copper Refinery” In *The Electrowinning and Winning of Copper*, ed. J.E. Hoffmann, R.G., Bautista, V.A., Ettl, V., Kudryk, R.J., Wesely, published by The Metallurgical Society Inc., 421-435.
- Uchida, I., Urushibata, H. and Toshima, S. (1981) “Electrocatalysis for Chlorine Electrode Reaction on  $\text{RuO}_2$  Electrode in  $\text{NaAlCl}_4$  Melt”, *Journal of Electrochemical Society*, 128 (11), 2351-2357.
- Vercesi, G.P., Salamin, J.Y. and Comninellis, Ch. (1991) “Morphological and Microstructural Study of the  $\text{Ti}/\text{IrO}_2\text{-Ta}_2\text{O}_5$  Electrode: Effect of the Preparation Temperature”, *Electrochimica Acta*, 36 (5-6), 991-998.
- Weems, D., Schledorn, M. and Farmer, M. D. (2005) “An Insoluble Titanium-Lead Anode for Sulphate Electrolytes”, Electrodes International, Inc. Technical Report.

- Xu, L. K. and Scantlebury, J. D. (2003), “Electrochemical Surface Characterisation of IrO<sub>2</sub>-Ta<sub>2</sub>O<sub>5</sub> Coated Titanium Electrodes in Na<sub>2</sub>SO<sub>4</sub> Solution”, *Journal of the Electrochemical Society*, 150 (6), B288-B293.
- Yoshio, T., Norihiro, Y. and Wataru, S., (2008) "Oxygen reduction behaviour of RuO<sub>2</sub>/Ti, IrO<sub>2</sub>/Ti and IrM (M: Ru, Mo, W, V) O<sub>x</sub>/Ti binary oxide electrodes in a sulphuric acid solution", *Electrochemistry Communications*, 10(4), 668-672.
- Yu, Pu. and O’Keefe, T.J. (1999) “Evaluation of Lead Anode Reactions in Acid Sulphate Electrolytes I. Lead Alloys with Cobalt Additive”, *Journal of the Electrochemical Society*, 146 (4), 1361-1369.
- Yu, Pu. and O’Keefe, T.J. (2002) “Evaluation of Lead Anode Reactions in Acid Sulphate Electrolytes II. Manganese Reactions”, *Journal of the Electrochemical Society*, 149 (5), A558-A569.
- Zhang, W. and Cheng, C.Y. (2007) “Manganese Metallurgy Review. Part III: Manganese Control in Zinc and Copper Electrolytes”, *Hydrometallurgy*, 89 (3-4), 178-188.

### **Other Bibliographic Sources Consulted and Used**

- Christensen, P. A., and Hamnett, A. “Techniques and Mechanisms in Electrochemistry”, Chapman and Hall, Oxford, UK, 1994.
- Comminellis, Ch. and Vercesi, G. P. (1991) “Problems in DSA Coating Deposition by Thermal Decomposition”, *Journal of Applied Electrochemistry*, 21 (2), 136-142.
- ([http://www.coleparmer.com/techinfo/techinfo.asp?htmlfile=pump\\_challenge.htm&ID=623](http://www.coleparmer.com/techinfo/techinfo.asp?htmlfile=pump_challenge.htm&ID=623))
- [http://www.permascand.com/content/leftmenu/electrochemical\\_systems-general/images/R&D0411.pdf](http://www.permascand.com/content/leftmenu/electrochemical_systems-general/images/R&D0411.pdf) (2 November 2007).
- <http://www.cp.umist.ac.uk>

- Kotz, R., and Stucki, S. (1986) “Stabilisation of RuO<sub>2</sub> by IrO<sub>2</sub> for Anodic Oxygen Evolution in Acid Media”, *Electrochimica Acta*, 31 (10).
- Laibach, S., Anastasijevic, N., Nepper, J.P., Bilson, E. and Grider J. (2001) “Innovations in Electrowinning Technology”, (11 November 2007). [www.hydrometallurgysection.org/2001electro/paperno2-6.pdf](http://www.hydrometallurgysection.org/2001electro/paperno2-6.pdf)
- Massot, L., Palau, P., A. Savall, A. and Taxil, P. (2006) “Comparison between Derived Sol-Gel and Conventional Methods for the Preparation of Dimensionally Stable Ta/IrO<sub>2</sub> Anodes for Oxygen Evolution”, *Journal of New Materials for Electrochemical Systems* 10, 123-128.
- Princeton Applied Research, “Electrochemistry and Corrosion Overview and Techniques”.
- Rashkov, S., Dobrev, T., Noncheva, Z., Stefanov, Y., Rashkova, B., and Petrova, M., (1999) “Lead-Cobalt Anodes for Electrowinning of Zinc from Sulphate Electrolytes”, *Hydrometallurgy*, 52(3), 223-230.
- Straumanis, M. and Chen, P. (1951) “The corrosion of titanium in acids: the rate of solution in sulphuric, hydrochloric, hydrobromic and hydroiodic acids”, *Corrosion* 7 (7), 229-237.
- Trasatti, S., and Buzzanca, G. (1971) “Ruthenium Dioxide: A New Interesting Electrode Material, Solid State Structure and Electrochemical Behaviour”, *Journal of Electroanalytical Chemistry*”, 29 (1), 1-5.

## **APPENDICES**

## APPENDIX A: FLOW RATE CALCULATIONS

Concentration of copper in BMR electrolyte = 55 g / l

Volume of electrolyte per cell = 16 l

∴ Total mass of copper in electrolyte per cell:

$$\begin{aligned} & 16l \times 55 \text{ g/l} \\ & = 880 \text{ g} \\ & 27.5\text{g} \end{aligned}$$

Minimum concentration of copper = 47.5 g / l

∴ Minimum mass of copper in spent electrolyte:

$$\begin{aligned} & 16l \times 47.5 \text{ g/l} \\ & = 760 \text{ g} \\ & 23.75 \end{aligned}$$

∴ Amount of copper deposited:

$$\begin{aligned} & 880 \text{ g} - 760 \text{ g} \\ & = 120 \text{ g} \\ & 3.75 \end{aligned}$$

Applied Current per cell:

$$I = \text{Current density}(j) \times \text{Area}(A)$$

$$\begin{aligned} \text{Anode area (A)} &= 0.36 \times 0.33 \times 2 \text{ faces} \\ &= 0.2376 \text{ m}^2 \end{aligned}$$

$$\begin{aligned} I &= 190 \text{ A/m}^2 \times 0.2376 \text{ m}^2 \\ &\approx 46 \text{ A} \end{aligned}$$

$$0.019 \text{ A}$$

Assuming 90% current efficiency:

$$t = \frac{nF\Delta W}{\varepsilon IM}$$

$$t = \frac{2 * 96500 * 120}{0.9 * 46 * 63.5} = 2.44 \text{ hrs } 666528.52$$

$$185.14$$

Since  $Q = \frac{V}{t}$ ; At  $t = 2.44$  hrs:

$$\begin{aligned} Q &= \frac{16}{2.44} = 0.021 \text{ l/min} \\ &= 6.56 \text{ l/hr} \\ &= 110 \text{ ml/min} \end{aligned}$$

## APPENDIX B: OPERATING PARAMETERS

|                    |                                    | Given parameter                |          | Set parameter   |           | Same <input type="checkbox"/> C<br>Same current density<br>Same cycle time | Same <input type="checkbox"/> C<br>Same current density<br>Same cycle time |
|--------------------|------------------------------------|--------------------------------|----------|-----------------|-----------|--|--|
|                    | Parameter                          | Unit                           | Plant    | Mini-cell (BMR) | Wits cell |  |  |
| Cell               | Length                             | m                              | 4.100    | 0.52            | 0.375     |  |  |
|                    | Width                              | m                              | 1.050    | 0.29            | 0.12      |  |  |
|                    | Depth                              | m                              | 1.300    | 0.3             |           |  |  |
|                    | Active depth                       | m                              | 1.092    | 0.275           | 0.37      |  |  |
|                    | Real volume                        | m <sup>3</sup>                 | 5.6      | 0.045           | 0.000     |  |  |
|                    | Active Volume                      | m <sup>3</sup>                 | 4.7      | 0.041           | 0.017     |  |  |
|                    | Flowrate                           | m <sup>3</sup> /hr             | 0.33     | 0.0026          | 0.0067    |  |  |
|                    |                                    | l/min                          | 5.5      | 0.0440          | 0.1112    |  |  |
|                    |                                    | l/hr                           | 330      | 2.639           | 6.670     |  |  |
|                    | Residence time                     | h                              | 14.2     | 15.7            | 2.5       |  |  |
|                    | Volume electrolyte per cycle       | L                              | 55440    | 443             | 1121      |  |  |
|                    | Inlet conc                         | g/L                            | 75       | 75              | 55        |  |  |
|                    | Outlet conc                        | g/L                            | 35       | 35              | 47.5      |  |  |
|                    | Rate of plating                    | g/h                            | 13200    | 106             | 50        |  |  |
|                    | Plating cycle                      | h                              | 168      | 168             | 168       |  |  |
|                    | Plated mass                        | kg                             | 2217.6   | 18              | 8         |  |  |
|                    | Current                            | A                              | 13000    | 99              | 47        |  |  |
| Current Density    | A/m <sup>2</sup>                   | 192                            | 192      | 192             |           |  |  |
| Cathode            | Thick                              | m                              | 0.00092  | 0.00092         | 0.00092   |  |  |
|                    | Width                              | m                              | 0.92     | 0.28            | 0.33      |  |  |
|                    | Height                             | m                              | 0.92     | 0.23            | 0.37      |  |  |
|                    | Surface area (one face)            | m <sup>2</sup>                 | 0.85     | 0.06            | 0.12      |  |  |
|                    | Surface area per cathode (2 sides) | m <sup>2</sup>                 | 1.7      | 0.13            | 0.244     |  |  |
|                    | No. of cathodes                    |                                | 40       | 4               | 1         |  |  |
|                    | Total surface area                 | m <sup>2</sup>                 | 68       | 0.515           | 0.244     |  |  |
|                    | Mass per cathode                   | kg                             | 55.440   | 4.433           | 8.404     |  |  |
|                    | Mass per cathode 'side'            | kg                             | 27.720   | 2.216           | 4.202     |  |  |
|                    | Specific mass cathode              | kg/m <sup>2</sup>              | 32.750   | 34.416          | 34.416    |  |  |
| Faraday            | mass plated                        | g                              | 2217600  | 17731           | 8404      |  |  |
|                    | mol                                |                                | 2        | 2               | 2         |  |  |
|                    | Faraday                            | As/mol                         | 96485    | 96485           | 96485     |  |  |
|                    | M                                  | g/mol                          | 63.55    | 63.55           | 63.55     |  |  |
|                    | time                               | s                              | 604800   | 604800          | 604800    |  |  |
|                    | Theoretical current                | A                              | 11133.86 | 89              | 42        |  |  |
| Current efficiency | %                                  | 86                             | 90       | 90              |           |  |  |
| Add info           | Catholyte to surface area          | m <sup>3</sup> /m <sup>2</sup> | 0.0694   | 0.0805          | 0.0682    |  |  |



## APPENDIX C: HEATER SIZING

### Assumptions:

- All calculations were based on synthetic electrolyte.
- Specific heat capacity of solution is similar to the specific heat capacity of water.

a) Calculation of the power required to heat the solution and container:

$$P = \frac{mc\Delta T}{860 * t_h} \dots\dots\dots 4.2$$

Where,

P- power (kW)

m- mass (kg)

c- specific heat capacity (kcalories/kg<sup>0</sup>C)

$\Delta T$  - temperature rise (<sup>0</sup>C)

$t_h$  - heat-up time (hours)

$$Mass(m) = Density * Volume$$

$$Mass(m) = 1.3 \text{ kg / l} * 16 \text{ l}$$

$$P(kW) = \frac{1.3 * 16 * 1 * 40}{860 * 2} = 0.48 \text{ kW}$$

b) Calculation of the power required to heat the container:

$$P(kW) = \frac{5.7 * 0.25 * 40}{860 * 1} = 0.066 \text{ kW}$$

c) Calculation of the power required to overcome heat losses:

$$\text{Heat losses} = 0.2 * (0.48 + 0.066)kW = 0.11kW$$

d) Total Heat Rating

$$\text{Heat rating} = 0.48 + 0.066 + 0.11 = 0.66kW$$

APPENDIX D: CURVES SHOWING REPRODUCIBILITY OF RESULTS

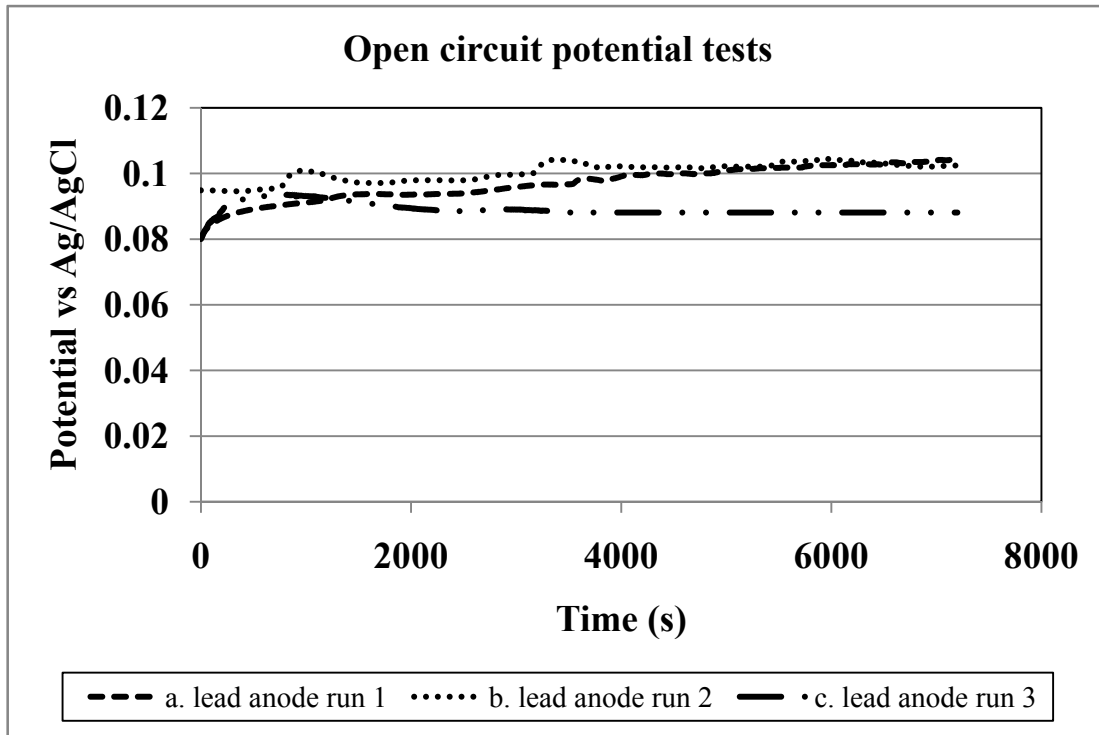


Figure 1: Open Circuit Potential Tests for the Lead Anode.

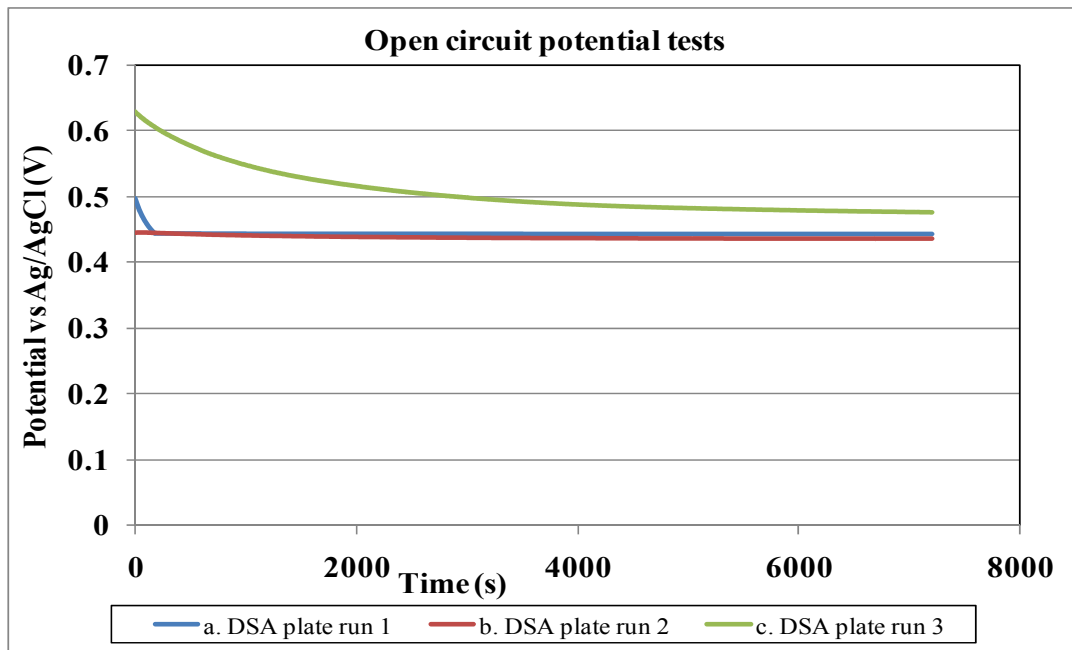


Figure 2: Open Circuit Potential Tests for the DSA Plate Anode.

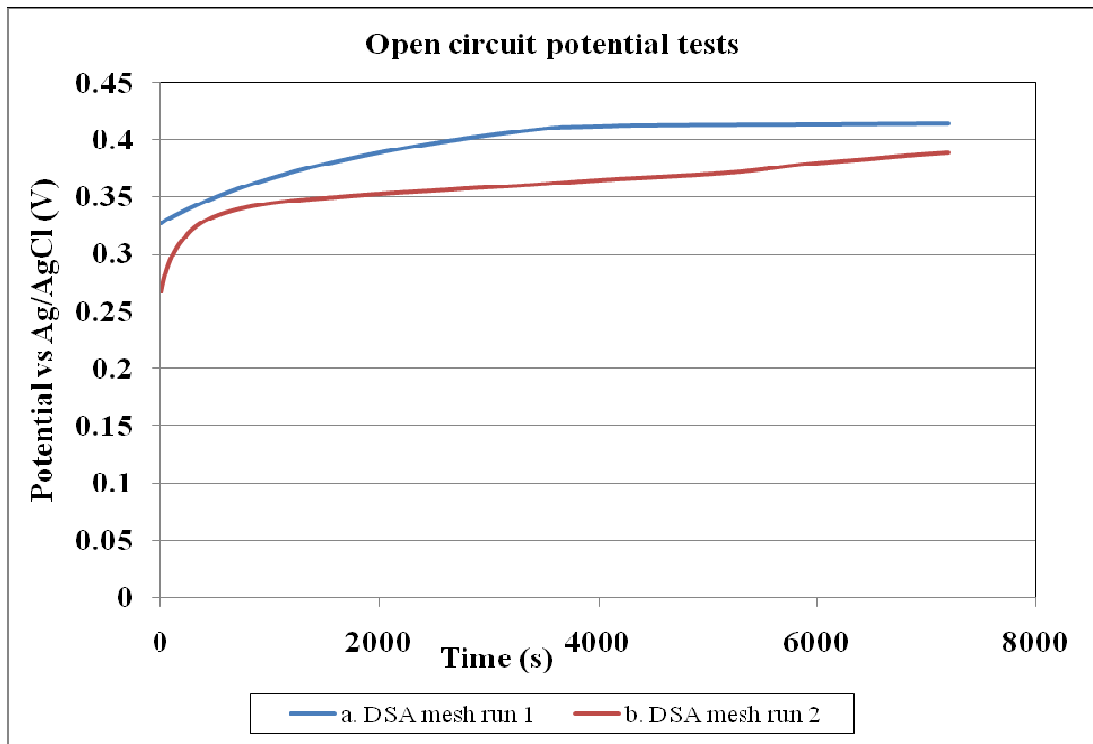


Figure 3: Open Circuit Potential Tests for the Lead Anode.

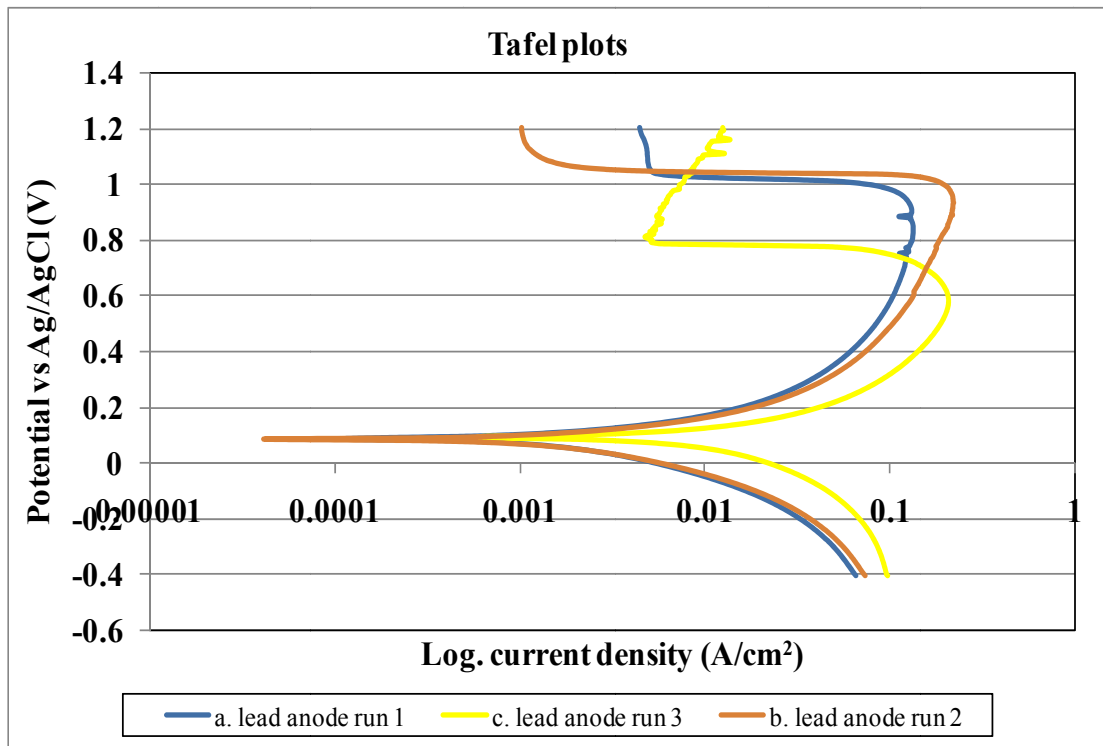


Figure 4: Tafel Plots for the Lead Anode.

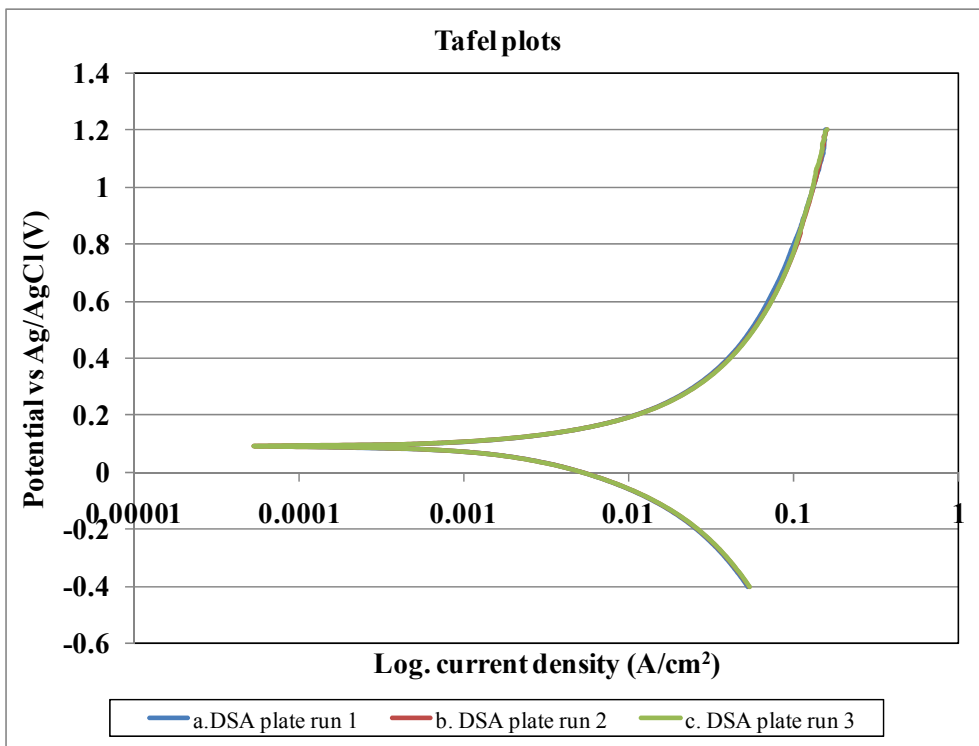


Figure 5: Tafel Plots for the DSA Plate Anode.

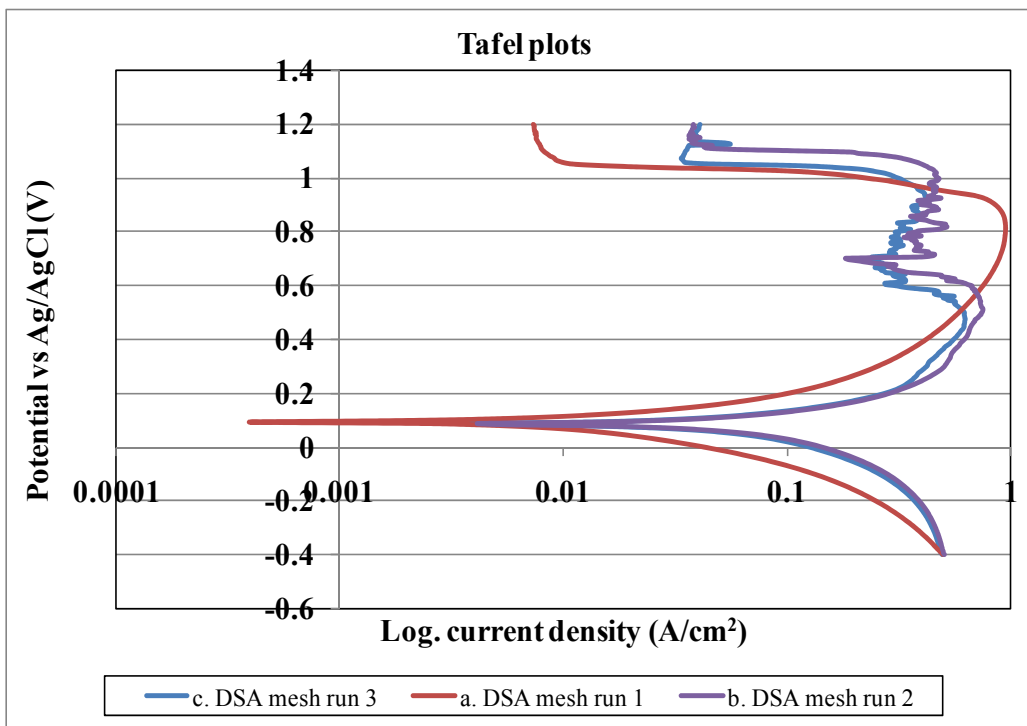


Figure 6: Tafel Plots for the DSA Mesh Anode.

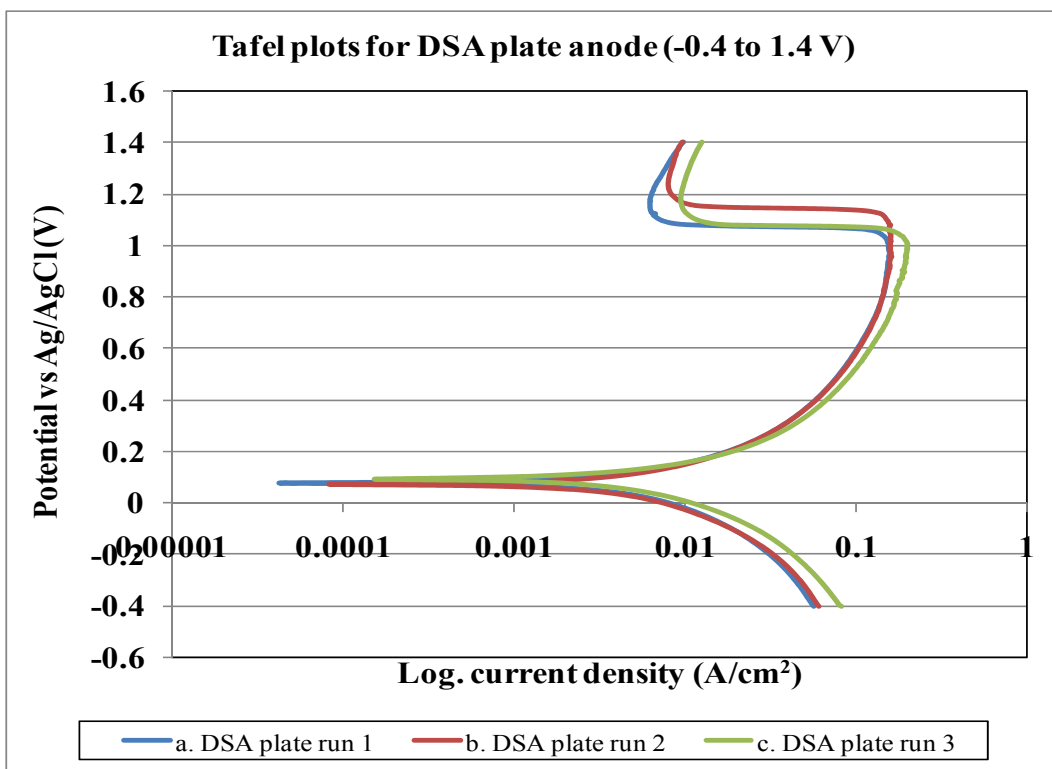


Figure 7: Tafel Plots for the DSA Plate Anode in the Potential Range (-0.4 V to 1.4 V).

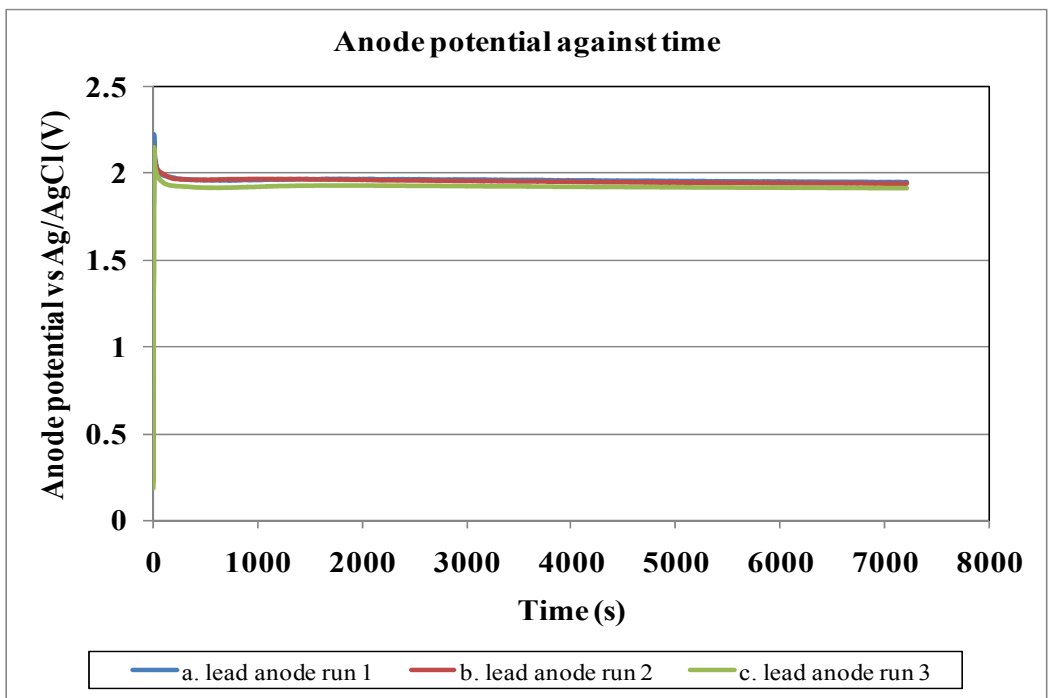


Figure 8: Galvanostatic Chronopotentiometry Curves for the Lead Anode.

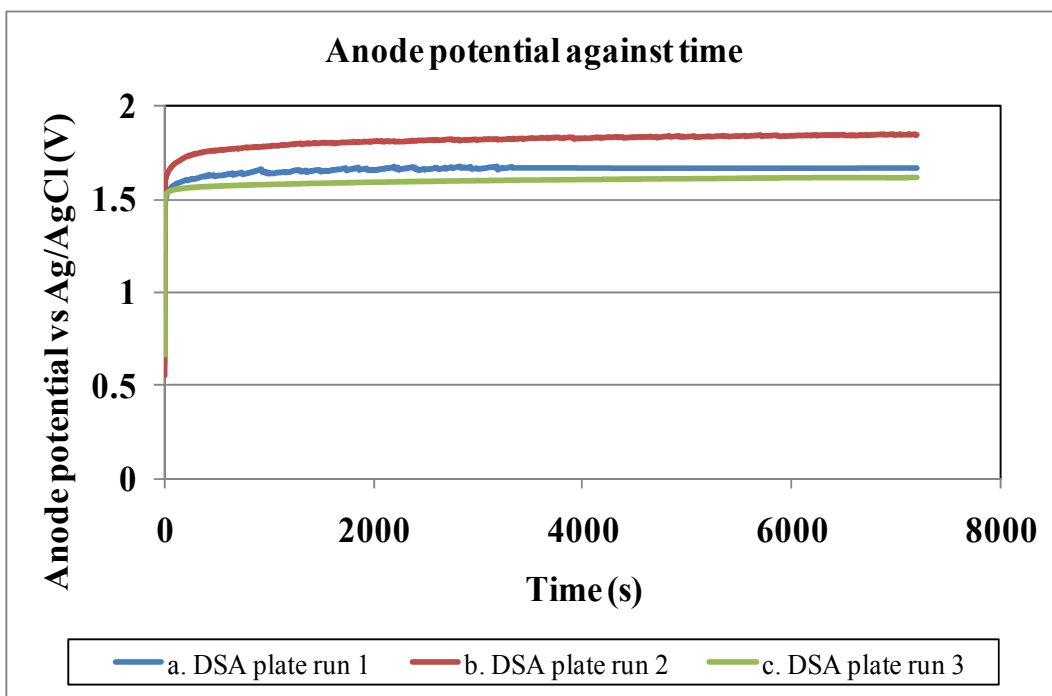


Figure 9: Galvanostatic Chronopotentiometry Curves for the DSA Plate Anode.

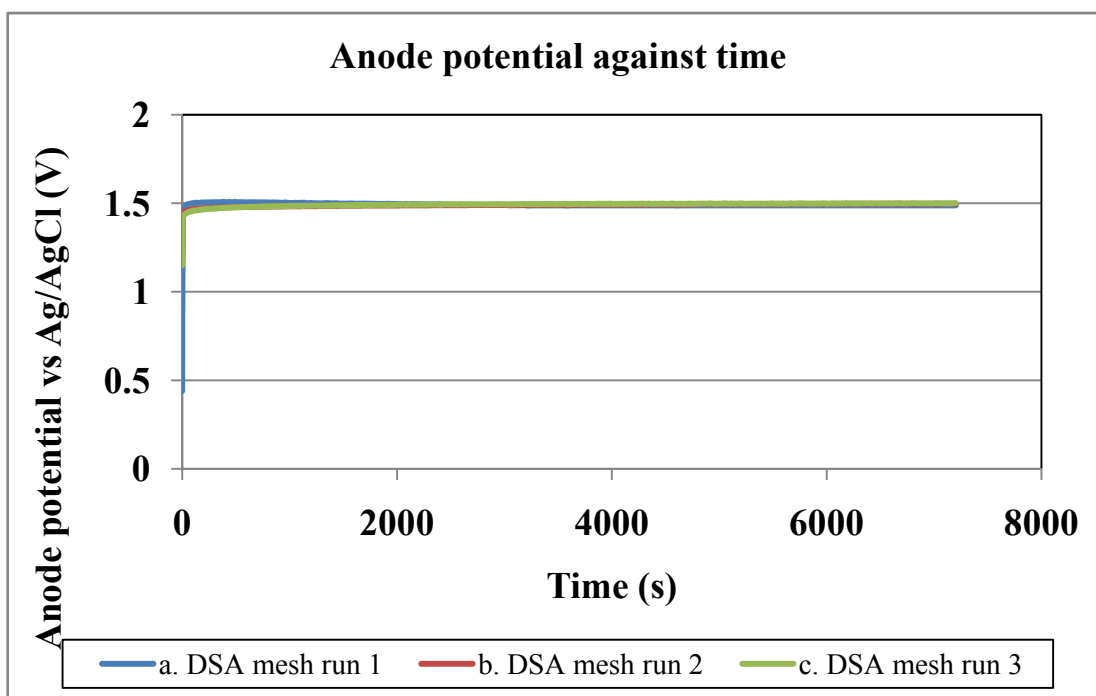


Figure 10: Galvanostatic Chronopotentiometry Curves for Mesh Anodes.

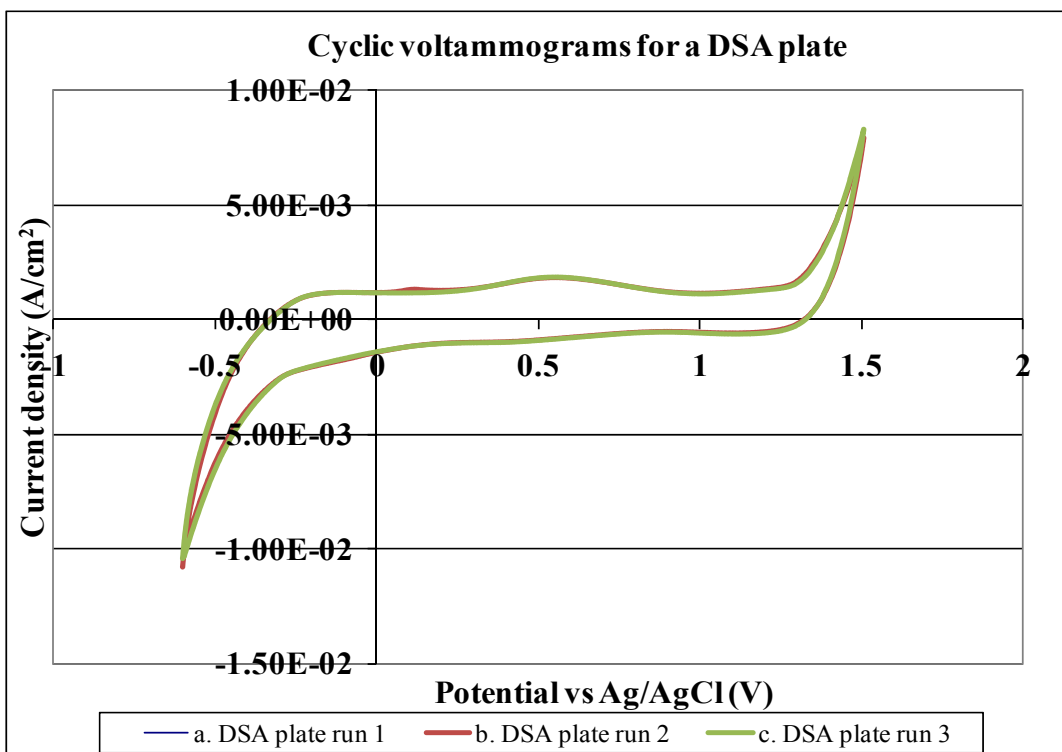


Figure 11: Cyclic Voltammograms for a DSA Plate Anode.

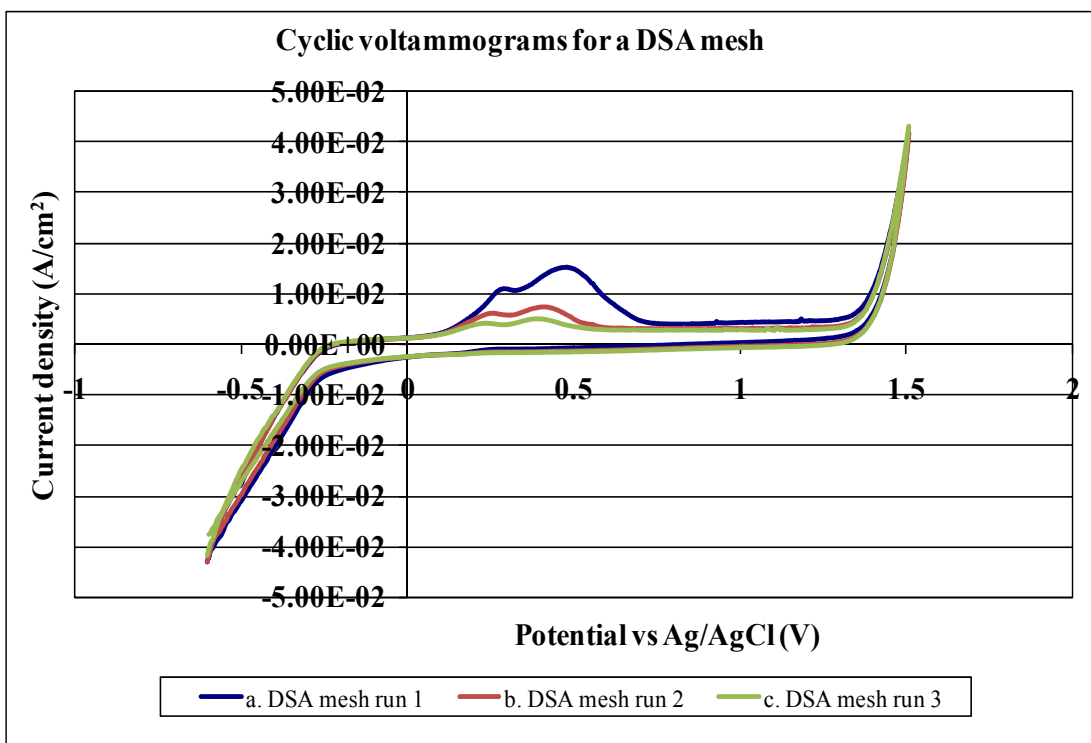


Figure 12: Cyclic Voltammograms for a DSA Mesh Anode.



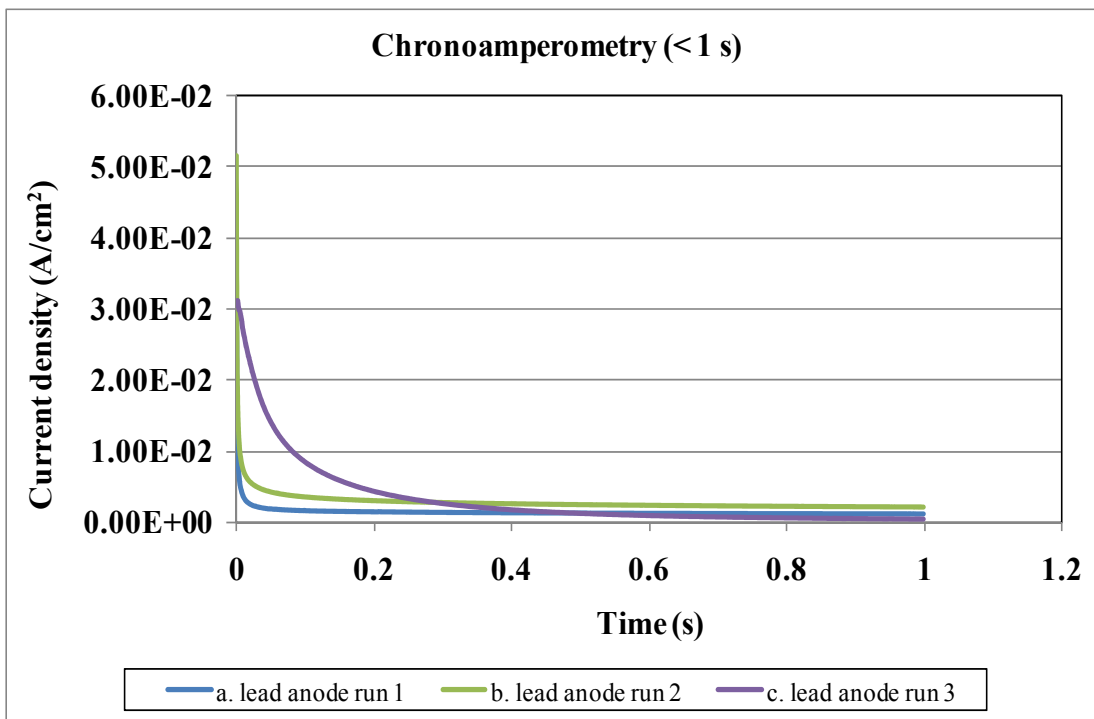


Figure 13: Chronoamperometry Tests for a Lead Anode.

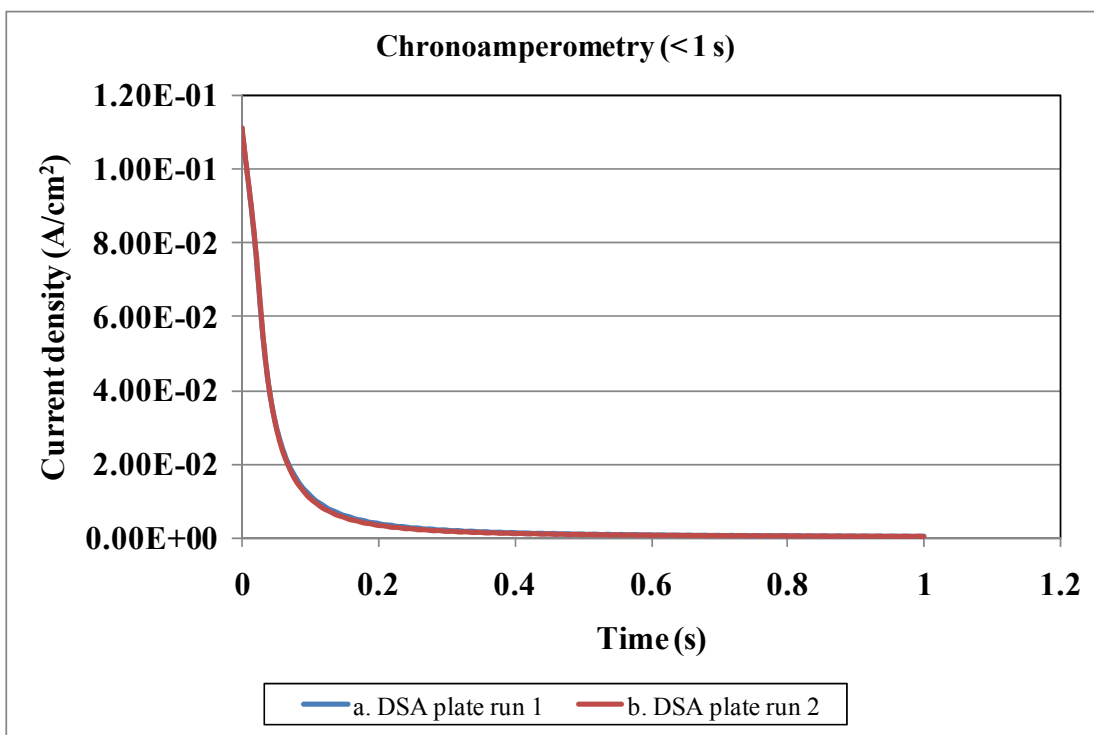


Figure 14: Chronoamperometry Tests for a DSA plate Anode.

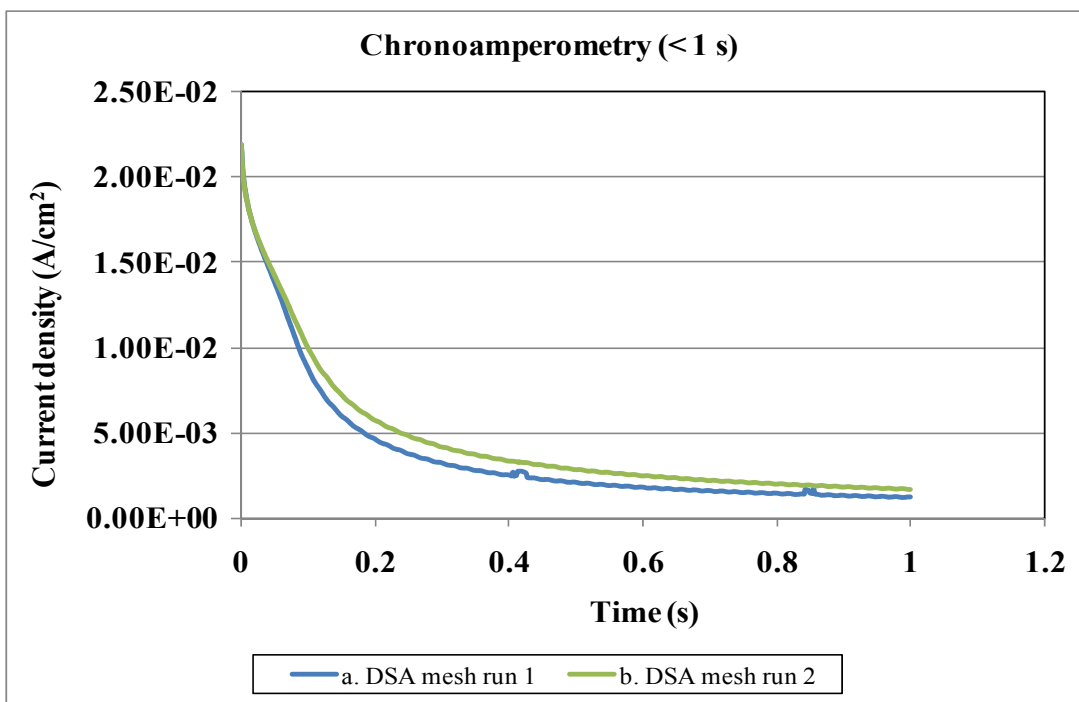


Figure 15: Chronoamperometry Tests for a DSA Mesh Anode.

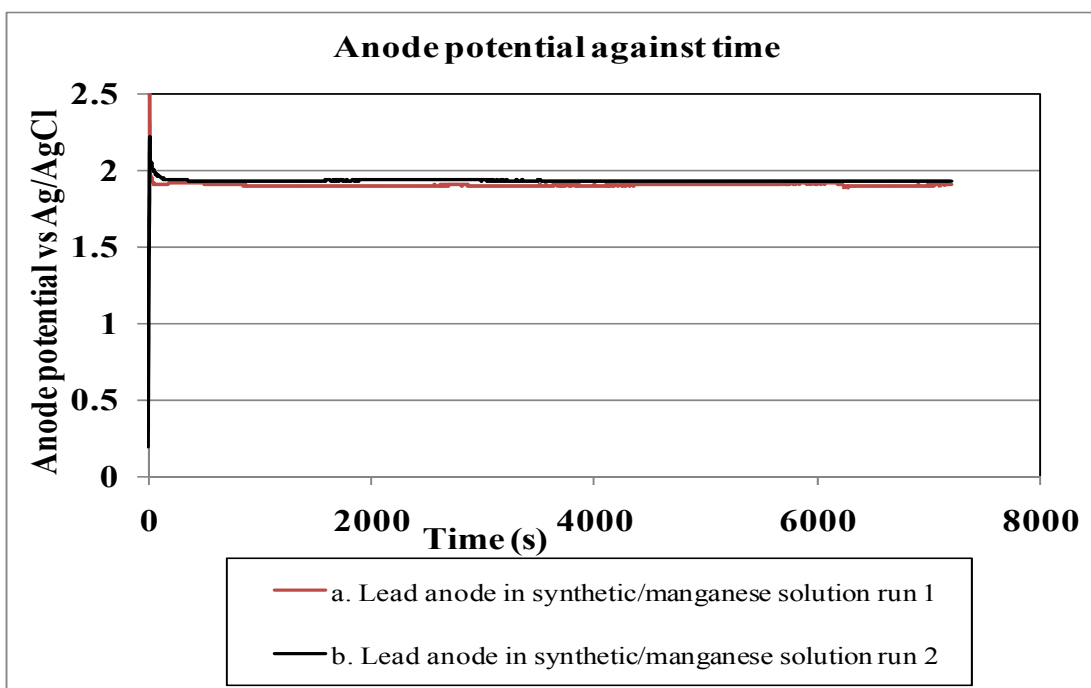


Figure 16: Galvanostatic Chronopotentiometry Curves for the Lead Anode in Synthetic/Manganese Solution.

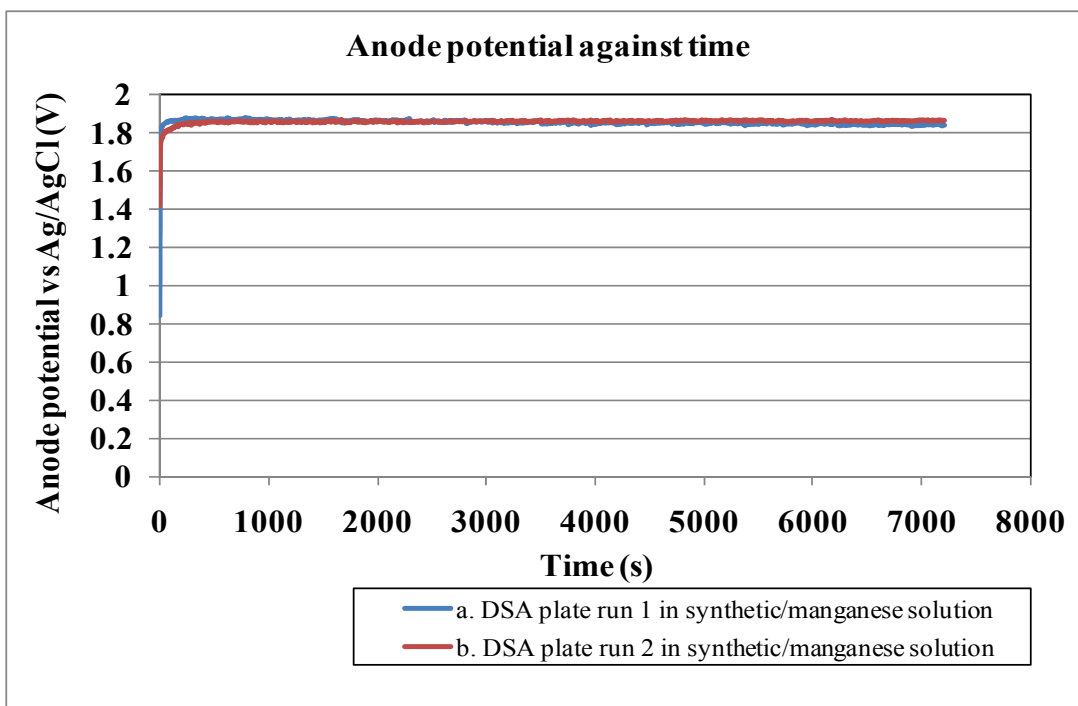


Figure 17: Galvanostatic Chronopotentiometry Curves for the DSA Plate Anode in Synthetic/Manganese Solution.

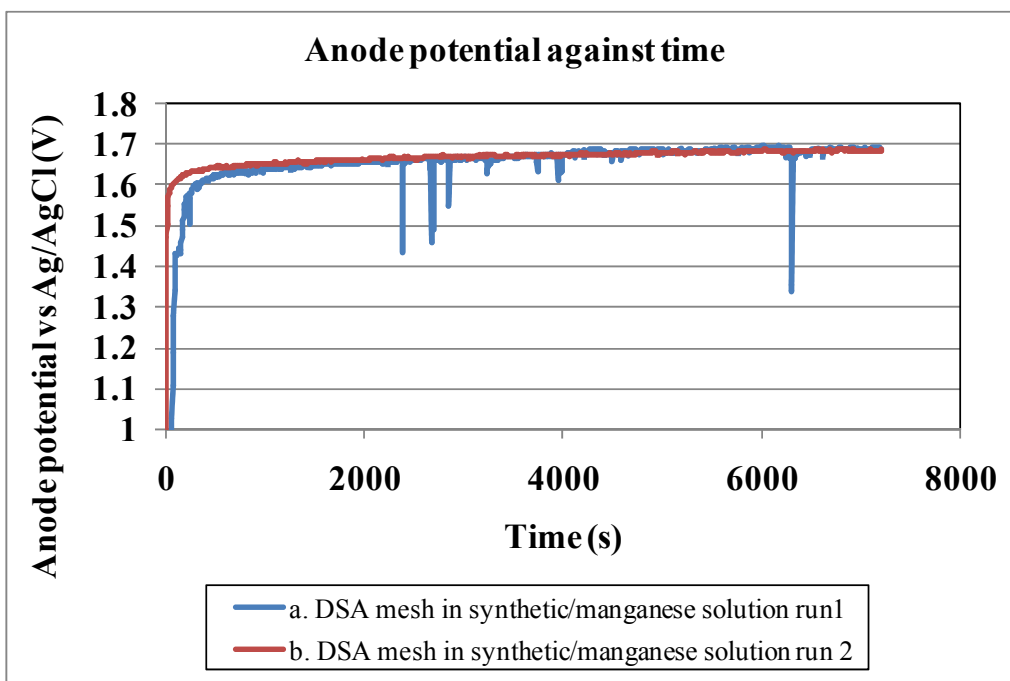
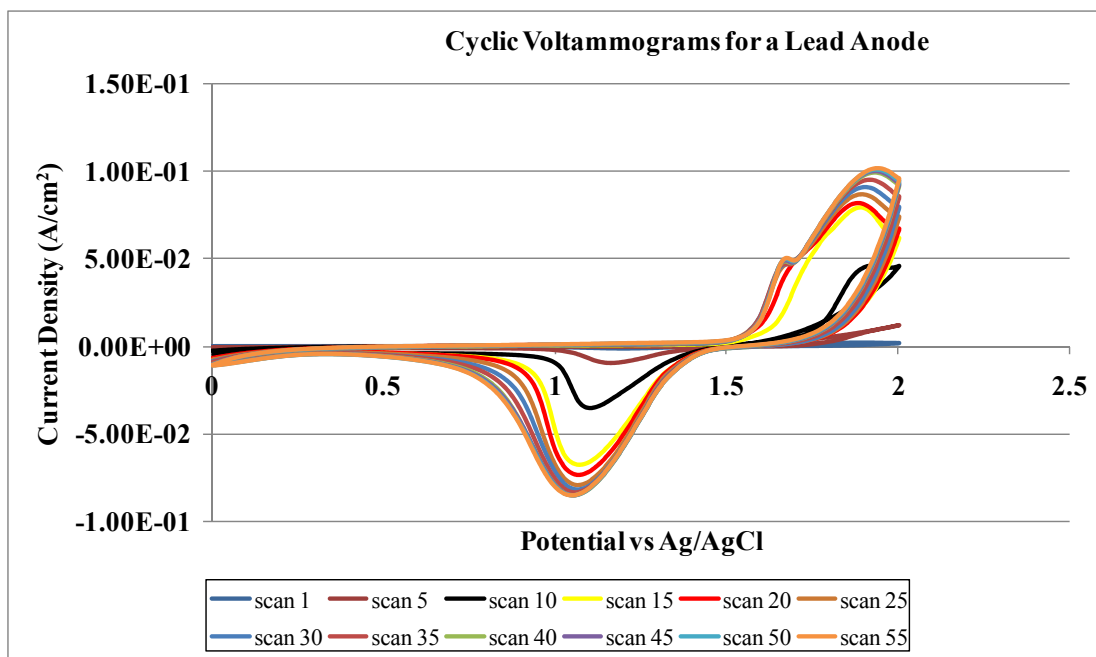


Figure 18: Galvanostatic Chronopotentiometry Curves for the DSA Mesh Anode in Synthetic/Manganese Solution.



**Figure 19: Consecutive Cyclic Voltammograms for the Lead Anode Performed Before Electrochemical Impedance Tests.**

**APPENDIX E: GALVANOSTATIC CHRONOPOTENTIOMETRY CURVES WITH SIMILAR ANODE/CATHODE AREAS AND CURRENT EFFICIENCIES**

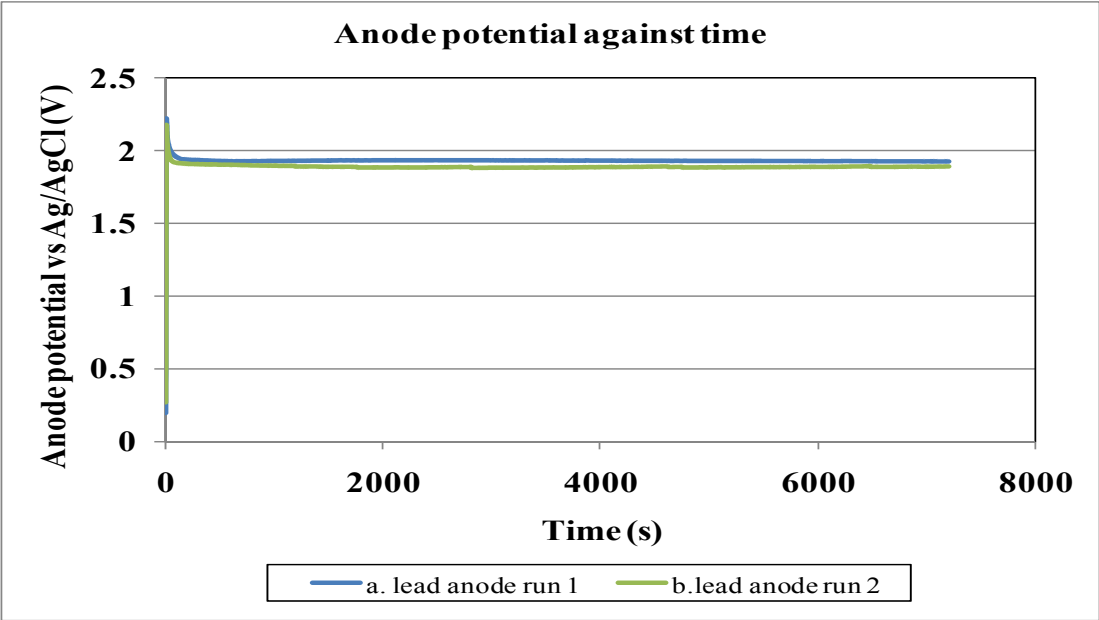


Figure 20: Galvanostatic Chronopotentiometry Curves for the Lead Anode.

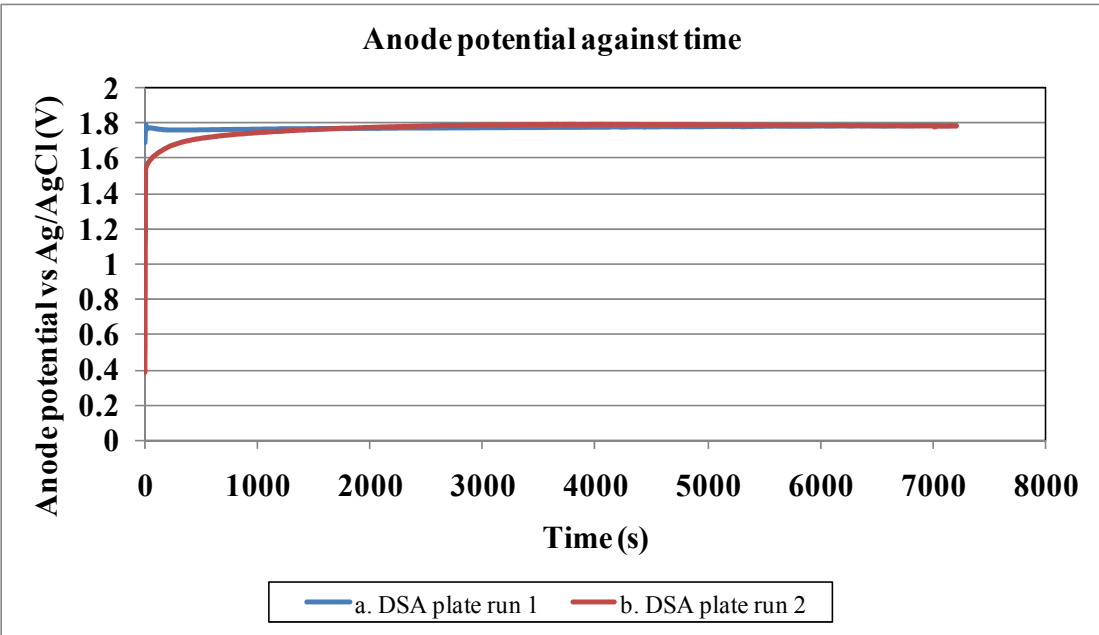


Figure 21: Galvanostatic Chronopotentiometry Curves for the DSA Plate Anode.

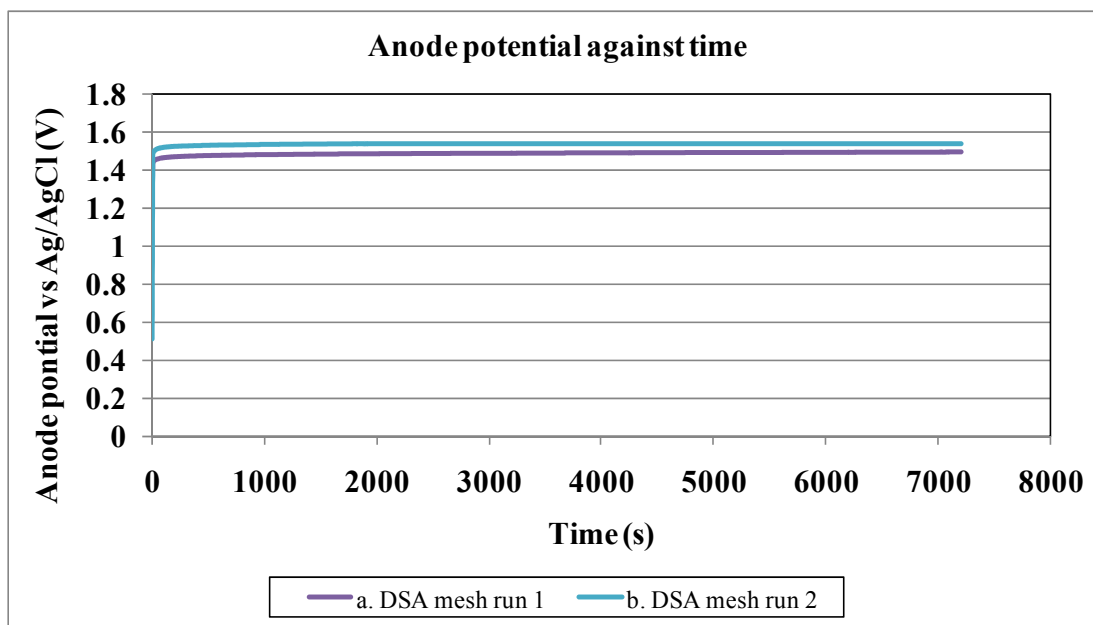


Figure 22: Galvanostatic Chronopotentiometry Curves for the DSA Mesh Anode.

Table 1: Determination of Current Efficiency

| Pb/Sb   | Value       |
|---|-------------|
| Weight gained by the cathode (g)                              | 0.044       |
| Anode/cathode area (cm <sup>2</sup> )                         | 1.00        |
| Current density (A/cm <sup>2</sup> )                          | 0.019       |
| Current (A)   | 0.019       |
| Volume of electrolyte injected (ml/hr)                        | 2.7         |
| <b>Current efficiency (%)</b>                                 | <b>97.8</b> |
| <b>Ti-Ta<sub>2</sub>O<sub>5</sub>/IrO<sub>2</sub> (plate)</b> |             |
| Weight gained by the cathode (g)                              | 0.056       |
| Anode/cathode area (cm <sup>2</sup> )                         | 1.28        |
| Current density (A/cm <sup>2</sup> )                          | 0.019       |
| Current (A)   | 0.024       |
| Volume of electrolyte injected (ml/hr)                        | 3.4         |
| <b>Current efficiency (%)</b>                                 | <b>97.8</b> |
| <b>Ti-Ta<sub>2</sub>O<sub>5</sub>/IrO<sub>2</sub> (mesh)</b>  |             |
| Weight gained by the cathode (g)                              | 0.032       |

|  |             |
|--|-------------|
| Anode/cathode area (cm <sup>2</sup> )  | 0.75        |
| Current density (A/cm <sup>2</sup> )   | 0.019       |
| Current (A)                            | 0.014       |
| Volume of electrolyte injected (ml/hr) | 2.0         |
| <b>Current efficiency (%)</b>          | <b>97.7</b> |

## APPENDIX F: DATA FOR FIGURES

A sample of part of the raw data used to plot figure 5.31 in the electrowinning tests is shown below. Real time monitoring of the cell voltage with time was done by means of data loggers for all the anodes.

| Anode            | Time        | Cell voltage (V) | Anode           | Cell voltage (V) | Anode       | Cell voltage (V) |
|------------------|-------------|------------------|-----------------|------------------|-------------|------------------|
| <b>DSA plate</b> | 0:00'0.000" | 2.131            | <b>DSA mesh</b> | 2.122            | <b>lead</b> | 2.374            |
|                  | 0:08'0.000" | 2.068            |                 | 2.006            |             | 2.188            |
|                  | 0:16'0.000" | 2.073            |                 | 1.957            |             | 2.143            |
|                  | 0:24'0.000" | 2.079            |                 | 1.949            |             | 2.106            |
|                  | 0:32'0.000" | 1.995            |                 | 1.919            |             | 2.05             |
|                  | 0:40'0.000" | 1.993            |                 | 1.933            |             | 2.027            |
|                  | 0:48'0.000" | 1.972            |                 | 1.924            |             | 2.025            |
|                  | 0:56'0.000" | 1.968            |                 | 1.9              |             | 2.032            |
|                  | 1:04'0.000" | 1.955            |                 | 1.868            |             | 2.023            |
|                  | 1:12'0.000" | 1.958            |                 | 1.907            |             | 2.003            |
|                  | 1:20'0.000" | 1.96             |                 | 1.879            |             | 2.002            |
|                  | 1:28'0.000" | 1.952            |                 | 1.845            |             | 2.01             |
|                  | 1:36'0.000" | 1.944            |                 | 1.874            |             | 2.008            |
|                  | 1:44'0.000" | 1.959            |                 | 1.883            |             | 2.003            |
|                  | 1:52'0.000" | 1.974            |                 | 1.886            |             | 1.999            |
|                  | 2:00'0.000" | 1.939            |                 | 1.894            |             | 1.998            |
|                  | 2:08'0.000" | 1.945            |                 | 1.845            |             | 2.009            |
|                  | 2:16'0.000" | 1.975            |                 | 1.8              |             | 2.01             |
|                  | 2:24'0.000" | 1.955            |                 | 1.886            |             | 1.982            |
|                  | 2:32'0.000" | 1.945            |                 | 1.878            |             | 1.992            |
|                  | 2:40'0.000" | 1.938            |                 | 1.865            |             | 2.003            |
|                  | 2:48'0.000" | 1.956            |                 | 1.863            |             | 2.002            |
|                  | 2:56'0.000" | 1.956            |                 | 1.876            |             | 1.988            |
|                  | 3:04'0.000" | 1.944            |                 | 1.893            |             | 1.986            |
|                  | 3:12'0.000" | 1.94             |                 | 1.845            |             | 1.999            |
|                  | 3:20'0.000" | 1.934            |                 | 1.884            |             | 1.98             |
|                  | 3:28'0.000" | 1.941            |                 | 1.867            |             | 1.974            |
|                  | 3:36'0.000" | 1.937            |                 | 1.847            |             | 1.978            |
|                  | 3:44'0.000" | 1.946            |                 | 1.891            |             | 2.001            |
|                  | 3:52'0.000" | 1.965            |                 | 1.9              |             | 1.977            |
|                  | 4:00'0.000" | 1.958            |                 | 1.848            |             | 1.981            |
|                  | 4:08'0.000" | 1.959            |                 | 1.851            |             | 1.987            |
|                  | 4:16'0.000" | 1.935            |                 | 1.899            |             | 1.998            |



|  |              |       |  |       |  |       |
|--|--------------|-------|--|-------|--|-------|
|  | 4:24'0.000"  | 1.953 |  | 1.884 |  | 1.987 |
|  | 4:32'0.000"  | 1.961 |  | 1.873 |  | 1.983 |
|  | 4:40'0.000"  | 1.96  |  | 1.905 |  | 1.986 |
|  | 4:48'0.000"  | 1.955 |  | 1.881 |  | 1.985 |
|  | 4:56'0.000"  | 1.932 |  | 1.867 |  | 1.973 |
|  | 5:04'0.000"  | 1.94  |  | 1.916 |  | 1.977 |
|  | 5:12'0.000"  | 1.93  |  | 1.88  |  | 1.968 |
|  | 5:20'0.000"  | 1.943 |  | 1.878 |  | 1.99  |
|  | 5:28'0.000"  | 1.944 |  | 1.908 |  | 1.977 |
|  | 5:36'0.000"  | 1.939 |  | 1.859 |  | 1.972 |
|  | 5:44'0.000"  | 1.933 |  | 1.877 |  | 1.968 |
|  | 5:52'0.000"  | 1.928 |  | 1.873 |  | 1.969 |
|  | 6:00'0.000"  | 1.932 |  | 1.872 |  | 1.972 |
|  | 6:08'0.000"  | 1.936 |  | 1.899 |  | 1.972 |
|  | 6:16'0.000"  | 1.957 |  | 1.893 |  | 1.99  |
|  | 6:24'0.000"  | 1.943 |  | 1.895 |  | 1.977 |
|  | 6:32'0.000"  | 1.923 |  | 1.878 |  | 1.967 |
|  | 6:40'0.000"  | 1.921 |  | 1.878 |  | 1.967 |
|  | 6:48'0.000"  | 1.92  |  | 1.885 |  | 1.964 |
|  | 6:56'0.000"  | 1.932 |  | 1.895 |  | 1.962 |
|  | 7:04'0.000"  | 1.966 |  | 1.744 |  | 1.977 |
|  | 7:12'0.000"  | 1.975 |  | 1.655 |  | 2.006 |
|  | 7:20'0.000"  | 1.921 |  | 1.945 |  | 1.956 |
|  | 7:28'0.000"  | 1.927 |  | 1.884 |  | 1.961 |
|  | 7:36'0.000"  | 1.985 |  | 1.633 |  | 2.01  |
|  | 7:44'0.000"  | 1.942 |  | 1.849 |  | 1.981 |
|  | 7:52'0.000"  | 1.994 |  | 1.743 |  | 1.977 |
|  | 8:00'0.000"  | 1.933 |  | 1.894 |  | 1.964 |
|  | 8:08'0.000"  | 1.956 |  | 1.652 |  | 1.998 |
|  | 8:16'0.000"  | 1.948 |  | 1.768 |  | 1.987 |
|  | 8:24'0.000"  | 1.926 |  | 1.872 |  | 1.951 |
|  | 8:32'0.000"  | 1.928 |  | 1.896 |  | 1.969 |
|  | 8:40'0.000"  | 2.022 |  | 1.521 |  | 2.033 |
|  | 8:48'0.000"  | 1.91  |  | 1.943 |  | 1.953 |
|  | 8:56'0.000"  | 1.951 |  | 1.905 |  | 1.971 |
|  | 9:04'0.000"  | 1.931 |  | 1.822 |  | 1.971 |
|  | 9:12'0.000"  | 1.919 |  | 1.889 |  | 1.974 |
|  | 9:20'0.000"  | 2.017 |  | 1.588 |  | 2.004 |
|  | 9:28'0.000"  | 1.928 |  | 1.815 |  | 1.962 |
|  | 9:36'0.000"  | 1.909 |  | 1.917 |  | 1.961 |
|  | 9:44'0.000"  | 1.898 |  | 1.882 |  | 1.966 |
|  | 9:52'0.000"  | 1.932 |  | 1.908 |  | 1.955 |
|  | 10:00'0.000" | 1.933 |  | 1.909 |  | 1.972 |

|  |              |       |  |       |  |       |
|--|--------------|-------|--|-------|--|-------|
|  | 10:08'0.000" | 1.965 |  | 1.686 |  | 2.002 |
|  | 10:16'0.000" | 1.954 |  | 1.758 |  | 1.973 |
|  | 10:24'0.000" | 1.991 |  | 1.653 |  | 1.992 |
|  | 10:32'0.000" | 1.922 |  | 1.836 |  | 1.967 |
|  | 10:40'0.000" | 1.883 |  | 1.927 |  | 1.951 |
|  | 10:48'0.000" | 1.957 |  | 1.697 |  | 1.975 |
|  | 10:56'0.000" | 1.951 |  | 1.759 |  | 1.974 |
|  | 11:04'0.000" | 1.922 |  | 1.815 |  | 1.972 |
|  | 11:12'0.000" | 1.913 |  | 1.853 |  | 1.956 |
|  | 11:20'0.000" | 1.973 |  | 1.6   |  | 1.991 |
|  | 11:28'0.000" | 1.933 |  | 1.817 |  | 1.967 |
|  | 11:36'0.000" | 1.903 |  | 1.906 |  | 1.96  |
|  | 11:44'0.000" | 1.931 |  | 1.815 |  | 1.959 |
|  | 11:52'0.000" | 1.915 |  | 1.891 |  | 1.961 |
|  | 12:00'0.000" | 1.922 |  | 1.918 |  | 1.967 |
|  | 12:08'0.000" | 1.913 |  | 1.917 |  | 1.956 |
|  | 12:16'0.000" | 1.905 |  | 1.911 |  | 1.953 |
|  | 12:24'0.000" | 1.937 |  | 1.883 |  | 1.956 |
|  | 12:32'0.000" | 1.919 |  | 1.828 |  | 1.96  |
|  | 12:40'0.000" | 1.899 |  | 1.894 |  | 1.946 |
|  | 12:48'0.000" | 1.908 |  | 1.867 |  | 1.957 |
|  | 12:56'0.000" | 1.91  |  | 1.863 |  | 1.962 |
|  | 13:04'0.000" | 1.914 |  | 1.85  |  | 1.954 |
|  | 13:12'0.000" | 1.899 |  | 1.89  |  | 1.954 |
|  | 13:20'0.000" | 1.982 |  | 1.621 |  | 2.002 |
|  | 13:28'0.000" | 1.945 |  | 1.807 |  | 1.971 |
|  | 13:36'0.000" | 1.982 |  | 1.632 |  | 1.995 |
|  | 13:44'0.000" | 1.986 |  | 1.568 |  | 2.007 |
|  | 13:52'0.000" | 2.005 |  | 1.547 |  | 2.016 |
|  | 14:00'0.000" | 1.915 |  | 1.876 |  | 1.946 |
|  | 14:08'0.000" | 1.906 |  | 1.892 |  | 1.959 |
|  | 14:16'0.000" | 1.916 |  | 1.884 |  | 1.965 |
|  | 14:24'0.000" | 1.933 |  | 1.885 |  | 1.964 |
|  | 14:32'0.000" | 1.927 |  | 1.837 |  | 1.961 |
|  | 14:40'0.000" | 1.904 |  | 1.887 |  | 1.955 |
|  | 14:48'0.000" | 1.898 |  | 1.895 |  | 1.954 |
|  | 14:56'0.000" | 2.001 |  | 1.541 |  | 2.001 |
|  | 15:04'0.000" | 1.958 |  | 1.687 |  | 1.99  |
|  | 15:12'0.000" | 1.969 |  | 1.654 |  | 2.005 |
|  | 15:20'0.000" | 1.979 |  | 1.703 |  | 1.977 |
|  | 15:28'0.000" | 1.904 |  | 1.938 |  | 1.95  |
|  | 15:36'0.000" | 1.903 |  | 1.882 |  | 1.962 |
|  | 15:44'0.000" | 1.919 |  | 1.86  |  | 1.962 |

|  |              |       |  |       |  |       |
|--|--------------|-------|--|-------|--|-------|
|  | 15:52'0.000" | 1.986 |  | 1.619 |  | 1.989 |
|  | 16:00'0.000" | 1.972 |  | 1.647 |  | 1.994 |
|  | 16:08'0.000" | 1.896 |  | 1.928 |  | 1.96  |
|  | 16:16'0.000" | 1.906 |  | 1.903 |  | 1.949 |
|  | 16:24'0.000" | 1.916 |  | 1.891 |  | 1.955 |
|  | 16:32'0.000" | 1.955 |  | 1.669 |  | 1.988 |
|  | 16:40'0.000" | 1.891 |  | 1.897 |  | 1.949 |
|  | 16:48'0.000" | 1.915 |  | 1.847 |  | 1.943 |
|  | 16:56'0.000" | 1.9   |  | 1.879 |  | 1.951 |
|  | 17:04'0.000" | 1.89  |  | 1.871 |  | 1.959 |
|  | 17:12'0.000" | 1.957 |  | 1.742 |  | 1.968 |
|  | 17:20'0.000" | 1.92  |  | 1.908 |  | 1.952 |
|  | 17:28'0.000" | 1.947 |  | 1.646 |  | 1.989 |
|  | 17:36'0.000" | 1.965 |  | 1.713 |  | 1.983 |
|  | 17:44'0.000" | 1.973 |  | 1.723 |  | 1.977 |
|  | 17:52'0.000" | 1.898 |  | 1.946 |  | 1.942 |
|  | 18:00'0.000" | 1.881 |  | 1.897 |  | 1.949 |
|  | 18:08'0.000" | 1.966 |  | 1.607 |  | 1.981 |
|  | 18:16'0.000" | 2.001 |  | 1.613 |  | 2.003 |
|  | 18:24'0.000" | 1.899 |  | 1.91  |  | 1.954 |
|  | 18:32'0.000" | 1.938 |  | 1.694 |  | 1.975 |
|  | 18:40'0.000" | 1.91  |  | 1.919 |  | 1.943 |
|  | 18:48'0.000" | 1.914 |  | 1.867 |  | 1.956 |
|  | 18:56'0.000" | 1.94  |  | 1.679 |  | 2.003 |
|  | 19:04'0.000" | 1.908 |  | 1.91  |  | 1.95  |
|  | 19:12'0.000" | 1.923 |  | 1.857 |  | 1.951 |
|  | 19:20'0.000" | 1.914 |  | 1.911 |  | 1.957 |
|  | 19:28'0.000" | 1.959 |  | 1.68  |  | 2.002 |
|  | 19:36'0.000" | 1.976 |  | 1.637 |  | 2.014 |
|  | 19:44'0.000" | 1.908 |  | 1.881 |  | 1.942 |
|  | 19:52'0.000" | 1.974 |  | 1.627 |  | 1.987 |
|  | 20:00'0.000" | 1.922 |  | 1.825 |  | 1.967 |
|  | 20:08'0.000" | 1.945 |  | 1.675 |  | 1.995 |
|  | 20:16'0.000" | 1.978 |  | 1.648 |  | 1.994 |
|  | 20:24'0.000" | 1.987 |  | 1.583 |  | 2.004 |
|  | 20:32'0.000" | 2.007 |  | 1.574 |  | 2.016 |
|  | 20:40'0.000" | 1.965 |  | 1.634 |  | 2.012 |
|  | 20:48'0.000" | 1.993 |  | 1.511 |  | 2.034 |
|  | 20:56'0.000" | 1.961 |  | 1.64  |  | 1.982 |
|  | 21:04'0.000" | 1.923 |  | 1.924 |  | 1.958 |
|  | 21:12'0.000" | 1.954 |  | 1.645 |  | 2.001 |
|  | 21:20'0.000" | 1.895 |  | 1.868 |  | 1.971 |
|  | 21:28'0.000" | 1.962 |  | 1.673 |  | 2.011 |

|  |              |       |  |       |  |       |
|--|--------------|-------|--|-------|--|-------|
|  | 21:36'0.000" | 1.984 |  | 1.629 |  | 2.004 |
|  | 21:44'0.000" | 1.991 |  | 1.576 |  | 2.021 |
|  | 21:52'0.000" | 1.896 |  | 1.456 |  | 1.959 |
|  | 22:00'0.000" | 1.886 |  | 1.901 |  | 1.959 |
|  | 22:08'0.000" | 1.906 |  | 1.86  |  | 1.959 |
|  | 22:16'0.000" | 1.903 |  | 1.859 |  | 1.942 |
|  | 22:24'0.000" | 1.895 |  | 1.893 |  | 2.005 |
|  | 22:32'0.000" | 1.962 |  | 1.662 |  | 2.008 |
|  | 22:40'0.000" | 1.977 |  | 1.646 |  | 1.98  |
|  | 22:48'0.000" | 1.98  |  | 1.682 |  | 1.981 |
|  | 22:56'0.000" | 1.918 |  | 1.844 |  | 1.961 |
|  | 23:04'0.000" | 1.899 |  | 1.919 |  | 1.936 |
|  | 23:12'0.000" | 1.9   |  | 1.858 |  | 1.917 |
|  | 23:20'0.000" | 1.919 |  | 1.636 |  | 1.954 |
|  | 23:28'0.000" | 1.909 |  | 1.674 |  | 1.957 |
|  | 23:36'0.000" | 1.884 |  | 1.786 |  | 1.926 |
|  | 23:44'0.000" | 1.877 |  | 1.874 |  | 1.906 |
|  | 23:52'0.000" | 1.916 |  | 1.702 |  | 1.948 |
|  | 24:00'0.000" | 1.864 |  | 1.63  |  | 1.933 |
|  | 24:08'0.000" | 1.889 |  | 1.601 |  | 1.905 |
|  | 24:16'0.000" | 1.888 |  | 1.594 |  | 1.922 |
|  | 24:24'0.000" | 1.9   |  | 1.539 |  | 1.943 |
|  | 24:32'0.000" | 1.799 |  | 1.86  |  | 1.937 |
|  | 24:40'0.000" | 1.916 |  | 1.575 |  | 1.928 |
|  | 24:48'0.000" | 1.92  |  | 1.565 |  | 1.948 |
|  | 24:56'0.000" | 1.878 |  | 1.707 |  | 1.927 |
|  | 25:04'0.000" | 1.866 |  | 1.988 |  | 1.915 |
|  | 25:12'0.000" | 1.958 |  | 1.653 |  | 1.96  |
|  | 25:20'0.000" | 1.951 |  | 1.634 |  | 1.973 |
|  | 25:28'0.000" | 1.987 |  | 1.452 |  | 2.001 |
|  | 25:36'0.000" | 1.905 |  | 1.838 |  | 1.926 |
|  | 25:44'0.000" | 1.891 |  | 1.903 |  | 1.914 |
|  | 25:52'0.000" | 1.88  |  | 1.908 |  | 1.931 |
|  | 26:00'0.000" | 1.963 |  | 1.626 |  | 1.975 |
|  | 26:08'0.000" | 1.972 |  | 1.61  |  | 1.96  |
|  | 26:16'0.000" | 1.925 |  | 1.694 |  | 1.952 |
|  | 26:24'0.000" | 1.94  |  | 1.636 |  | 1.962 |
|  | 26:32'0.000" | 1.944 |  | 1.661 |  | 1.95  |
|  | 26:40'0.000" | 1.957 |  | 1.681 |  | 1.951 |
|  | 26:48'0.000" | 1.893 |  | 1.913 |  | 1.927 |
|  | 26:56'0.000" | 1.946 |  | 1.683 |  | 1.963 |
|  | 27:04'0.000" | 1.931 |  | 1.81  |  | 1.929 |
|  | 27:12'0.000" | 1.915 |  | 1.839 |  | 1.92  |

|  |              |       |  |       |  |       |
|--|--------------|-------|--|-------|--|-------|
|  | 27:20'0.000" | 1.898 |  | 1.874 |  | 1.916 |
|  | 27:28'0.000" | 1.965 |  | 1.632 |  | 1.966 |
|  | 27:36'0.000" | 1.915 |  | 1.898 |  | 1.907 |
|  | 27:44'0.000" | 1.985 |  | 1.624 |  | 1.964 |
|  | 27:52'0.000" | 1.978 |  | 1.585 |  | 1.972 |
|  | 28:00'0.000" | 1.977 |  | 1.633 |  | 1.963 |
|  | 28:08'0.000" | 1.971 |  | 1.801 |  | 1.931 |
|  | 28:16'0.000" | 1.953 |  | 1.669 |  | 1.937 |
|  | 28:24'0.000" | 1.999 |  | 1.489 |  | 1.976 |
|  | 28:32'0.000" | 1.993 |  | 1.581 |  | 1.946 |
|  | 28:40'0.000" | 1.905 |  | 1.898 |  | 1.906 |
|  | 28:48'0.000" | 1.968 |  | 1.647 |  | 1.957 |
|  | 28:56'0.000" | 1.958 |  | 1.714 |  | 1.937 |
|  | 29:04'0.000" | 1.906 |  | 1.908 |  | 1.899 |
|  | 29:12'0.000" | 1.972 |  | 1.626 |  | 1.95  |
|  | 29:20'0.000" | 2.002 |  | 1.52  |  | 1.959 |
|  | 29:28'0.000" | 1.955 |  | 1.639 |  | 1.941 |
|  | 29:36'0.000" | 1.911 |  | 1.789 |  | 1.898 |
|  | 29:44'0.000" | 1.973 |  | 1.649 |  | 1.944 |
|  | 29:52'0.000" | 1.985 |  | 1.621 |  | 1.956 |
|  | 30:00'0.000" | 2.001 |  | 1.208 |  | 1.925 |
|  | 30:08'0.000" | 2.035 |  | 1.621 |  | 1.936 |
|  | 30:16'0.000" | 2.039 |  | 1.564 |  | 1.931 |
|  | 30:24'0.000" | 2.025 |  | 1.686 |  | 1.923 |
|  | 30:32'0.000" | 1.975 |  | 1.625 |  | 1.921 |
|  | 30:40'0.000" | 2.04  |  | 1.645 |  | 1.919 |
|  | 30:48'0.000" | 1.975 |  | 1.882 |  | 1.888 |
|  | 30:56'0.000" | 1.975 |  | 1.87  |  | 1.884 |
|  | 31:04'0.000" | 2.047 |  | 1.609 |  | 1.917 |
|  | 31:12'0.000" | 2.028 |  | 1.713 |  | 1.905 |
|  | 31:20'0.000" | 1.986 |  | 1.912 |  | 1.889 |
|  | 31:28'0.000" | 2.052 |  | 1.588 |  | 1.922 |
|  | 31:36'0.000" | 2.024 |  | 1.634 |  | 1.907 |
|  | 31:44'0.000" | 1.992 |  | 1.785 |  | 1.9   |
|  | 31:52'0.000" | 1.99  |  | 1.747 |  | 1.895 |
|  | 32:00'0.000" | 2.041 |  | 1.731 |  | 1.907 |
|  | 32:08'0.000" | 2.017 |  | 1.808 |  | 1.901 |
|  | 32:16'0.000" | 1.993 |  | 1.837 |  | 1.892 |
|  | 32:24'0.000" | 2.045 |  | 1.684 |  | 1.922 |
|  | 32:32'0.000" | 2.01  |  | 1.852 |  | 1.892 |
|  | 32:40'0.000" | 2.038 |  | 1.515 |  | 1.969 |
|  | 32:48'0.000" | 1.923 |  | 1.882 |  | 1.912 |
|  | 32:56'0.000" | 2.022 |  | 1.699 |  | 1.954 |

|  |              |       |  |       |  |       |
|--|--------------|-------|--|-------|--|-------|
|  | 33:04'0.000" | 1.945 |  | 1.901 |  | 1.914 |
|  | 33:12'0.000" | 2.029 |  | 1.715 |  | 1.959 |
|  | 33:20'0.000" | 2.003 |  | 1.642 |  | 1.951 |
|  | 33:28'0.000" | 2.009 |  | 1.659 |  | 1.941 |
|  | 33:36'0.000" | 1.943 |  | 1.926 |  | 1.951 |
|  | 33:44'0.000" | 1.905 |  | 1.864 |  | 1.914 |
|  | 33:52'0.000" | 1.991 |  | 1.675 |  | 1.941 |
|  | 34:00'0.000" | 2.019 |  | 1.596 |  | 1.948 |
|  | 34:08'0.000" | 2.031 |  | 1.586 |  | 1.958 |
|  | 34:16'0.000" | 1.917 |  | 1.85  |  | 1.906 |
|  | 34:24'0.000" | 1.994 |  | 1.678 |  | 1.928 |
|  | 34:32'0.000" | 1.977 |  | 1.747 |  | 1.923 |
|  | 34:40'0.000" | 1.947 |  | 1.887 |  | 1.915 |
|  | 34:48'0.000" | 1.94  |  | 1.9   |  | 1.982 |
|  | 34:56'0.000" | 1.996 |  | 1.78  |  | 1.917 |
|  | 35:04'0.000" | 1.956 |  | 1.91  |  | 1.915 |
|  | 35:12'0.000" | 1.939 |  | 1.909 |  | 1.921 |
|  | 35:20'0.000" | 2.008 |  | 1.683 |  | 1.942 |
|  | 35:28'0.000" | 2.029 |  | 1.611 |  | 1.949 |
|  | 35:36'0.000" | 2.033 |  | 1.642 |  | 1.951 |
|  | 35:44'0.000" | 2.007 |  | 1.741 |  | 1.955 |
|  | 35:52'0.000" | 1.988 |  | 1.724 |  | 1.925 |
|  | 36:00'0.000" | 1.992 |  | 1.696 |  | 1.931 |
|  | 36:08'0.000" | 1.971 |  | 1.738 |  | 1.927 |
|  | 36:16'0.000" | 1.97  |  | 1.72  |  | 1.919 |
|  | 36:24'0.000" | 1.942 |  | 1.853 |  | 1.905 |
|  | 36:32'0.000" | 1.947 |  | 1.859 |  | 1.914 |
|  | 36:40'0.000" | 1.939 |  | 1.921 |  | 1.919 |
|  | 36:48'0.000" | 1.95  |  | 1.885 |  | 1.9   |
|  | 36:56'0.000" | 1.969 |  | 1.869 |  | 1.908 |
|  | 37:04'0.000" | 2.023 |  | 1.643 |  | 1.95  |
|  | 37:12'0.000" | 1.985 |  | 1.779 |  | 1.926 |
|  | 37:20'0.000" | 2.027 |  | 1.691 |  | 1.922 |
|  | 37:28'0.000" | 1.98  |  | 1.749 |  | 1.934 |
|  | 37:36'0.000" | 2.009 |  | 1.724 |  | 1.936 |
|  | 37:44'0.000" | 1.957 |  | 1.929 |  | 1.898 |
|  | 37:52'0.000" | 2.023 |  | 1.701 |  | 1.946 |
|  | 38:00'0.000" | 2.056 |  | 1.556 |  | 1.961 |
|  | 38:08'0.000" | 1.946 |  | 1.918 |  | 1.91  |
|  | 38:16'0.000" | 2.019 |  | 1.677 |  | 1.929 |
|  | 38:24'0.000" | 2.026 |  | 1.692 |  | 1.944 |
|  | 38:32'0.000" | 1.977 |  | 1.839 |  | 1.931 |
|  | 38:40'0.000" | 2.017 |  | 1.734 |  | 1.927 |

|  |              |       |  |       |  |       |
|--|--------------|-------|--|-------|--|-------|
|  | 38:48'0.000" | 1.957 |  | 1.958 |  | 1.899 |
|  | 38:56'0.000" | 2.034 |  | 1.663 |  | 1.948 |
|  | 39:04'0.000" | 2.01  |  | 1.617 |  | 1.936 |
|  | 39:12'0.000" | 2.004 |  | 1.691 |  | 1.916 |
|  | 39:20'0.000" | 1.946 |  | 1.903 |  | 1.895 |
|  | 39:28'0.000" | 1.962 |  | 1.906 |  | 1.92  |
|  | 39:36'0.000" | 2.026 |  | 1.718 |  | 1.929 |
|  | 39:44'0.000" | 2.001 |  | 1.806 |  | 1.918 |
|  | 39:52'0.000" | 2.027 |  | 1.689 |  | 1.937 |
|  | 40:00'0.000" | 2.021 |  | 1.678 |  | 1.941 |
|  | 40:08'0.000" | 2.01  |  | 1.829 |  | 1.908 |
|  | 40:16'0.000" | 1.979 |  | 1.901 |  | 1.908 |
|  | 40:24'0.000" | 1.962 |  | 1.542 |  | 1.965 |
|  | 40:32'0.000" | 2.042 |  | 1.618 |  | 1.938 |
|  | 40:40'0.000" | 2.06  |  | 1.565 |  | 1.944 |
|  | 40:48'0.000" | 2.108 |  | 1.332 |  | 1.983 |
|  | 40:56'0.000" | 1.946 |  | 1.893 |  | 1.906 |
|  | 41:04'0.000" | 2.004 |  | 1.704 |  | 1.916 |
|  | 41:12'0.000" | 1.962 |  | 1.893 |  | 1.908 |
|  | 41:20'0.000" | 2.002 |  | 1.692 |  | 1.943 |
|  | 41:28'0.000" | 2.009 |  | 1.661 |  | 1.929 |
|  | 41:36'0.000" | 2.009 |  | 1.663 |  | 1.926 |
|  | 41:44'0.000" | 1.998 |  | 1.689 |  | 1.932 |
|  | 41:52'0.000" | 2.008 |  | 1.647 |  | 1.936 |
|  | 42:00'0.000" | 2.018 |  | 1.742 |  | 1.914 |
|  | 42:08'0.000" | 1.962 |  | 1.9   |  | 1.903 |
|  | 42:16'0.000" | 2.015 |  | 1.653 |  | 1.942 |
|  | 42:24'0.000" | 2     |  | 1.636 |  | 1.936 |
|  | 42:32'0.000" | 1.995 |  | 1.694 |  | 1.915 |
|  | 42:40'0.000" | 1.991 |  | 1.779 |  | 1.923 |
|  | 42:48'0.000" | 1.995 |  | 1.793 |  | 1.92  |
|  | 42:56'0.000" | 2.028 |  | 1.64  |  | 1.93  |
|  | 43:04'0.000" | 2.037 |  | 1.668 |  | 1.946 |
|  | 43:12'0.000" | 1.96  |  | 1.885 |  | 1.926 |
|  | 43:20'0.000" | 1.947 |  | 1.903 |  | 1.908 |
|  | 43:28'0.000" | 2.03  |  | 1.665 |  | 1.933 |
|  | 43:36'0.000" | 2.024 |  | 1.678 |  | 1.941 |
|  | 43:44'0.000" | 2.017 |  | 1.645 |  | 1.948 |
|  | 43:52'0.000" | 2.024 |  | 1.638 |  | 1.926 |
|  | 44:00'0.000" | 2.043 |  | 1.634 |  | 1.945 |
|  | 44:08'0.000" | 2.033 |  | 1.698 |  | 1.942 |
|  | 44:16'0.000" | 2.01  |  | 1.77  |  | 1.93  |
|  | 44:24'0.000" | 1.996 |  | 1.905 |  | 1.91  |

|  |              |       |  |       |  |       |
|--|--------------|-------|--|-------|--|-------|
|  | 44:32'0.000" | 2.024 |  | 1.695 |  | 1.925 |
|  | 44:40'0.000" | 1.946 |  | 1.931 |  | 1.898 |
|  | 44:48'0.000" | 1.984 |  | 1.848 |  | 1.906 |
|  | 44:56'0.000" | 1.95  |  | 1.917 |  | 1.884 |
|  | 45:04'0.000" | 2.039 |  | 1.657 |  | 1.933 |
|  | 45:12'0.000" | 2.001 |  | 1.771 |  | 1.919 |
|  | 45:20'0.000" | 2.067 |  | 1.576 |  | 1.933 |
|  | 45:28'0.000" | 2.058 |  | 1.663 |  | 1.938 |
|  | 45:36'0.000" | 2.074 |  | 1.58  |  | 1.955 |
|  | 45:44'0.000" | 2.072 |  | 1.564 |  | 1.954 |
|  | 45:52'0.000" | 1.979 |  | 1.883 |  | 1.89  |
|  | 46:00'0.000" | 2.024 |  | 1.681 |  | 1.92  |
|  | 46:08'0.000" | 2.064 |  | 1.608 |  | 1.951 |
|  | 46:16'0.000" | 2.059 |  | 1.581 |  | 1.917 |
|  | 46:24'0.000" | 2.068 |  | 1.676 |  | 1.921 |
|  | 46:32'0.000" | 2.052 |  | 1.54  |  | 1.921 |
|  | 46:40'0.000" | 1.965 |  | 1.873 |  | 1.888 |
|  | 46:48'0.000" | 2.041 |  | 1.669 |  | 1.902 |
|  | 46:56'0.000" | 2.036 |  | 1.662 |  | 1.908 |
|  | 47:04'0.000" | 1.961 |  | 1.822 |  | 1.887 |
|  | 47:12'0.000" | 2.04  |  | 1.675 |  | 1.915 |
|  | 47:20'0.000" | 2.021 |  | 1.671 |  | 1.894 |
|  | 47:28'0.000" | 1.979 |  | 1.797 |  | 1.877 |
|  | 47:36'0.000" | 1.967 |  | 1.821 |  | 1.886 |
|  | 47:44'0.000" | 1.96  |  | 1.899 |  | 1.872 |
|  | 47:52'0.000" | 2.021 |  | 1.661 |  | 1.902 |
|  | 48:00'0.000" | 2.005 |  | 1.659 |  | 1.899 |
|  | 48:08'0.000" | 1.938 |  | 1.897 |  | 1.872 |
|  | 48:16'0.000" | 1.971 |  | 1.862 |  | 1.872 |
|  | 48:24'0.000" | 2.011 |  | 1.715 |  | 1.895 |
|  | 48:32'0.000" | 1.974 |  | 1.885 |  | 1.882 |
|  | 48:40'0.000" | 1.972 |  | 1.892 |  | 1.883 |
|  | 48:48'0.000" | 2.005 |  | 1.726 |  | 1.887 |
|  | 48:56'0.000" | 1.993 |  | 1.766 |  | 1.886 |
|  | 49:04'0.000" | 1.944 |  | 1.883 |  | 1.87  |
|  | 49:12'0.000" | 1.969 |  | 1.813 |  | 1.87  |
|  | 49:20'0.000" | 1.984 |  | 1.89  |  | 1.876 |
|  | 49:28'0.000" | 2.055 |  | 1.663 |  | 1.906 |
|  | 49:36'0.000" | 2.068 |  | 1.668 |  | 1.915 |
|  | 49:44'0.000" | 2.049 |  | 1.706 |  | 1.902 |
|  | 49:52'0.000" | 2.035 |  | 1.758 |  | 1.894 |
|  | 50:00'0.000" | 1.967 |  | 1.818 |  | 1.874 |
|  | 50:08'0.000" | 2.037 |  | 1.63  |  | 1.877 |



|  |              |       |  |       |  |       |
|--|--------------|-------|--|-------|--|-------|
|  | 50:16'0.000" | 2.023 |  | 1.918 |  | 1.933 |
|  | 50:24'0.000" | 2.087 |  | 1.7   |  | 1.92  |
|  | 50:32'0.000" | 2.095 |  | 1.676 |  | 1.925 |
|  | 50:40'0.000" | 2.037 |  | 1.852 |  | 1.905 |
|  | 50:48'0.000" | 2.089 |  | 1.654 |  | 1.917 |
|  | 50:56'0.000" | 2.082 |  | 1.65  |  | 1.915 |
|  | 51:04'0.000" | 2.093 |  | 1.642 |  | 1.926 |
|  | 51:12'0.000" | 2.016 |  | 1.887 |  | 1.892 |
|  | 51:20'0.000" | 2.1   |  | 1.703 |  | 1.921 |
|  | 51:28'0.000" | 2.113 |  | 1.625 |  | 1.928 |
|  | 51:36'0.000" | 2.127 |  | 1.587 |  | 1.94  |
|  | 51:44'0.000" | 2.091 |  | 1.705 |  | 1.913 |
|  | 51:52'0.000" | 2.029 |  | 1.889 |  | 1.889 |
|  | 52:00'0.000" | 2.018 |  | 1.93  |  | 1.888 |
|  | 52:08'0.000" | 2.14  |  | 1.521 |  | 1.94  |
|  | 52:16'0.000" | 2.041 |  | 1.818 |  | 1.888 |
|  | 52:24'0.000" | 2.008 |  | 1.865 |  | 1.892 |
|  | 52:32'0.000" | 2.019 |  | 1.908 |  | 1.893 |
|  | 52:40'0.000" | 2.054 |  | 1.78  |  | 1.914 |
|  | 52:48'0.000" | 2.052 |  | 1.725 |  | 1.891 |
|  | 52:56'0.000" | 2.078 |  | 1.618 |  | 1.917 |
|  | 53:04'0.000" | 2.05  |  | 1.605 |  | 1.912 |
|  | 53:12'0.000" | 1.984 |  | 1.873 |  | 1.876 |
|  | 53:20'0.000" | 2.077 |  | 1.687 |  | 1.896 |
|  | 53:28'0.000" | 2.068 |  | 1.671 |  | 1.908 |
|  | 53:36'0.000" | 2.053 |  | 1.61  |  | 1.91  |
|  | 53:44'0.000" | 2.034 |  | 1.72  |  | 1.885 |
|  | 53:52'0.000" | 2.013 |  | 1.767 |  | 1.873 |
|  | 54:00'0.000" | 1.969 |  | 1.878 |  | 1.92  |
|  | 54:08'0.000" | 2.068 |  | 1.552 |  | 1.914 |
|  | 54:16'0.000" | 2.112 |  | 1.481 |  | 1.92  |
|  | 54:24'0.000" | 2.16  |  | 1.467 |  | 1.936 |
|  | 54:32'0.000" | 2.059 |  | 1.522 |  | 1.918 |
|  | 54:40'0.000" | 2.065 |  | 1.614 |  | 1.907 |
|  | 54:48'0.000" | 2.077 |  | 1.571 |  | 1.897 |
|  | 54:56'0.000" | 2.089 |  | 1.459 |  | 1.914 |
|  | 55:04'0.000" | 2.117 |  | 1.491 |  | 1.93  |
|  | 55:12'0.000" | 2.117 |  | 1.441 |  | 1.932 |
|  | 55:20'0.000" | 2.082 |  | 1.598 |  | 1.897 |
|  | 55:28'0.000" | 2.107 |  | 1.529 |  | 1.918 |
|  | 55:36'0.000" | 2.099 |  | 1.528 |  | 1.926 |
|  | 55:44'0.000" | 2.09  |  | 1.609 |  | 1.918 |
|  | 55:52'0.000" | 2.073 |  | 1.616 |  | 1.893 |

|  |              |       |  |       |  |       |
|--|--------------|-------|--|-------|--|-------|
|  | 56:00'0.000" | 1.966 |  | 1.844 |  | 1.859 |
|  | 56:08'0.000" | 2.034 |  | 1.782 |  | 1.891 |
|  | 56:16'0.000" | 2.017 |  | 1.902 |  | 1.878 |
|  | 56:24'0.000" | 2.055 |  | 1.681 |  | 1.89  |
|  | 56:32'0.000" | 1.997 |  | 1.831 |  | 1.874 |
|  | 56:40'0.000" | 1.996 |  | 1.804 |  | 1.88  |
|  | 56:48'0.000" | 1.988 |  | 1.87  |  | 1.868 |
|  | 56:56'0.000" | 2.003 |  | 1.768 |  | 1.872 |
|  | 57:04'0.000" | 1.974 |  | 1.879 |  | 1.865 |
|  | 57:12'0.000" | 2.399 |  | 1.569 |  | 1.864 |
|  | 57:20'0.000" | 2.424 |  | 1.527 |  | 1.862 |
|  | 57:28'0.000" | 2.496 |  | 1.161 |  | 1.901 |
|  | 57:36'0.000" | 2.523 |  | 1.206 |  | 1.903 |
|  | 57:44'0.000" | 2.385 |  | 1.387 |  | 1.865 |
|  | 57:52'0.000" | 2.253 |  | 1.811 |  | 1.818 |
|  | 58:00'0.000" | 2.361 |  | 1.568 |  | 1.864 |
|  | 58:08'0.000" | 2.393 |  | 1.487 |  | 1.876 |
|  | 58:16'0.000" | 2.555 |  | 1.121 |  | 1.913 |
|  | 58:24'0.000" | 2.487 |  | 1.235 |  | 1.879 |
|  | 58:32'0.000" | 2.24  |  | 1.762 |  | 1.827 |
|  | 58:40'0.000" | 2.411 |  | 1.499 |  | 1.882 |
|  | 58:48'0.000" | 2.365 |  | 1.472 |  | 1.853 |
|  | 58:56'0.000" | 2.22  |  | 1.806 |  | 1.827 |
|  | 59:04'0.000" | 2.338 |  | 1.556 |  | 1.863 |
|  | 59:12'0.000" | 2.282 |  | 1.719 |  | 1.842 |
|  | 59:20'0.000" | 2.315 |  | 1.619 |  | 1.853 |
|  | 59:28'0.000" | 2.356 |  | 1.563 |  | 1.865 |
|  | 59:36'0.000" | 2.361 |  | 1.467 |  | 1.88  |
|  | 59:44'0.000" | 2.386 |  | 1.42  |  | 1.869 |
|  | 59:52'0.000" | 2.343 |  | 1.544 |  | 1.859 |
|  | 60:00'0.000" | 2.217 |  | 1.831 |  | 1.833 |
|  | 60:08'0.000" | 2.359 |  | 1.524 |  | 1.866 |
|  | 60:16'0.000" | 2.365 |  | 1.53  |  | 1.863 |
|  | 60:24'0.000" | 2.261 |  | 1.76  |  | 1.841 |
|  | 60:32'0.000" | 2.239 |  | 1.821 |  | 1.842 |
|  | 60:40'0.000" | 2.285 |  | 1.704 |  | 1.843 |
|  | 60:48'0.000" | 2.368 |  | 1.476 |  | 1.87  |
|  | 60:56'0.000" | 2.359 |  | 1.464 |  | 1.878 |
|  | 61:04'0.000" | 2.25  |  | 1.798 |  | 1.838 |
|  | 61:12'0.000" | 2.31  |  | 1.656 |  | 1.848 |
|  | 61:20'0.000" | 2.292 |  | 1.697 |  | 1.854 |
|  | 61:28'0.000" | 2.289 |  | 1.75  |  | 1.858 |
|  | 61:36'0.000" | 2.243 |  | 1.826 |  | 1.834 |

|  |              |       |  |       |  |       |
|--|--------------|-------|--|-------|--|-------|
|  | 61:44'0.000" | 2.32  |  | 1.532 |  | 1.86  |
|  | 61:52'0.000" | 2.289 |  | 1.59  |  | 1.857 |
|  | 62:00'0.000" | 2.325 |  | 1.53  |  | 1.867 |
|  | 62:08'0.000" | 2.222 |  | 1.495 |  | 1.856 |
|  | 62:16'0.000" | 2.249 |  | 1.849 |  | 1.843 |
|  | 62:24'0.000" | 2.141 |  | 1.839 |  | 1.851 |
|  | 62:32'0.000" | 2.134 |  | 1.661 |  | 1.872 |
|  | 62:40'0.000" | 2.174 |  | 1.562 |  | 1.9   |
|  | 62:48'0.000" | 2.122 |  | 1.607 |  | 1.89  |
|  | 62:56'0.000" | 2.057 |  | 1.778 |  | 1.876 |
|  | 63:04'0.000" | 2.133 |  | 1.689 |  | 1.879 |
|  | 63:12'0.000" | 2.057 |  | 1.891 |  | 1.868 |
|  | 63:20'0.000" | 2.15  |  | 1.571 |  | 1.899 |
|  | 63:28'0.000" | 2.158 |  | 1.526 |  | 1.891 |
|  | 63:36'0.000" | 2.149 |  | 1.576 |  | 1.899 |
|  | 63:44'0.000" | 2.128 |  | 1.677 |  | 1.899 |
|  | 63:52'0.000" | 2.122 |  | 1.69  |  | 1.886 |
|  | 64:00'0.000" | 2.129 |  | 1.645 |  | 1.888 |
|  | 64:08'0.000" | 2.193 |  | 1.442 |  | 1.922 |
|  | 64:16'0.000" | 2.067 |  | 1.79  |  | 1.871 |
|  | 64:24'0.000" | 2.139 |  | 1.574 |  | 1.884 |
|  | 64:32'0.000" | 2.152 |  | 1.538 |  | 1.904 |
|  | 64:40'0.000" | 2.164 |  | 1.519 |  | 1.915 |
|  | 64:48'0.000" | 2.179 |  | 1.522 |  | 1.9   |
|  | 64:56'0.000" | 2.032 |  | 1.869 |  | 1.856 |
|  | 65:04'0.000" | 2.133 |  | 1.552 |  | 1.898 |
|  | 65:12'0.000" | 2.162 |  | 1.526 |  | 1.903 |
|  | 65:20'0.000" | 2.198 |  | 1.484 |  | 1.906 |
|  | 65:28'0.000" | 2.059 |  | 1.805 |  | 1.87  |
|  | 65:36'0.000" | 2.072 |  | 1.852 |  | 1.874 |
|  | 65:44'0.000" | 2.12  |  | 1.656 |  | 1.881 |
|  | 65:52'0.000" | 2.097 |  | 1.767 |  | 1.875 |
|  | 66:00'0.000" | 2.024 |  | 1.859 |  | 1.861 |
|  | 66:08'0.000" | 2.049 |  | 1.841 |  | 1.88  |
|  | 66:16'0.000" | 2.133 |  | 1.589 |  | 1.89  |
|  | 66:24'0.000" | 2.097 |  | 1.78  |  | 1.884 |
|  | 66:32'0.000" | 2.047 |  | 1.853 |  | 1.855 |
|  | 66:40'0.000" | 2.084 |  | 1.803 |  | 1.868 |
|  | 66:48'0.000" | 2.067 |  | 1.78  |  | 1.869 |
|  | 66:56'0.000" | 2.181 |  | 1.588 |  | 1.909 |
|  | 67:04'0.000" | 2.148 |  | 1.643 |  | 1.882 |
|  | 67:12'0.000" | 2.068 |  | 1.843 |  | 1.869 |
|  | 67:20'0.000" | 2.155 |  | 1.599 |  | 1.903 |

|  |              |       |  |       |  |       |
|--|--------------|-------|--|-------|--|-------|
|  | 67:28'0.000" | 2.145 |  | 1.623 |  | 1.888 |
|  | 67:36'0.000" | 2.112 |  | 1.622 |  | 1.892 |
|  | 67:44'0.000" | 2.154 |  | 1.513 |  | 1.924 |
|  | 67:52'0.000" | 2.047 |  | 1.871 |  | 1.856 |
|  | 68:00'0.000" | 2.163 |  | 1.569 |  | 1.905 |
|  | 68:08'0.000" | 2.167 |  | 1.518 |  | 1.911 |
|  | 68:16'0.000" | 2.177 |  | 1.542 |  | 1.903 |
|  | 68:24'0.000" | 2.03  |  | 1.904 |  | 1.852 |
|  | 68:32'0.000" | 2.133 |  | 1.651 |  | 1.891 |
|  | 68:40'0.000" | 2.141 |  | 1.627 |  | 1.892 |
|  | 68:48'0.000" | 2.13  |  | 1.588 |  | 1.88  |
|  | 68:56'0.000" | 2.158 |  | 1.581 |  | 1.897 |
|  | 69:04'0.000" | 2.188 |  | 1.595 |  | 1.911 |
|  | 69:12'0.000" | 2.197 |  | 1.536 |  | 1.899 |
|  | 69:20'0.000" | 2.189 |  | 1.575 |  | 1.905 |
|  | 69:28'0.000" | 2.262 |  | 1.303 |  | 1.955 |
|  | 69:36'0.000" | 2.165 |  | 1.728 |  | 1.909 |
|  | 69:44'0.000" | 2.151 |  | 1.766 |  | 1.899 |
|  | 69:52'0.000" | 2.171 |  | 1.66  |  | 1.911 |
|  | 70:00'0.000" | 2.152 |  | 1.819 |  | 1.908 |
|  | 70:08'0.000" | 2.124 |  | 1.923 |  | 1.885 |
|  | 70:16'0.000" | 2.25  |  | 1.577 |  | 1.94  |
|  | 70:24'0.000" | 2.257 |  | 1.552 |  | 1.943 |
|  | 70:32'0.000" | 2.139 |  | 1.896 |  | 1.899 |
|  | 70:40'0.000" | 2.224 |  | 1.565 |  | 1.919 |
|  | 70:48'0.000" | 2.214 |  | 1.533 |  | 1.93  |
|  | 70:56'0.000" | 2.268 |  | 1.545 |  | 1.947 |
|  | 71:04'0.000" | 2.165 |  | 1.751 |  | 1.897 |
|  | 71:12'0.000" | 2.148 |  | 1.802 |  | 1.896 |
|  | 71:20'0.000" | 2.2   |  | 1.654 |  | 1.924 |
|  | 71:28'0.000" | 2.147 |  | 1.788 |  | 1.901 |
|  | 71:36'0.000" | 2.133 |  | 1.83  |  | 1.884 |
|  | 71:44'0.000" | 2.235 |  | 1.619 |  | 1.932 |
|  | 71:52'0.000" | 2.223 |  | 1.586 |  | 1.931 |
|  | 72:00'0.000" | 2.162 |  | 1.811 |  | 1.892 |
|  | 72:08'0.000" | 2.14  |  | 1.867 |  | 1.883 |
|  | 72:16'0.000" | 2.236 |  | 1.592 |  | 1.929 |
|  | 72:24'0.000" | 2.266 |  | 1.523 |  | 1.935 |
|  | 72:32'0.000" | 2.148 |  | 1.916 |  | 1.88  |
|  | 72:40'0.000" | 2.255 |  | 1.601 |  | 1.92  |
|  | 72:48'0.000" | 2.199 |  | 1.804 |  | 1.931 |
|  | 72:56'0.000" | 2.173 |  | 1.877 |  | 1.9   |
|  | 73:04'0.000" | 2.262 |  | 1.611 |  | 1.92  |

|  |              |       |  |       |  |       |
|--|--------------|-------|--|-------|--|-------|
|  | 73:12'0.000" | 2.304 |  | 1.535 |  | 1.933 |
|  | 73:20'0.000" | 2.287 |  | 1.519 |  | 1.944 |
|  | 73:28'0.000" | 2.293 |  | 1.533 |  | 1.94  |
|  | 73:36'0.000" | 2.32  |  | 1.369 |  | 1.941 |
|  | 73:44'0.000" | 2.311 |  | 1.463 |  | 1.927 |
|  | 73:52'0.000" | 2.242 |  | 1.644 |  | 1.924 |
|  | 74:00'0.000" | 2.297 |  | 1.54  |  | 1.928 |
|  | 74:08'0.000" | 2.245 |  | 1.594 |  | 1.909 |
|  | 74:16'0.000" | 2.254 |  | 1.547 |  | 1.924 |
|  | 74:24'0.000" | 2.228 |  | 1.637 |  | 1.92  |
|  | 74:32'0.000" | 2.176 |  | 1.814 |  | 1.889 |
|  | 74:40'0.000" | 2.178 |  | 1.854 |  | 1.933 |
|  | 74:48'0.000" | 2.294 |  | 1.53  |  | 1.942 |
|  | 74:56'0.000" | 2.37  |  | 1.514 |  | 1.927 |
|  | 75:04'0.000" | 2.391 |  | 1.674 |  | 1.88  |
|  | 75:12'0.000" | 2.326 |  | 1.779 |  | 1.872 |
|  | 75:20'0.000" | 2.314 |  | 1.845 |  | 1.871 |
|  | 75:28'0.000" | 2.385 |  | 1.712 |  | 1.892 |
|  | 75:36'0.000" | 2.36  |  | 1.731 |  | 1.882 |
|  | 75:44'0.000" | 2.317 |  | 1.738 |  | 1.886 |
|  | 75:52'0.000" | 2.42  |  | 1.529 |  | 1.913 |
|  | 76:00'0.000" | 2.405 |  | 1.573 |  | 1.897 |
|  | 76:08'0.000" | 2.391 |  | 1.609 |  | 1.889 |
|  | 76:16'0.000" | 2.319 |  | 1.837 |  | 1.866 |
|  | 76:24'0.000" | 2.301 |  | 1.545 |  | 1.867 |
|  | 76:32'0.000" | 2.284 |  | 1.564 |  | 1.853 |
|  | 76:40'0.000" | 2.239 |  | 1.715 |  | 1.845 |
|  | 76:48'0.000" | 2.201 |  | 1.786 |  | 1.837 |
|  | 76:56'0.000" | 2.315 |  | 1.492 |  | 1.873 |
|  | 77:04'0.000" | 2.311 |  | 1.514 |  | 1.864 |
|  | 77:12'0.000" | 2.306 |  | 1.534 |  | 1.848 |
|  | 77:20'0.000" | 2.215 |  | 1.776 |  | 1.849 |
|  | 77:28'0.000" | 2.307 |  | 1.57  |  | 1.861 |
|  | 77:36'0.000" | 2.309 |  | 1.53  |  | 1.872 |
|  | 77:44'0.000" | 2.322 |  | 1.427 |  | 1.875 |
|  | 77:52'0.000" | 2.159 |  | 1.832 |  | 1.885 |
|  | 78:00'0.000" | 2.279 |  | 1.53  |  | 1.853 |
|  | 78:08'0.000" | 2.286 |  | 1.572 |  | 1.856 |
|  | 78:16'0.000" | 2.268 |  | 1.559 |  | 1.858 |
|  | 78:24'0.000" | 2.231 |  | 1.702 |  | 1.852 |
|  | 78:32'0.000" | 2.096 |  | 1.779 |  | 2.055 |
|  | 78:40'0.000" | 2.206 |  | 1.454 |  | 2.115 |
|  | 78:48'0.000" | 2.209 |  | 1.385 |  | 2.127 |

|  |              |       |  |       |  |       |
|--|--------------|-------|--|-------|--|-------|
|  | 78:56'0.000" | 2.186 |  | 1.421 |  | 2.13  |
|  | 79:04'0.000" | 2.278 |  | 1.337 |  | 2.15  |
|  | 79:12'0.000" | 2.19  |  | 1.412 |  | 2.091 |
|  | 79:20'0.000" | 2.161 |  | 1.457 |  | 2.083 |
|  | 79:28'0.000" | 2.24  |  | 1.426 |  | 2.135 |
|  | 79:36'0.000" | 2.077 |  | 1.796 |  | 2.029 |
|  | 79:44'0.000" | 2.108 |  | 1.729 |  | 2.033 |
|  | 79:52'0.000" | 2.175 |  | 1.528 |  | 2.079 |
|  | 80:00'0.000" | 2.216 |  | 1.409 |  | 2.114 |
|  | 80:08'0.000" | 2.214 |  | 1.443 |  | 2.104 |
|  | 80:16'0.000" | 2.225 |  | 1.398 |  | 2.093 |
|  | 80:24'0.000" | 2.1   |  | 1.742 |  | 2.028 |
|  | 80:32'0.000" | 2.194 |  | 1.485 |  | 2.087 |
|  | 80:40'0.000" | 2.242 |  | 1.328 |  | 2.126 |
|  | 80:48'0.000" | 2.244 |  | 1.411 |  | 2.098 |
|  | 80:56'0.000" | 2.142 |  | 1.361 |  | 2.134 |
|  | 81:04'0.000" | 2.037 |  | 1.53  |  | 2.116 |
|  | 81:12'0.000" | 1.996 |  | 1.423 |  | 2.118 |
|  | 81:20'0.000" | 2.017 |  | 1.349 |  | 2.168 |
|  | 81:28'0.000" | 2.009 |  | 1.529 |  | 2.106 |
|  | 81:36'0.000" | 1.929 |  | 1.792 |  | 2.054 |
|  | 81:44'0.000" | 1.946 |  | 1.784 |  | 2.067 |
|  | 81:52'0.000" | 1.943 |  | 1.786 |  | 2.123 |
|  | 82:00'0.000" | 2.025 |  | 1.482 |  | 2.118 |
|  | 82:08'0.000" | 2.056 |  | 1.44  |  | 2.129 |
|  | 82:16'0.000" | 2.084 |  | 1.299 |  | 2.151 |
|  | 82:24'0.000" | 2.002 |  | 1.627 |  | 2.066 |
|  | 82:32'0.000" | 2.001 |  | 1.631 |  | 2.116 |
|  | 82:40'0.000" | 1.997 |  | 1.664 |  | 2.087 |
|  | 82:48'0.000" | 1.938 |  | 1.738 |  | 2.048 |
|  | 82:56'0.000" | 2.013 |  | 1.553 |  | 2.112 |
|  | 83:04'0.000" | 2.021 |  | 1.553 |  | 2.125 |
|  | 83:12'0.000" | 1.98  |  | 1.737 |  | 2.072 |
|  | 83:20'0.000" | 2.015 |  | 1.566 |  | 2.095 |
|  | 83:28'0.000" | 2.039 |  | 1.486 |  | 2.108 |
|  | 83:36'0.000" | 2.038 |  | 1.43  |  | 2.122 |
|  | 83:44'0.000" | 2.033 |  | 1.48  |  | 2.121 |
|  | 83:52'0.000" | 2.079 |  | 1.532 |  | 2.073 |
|  | 84:00'0.000" | 2.043 |  | 1.657 |  | 1.885 |
|  | 84:08'0.000" | 2.081 |  | 1.608 |  | 1.915 |
|  | 84:16'0.000" | 2.038 |  | 1.553 |  | 1.912 |
|  | 84:24'0.000" | 2.024 |  | 1.718 |  | 1.874 |
|  | 84:32'0.000" | 1.948 |  | 1.701 |  | 2.346 |

|  |              |       |  |       |  |       |
|--|--------------|-------|--|-------|--|-------|
|  | 84:40'0.000" | 1.915 |  | 1.741 |  | 2.234 |
|  | 84:48'0.000" | 1.944 |  | 1.657 |  | 2.233 |
|  | 84:56'0.000" | 1.939 |  | 1.746 |  | 2.208 |
|  | 85:04'0.000" | 1.914 |  | 1.761 |  | 2.194 |
|  | 85:12'0.000" | 1.921 |  | 1.742 |  | 2.188 |
|  | 85:20'0.000" | 2.013 |  | 1.485 |  | 2.239 |
|  | 85:28'0.000" | 2.043 |  | 1.462 |  | 2.273 |
|  | 85:36'0.000" | 1.929 |  | 1.816 |  | 2.18  |
|  | 85:44'0.000" | 2.031 |  | 1.484 |  | 2.244 |
|  | 85:52'0.000" | 2.036 |  | 1.423 |  | 2.256 |
|  | 86:00'0.000" | 2.07  |  | 1.328 |  | 2.284 |
|  | 86:08'0.000" | 2.035 |  | 1.464 |  | 2.243 |
|  | 86:16'0.000" | 2.032 |  | 1.518 |  | 2.231 |
|  | 86:24'0.000" | 2.026 |  | 1.511 |  | 2.236 |
|  | 86:32'0.000" | 2.037 |  | 1.489 |  | 2.219 |
|  | 86:40'0.000" | 2.007 |  | 1.557 |  | 2.206 |
|  | 86:48'0.000" | 1.956 |  | 1.714 |  | 2.163 |
|  | 86:56'0.000" | 1.97  |  | 1.68  |  | 2.17  |
|  | 87:04'0.000" | 1.959 |  | 1.71  |  | 2.152 |
|  | 87:12'0.000" | 1.968 |  | 1.702 |  | 2.171 |
|  | 87:20'0.000" | 1.963 |  | 1.73  |  | 2.161 |
|  | 87:28'0.000" | 2.019 |  | 1.577 |  | 2.189 |
|  | 87:36'0.000" | 2.005 |  | 1.606 |  | 2.19  |
|  | 87:44'0.000" | 2.024 |  | 1.58  |  | 2.207 |
|  | 87:52'0.000" | 1.978 |  | 1.644 |  | 2.167 |
|  | 88:00'0.000" | 1.962 |  | 1.779 |  | 2.144 |
|  | 88:08'0.000" | 2.02  |  | 1.539 |  | 2.219 |
|  | 88:16'0.000" | 2.021 |  | 1.583 |  | 2.176 |
|  | 88:24'0.000" | 2.007 |  | 1.596 |  | 2.188 |
|  | 88:32'0.000" | 2.008 |  | 1.577 |  | 2.184 |
|  | 88:40'0.000" | 1.979 |  | 1.659 |  | 2.156 |
|  | 88:48'0.000" | 1.968 |  | 1.78  |  | 2.125 |
|  | 88:56'0.000" | 2.007 |  | 1.569 |  | 2.193 |
|  | 89:04'0.000" | 2.035 |  | 1.498 |  | 2.196 |
|  | 89:12'0.000" | 2.061 |  | 1.412 |  | 2.204 |
|  | 89:20'0.000" | 2.002 |  | 1.559 |  | 2.173 |
|  | 89:28'0.000" | 1.991 |  | 1.552 |  | 2.169 |
|  | 89:36'0.000" | 1.996 |  | 1.642 |  | 2.145 |
|  | 89:44'0.000" | 1.955 |  | 1.75  |  | 2.136 |
|  | 89:52'0.000" | 1.95  |  | 1.779 |  | 2.132 |
|  | 90:00'0.000" | 2.045 |  | 1.48  |  | 2.186 |
|  | 90:08'0.000" | 2.033 |  | 1.438 |  | 2.184 |
|  | 90:16'0.000" | 1.958 |  | 1.678 |  | 2.145 |

|              |       |  |       |  |       |
|--------------|-------|--|-------|--|-------|
| 90:24'0.000" | 1.941 |  | 1.795 |  | 2.1   |
| 90:32'0.000" | 2.082 |  | 1.457 |  | 2.21  |
| 90:40'0.000" | 2.019 |  | 1.529 |  | 2.176 |
| 90:48'0.000" | 2     |  | 1.61  |  | 2.137 |
| 90:56'0.000" | 2.053 |  | 1.459 |  | 2.178 |
| 91:04'0.000" | 2.008 |  | 1.712 |  | 2.164 |
| 91:12'0.000" | 2.019 |  | 1.549 |  | 2.192 |
| 91:20'0.000" | 2.078 |  | 1.399 |  | 2.191 |
| 91:28'0.000" | 2.051 |  | 1.435 |  | 2.185 |
| 91:36'0.000" | 1.926 |  | 1.81  |  | 2.124 |
| 91:44'0.000" | 2.053 |  | 1.469 |  | 2.178 |
| 91:52'0.000" | 2.074 |  | 1.435 |  | 2.209 |
| 92:00'0.000" | 2.07  |  | 1.436 |  | 2.201 |
| 92:08'0.000" | 2.05  |  | 1.465 |  | 2.187 |
| 92:16'0.000" | 2.055 |  | 1.479 |  | 2.192 |
| 92:24'0.000" | 2.04  |  | 1.468 |  | 2.187 |
| 92:32'0.000" | 2.05  |  | 1.388 |  | 2.196 |
| 92:40'0.000" | 2.059 |  | 1.483 |  | 2.203 |
| 92:48'0.000" | 2.036 |  | 1.406 |  | 2.196 |
| 92:56'0.000" | 1.906 |  | 1.785 |  | 2.169 |
| 93:04'0.000" | 2.085 |  | 1.456 |  | 2.002 |
| 93:12'0.000" | 2.048 |  | 1.649 |  | 1.903 |
| 93:20'0.000" | 2.097 |  | 1.562 |  | 1.896 |
| 93:28'0.000" | 2.092 |  | 1.574 |  | 1.891 |
| 93:36'0.000" | 2.121 |  | 1.494 |  | 1.895 |
| 93:44'0.000" | 2.139 |  | 1.518 |  | 1.908 |
| 93:52'0.000" | 2.089 |  | 1.507 |  | 1.901 |
| 94:00'0.000" | 2.108 |  | 1.471 |  | 1.889 |
| 94:08'0.000" | 2.097 |  | 1.492 |  | 1.89  |
| 94:16'0.000" | 2.113 |  | 1.44  |  | 1.902 |
| 94:24'0.000" | 2.137 |  | 1.382 |  | 1.916 |
| 94:32'0.000" | 2.119 |  | 1.431 |  | 1.903 |
| 94:40'0.000" | 2.082 |  | 1.569 |  | 1.869 |
| 94:48'0.000" | 2     |  | 1.813 |  | 1.85  |
| 94:56'0.000" | 2.075 |  | 1.564 |  | 1.888 |
| 95:04'0.000" | 2.112 |  | 1.48  |  | 1.892 |
| 95:12'0.000" | 2.042 |  | 1.659 |  | 1.859 |
| 95:20'0.000" | 2.061 |  | 1.598 |  | 1.877 |
| 95:28'0.000" | 2.05  |  | 1.633 |  | 1.878 |
| 95:36'0.000" | 2.077 |  | 1.652 |  | 1.864 |
| 95:44'0.000" | 2.096 |  | 1.573 |  | 1.871 |
| 95:52'0.000" | 2.044 |  | 1.845 |  | 1.884 |
| 96:00'0.000" | 2.134 |  | 1.485 |  | 1.89  |



|  |               |       |  |       |  |       |
|--|---------------|-------|--|-------|--|-------|
|  | 96:08'0.000"  | 2.091 |  | 1.546 |  | 1.873 |
|  | 96:16'0.000"  | 2.152 |  | 1.535 |  | 1.879 |
|  | 96:24'0.000"  | 2.146 |  | 1.539 |  | 1.886 |
|  | 96:32'0.000"  | 2.096 |  | 1.6   |  | 1.868 |
|  | 96:40'0.000"  | 2.106 |  | 1.511 |  | 1.888 |
|  | 96:48'0.000"  | 2.121 |  | 1.549 |  | 1.884 |
|  | 96:56'0.000"  | 2.108 |  | 1.562 |  | 1.866 |
|  | 97:04'0.000"  | 2.134 |  | 1.484 |  | 1.883 |
|  | 97:12'0.000"  | 2.104 |  | 1.543 |  | 1.876 |
|  | 97:20'0.000"  | 2.014 |  | 1.855 |  | 1.865 |
|  | 97:28'0.000"  | 2.115 |  | 1.571 |  | 1.885 |
|  | 97:36'0.000"  | 2.058 |  | 1.791 |  | 1.846 |
|  | 97:44'0.000"  | 2.001 |  | 1.802 |  | 1.836 |
|  | 97:52'0.000"  | 2.098 |  | 1.535 |  | 1.884 |
|  | 98:00'0.000"  | 2.084 |  | 1.601 |  | 1.874 |
|  | 98:08'0.000"  | 2.159 |  | 1.531 |  | 1.887 |
|  | 98:16'0.000"  | 2.127 |  | 1.52  |  | 1.877 |
|  | 98:24'0.000"  | 2.137 |  | 1.493 |  | 1.888 |
|  | 98:32'0.000"  | 2.125 |  | 1.497 |  | 1.889 |
|  | 98:40'0.000"  | 2.063 |  | 1.662 |  | 1.857 |
|  | 98:48'0.000"  | 2.03  |  | 1.772 |  | 1.837 |
|  | 98:56'0.000"  | 2.094 |  | 1.622 |  | 1.866 |
|  | 99:04'0.000"  | 2.012 |  | 1.872 |  | 1.895 |
|  | 99:12'0.000"  | 2.134 |  | 1.522 |  | 1.892 |
|  | 99:20'0.000"  | 2.136 |  | 1.539 |  | 1.882 |
|  | 99:28'0.000"  | 2.033 |  | 1.88  |  | 1.832 |
|  | 99:36'0.000"  | 2.211 |  | 1.299 |  | 1.909 |
|  | 99:44'0.000"  | 2.17  |  | 1.336 |  | 1.892 |
|  | 99:52'0.000"  | 2.117 |  | 1.658 |  | 1.868 |
|  | 100:00'0.000" | 2.071 |  | 1.777 |  | 1.844 |

A sample of the raw data used to plot figure 5.2 in the potentiodynamic polarisation tests is shown below.

|             | Potential vs Ag/AgCl (V) | Log. Current density (A/cm <sup>2</sup> ) |                 | Log. Current density (A/cm <sup>2</sup> ) |                  | Log. Current density (A/cm <sup>2</sup> ) |
|-------------|--------------------------|---|-----------------|---|------------------|---|
| <b>lead</b> | -0.3999                  | 0.06528                                   | <b>DSA mesh</b> | 0.009888                                  | <b>DSA plate</b> | 0.501                                     |
|             | -0.3951                  | 0.06442                                   |                 | 0.009448                                  |                  | 0.4942                                    |
|             | -0.3902                  | 0.06363                                   |                 | 0.009                                     |                  | 0.4876                                    |
|             | -0.3853                  | 0.06284                                   |                 | 0.008624                                  |                  | 0.4814                                    |
|             | -0.3804                  | 0.0621                                    |                 | 0.008362                                  |                  | 0.4749                                    |

|         |         |  |             |        |
|---------|---------|--|-------------|--------|
| -0.3755 | 0.06137 |  | 0.007837    | 0.469  |
| -0.3706 | 0.06064 |  | 0.007504    | 0.4629 |
| -0.3658 | 0.05994 |  | 0.00719     | 0.4571 |
| -0.3609 | 0.0592  |  | 0.006778    | 0.4517 |
| -0.356  | 0.05847 |  | 0.006445    | 0.4457 |
| -0.3511 | 0.05777 |  | 0.006076    | 0.4399 |
| -0.3462 | 0.05707 |  | 0.005661    | 0.4338 |
| -0.3413 | 0.05634 |  | 0.00535     | 0.4279 |
| -0.3365 | 0.0556  |  | 0.005017    | 0.4218 |
| -0.3316 | 0.05487 |  | 0.004648    | 0.4155 |
| -0.3267 | 0.05414 |  | 0.004315    | 0.4094 |
| -0.3218 | 0.05341 |  | 0.003952    | 0.4033 |
| -0.3169 | 0.05267 |  | 0.00365     | 0.3972 |
| -0.312  | 0.05191 |  | 0.003339    | 0.3916 |
| -0.3072 | 0.05115 |  | 0.003009    | 0.3853 |
| -0.3023 | 0.05038 |  | 0.002702    | 0.3792 |
| -0.2974 | 0.04962 |  | 0.002483    | 0.373  |
| -0.2925 | 0.04883 |  | 0.002218    | 0.367  |
| -0.2876 | 0.04807 |  | 0.001948    | 0.3607 |
| -0.2827 | 0.04727 |  | 0.001699    | 0.3546 |
| -0.2779 | 0.04648 |  | 0.001465    | 0.3484 |
| -0.273  | 0.04568 |  | 0.001239    | 0.3421 |
| -0.2681 | 0.04471 |  | 0.001037    | 0.336  |
| -0.2632 | 0.04391 |  | 0.0008493   | 0.3299 |
| -0.2583 | 0.04309 |  | 0.0006821   | 0.3236 |
| -0.2534 | 0.04228 |  | 0.0005368   | 0.3175 |
| -0.2486 | 0.04146 |  | 0.0004083   | 0.3114 |
| -0.2437 | 0.04063 |  | 0.0002982   | 0.3053 |
| -0.2388 | 0.03981 |  | 0.0002042   | 0.2991 |
| -0.2339 | 0.03898 |  | 0.0001254   | 0.2928 |
| -0.229  | 0.03815 |  | 0.00005829  | 0.2867 |
| -0.2242 | 0.03731 |  | 0.000002136 | 0.2808 |
| -0.2193 | 0.03648 |  | 0.00004761  | 0.2747 |
| -0.2144 | 0.03565 |  | 0.00008661  | 0.2686 |
| -0.2095 | 0.03481 |  | 0.00012     | 0.2622 |
| -0.2046 | 0.03398 |  | 0.0001487   | 0.256  |
| -0.1997 | 0.03315 |  | 0.0001738   | 0.25   |
| -0.1949 | 0.03231 |  | 0.0001951   | 0.244  |
| -0.19   | 0.03148 |  | 0.0002147   | 0.2379 |
| -0.1851 | 0.03065 |  | 0.0002325   | 0.2319 |
| -0.1802 | 0.02982 |  | 0.000248    | 0.226  |
| -0.1753 | 0.029   |  | 0.0002629   | 0.2202 |
| -0.1704 | 0.02818 |  | 0.0002762   | 0.2142 |

|  |         |          |  |           |  |          |
|--|---------|----------|--|-----------|--|----------|
|  | -0.1656 | 0.02737  |  | 0.0002888 |  | 0.2083   |
|  | -0.1607 | 0.02656  |  | 0.0003008 |  | 0.2024   |
|  | -0.1558 | 0.02575  |  | 0.0003116 |  | 0.1966   |
|  | -0.1509 | 0.02495  |  | 0.0003225 |  | 0.1908   |
|  | -0.146  | 0.02415  |  | 0.0003318 |  | 0.185    |
|  | -0.1411 | 0.02336  |  | 0.0003417 |  | 0.1793   |
|  | -0.1363 | 0.02258  |  | 0.0003506 |  | 0.1736   |
|  | 1.119   | 0.00485  |  | 0.001144  |  | 0.007938 |
|  | 1.124   | 0.004843 |  | 0.001153  |  | 0.007866 |
|  | 1.128   | 0.004829 |  | 0.001159  |  | 0.00784  |
|  | 1.133   | 0.004813 |  | 0.001167  |  | 0.00775  |
|  | 1.138   | 0.004796 |  | 0.001174  |  | 0.007687 |
|  | 1.143   | 0.00477  |  | 0.001182  |  | 0.007633 |
|  | 1.148   | 0.004744 |  | 0.001191  |  | 0.007567 |
|  | 1.153   | 0.004715 |  | 0.0012    |  | 0.007557 |
|  | 1.158   | 0.004683 |  | 0.001208  |  | 0.007578 |
|  | 1.163   | 0.004649 |  | 0.001217  |  | 0.00757  |
|  | 1.167   | 0.004611 |  | 0.001227  |  | 0.007475 |
|  | 1.172   | 0.004569 |  | 0.001238  |  | 0.00756  |
|  | 1.177   | 0.004534 |  | 0.001247  |  | 0.007438 |
|  | 1.182   | 0.004507 |  | 0.001258  |  | 0.007437 |
|  | 1.187   | 0.004484 |  | 0.001269  |  | 0.007406 |
|  | 1.192   | 0.004458 |  | 0.001281  |  | 0.007405 |
|  | 1.197   | 0.004445 |  | 0.001293  |  | 0.007416 |
|  | 1.202   | 0.004425 |  | 0.001306  |  | 0.007348 |

A sample of part of the raw data used to plot figure 19 showing 55 cyclic voltammetry scans for the lead anode is shown below.

|        | Potential | Current density |         | Potential | Current density |         | Potential | Current density |         | Potential | Current density |         | Potential | Current density |
|--------|-----------|-----------------|---------|-----------|-----------------|---------|-----------|-----------------|---------|-----------|-----------------|---------|-----------|-----------------|
| scan 5 | 0         | -3.27E-04       | scan 10 | 0         | -2.61E-03       | scan 15 | 0         | -6.93E-03       | scan 20 | 0         | -6.76E-03       | scan 25 | 0         | -7.58E-03       |
|        | 4.88E-03  | -3.12E-04       |         | 4.88E-03  | -2.53E-03       |         | 4.88E-03  | -6.77E-03       |         | 4.88E-03  | -6.60E-03       |         | 4.88E-03  | -7.39E-03       |
|        | 9.77E-03  | -2.99E-04       |         | 9.77E-03  | -2.46E-03       |         | 9.77E-03  | -6.60E-03       |         | 9.77E-03  | -6.43E-03       |         | 9.77E-03  | -7.19E-03       |
|        | 1.47E-02  | -2.86E-04       |         | 1.47E-02  | -2.39E-03       |         | 1.47E-02  | -6.43E-03       |         | 1.47E-02  | -6.26E-03       |         | 1.47E-02  | -7.00E-03       |
|        | 1.95E-02  | -2.75E-04       |         | 1.95E-02  | -2.33E-03       |         | 1.95E-02  | -6.26E-03       |         | 1.95E-02  | -6.09E-03       |         | 1.95E-02  | -6.80E-03       |
|        | 2.44E-02  | -2.64E-04       |         | 2.44E-02  | -2.26E-03       |         | 2.44E-02  | -6.09E-03       |         | 2.44E-02  | -5.92E-03       |         | 2.44E-02  | -6.61E-03       |
|        | 2.93E-02  | -2.54E-04       |         | 2.93E-02  | -2.20E-03       |         | 2.93E-02  | -5.93E-03       |         | 2.93E-02  | -5.76E-03       |         | 2.93E-02  | -6.42E-03       |
|        | 3.42E-02  | -2.44E-04       |         | 3.42E-02  | -2.15E-03       |         | 3.42E-02  | -5.77E-03       |         | 3.42E-02  | -5.61E-03       |         | 3.42E-02  | -6.24E-03       |
|        | 3.91E-02  | -2.35E-04       |         | 3.91E-02  | -2.09E-03       |         | 3.91E-02  | -5.61E-03       |         | 3.91E-02  | -5.45E-03       |         | 3.91E-02  | -6.06E-03       |
|        | 4.40E-02  | -2.27E-04       |         | 4.40E-02  | -2.03E-03       |         | 4.40E-02  | -5.45E-03       |         | 4.40E-02  | -5.30E-03       |         | 4.40E-02  | -5.89E-03       |
|        | 4.88E-02  | -2.19E-04       |         | 4.88E-02  | -1.98E-03       |         | 4.88E-02  | -5.30E-03       |         | 4.88E-02  | -5.15E-03       |         | 4.88E-02  | -5.73E-03       |
|        | 5.37E-02  | -2.11E-04       |         | 5.37E-02  | -1.93E-03       |         | 5.37E-02  | -5.15E-03       |         | 5.37E-02  | -5.01E-03       |         | 5.37E-02  | -5.56E-03       |
|        | 5.86E-02  | -2.04E-04       |         | 5.86E-02  | -1.88E-03       |         | 5.86E-02  | -5.01E-03       |         | 5.86E-02  | -4.87E-03       |         | 5.86E-02  | -5.41E-03       |
|        | 6.35E-02  | -1.97E-04       |         | 6.35E-02  | -1.83E-03       |         | 6.35E-02  | -4.87E-03       |         | 6.35E-02  | -4.74E-03       |         | 6.35E-02  | -5.26E-03       |
|        | 6.84E-02  | -1.91E-04       |         | 6.84E-02  | -1.79E-03       |         | 6.84E-02  | -4.73E-03       |         | 6.84E-02  | -4.61E-03       |         | 6.84E-02  | -5.11E-03       |
|        | 7.32E-02  | -1.85E-04       |         | 7.32E-02  | -1.74E-03       |         | 7.32E-02  | -4.60E-03       |         | 7.32E-02  | -4.48E-03       |         | 7.32E-02  | -4.96E-03       |
|        | 7.81E-02  | -1.79E-04       |         | 7.81E-02  | -1.70E-03       |         | 7.81E-02  | -4.47E-03       |         | 7.81E-02  | -4.36E-03       |         | 7.81E-02  | -4.82E-03       |
|        | 8.30E-02  | -1.73E-04       |         | 8.30E-02  | -1.66E-03       |         | 8.30E-02  | -4.34E-03       |         | 8.30E-02  | -4.24E-03       |         | 8.30E-02  | -4.69E-03       |
|        | 8.79E-02  | -1.67E-04       |         | 8.79E-02  | -1.62E-03       |         | 8.79E-02  | -4.21E-03       |         | 8.79E-02  | -4.12E-03       |         | 8.79E-02  | -4.56E-03       |
|        | 9.28E-02  | -1.62E-04       |         | 9.28E-02  | -1.58E-03       |         | 9.28E-02  | -4.09E-03       |         | 9.28E-02  | -4.00E-03       |         | 9.28E-02  | -4.43E-03       |
|        | 9.77E-02  | -1.57E-04       |         | 9.77E-02  | -1.54E-03       |         | 9.77E-02  | -3.97E-03       |         | 9.77E-02  | -3.89E-03       |         | 9.77E-02  | -4.30E-03       |
|        | 0.1025    | -1.53E-04       |         | 0.1025    | -1.50E-03       |         | 0.1025    | -3.86E-03       |         | 0.1025    | -3.78E-03       |         | 0.1025    | -4.18E-03       |

|  |        |           |  |        |           |  |        |           |  |        |           |  |        |           |
|--|--------|-----------|--|--------|-----------|--|--------|-----------|--|--------|-----------|--|--------|-----------|
|  | 0.1074 | -1.48E-04 |  | 0.1074 | -1.46E-03 |  | 0.1074 | -3.75E-03 |  | 0.1074 | -3.67E-03 |  | 0.1074 | -4.06E-03 |
|  | 0.1123 | -1.44E-04 |  | 0.1123 | -1.43E-03 |  | 0.1123 | -3.63E-03 |  | 0.1123 | -3.57E-03 |  | 0.1123 | -3.95E-03 |
|  | 0.1172 | -1.40E-04 |  | 0.1172 | -1.39E-03 |  | 0.1172 | -3.53E-03 |  | 0.1172 | -3.47E-03 |  | 0.1172 | -3.84E-03 |
|  | 0.1221 | -1.35E-04 |  | 0.1221 | -1.36E-03 |  | 0.1221 | -3.42E-03 |  | 0.1221 | -3.37E-03 |  | 0.1221 | -3.73E-03 |
|  | 0.127  | -1.32E-04 |  | 0.127  | -1.32E-03 |  | 0.127  | -3.32E-03 |  | 0.127  | -3.27E-03 |  | 0.127  | -3.62E-03 |
|  | 0.1318 | -1.28E-04 |  | 0.1318 | -1.29E-03 |  | 0.1318 | -3.22E-03 |  | 0.1318 | -3.18E-03 |  | 0.1318 | -3.52E-03 |
|  | 0.1367 | -1.24E-04 |  | 0.1367 | -1.26E-03 |  | 0.1367 | -3.12E-03 |  | 0.1367 | -3.09E-03 |  | 0.1367 | -3.42E-03 |
|  | 0.1416 | -1.21E-04 |  | 0.1416 | -1.23E-03 |  | 0.1416 | -3.03E-03 |  | 0.1416 | -3.00E-03 |  | 0.1416 | -3.32E-03 |
|  | 0.1465 | -1.17E-04 |  | 0.1465 | -1.20E-03 |  | 0.1465 | -2.94E-03 |  | 0.1465 | -2.91E-03 |  | 0.1465 | -3.23E-03 |
|  | 0.1514 | -1.14E-04 |  | 0.1514 | -1.17E-03 |  | 0.1514 | -2.85E-03 |  | 0.1514 | -2.83E-03 |  | 0.1514 | -3.14E-03 |
|  | 0.1563 | -1.11E-04 |  | 0.1563 | -1.14E-03 |  | 0.1563 | -2.76E-03 |  | 0.1563 | -2.75E-03 |  | 0.1563 | -3.05E-03 |
|  | 0.1611 | -1.08E-04 |  | 0.1611 | -1.11E-03 |  | 0.1611 | -2.68E-03 |  | 0.1611 | -2.67E-03 |  | 0.1611 | -2.96E-03 |
|  | 0.166  | -1.05E-04 |  | 0.166  | -1.08E-03 |  | 0.166  | -2.59E-03 |  | 0.166  | -2.59E-03 |  | 0.166  | -2.87E-03 |
|  | 0.1709 | -1.02E-04 |  | 0.1709 | -1.06E-03 |  | 0.1709 | -2.51E-03 |  | 0.1709 | -2.52E-03 |  | 0.1709 | -2.79E-03 |
|  | 0.1758 | -9.97E-05 |  | 0.1758 | -1.03E-03 |  | 0.1758 | -2.44E-03 |  | 0.1758 | -2.44E-03 |  | 0.1758 | -2.71E-03 |
|  | 0.1807 | -9.70E-05 |  | 0.1807 | -1.00E-03 |  | 0.1807 | -2.36E-03 |  | 0.1807 | -2.37E-03 |  | 0.1807 | -2.63E-03 |
|  | 0.1855 | -9.45E-05 |  | 0.1855 | -9.76E-04 |  | 0.1855 | -2.29E-03 |  | 0.1855 | -2.30E-03 |  | 0.1855 | -2.56E-03 |
|  | 0.1904 | -9.20E-05 |  | 0.1904 | -9.51E-04 |  | 0.1904 | -2.21E-03 |  | 0.1904 | -2.24E-03 |  | 0.1904 | -2.48E-03 |
|  | 0.1953 | -8.96E-05 |  | 0.1953 | -9.27E-04 |  | 0.1953 | -2.14E-03 |  | 0.1953 | -2.17E-03 |  | 0.1953 | -2.41E-03 |
|  | 0.2002 | -8.74E-05 |  | 0.2002 | -9.03E-04 |  | 0.2002 | -2.08E-03 |  | 0.2002 | -2.11E-03 |  | 0.2002 | -2.34E-03 |
|  | 0.2051 | -8.52E-05 |  | 0.2051 | -8.80E-04 |  | 0.2051 | -2.01E-03 |  | 0.2051 | -2.05E-03 |  | 0.2051 | -2.28E-03 |
|  | 0.21   | -8.29E-05 |  | 0.21   | -8.57E-04 |  | 0.21   | -1.94E-03 |  | 0.21   | -1.99E-03 |  | 0.21   | -2.21E-03 |
|  | 0.2148 | -8.09E-05 |  | 0.2148 | -8.34E-04 |  | 0.2148 | -1.88E-03 |  | 0.2148 | -1.93E-03 |  | 0.2148 | -2.15E-03 |
|  | 0.2197 | -7.88E-05 |  | 0.2197 | -8.12E-04 |  | 0.2197 | -1.82E-03 |  | 0.2197 | -1.87E-03 |  | 0.2197 | -2.08E-03 |
|  | 0.2246 | -7.67E-05 |  | 0.2246 | -7.90E-04 |  | 0.2246 | -1.76E-03 |  | 0.2246 | -1.82E-03 |  | 0.2246 | -2.02E-03 |
|  | 0.2295 | -7.47E-05 |  | 0.2295 | -7.69E-04 |  | 0.2295 | -1.71E-03 |  | 0.2295 | -1.76E-03 |  | 0.2295 | -1.97E-03 |

|  |        |           |  |        |           |  |        |           |  |        |           |  |        |           |
|--|--------|-----------|--|--------|-----------|--|--------|-----------|--|--------|-----------|--|--------|-----------|
|  | 0.2344 | -7.29E-05 |  | 0.2344 | -7.49E-04 |  | 0.2344 | -1.65E-03 |  | 0.2344 | -1.71E-03 |  | 0.2344 | -1.91E-03 |
|  | 0.2393 | -7.10E-05 |  | 0.2393 | -7.28E-04 |  | 0.2393 | -1.60E-03 |  | 0.2393 | -1.66E-03 |  | 0.2393 | -1.85E-03 |
|  | 0.2441 | -6.90E-05 |  | 0.2441 | -7.08E-04 |  | 0.2441 | -1.54E-03 |  | 0.2441 | -1.61E-03 |  | 0.2441 | -1.80E-03 |
|  | 0.249  | -6.74E-05 |  | 0.249  | -6.89E-04 |  | 0.249  | -1.49E-03 |  | 0.249  | -1.57E-03 |  | 0.249  | -1.75E-03 |
|  | 0.2539 | -6.56E-05 |  | 0.2539 | -6.70E-04 |  | 0.2539 | -1.44E-03 |  | 0.2539 | -1.52E-03 |  | 0.2539 | -1.70E-03 |
|  | 0.2588 | -6.39E-05 |  | 0.2588 | -6.51E-04 |  | 0.2588 | -1.39E-03 |  | 0.2588 | -1.48E-03 |  | 0.2588 | -1.65E-03 |
|  | 0.2637 | -6.23E-05 |  | 0.2637 | -6.33E-04 |  | 0.2637 | -1.35E-03 |  | 0.2637 | -1.43E-03 |  | 0.2637 | -1.60E-03 |
|  | 0.2686 | -6.08E-05 |  | 0.2686 | -6.15E-04 |  | 0.2686 | -1.30E-03 |  | 0.2686 | -1.39E-03 |  | 0.2686 | -1.55E-03 |
|  | 0.2734 | -5.93E-05 |  | 0.2734 | -5.97E-04 |  | 0.2734 | -1.26E-03 |  | 0.2734 | -1.35E-03 |  | 0.2734 | -1.51E-03 |
|  | 0.2783 | -5.78E-05 |  | 0.2783 | -5.80E-04 |  | 0.2783 | -1.22E-03 |  | 0.2783 | -1.31E-03 |  | 0.2783 | -1.46E-03 |
|  | 0.2832 | -5.63E-05 |  | 0.2832 | -5.63E-04 |  | 0.2832 | -1.17E-03 |  | 0.2832 | -1.27E-03 |  | 0.2832 | -1.42E-03 |
|  | 0.2881 | -5.48E-05 |  | 0.2881 | -5.46E-04 |  | 0.2881 | -1.13E-03 |  | 0.2881 | -1.23E-03 |  | 0.2881 | -1.38E-03 |
|  | 0.293  | -5.34E-05 |  | 0.293  | -5.30E-04 |  | 0.293  | -1.09E-03 |  | 0.293  | -1.19E-03 |  | 0.293  | -1.34E-03 |
|  | 0.2979 | -5.21E-05 |  | 0.2979 | -5.14E-04 |  | 0.2979 | -1.06E-03 |  | 0.2979 | -1.16E-03 |  | 0.2979 | -1.30E-03 |
|  | 0.3027 | -5.08E-05 |  | 0.3027 | -4.98E-04 |  | 0.3027 | -1.02E-03 |  | 0.3027 | -1.12E-03 |  | 0.3027 | -1.26E-03 |
|  | 0.3076 | -4.94E-05 |  | 0.3076 | -4.83E-04 |  | 0.3076 | -9.82E-04 |  | 0.3076 | -1.09E-03 |  | 0.3076 | -1.22E-03 |
|  | 0.3125 | -4.81E-05 |  | 0.3125 | -4.68E-04 |  | 0.3125 | -9.47E-04 |  | 0.3125 | -1.06E-03 |  | 0.3125 | -1.19E-03 |
|  | 0.3174 | -4.68E-05 |  | 0.3174 | -4.54E-04 |  | 0.3174 | -9.13E-04 |  | 0.3174 | -1.02E-03 |  | 0.3174 | -1.15E-03 |
|  | 0.3223 | -4.56E-05 |  | 0.3223 | -4.39E-04 |  | 0.3223 | -8.80E-04 |  | 0.3223 | -9.92E-04 |  | 0.3223 | -1.12E-03 |
|  | 0.3271 | -4.44E-05 |  | 0.3271 | -4.25E-04 |  | 0.3271 | -8.48E-04 |  | 0.3271 | -9.61E-04 |  | 0.3271 | -1.08E-03 |
|  | 0.332  | -4.31E-05 |  | 0.332  | -4.11E-04 |  | 0.332  | -8.17E-04 |  | 0.332  | -9.31E-04 |  | 0.332  | -1.05E-03 |
|  | 0.3369 | -4.19E-05 |  | 0.3369 | -3.98E-04 |  | 0.3369 | -7.86E-04 |  | 0.3369 | -9.02E-04 |  | 0.3369 | -1.02E-03 |
|  | 0.3418 | -4.08E-05 |  | 0.3418 | -3.84E-04 |  | 0.3418 | -7.56E-04 |  | 0.3418 | -8.73E-04 |  | 0.3418 | -9.84E-04 |
|  | 0.3467 | -3.96E-05 |  | 0.3467 | -3.71E-04 |  | 0.3467 | -7.27E-04 |  | 0.3467 | -8.45E-04 |  | 0.3467 | -9.53E-04 |
|  | 0.3516 | -3.85E-05 |  | 0.3516 | -3.59E-04 |  | 0.3516 | -6.99E-04 |  | 0.3516 | -8.18E-04 |  | 0.3516 | -9.23E-04 |
|  | 0.3564 | -3.74E-05 |  | 0.3564 | -3.46E-04 |  | 0.3564 | -6.72E-04 |  | 0.3564 | -7.92E-04 |  | 0.3564 | -8.93E-04 |

|  |        |           |  |        |           |  |        |           |  |        |           |  |        |           |
|--|--------|-----------|--|--------|-----------|--|--------|-----------|--|--------|-----------|--|--------|-----------|
|  | 0.3613 | -3.64E-05 |  | 0.3613 | -3.34E-04 |  | 0.3613 | -6.45E-04 |  | 0.3613 | -7.66E-04 |  | 0.3613 | -8.64E-04 |
|  | 0.3662 | -3.54E-05 |  | 0.3662 | -3.22E-04 |  | 0.3662 | -6.19E-04 |  | 0.3662 | -7.41E-04 |  | 0.3662 | -8.35E-04 |
|  | 0.3711 | -3.44E-05 |  | 0.3711 | -3.10E-04 |  | 0.3711 | -5.94E-04 |  | 0.3711 | -7.16E-04 |  | 0.3711 | -8.07E-04 |
|  | 0.376  | -3.34E-05 |  | 0.376  | -2.98E-04 |  | 0.376  | -5.69E-04 |  | 0.376  | -6.92E-04 |  | 0.376  | -7.80E-04 |
|  | 0.3809 | -3.24E-05 |  | 0.3809 | -2.87E-04 |  | 0.3809 | -5.44E-04 |  | 0.3809 | -6.68E-04 |  | 0.3809 | -7.54E-04 |
|  | 0.3857 | -3.14E-05 |  | 0.3857 | -2.76E-04 |  | 0.3857 | -5.21E-04 |  | 0.3857 | -6.45E-04 |  | 0.3857 | -7.27E-04 |
|  | 0.3906 | -3.05E-05 |  | 0.3906 | -2.65E-04 |  | 0.3906 | -4.98E-04 |  | 0.3906 | -6.22E-04 |  | 0.3906 | -7.02E-04 |
|  | 0.3955 | -2.96E-05 |  | 0.3955 | -2.54E-04 |  | 0.3955 | -4.76E-04 |  | 0.3955 | -6.00E-04 |  | 0.3955 | -6.76E-04 |
|  | 0.4004 | -2.86E-05 |  | 0.4004 | -2.44E-04 |  | 0.4004 | -4.54E-04 |  | 0.4004 | -5.78E-04 |  | 0.4004 | -6.52E-04 |
|  | 0.4053 | -2.78E-05 |  | 0.4053 | -2.33E-04 |  | 0.4053 | -4.32E-04 |  | 0.4053 | -5.56E-04 |  | 0.4053 | -6.27E-04 |
|  | 0.4102 | -2.69E-05 |  | 0.4102 | -2.23E-04 |  | 0.4102 | -4.11E-04 |  | 0.4102 | -5.35E-04 |  | 0.4102 | -6.04E-04 |
|  | 0.415  | -2.60E-05 |  | 0.415  | -2.13E-04 |  | 0.415  | -3.91E-04 |  | 0.415  | -5.15E-04 |  | 0.415  | -5.80E-04 |
|  | 0.4199 | -2.51E-05 |  | 0.4199 | -2.03E-04 |  | 0.4199 | -3.71E-04 |  | 0.4199 | -4.94E-04 |  | 0.4199 | -5.57E-04 |
|  | 0.4248 | -2.43E-05 |  | 0.4248 | -1.94E-04 |  | 0.4248 | -3.51E-04 |  | 0.4248 | -4.75E-04 |  | 0.4248 | -5.34E-04 |
|  | 0.4297 | -2.35E-05 |  | 0.4297 | -1.84E-04 |  | 0.4297 | -3.32E-04 |  | 0.4297 | -4.55E-04 |  | 0.4297 | -5.12E-04 |
|  | 0.4346 | -2.24E-05 |  | 0.4346 | -1.75E-04 |  | 0.4346 | -3.13E-04 |  | 0.4346 | -4.36E-04 |  | 0.4346 | -4.90E-04 |
|  | 0.4395 | -2.16E-05 |  | 0.4395 | -1.66E-04 |  | 0.4395 | -2.95E-04 |  | 0.4395 | -4.17E-04 |  | 0.4395 | -4.68E-04 |
|  | 0.4443 | -2.08E-05 |  | 0.4443 | -1.57E-04 |  | 0.4443 | -2.77E-04 |  | 0.4443 | -3.98E-04 |  | 0.4443 | -4.47E-04 |
|  | 0.4492 | -2.00E-05 |  | 0.4492 | -1.48E-04 |  | 0.4492 | -2.59E-04 |  | 0.4492 | -3.80E-04 |  | 0.4492 | -4.26E-04 |
|  | 0.4541 | -1.93E-05 |  | 0.4541 | -1.39E-04 |  | 0.4541 | -2.42E-04 |  | 0.4541 | -3.62E-04 |  | 0.4541 | -4.05E-04 |
|  | 0.459  | -1.86E-05 |  | 0.459  | -1.31E-04 |  | 0.459  | -2.25E-04 |  | 0.459  | -3.44E-04 |  | 0.459  | -3.85E-04 |
|  | 0.4639 | -1.79E-05 |  | 0.4639 | -1.22E-04 |  | 0.4639 | -2.09E-04 |  | 0.4639 | -3.26E-04 |  | 0.4639 | -3.65E-04 |
|  | 0.4688 | -1.71E-05 |  | 0.4688 | -1.14E-04 |  | 0.4688 | -1.92E-04 |  | 0.4688 | -3.09E-04 |  | 0.4688 | -3.45E-04 |
|  | 0.4736 | -1.64E-05 |  | 0.4736 | -1.06E-04 |  | 0.4736 | -1.77E-04 |  | 0.4736 | -2.92E-04 |  | 0.4736 | -3.26E-04 |
|  | 0.4785 | -1.57E-05 |  | 0.4785 | -9.78E-05 |  | 0.4785 | -1.61E-04 |  | 0.4785 | -2.75E-04 |  | 0.4785 | -3.07E-04 |
|  | 0.4834 | -1.50E-05 |  | 0.4834 | -8.98E-05 |  | 0.4834 | -1.45E-04 |  | 0.4834 | -2.59E-04 |  | 0.4834 | -2.88E-04 |

|  |        |           |  |        |           |  |        |           |  |        |           |  |        |           |
|--|--------|-----------|--|--------|-----------|--|--------|-----------|--|--------|-----------|--|--------|-----------|
|  | 0.4883 | -1.43E-05 |  | 0.4883 | -8.20E-05 |  | 0.4883 | -1.30E-04 |  | 0.4883 | -2.42E-04 |  | 0.4883 | -2.69E-04 |
|  | 0.4932 | -1.36E-05 |  | 0.4932 | -7.43E-05 |  | 0.4932 | -1.15E-04 |  | 0.4932 | -2.26E-04 |  | 0.4932 | -2.51E-04 |
|  | 0.498  | -1.29E-05 |  | 0.498  | -6.67E-05 |  | 0.498  | -1.01E-04 |  | 0.498  | -2.10E-04 |  | 0.498  | -2.33E-04 |
|  | 0.5029 | -1.22E-05 |  | 0.5029 | -5.93E-05 |  | 0.5029 | -8.64E-05 |  | 0.5029 | -1.95E-04 |  | 0.5029 | -2.15E-04 |
|  | 0.5078 | -1.16E-05 |  | 0.5078 | -5.19E-05 |  | 0.5078 | -7.22E-05 |  | 0.5078 | -1.79E-04 |  | 0.5078 | -1.97E-04 |
|  | 0.5127 | -1.09E-05 |  | 0.5127 | -4.46E-05 |  | 0.5127 | -5.83E-05 |  | 0.5127 | -1.64E-04 |  | 0.5127 | -1.80E-04 |
|  | 0.5176 | -1.03E-05 |  | 0.5176 | -3.74E-05 |  | 0.5176 | -4.45E-05 |  | 0.5176 | -1.49E-04 |  | 0.5176 | -1.62E-04 |
|  | 0.5225 | -9.69E-06 |  | 0.5225 | -3.03E-05 |  | 0.5225 | -3.10E-05 |  | 0.5225 | -1.34E-04 |  | 0.5225 | -1.45E-04 |
|  | 0.5273 | -9.05E-06 |  | 0.5273 | -2.33E-05 |  | 0.5273 | -1.76E-05 |  | 0.5273 | -1.19E-04 |  | 0.5273 | -1.29E-04 |
|  | 0.5322 | -8.38E-06 |  | 0.5322 | -1.63E-05 |  | 0.5322 | -4.46E-06 |  | 0.5322 | -1.04E-04 |  | 0.5322 | -1.12E-04 |
|  | 0.5371 | -7.83E-06 |  | 0.5371 | -9.40E-06 |  | 0.5371 | 8.55E-06  |  | 0.5371 | -8.92E-05 |  | 0.5371 | -9.56E-05 |
|  | 0.542  | -7.23E-06 |  | 0.542  | -2.64E-06 |  | 0.542  | 2.14E-05  |  | 0.542  | -7.46E-05 |  | 0.542  | -7.94E-05 |
|  | 0.5469 | -6.59E-06 |  | 0.5469 | 4.07E-06  |  | 0.5469 | 3.41E-05  |  | 0.5469 | -6.02E-05 |  | 0.5469 | -6.34E-05 |
|  | 0.5518 | -6.01E-06 |  | 0.5518 | 1.07E-05  |  | 0.5518 | 4.66E-05  |  | 0.5518 | -4.59E-05 |  | 0.5518 | -4.73E-05 |
|  | 0.5566 | -5.44E-06 |  | 0.5566 | 1.74E-05  |  | 0.5566 | 5.91E-05  |  | 0.5566 | -3.17E-05 |  | 0.5566 | -3.15E-05 |
|  | 0.5615 | -4.87E-06 |  | 0.5615 | 2.39E-05  |  | 0.5615 | 7.14E-05  |  | 0.5615 | -1.76E-05 |  | 0.5615 | -1.58E-05 |
|  | 0.5664 | -4.29E-06 |  | 0.5664 | 3.03E-05  |  | 0.5664 | 8.36E-05  |  | 0.5664 | -3.69E-06 |  | 0.5664 | -2.14E-07 |
|  | 0.5713 | -3.71E-06 |  | 0.5713 | 3.67E-05  |  | 0.5713 | 9.56E-05  |  | 0.5713 | 1.02E-05  |  | 0.5713 | 1.52E-05  |
|  | 0.5762 | -3.19E-06 |  | 0.5762 | 4.31E-05  |  | 0.5762 | 1.08E-04  |  | 0.5762 | 2.39E-05  |  | 0.5762 | 3.04E-05  |
|  | 0.5811 | -2.62E-06 |  | 0.5811 | 4.94E-05  |  | 0.5811 | 1.19E-04  |  | 0.5811 | 3.75E-05  |  | 0.5811 | 4.54E-05  |
|  | 0.5859 | -2.07E-06 |  | 0.5859 | 5.57E-05  |  | 0.5859 | 1.31E-04  |  | 0.5859 | 5.10E-05  |  | 0.5859 | 6.03E-05  |
|  | 0.5908 | -1.56E-06 |  | 0.5908 | 6.19E-05  |  | 0.5908 | 1.43E-04  |  | 0.5908 | 6.45E-05  |  | 0.5908 | 7.51E-05  |
|  | 0.5957 | -1.05E-06 |  | 0.5957 | 6.81E-05  |  | 0.5957 | 1.54E-04  |  | 0.5957 | 7.78E-05  |  | 0.5957 | 8.98E-05  |
|  | 0.6006 | -4.93E-07 |  | 0.6006 | 7.42E-05  |  | 0.6006 | 1.66E-04  |  | 0.6006 | 9.10E-05  |  | 0.6006 | 1.04E-04  |
|  | 0.6055 | 3.45E-08  |  | 0.6055 | 8.03E-05  |  | 0.6055 | 1.77E-04  |  | 0.6055 | 1.04E-04  |  | 0.6055 | 1.19E-04  |
|  | 0.6104 | 5.46E-07  |  | 0.6104 | 8.63E-05  |  | 0.6104 | 1.88E-04  |  | 0.6104 | 1.17E-04  |  | 0.6104 | 1.33E-04  |



|  |        |          |  |        |          |  |        |          |  |        |          |  |        |          |
|--|--------|----------|--|--------|----------|--|--------|----------|--|--------|----------|--|--------|----------|
|  | 0.6152 | 1.08E-06 |  | 0.6152 | 9.23E-05 |  | 0.6152 | 1.99E-04 |  | 0.6152 | 1.30E-04 |  | 0.6152 | 1.47E-04 |
|  | 0.6201 | 1.62E-06 |  | 0.6201 | 9.83E-05 |  | 0.6201 | 2.10E-04 |  | 0.6201 | 1.43E-04 |  | 0.6201 | 1.61E-04 |
|  | 0.625  | 2.10E-06 |  | 0.625  | 1.04E-04 |  | 0.625  | 2.21E-04 |  | 0.625  | 1.56E-04 |  | 0.625  | 1.75E-04 |
|  | 0.6299 | 2.60E-06 |  | 0.6299 | 1.10E-04 |  | 0.6299 | 2.32E-04 |  | 0.6299 | 1.69E-04 |  | 0.6299 | 1.89E-04 |
|  | 0.6348 | 3.11E-06 |  | 0.6348 | 1.16E-04 |  | 0.6348 | 2.43E-04 |  | 0.6348 | 1.81E-04 |  | 0.6348 | 2.02E-04 |
|  | 0.6396 | 3.60E-06 |  | 0.6396 | 1.22E-04 |  | 0.6396 | 2.54E-04 |  | 0.6396 | 1.94E-04 |  | 0.6396 | 2.16E-04 |
|  | 0.6445 | 4.08E-06 |  | 0.6445 | 1.28E-04 |  | 0.6445 | 2.65E-04 |  | 0.6445 | 2.06E-04 |  | 0.6445 | 2.29E-04 |
|  | 0.6494 | 4.56E-06 |  | 0.6494 | 1.34E-04 |  | 0.6494 | 2.75E-04 |  | 0.6494 | 2.19E-04 |  | 0.6494 | 2.42E-04 |
|  | 0.6543 | 5.06E-06 |  | 0.6543 | 1.39E-04 |  | 0.6543 | 2.86E-04 |  | 0.6543 | 2.31E-04 |  | 0.6543 | 2.55E-04 |
|  | 0.6592 | 5.52E-06 |  | 0.6592 | 1.45E-04 |  | 0.6592 | 2.97E-04 |  | 0.6592 | 2.43E-04 |  | 0.6592 | 2.68E-04 |
|  | 0.6641 | 5.96E-06 |  | 0.6641 | 1.51E-04 |  | 0.6641 | 3.07E-04 |  | 0.6641 | 2.55E-04 |  | 0.6641 | 2.81E-04 |
|  | 0.6689 | 6.42E-06 |  | 0.6689 | 1.56E-04 |  | 0.6689 | 3.18E-04 |  | 0.6689 | 2.67E-04 |  | 0.6689 | 2.94E-04 |
|  | 0.6738 | 6.87E-06 |  | 0.6738 | 1.62E-04 |  | 0.6738 | 3.28E-04 |  | 0.6738 | 2.79E-04 |  | 0.6738 | 3.06E-04 |
|  | 0.6787 | 7.33E-06 |  | 0.6787 | 1.68E-04 |  | 0.6787 | 3.39E-04 |  | 0.6787 | 2.91E-04 |  | 0.6787 | 3.19E-04 |
|  | 0.6836 | 7.76E-06 |  | 0.6836 | 1.73E-04 |  | 0.6836 | 3.49E-04 |  | 0.6836 | 3.03E-04 |  | 0.6836 | 3.31E-04 |
|  | 0.6885 | 8.21E-06 |  | 0.6885 | 1.79E-04 |  | 0.6885 | 3.59E-04 |  | 0.6885 | 3.14E-04 |  | 0.6885 | 3.44E-04 |
|  | 0.6934 | 8.67E-06 |  | 0.6934 | 1.84E-04 |  | 0.6934 | 3.70E-04 |  | 0.6934 | 3.26E-04 |  | 0.6934 | 3.56E-04 |
|  | 0.6982 | 9.11E-06 |  | 0.6982 | 1.90E-04 |  | 0.6982 | 3.80E-04 |  | 0.6982 | 3.37E-04 |  | 0.6982 | 3.68E-04 |
|  | 0.7031 | 9.56E-06 |  | 0.7031 | 1.96E-04 |  | 0.7031 | 3.90E-04 |  | 0.7031 | 3.49E-04 |  | 0.7031 | 3.79E-04 |

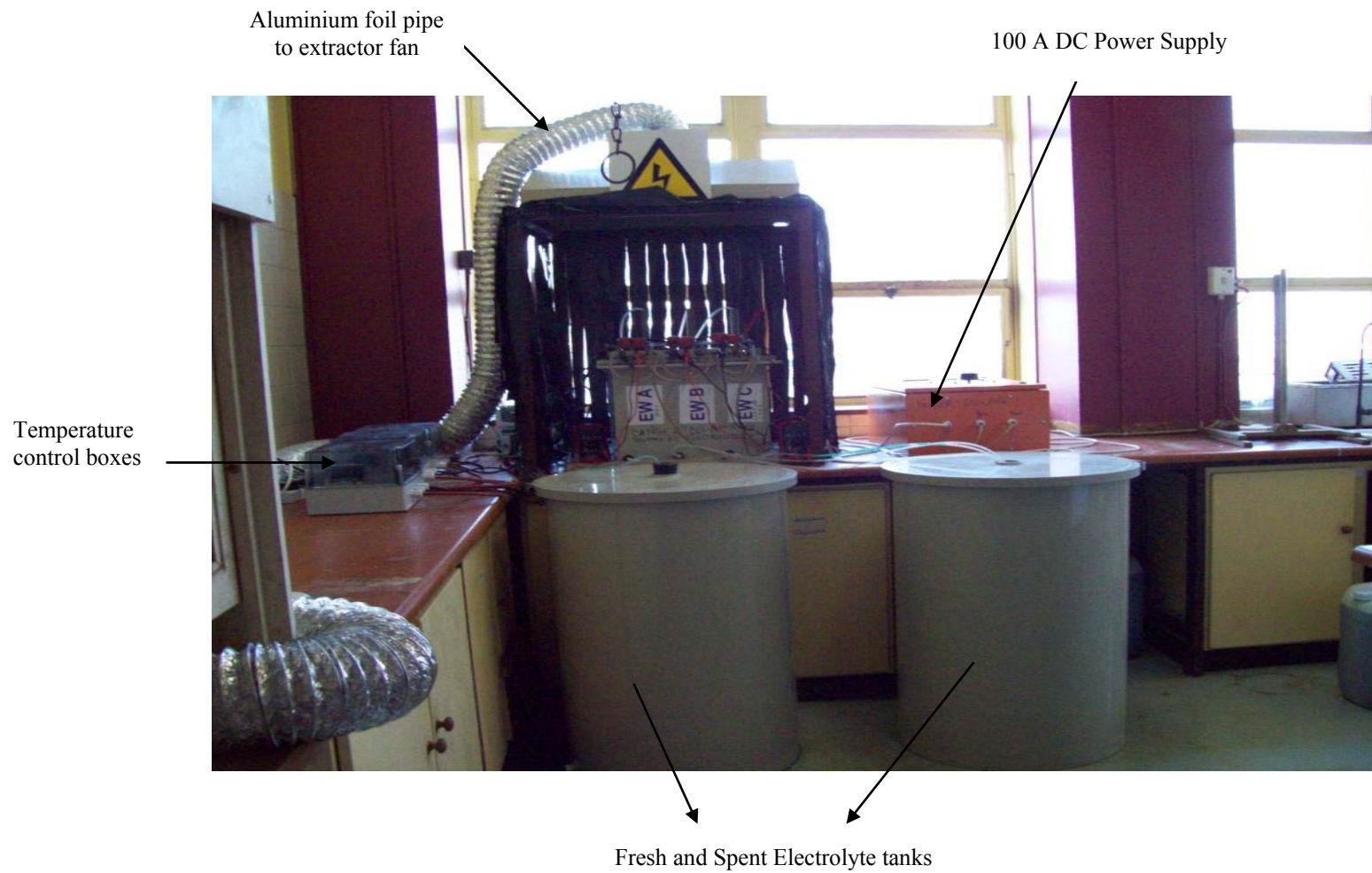
\* Potential in volts.

\* Current density in amperes per square centimetre

## APPENDIX G: COMPOSITION OF BMR ELECTROLYTE

| <b>Sample</b> | <b>Pt</b>      | <b>Pd</b>      | <b>Au</b>      | <b>Rh</b>      | <b>Ru</b>      | <b>Ir</b>      | <b>Os</b>      |
|---------------|----------------|----------------|----------------|----------------|----------------|----------------|----------------|
| <b>Unit</b>   | <b>mg/l</b>    | <b>mg/l</b>    | <b>mg/l</b>    | <b>mg/l</b>    | <b>mg/l</b>    | <b>mg/l</b>    | <b>mg/l</b>    |
| <b>Method</b> | <b>*ICP-MS</b> | <b>*ICP-MS</b> | <b>*ICP-MS</b> | <b>*ICP-MS</b> | <b>*ICP-MS</b> | <b>*ICP-MS</b> | <b>*ICP-MS</b> |
| TANK 1        | <0.2           | <0.2           | <0.2           | 3.9            | 30             | 1.0            | 0.4            |
| TANK 2        | <0.2           | <0.2           | <0.2           | 4.0            | 32             | 1.0            | <0.2           |
| <b>Sample</b> | <b>Ag</b>      | <b>Bi</b>      | <b>Pb</b>      | <b>Se</b>      | <b>As</b>      | <b>Cu</b>      | <b>Ni</b>      |
| <b>Unit</b>   | <b>mg/l</b>    | <b>mg/l</b>    | <b>mg/l</b>    | <b>mg/l</b>    | <b>mg/l</b>    | <b>mg/l</b>    | <b>mg/l</b>    |
| <b>Method</b> | <b>*ICP-MS</b> | <b>*ICP-MS</b> | <b>*ICP-MS</b> | <b>*ICP-MS</b> | <b>*ICP-MS</b> | <b>*ICP</b>    | <b>*ICP</b>    |
| TANK 1        | <0.2           | 5.6            | 2.2            | 11             | 150            | 55.73g/l       | 59.28g/l       |
| TANK 2        | <0.2           | 5.7            | 2.6            | 11             | 158            | 53.43g/l       | 61.45g/l       |
| <b>Sample</b> | <b>Co</b>      | <b>S</b>       | <b>Al</b>      | <b>Ca</b>      | <b>Cr</b>      | <b>Mn</b>      | <b>Fe</b>      |
| <b>Unit</b>   | <b>mg/l</b>    | <b>mg/l</b>    | <b>mg/l</b>    | <b>mg/l</b>    | <b>mg/l</b>    | <b>mg/l</b>    | <b>mg/l</b>    |
| <b>Method</b> | <b>*ICP</b>    | <b>*ICP</b>    | <b>*ICP</b>    | <b>*ICP</b>    | <b>*ICP</b>    | <b>*ICP</b>    | <b>*ICP</b>    |
| TANK 1        | 1434           | 90.23g/l       | 121            | 77.60          | 23.45          | 8.05           | 12.4g/l        |
| TANK 2        | 1436           | 89.18g/l       | 116            | 73.70          | 22.70          | 8.4            | 12.3g/l        |

## APPENDIX H: PHOTOGRAPH OF THE EXPERIMENTAL SETUP (ELECTROWINNING)



## **SUBMISSION OF RESEARCH PAPER**

The following article from a section of the results has been accepted for publication in an ISI-peer-reviewed journal after the corrections suggested by both examiners have been made:

Z.S. Msindo, V. Sibanda and J.H. Potgieter, Electrochemical and physical characterization of lead based anodes in comparison to Ti- (70%) IrO<sub>2</sub>/ (30%) Ta<sub>2</sub>O<sub>5</sub> dimensionally stable anodes for use in copper electrowinning, Journal of Applied Electrochemistry (in press)